A.C. LOSSES IN SUPERCONDUCTING NIOBIUM

by

Paul Robert Brankin

A thesis submitted to the

UNIVERSITY OF WARWICK

for the degree of Doctor of Philosophy

November 1970

ABSTRACT

The thesis is introduced by a discussion of the technological importance of developing superconducting materials having low losses at power frequencies. The following two chapters are devoted to a presentation of the reversible magnetic properties of superconductors using the Ginzburg-Landau equations, and a discussion of the irreversible behaviour of real materials in terms of flux pinning and the critical state concept. Following this background discussion, previous work on a.c. losses is reviewed. Particular emphasis is given to the losses below H_{c1} and it is shown that, while losses above H_{c1} can be interpreted using the critical state model, below H_{c1} they are only partially understood.

Modifications to an electronic wattmeter which enable accurate measurements to be made at 10^{-4} WHz^{-1} m^{-2} are discussed. An improved vibrating sample magnetometer is described, together with the theory and design of an a.c. permeability apparatus used to obtain critical current values.

The preparation of a range of niobium samples is described. The techniques employed include annealing, spark-machining, mechanical, chemical and electropolishing, neutron irradiation and ion-implantation. The magnetization curves, surface profiles and other data for the treated specimens are presented.

Measurements of the low frequency losses in these samples at 4.2 K are described. It is shown that in rough samples hysteretic losses arise below H_{c1} from the penetration of surface asperities and that the results are in good agreement with an expression, similar to Buchhold's (1963), which is derived, namely :

$$L = 4 \mu_o H_m^2 f(H_m/H_{CL}) KD$$

where H_m is the peak field, H_{CL} the lower critical field, H_{c1} or H_c, D the centre line average height of the surface profile and K a 'hysteresis factor'. The losses in cold-worked and annealed niobium samples and lead, tin and indium specimens with values for D between 0.33 and 20 μm are found to fit

(within a factor of two) the expression :

$$L = \tfrac{1}{2} \mu_o H_m^2 (H_m/H_{CL})^2 D$$

Different results are observed in smooth samples and explanations for these are suggested. The losses in samples previously penetrated by a large a.c. field are found to be increased by a factor of up to thirty. This increase is related to trapped flux and possible loss mechanisms are discussed.

The losses above H_{cl} are shown to be reduced in damaged samples. Neutron irradiation induces heavy bulk damage but has little effect on the surface. Mechanical treatment produces large surface currents and is most effective in reducing the loss, the dissipation at 50 Hz being below 0.1 W m^{-2} at fields up to 85 kA(RMS)m^{-1} (1500 Oe - Peak) in a mechanically polished, annealed polycrystalline sample. Implantation of niobium ions to a depth of 10 nm does not alter the losses.

Measurements of the critical currents and flux profiles in two annealed samples are presented and it is shown that a critical state exists within them. The losses above H_{cl} in both irreversible and annealed samples fit the Ullmaier (1966) expression $L = \frac{2}{3} \mu_o (H_m - \Delta H/2)^3 / J_c$, but it is found that equating $\Delta H/2$ with H_{cl} gives critical currents an order of magnitude smaller than those obtained in other measurements. It is shown that $\Delta H/2$ is not constant and that the shielding currents are negligible except near H_{cl}.

THE AUTHOR obtained a Bachelor's degree in Physics at King's College, London University, in August 1964. He worked as a Logic Design Engineer for Elliott Automation, Borehamwood until 1965 when he joined the Low Temperature Group in the Physics Department at Manchester University. During his first year at Manchester he obtained a Diploma for Advanced Studies in Science, and commenced measurement of the magnetic susceptibility of superconductors. He was awarded the Degree of Master of Science in 1968 by the University of Manchester for a thesis entitled, "Critical Currents in the Superconducting Surface Sheaths of Some Indium-Lead Alloys". In 1967 he moved to the School of Engineering Science at the University of Warwick where he performed the work described in this thesis. At present the author is employed as a physicist in the Superconductivity Department of the British Oxygen Company.

DECLARATION

I, the undersigned Paul Robert Brankin, declare that the concept and execution of the work described in this thesis has been my own responsibility, and that none of my work presented here has been submitted in support of an application for another degree or qualification at this or any other university or other institute of learning.

Paul Robert Brankin

ACKNOWLEDGEMENTS

I wish to express my gratitude to the authorities at Warwick University and Professor J.A. Shercliff for extending to me the facilities of the University during the period of my work for this thesis. I am grateful to the British Oxygen Company (and in particular Dr. B.B. Goodman) for financial support over the same period.

I would like to thank my supervisor Dr. R.G. Rhodes for his advice and guidance during the past three years and for reading the manuscript. Little experimental work is possible without technical assistance and I am grateful to Mr. H. Woodgate and the many other technicians who have constructed apparatus and undertaken measurements for me. I have also benefited from many useful discussions with my erstwhile colleagues Drs. J.E. Goodfellow, R.M.F. Linford and R.J.A. Seebold and, more recently, Dr. A.R. Eastham whom I must also thank for proof reading the typescript. Single crystal samples were provided for this work by Dr. D. Jones of Birmingham University, Centre for Materials Science, and Dr. D.K. Bowen of Warwick University to whom I am grateful for metallurgical advice. Finally, I must thank Miss Daphne Twigger for her patience in turning the manuscript into a presentable typescript, Mrs. Christine Allsop for tracing the drawings and my wife and children for tolerating my single-minded pursuit of science for the past three years, to them my apologies for the neglect they have suffered.

P.R. BRANKIN NOVEMBER 1970

CONTENTS

1. INTRODUCTION

The last decade has seen a phenomenal expansion in the use of superconductors. The first high-field solenoids were constructed in 1961 by Frazer et al (1961) and Kunzler (1962). Since then superconductors have been used in the construction of a 2.4 MW D.C. motor by the International Research and Development Co., two large bubble-chamber magnets at Brookhaven and Argonne, the former of 2.44 m and the latter of 4.83 m internal diameter, an 0.7 m quadrupole, focussing magnet for the Cern 28 GeV proton synchroton and in microwave cavities for a linear accelerator at Stanford. Beside these large scale projects, superconducting magnets of a variety of designs have become common place research tools in many laboratories. A superconducting picovoltmeter is available, and quantum interference devices (Josephson junctions) have found many uses. Superconducting wire is produced by firms in Britain, Japan, Germany and North America. Superconducting magnets are available from numerous commercial enterprises.

Feasibility and design studies have been undertaken for many other applications. For example, Powell and Danby (1966) have examined the possibilities of using superconducting magnets in the suspension of high-speed trains, Garwin and Matisoo (1967) studied the transmission of powers of the order of 100 GW over distances of 1000 km using a D.C. superconducting cable, workers at the Rutherford laboratory are actively engaged in developing a superconducting synchrotron (Smith, 1968).

Apart from the IRDC motor all the large-scale applications of superconductors have been in nuclear research; in none of them are superconductors used to carry power-frequency alternating currents. Since almost all electric power is generated, transmitted and utilized as alternating current the widespread use of superconductors in everyday industrial applications now awaits the development of materials suitable for use with alternating currents.

The advance in the use of superconductors detailed above depended on the development of such high-field superconducting materials as Nb_3Sn and NbZr

by Kunzler et al (1961) and Berlincourt et al (1961). These materials can carry currents of up to 10,000 MA m^{-2} at fields of 2 Tesla, and 100 MA m^{-2} at up to 20 Tesla. Their ability to carry such large currents with apparently zero power dissipation arises because flux penetrates the material and is pinned at metallurgical defects. However, when an alternating field is applied this behaviour leads to dissipation. The motion of flux into and out of the superconductor as the field changes is hysteretic, and produces losses.

Although the losses are small compared to normal joule heating in good conductors at room temperature, they are significant for two reasons. First the rate at which heat can be transferred from a metal surface to liquid helium without producing a large temperature gradient is about 100 Wm^{-2}. Consequently there is a limit to the loss level at which a superconductor can be operated without producing thermal runaway. Second it requires a power input of λ order 400 watts at room temperature to produce 1 watt of refrigeration at 4.2 K, any loss in a superconductor must therefore be at least a factor of 400 smaller than in a conventional conductor to obtain a real reduction in power losses.

Most devices utilizing superconductors fall into two categories, those which exploit the high-field characteristics of superconductors e.g. magnets and those which utilize their high current-carrying capacities e.g. cables. For the former only the high-field superconductors are available, and the problems of 50 Hz a.c. losses already mentioned are severe. For high current applications the elemental superconductors provide a second possibility. Some of these prevent flux penetration up to moderately high fields. In this field region, the so called Meissner state, they can carry high alternating current densities at the surface with very little loss. Lead and niobium are two materials which have been considered (Rogers and Edwards, 1967). Niobium is the basis for most of the high-field alloys, but, in pure form it remains in the Meissner state to fields of 110 kA m^{-1} (1400 Oe) at 4.2 K, and has a critical temperature of 9.2 K.

No other material excludes flux to as high a field at 4.2 K.

One of the high-current applications for which niobium could be used is an a.c. power transmission cable. A number of design and feasibility studies have been undertaken of such a device e.g. Rogers and Edwards (1967), Cairns et al (1969). Its potential advantages are enormous; it could carry high currents over long distances, and might solve the problems of increasing voltage and size which hamper conventional cable design. Cairns et al (1969) and Rogers (1969) have shown that an a.c. cable to carry powers of the order of 1GW might be economically and technically feasible. The conductor (Taylor, 1969) would be a thin layer of niobium operated at a surface current density below 100 kA m^{-1}. This would be attached to a layer of high-field superconductor on a copper base which could carry any overload currents that produced fields sufficient to drive the niobium normal.

One of the problems in designing an a.c. cable or other device is a lack of reliable information about the mechanisms which produce the small losses that occur in the Meissner State. For example, the relationships between loss and metallurgical parameters are uncertain, the desirable degree of surface smoothness is not known. It is not clear if the performance of niobium can be improved. Any increase in its current carrying capacity would certainly enhance the feasibility of the concept.

This thesis describes an experimental programme which has been undertaken to clarify some of these points. A.C. losses in niobium both in and above the Meissner state have been measured with the objectives of identifying the loss mechanisms, defining the important material parameters and investigating ways of reducing losses particularly in fields above the Meissner state.

The next two chapters describe the basic reversible and irreversible magnetic properties of superconductors. The fourth chapter outlines the current understanding of a.c. losses and the specific objects of our experiments. The experimental apparatus and the results obtained are then discussed. S.I. units are used throughout except that, for convenience, a magnetic field, H, is quoted in both Am^{-1} and Oe.

* Recent pulsed-field measurements by Foner et al have shown the upper critical field of NbAlGe to be 41T at 4.2K.

see Foner, S., McNiff, E.J. (Jr), Matthias, B.T., Geballe, T.H., Willens R.H. and Corenzwit, E., 1970, Phys. Lett., 31a, 349-50

2. THE REVERSIBLE BEHAVIOUR OF SUPERCONDUCTORS

2.1. Superconductivity

A superconductor is a material which below its critical temperature, T_c, has an immeasurably small resistance to the flow of electrical current. In a magnetic field a superconductor will regain its normal properties when the field exceeds a critical value. This critical field is temperature dependent increasing from zero at T_c to its maximum value at absolute zero.

The phenomenon of superconductivity was first observed in 1911 at the University of Leiden when Kamerlingh Onnes (1913) attempted to measure the resistance of mercury in liquid helium. He found that below 4K he could measure no resistance. Since that time a further 23 elements have been shown to be superconductors with critical temperatures ranging from 11.2K for technitium to 0.01K for tungsten (Roberts 1963), and with critical fields up to 0.26 Tesla for niobium. Much higher critical fields and temperatures are exhibited by alloys. Roberts (1963) has listed hundreds of superconducting alloy systems and compounds. The highest critical temperature so far recorded (Foner et al, 1968) is 20.7K for a composite of niobium, aluminium and germanium; niobium-tin with a critical temperature of 18.5K has the highest upper critical field of over 20 Tesla at OK.*

Superconductors have other important properties besides zero resistivity. A weak magnetic field is completely excluded from their interiors; they are completely diamagnetic with magnetic moment, M, equal to -H. For suitably prepared samples this effect is reversible. When flux does penetrate a superconductor it is quantized. Other properties are also affected. At the critical temperature a second order phase transition into the superconducting state takes place in zero magnetic field. This transition involves no latent heat. There is a discontinuity in the specific heat which rises to a high value at T_c then falls below its normal state value as the temperature is lowered towards zero. There are also small changes in bulk rigidity modulus and thermal expansion coefficient at the transition temperature.

A microscopic interpretation of these and other properties of superconductors has been developed by Bardeen, Cooper and Schrieffer (1957). With some modifications, their theory which is now known as the BCS theory, has been shown to be in agreement with the data from a wide range of thermal, electromagnetic, nuclear, acoustic and mechanical measurements. The theory shows that the properties of a superconductor are produced by a condensed state involving pairs of electrons with opposite spin and equal and opposite momentum. This state extends over the whole of a macroscopic sample, and can be described by a superconducting order parameter, ψ, which is a function of position and time only. Such a condensed state will be produced by any attractive force between electrons, but in the BCS theory this is supposed to arise from phonon coupling over a characteristic distance called the coherence length, $\xi(T)$.

An alternative and simpler approach to the understanding of the electromagnetic properties of superconductors in particular is the Ginzburg-Landau (1950) theory. In the remainder of this chapter the reversible properties of superconductors are described, the Ginzburg-Landau equations are introduced and the magnetic properties they predict are presented. Many sources have been referred to while writing this chapter but the author has drawn in particular from the books by Lynton (1969), DeGennes (1966) and Rose-Innes and Rhoderick (1969), and the review article on Type II superconductors by Goodman (1966).

2.2. Early Theories of Superconductivity

If an infinitely long cylinder of one of the superconducting elements is placed in a uniform, axial, magnetic field which increases from zero, the magnetization, M, of the sample follows the path shown in Fig. 2.1. The superconductor exhibits perfect diamagnetism, that is M equals -H, up to a critical field, H_c. At H_c the superconductor reverts to the normal state, where resistance reappears and M is almost zero. Generally, the transition is not reversible. There is some hysteresis due, for example to multiply-

connected, internal regions with critical fields higher than that of the bulk material. On field reversal, these become superconducting before the bulk, and flux is trapped within them.

However, Meissner and Ochsenfeld (1933) showed that for pure, defect-free samples of good crystallinity the phase change is reversible. This enabled Gorter and Casimir (1933) to develop a thermodynamic treatment of superconductivity. The Gibb's free energy, $G_s(H)$, of a superconductor in a magnetic field, H, is given by

$$2.2.1. \qquad G_s(H) - G_s(o) = \int_o^V dV \; \mu_o \int_o^H -M(H)dH$$

where $G_s(o)$ is the free-energy in zero field.
Volume changes are negligible so $\int dV$ equals V, and for an infinite sample M equals -H. At the transition $G_s(H_c) \equiv G_n(H_c)$, where $G_n(H)$ is the free energy of the normal phase in a magnetic field. For most materials $G_n(H)$ will be almost equal to $G_n(o)$. Hence it can be shown that

$$2.2.2. \qquad G_n(o) - G_s(o) = V\mu_o H_c^2/2$$

Thus the condensation energy, $\mu_o H_c^2/2 (Jm^{-3})$, of the superconducting state is equal to the area under the reversible magnetization curve, $\int_o^{H_T} MdH$ and is of the order of 10^{-8} eV per atom. Its smallness was the principal reason for the long delay (1911-1957) in deriving a satisfactory theory of the superconducting state.

Successive differentiations of Equation 2.2.2. with respect to temperature yield expressions for the entropy and specific heat of a superconductor in terms of the variation of the critical field with temperature. Gorter and Casimir also predicted how the thermal properties would vary with temperature by using a two-fluid model of a superconductor. This model supposes that the superconductor contains two types of conducting electrons, a number n_s which are superconducting, and $n - n_s$ which are normal. As the temperature changes from T_c to zero, n_s changes from zero to n.

Thus, the Meissner-Ochsenfeld experiments led the way to a thermo-

dynamic description of superconductivity. They also led F. and H. London (1935) to develop an electromagnetic theory of superconductors. Becker et al (1933) had developed an electromagnetic treatment based on the assumption that a superconductor contained perfectly conducting electrons. The current density $\underline{J}$ in a material subject to a field $\underline{E}$, and containing n perfectly conducting electrons of charge e and mass m can be shown to be

2.2.3. $$\underline{E} = \frac{m}{ne^2} \dot{\underline{J}}$$

Using the Maxwell equation curl $\underline{E} = -\dot{\underline{B}}$ this leads to

2.2.4. $$-\dot{B} = \frac{m}{ne^2} \text{ curl } \dot{\underline{J}}$$

Equation 2.2.4. shows that a perfect conductor would generate shielding currents near the surface opposing any change in an applied magnetic field and keeping the internal flux constant. Hence if the normal-superconducting transition occurred in a magnetic field, the flux present in the conductor would be trapped. The Meissner experiments showed that in a superconductor this does not happen.

F. and H. London (1935) suggested that the superconducting electrons of the Gorter-Casimir two-fluid model should obey Equation 2.2.3. which becomes

2.2.5. $$\underline{E} = \frac{m}{n_s e^2} \dot{\underline{J}}$$

and that the Meissner effect would occur if Equation 2.2.4. was replaced by the more restrictive condition

2.2.6. $$-\underline{B} = \frac{m}{n_s e^2} \text{ curl } \underline{J}$$

where n_s is the number of superconducting electrons.

Equations 2.2.5. and 6 describe the electromagnetic behaviour of a superconductor, and are known as London's equations. Equation 2.2.6. may be combined with the Maxwell equation curl $\underline{B} = \mu_o \underline{J}$ to obtain the expression

2.2.7. $$\underline{B} + \lambda_L^2 \, \text{curl curl} \, \underline{B} = 0$$ where

2.2.8. $$\lambda_L = \left(\frac{m}{\mu_0 n_s e^2} \right)^{\frac{1}{2}}$$

The solution to Equation 2.2.7. for a one-dimensional case shows that an external field penetrates a superconductor, but decays exponentially from the surface over a characteristic distance λ_L which is approximately 10 nm. λ_L is called the London penetration depth.

The experiments of Schoenberg (1940) and others confirmed the London prediction that an external field should penetrate a small distance into a superconductor. They also showed that the temperature variation of the penetration depth agreed with the temperature variation of $n_s^{-\frac{1}{2}}$ predicted by the two-fluid model. However the actual value of the penetration depth was found to be larger than λ_L. Pippard (1953) used measurements of the anomalous skin effect in superconducting tin samples to obtain the actual penetration depth, λ. He found that λ was greater than λ_L, that it increased as the applied field increased and that it was anisotropic in single crystals. Even more significant was his discovery that the penetration depth in zero field, λ_0, increased as the mean free path, l, of the tin was decreased by the addition of indium.

To explain his results Pippard (1950 and 1953) suggested that there was a characteristic length associated with superconductors which was the minimum distance over which changes in the parameters describing the superconducting state could change under the influence of perturbations. This characteristic length was of the order of 1 μm for pure materials, and decreased with the electron mean free path in impure specimens. Such a characteristic length, the coherence length $\xi(T)$, does appear in the microscopic BCS theory.

Pippard drew an analogy with the theory of the anomalous skin effect to suggest that the relationship between the super currents and the external field was non-local. Using a non-local expression for the conductivity in a region of characteristic dimension ξ, similar to expressions developed

for the anomalous skin effect, he predicted that the actual penetration depth should be given by the expressions

2.2.9. $\lambda = (\xi_0/\xi)^{\frac{1}{2}} \lambda_L \qquad \xi << \lambda \qquad$ (London Limit)

2.2.10 $\lambda_\infty = 0.62\, \xi_0^{1/3}\, \lambda_L^{2/3} \qquad \xi >> \lambda$ (Pippard Limit)

where ξ_0 is the coherence length for pure materials, and λ_∞ is the corresponding penetration depth in the limit of infinite electron mean free path. These expressions are found to be in agreement with experiment.

2.3. The Ginzburg-Landau Equations

While Pippard was developing the concept of the coherence length, Ginzburg and Landau (1950) suggested a phenomenological theory of superconductors which leads to a similar idea. Their aim was to improve on the London theory which did not permit a calculation of the normal-superconducting surface energy, nor correctly describe the destruction of superconductivity by a magnetic field and current.

According to the Landau-Lifshitz (1958) theory of second order phase transitions, the free energy difference of the phases can be expressed as an even power series of an 'order parameter' of the more ordered phase. Ginzburg and Landau assumed that for a superconductor near T_c only the first two terms of the expansion needed to be considered, and hence in zero-field one could write :

$$G_s = G_n + \alpha|\psi|^2 + \beta/2|\psi|^4$$

where ψ is the superconducting order parameter, α and β are two variable parameters, and G is the Gibbs free energy per unit volume. If G_s is required to be a minimum in zero field then $\partial G_s/\partial(|\psi|^2) = 0$ and

2.3.1. $$|\psi_0|^2 = -\alpha/\beta$$

Since $G_n(o) - G_s(o) = \mu_o H_c^2/2$ (Equation 2.2.2.)

this gives :

2.3.2. $$\mu_o \frac{H_c^2}{2} = \frac{\alpha^2}{2\beta}$$

In a magnetic field there will be a contribution to the free energy of $\mu_o H^2/2$ from the field, and a kinetic energy contribution where variations in ψ take place which Ginzburg and Landau supposed to be

$$\frac{1}{2m} |\psi(-i\hbar\nabla - 2e\underline{A})^2 \psi^*|$$

Where curl $\underline{A} = \underline{B}$, and the current carriers are assumed to be electron pairs of charge 2e. They then added these terms, and by minimizing the resulting expression for the energy with respect to both $\underline{A}$ and ψ^* obtained the two Ginzburg Landau equations :

2.3.3. $$\alpha\psi + \beta|\psi|^2\psi + \frac{1}{2m}(-i\hbar\nabla - 2e\underline{A})^2 \psi = 0$$

2.3.4. $$\underline{J} = -\frac{e\hbar}{im}(\psi^*\nabla\psi - \psi\nabla\psi^*) - \frac{4e^2}{m}|\psi|^2\underline{A}$$

and also the Ginzburg-Landau boundary condition

2.3.5. $$(-i\hbar\nabla - 2e\underline{A})_n \psi = 0$$

Where n denotes the component normal to the boundary.

These equations describe the time-independent, electromagnetic behaviour of a superconductor and Gorkov (1959) showed that, sufficiently near to T_c, they can be derived from the microscopic BCS theory. In practice they appear to apply reasonably well at all temperatures.

The equations can be written so as to contain both ξ and λ as parameters. For a semi-infinite slab occupying $o < x < \infty$ where there are no fields or currents, equation 2.3.3. may be written :

2.3.6. $$-\frac{\hbar^2}{2m}\frac{d^2\psi}{dx^2} + \alpha\psi + \beta\psi^3 = 0$$

If $\psi(x)$ is non-uniform we may substitute

$$\psi = \psi_o f(x) \quad \text{and} \quad \xi^2(T) = \hbar^2/2m\alpha$$

into 2.3.6. and obtain the equation

$$-\xi^2 \frac{d^2f}{dx^2} - f + f^3 = 0$$

which shows that changes in f and hence ψ will take place over distances of order ξ.

In weak magnetic fields $|\psi|^2 \approx |\psi_0|^2$ and 2.3.4. may be written

$$\underline{J} = -\frac{4e^2}{m} |\psi_0|^2 \underline{A}$$

Taking the curl of both sides we obtain :

2.3.7. $$-\underline{B} = \frac{m}{4e^2|\psi_0|^2} \text{ curl } \underline{J}$$

Provided that $|\psi_0|^2$ is interpreted as the number of superconducting electrons n_s, this is identical to the London equation 2.2.6. for particles of charge 2e. Although Ginzburg and Landau derived Equation 2.3.7. in the same way as this and defined a penetration depth λ_0 by

$$\lambda_0 = \left(\frac{m}{4\mu_0 e^2|\psi_0|^2}\right)^{\frac{1}{2}}$$

they did not explicity define the parameter ξ. They did however define another parameter, χ, now usually denoted by κ and known as the Ginzburg-Landau parameter, by the equation

2.3.8. $$\kappa = \frac{m}{e\hbar} \left(\frac{\beta}{2\mu_0}\right)^{\frac{1}{2}}$$

They pointed out that experimentally the ratio λ_0/κ (which using Equation 2.3.1. can be shown to be equal to ξ as defined by $\xi^2 = \hbar^2/2m\alpha$) was of the order of $10\lambda_0$, and that this was the thickness of the normal-superconducting surface region. The significance of this conclusion, and the parameter κ will be discussed in the next section.

2.4. Type II Superconductors and the Mixed State

The importance of the Ginzburg-Landau equations was not fully recognized until ten years after they were first published. Until this time the behaviour

of superconducting alloys in allowing flux to penetrate at a field lower than that at which superconductivity disappeared, had been associated with the magnetic irreversibility of such materials. Both effects were supposed to arise from inhomogeneities and defects in the samples. The discovery that Nb_3Sn remained superconducting up to a field of 8 Teslas which was almost one hundred times greater than that at which complete diamagnetism ceased, presented a major problem. Goodman (1961), however, pointed out that a superconductor could reduce its free energy by allowing flux to penetrate, because in that case the magnetization, M, which appears in equation 2.2.1. would be less than 1. London (1950) had reached a similar conclusion. He showed that a superconductor which did exclude flux up to H_c must have a positive surface energy so that the creation of extra normal-superconducting surfaces would, in fact, increase the free energy. This can be seen by considering Fig. 2.3. which shows the variation of the super electron order parameter, ψ, and the magnetic field, H, at the surface of a superconductor. The field penetrates a distance λ, and the free energy per unit surface area is therefore reduced by $\lambda\mu_0 H^2/2$. The order parameter changes over a coherence length, ξ, and the loss of superconducting volume increases the free energy per unit surface area by $\xi\mu_0 H_c^2/2$. Therefore, the surface energy per unit area α_{ns} is approximately $\frac{1}{2}\mu_0(\xi H_c^2 - \lambda H^2)$. Pippard (1953) showed that for pure materials $\xi > \lambda$, and α_{ns} is therefore positive at all fields. However in alloys the mean free path and the coherence length are small, while the penetration depth is large. Goodman suggested that, in this case, ξ might become smaller than λ, α_{ns} would then be negative at a sufficiently high field. Homogeneous alloy specimens might therefore exhibit a new type of magnetic behaviour, characteristic of negative surface energy superconductors, in which superconductivity remained to fields well above the thermodynamic critical field H_c defined by Equation 2.2.2.

Goodman's theory drew attention to a paper written four years earlier by Abrikosov (1957). In it Abrikosov pointed out that the Ginzburg-Landau equations lead to the conclusion that there are two types

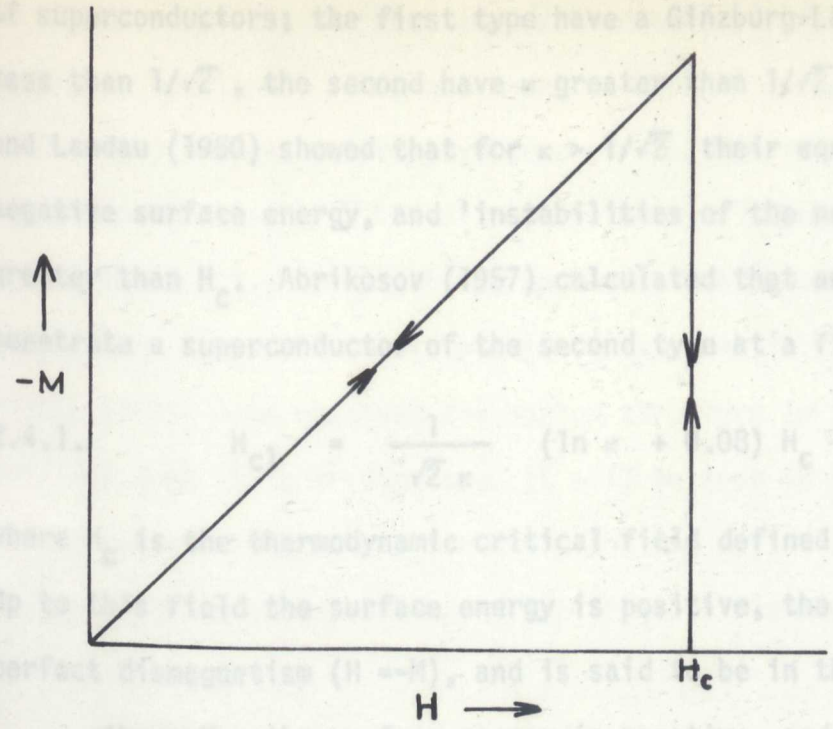

FIGURE 2.1

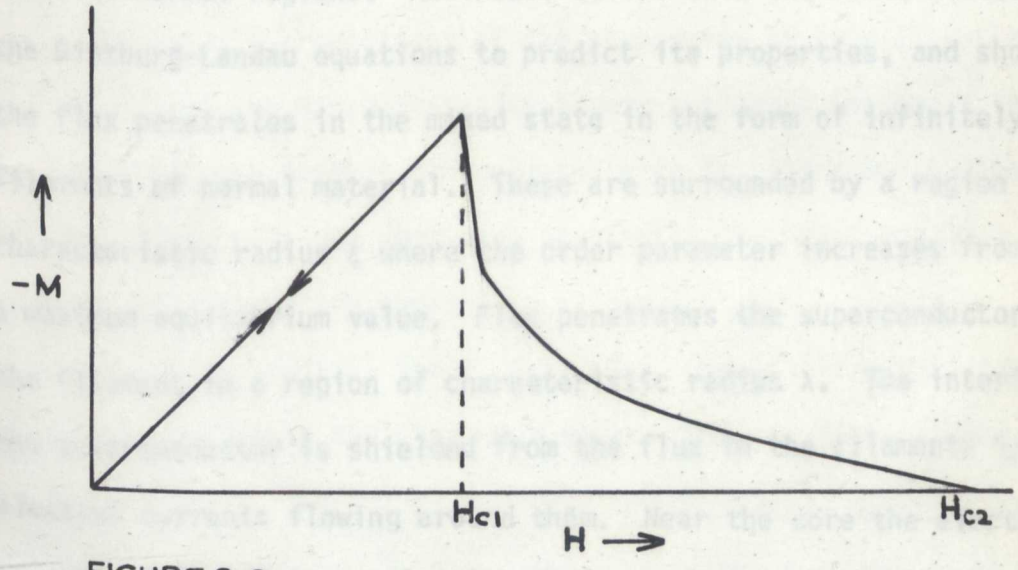

FIGURE 2.2

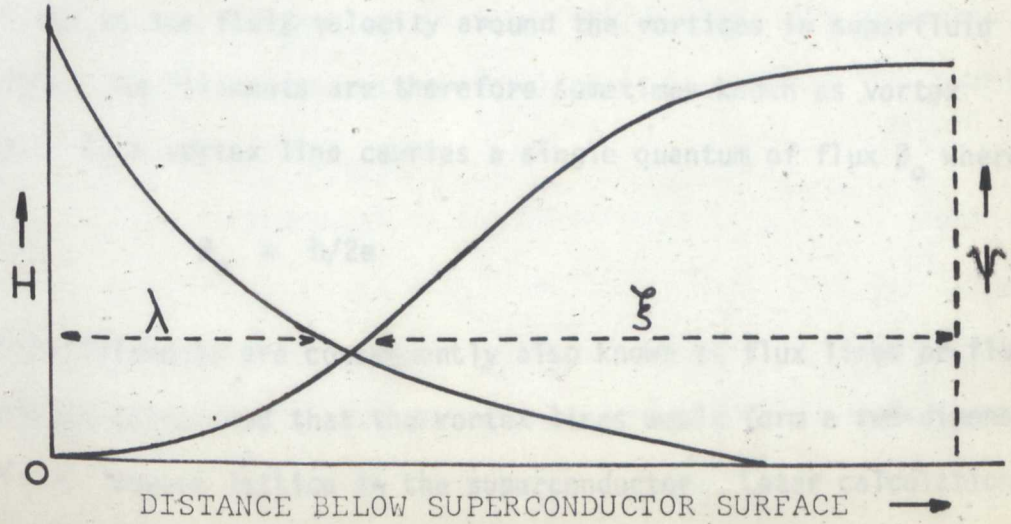

FIGURE 2.3

of superconductors; the first type have a Ginzburg-Landau parameter κ less than $1/\sqrt{2}$, the second have κ greater than $1/\sqrt{2}$. Moreover, Ginzburg and Landau (1950) showed that for $\kappa > 1/\sqrt{2}$ their equations lead to a negative surface energy, and 'instabilities of the normal phase' in fields greater than H_c. Abrikosov (1957) calculated that an applied field should penetrate a superconductor of the second type at a field H_{c1} given by

2.4.1. $$H_{c1} = \frac{1}{\sqrt{2}\,\kappa} (\ln \kappa + 0.08)\, H_c \qquad (\kappa >> 1)$$

where H_c is the thermodynamic critical field defined by 2.2.2. Up to this field the surface energy is positive, the material exhibits perfect diamagnetism ($H = -M$), and is said to be in the Meissner state.

Above H_{c1} the surface energy is negative, and the superconductor contains normal regions. Abrikosov called this the mixed state. He used the Ginzburg-Landau equations to predict its properties, and showed that the flux penetrates in the mixed state in the form of infinitely thin filaments of normal material. These are surrounded by a region of characteristic radius ξ where the order parameter increases from zero to a maximum equilibrium value. Flux penetrates the superconductor around the filament in a region of characteristic radius λ. The interior of the superconductor is shielded from the flux in the filaments by super-electron currents flowing around them. Near the core the electron velocity falls off inversely with distance from the filament in the same way as the fluid velocity around the vortices in superfluid helium. The filaments are therefore sometimes known as vortex lines. Each vortex line carries a single quantum of flux ϕ_0 where

$$\phi_0 = h/2e$$

and the filaments are consequently also known as flux lines or fluxoids. Abrikosov calculated that the vortex lines would form a two-dimensional periodic, square lattice in the superconductor. Later calculations (Matricon 1964, Kleiner et al 1964) showed that under most conditions a triangular lattice is more stable than a square one.

The existence of 'negative surface energy' superconductors is now adequately confirmed. They are known as type II superconductors. French et al (1967) amongst others have demonstrated the existence of materials with κ greater than $1/\sqrt{2}$, first penetrated by flux at a field H_{c1} given by Equation 2.4.1., for which the magnetization curves are completely reversible. A typical reversible curve is shown in Fig. 2.2. Essmann and Träuble (1967) have observed the vortex structure in the mixed state, and confirmed that it is triangular. It will be seen in Chapter 3 that interactions between this vortex structure and the crystalline lattice provide the basis for an understanding of the irreversible magnetic properties of superconductors.

2.5. The Upper Critical Fields

Abrikosov's predictions of the properties of type II superconductors on the basis of the Ginzburg-Landau theory confirmed its great importance. Its usefulness was further demonstrated when St. James and DeGennes (1963) used the Ginzburg-Landau equations to predict the existence of a phenomenon now known as the surface sheath.

The upper critical field, H_{c2}, of a type II superconductor may be determined by solving the Ginzburg-Landau equations in high fields. Near the critical field ψ will be small and terms in $|\psi|^2$ can be ignored. Equations 2.3.3. and 2.3.4. then become

2.5.1. $$1/2m(-i\hbar\nabla - 2e\underline{A})^2\psi = -\alpha\psi$$

2.5.2. $$\underline{J} = 0$$

Equation 2.5.1. is identical to the Schrodinger equation of a particle of charge 2e and mass m in a uniform magnetic field $\underline{B}$ = curl $\underline{A}$. Landau and Lifshitz (1958) show that, in an infinite medium, this equation predicts that the particles will move in circular orbits of frequency $\omega_c = 2eB/m$ with velocity v. The energy of a particle has the form $\frac{1}{2}mv^2 + (n + 1/2)\hbar\omega_c$, and the lowest energy state corresponding to v = n = 0 gives :

2.5.3. $$-\alpha = \frac{e\hbar B}{m}$$

Other energy states give lower values for B consequently 2.5.3. gives the upper critical field i.e.

$$H_{c2} = \frac{\alpha m}{\mu_o e\hbar}$$

Using Equations 2.3.2. and 2.3.8. this may be rewritten as

2.5.4. $$H_{c2} = \kappa\sqrt{2}\ H_c$$

St. James and DeGennes showed that the above solution also satisfied the boundary condition (Equation 2.3.5.) in the case of a semi-infinite slab with the field normal to the surface. However, when the field was parallel to the surface the boundary condition was not satisfied for a region of order ξ below the surface. The correct solution in this case led to a higher surface critical field H_{c3} given by

2.5.5. $$H_{c3} = 2.4\ \kappa\ H_c = 1.7\ H_{c2}$$

The prediction that a region of thickness ξ at the surface of a sample would remain superconducting up to fields greater than H_{c2} applied parallel to the surface was rapidly confirmed by a number of workers e.g. Bon Mardion et al (1964). Since H_{c3} will be greater than H_c for $\kappa > 0.417$, some Type I superconductors also exhibit surface superconductivity. The phenomenon is usually known as the DeGennes surface sheath.

2.6. Summary of Magnetic Properties

The magnetic properties of superconductors described by the Ginzburg-Landau theory may be summarized as follows.

For all superconductors :-

There is a thermodynamic critical field H_c defined by :

$$\mu_o H_c^{\,2}/2 = \mu_o \int_0^{H_T} M\,dH$$

where H_T is the maximum field at which superconductivity exists.

Superconductors may be divided into two types depending on their Ginzburg-Landau parameter κ.

For Type I superconductors :

$\kappa < 1/\sqrt{2}$, the surface energy is positive, $\lambda < \xi$ and flux is excluded from an ideal sample up to H_c.

For Type I and II superconductors :

When $\kappa > 0.417$ the surface remains superconducting in fields parallel to the surface up to H_{c3} given by :

$$H_{c3} = 2.4\,\kappa\,H_c$$

For Type II superconductors :

$\kappa > 1/\sqrt{2}$, the surface energy becomes negative and flux penetrates below H_c at a field H_{c1} given by

$$H_{c1} = \frac{1}{\sqrt{2}\,\kappa}\,(\ln\kappa + 0.08)\,H_c \qquad (\kappa \gg 1)$$

Flux penetrates in the form of quantized flux lines and the bulk material remains superconducting up to a field H_{c2} given by

$$H_{c2} = \sqrt{2}\,\kappa\,H_c$$

3. IRREVERSIBLE PROPERTIES

3.1. Magnetization Curves and Critical Currents

The magnetization curve of a real superconductor will, in general, be irreversible. The degree of irreversibility will be greater in less homogeneous materials. This is illustrated by Figure 3.1. which shows the magnetization curves of two niobium samples : one well-annealed and polished, and the other cold worked and rough. Some flux remains trapped even in the annealed sample once the field exceeds H_{c1}. The reverse magnetization curve shows that the exit of flux from the sample is impeded. The magnetization curve of the cold-worked sample is almost completely irreversible, with little flux leaving the sample when the field is reduced to zero. Flux penetration is also impeded in this sample. Large scale penetration is delayed to over 240 kA m^{-1} (3000 Oe) even though H_{c1} is about 110 kA m^{-1} (1400 Oe).

The flux distribution within an irreversible sample is difficult to examine directly, but considerable understanding has been gained by observation of the distribution at surfaces perpendicular to the applied fields. Various techniques have been developed to do this. In the powder pattern method the surface is either covered with ferromagnetic particles which are attracted to the normal, flux-carrying regions or superconducting particles which are repelled from the normal areas. Essmann and Träuble (1967) have developed a sophisticated version of this technique. They decorate the exit points of flux lines with ferromagnetic particles about 10 nm in diameter, produced by evaporating iron over the surface at helium temperatures. The particle distribution may then be examined by either electron or optical microscopy using a carbon replica technique. Other methods utilize the change produced by a magnetic field in some physical parameter of a material. For example, DeSorbo and Healey (1964) observed the rotation of the plane of polarization of incident light produced in a sheet of paramagnetic cerium phosphate layed on the surface of a specimen. Examination of the reflected

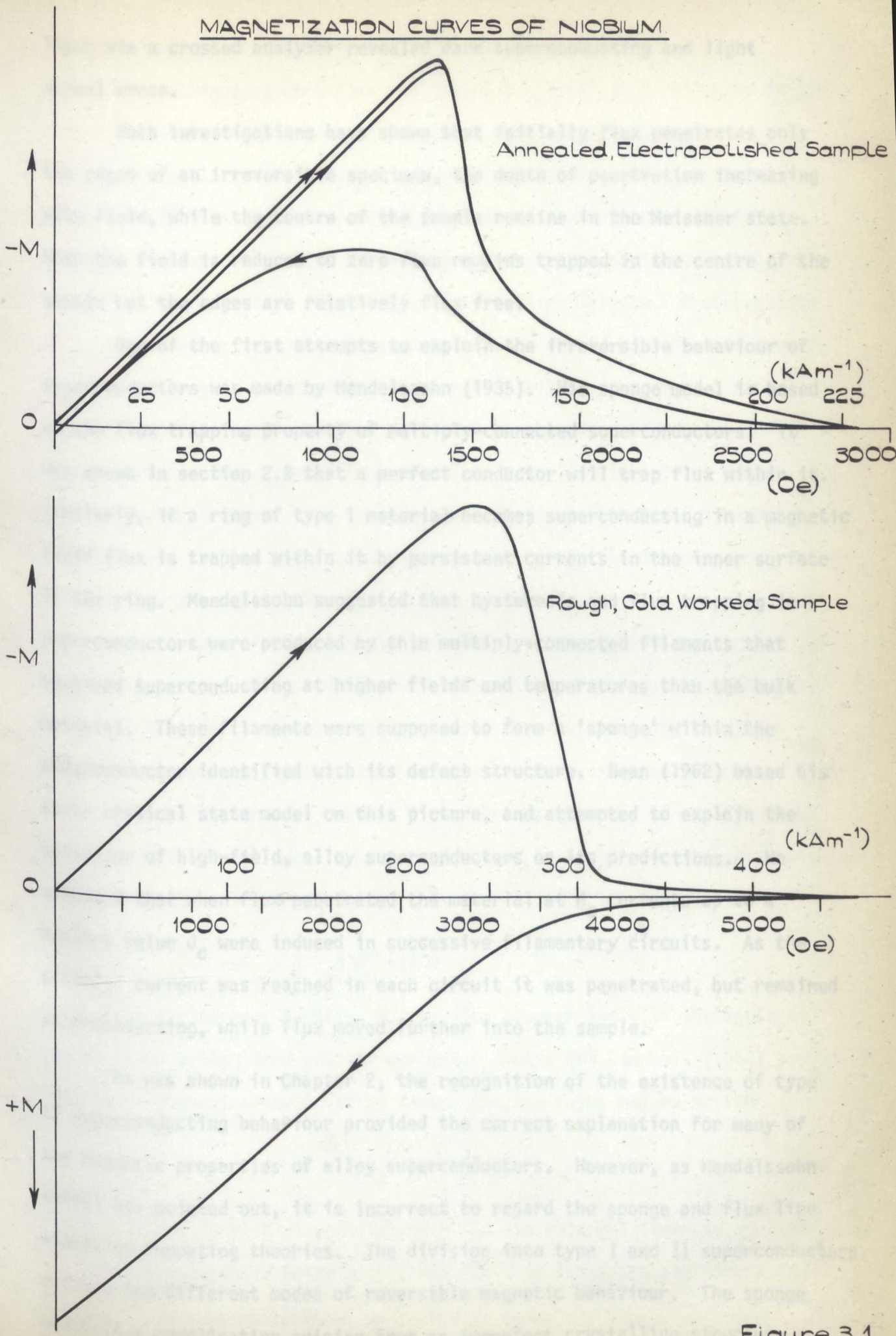
MAGNETIZATION CURVES OF NIOBIUM
Annealed, Electropolished Sample
-M
0
25
50
100
150
200
225
(kAm⁻¹)
500
1000
1500
2000
2500
3000
(Oe)
Rough, Cold Worked Sample
-M
0
100
200
300
400
(kAm⁻¹)
1000
2000
3000
4000
5000
(Oe)
+M

Figure 3.1

light via a crossed analyser revealed dark superconducting and light normal areas.

Such investigations have shown that initially flux penetrates only the edges of an irreversible specimen, the depth of penetration increasing with field, while the centre of the sample remains in the Meissner state. When the field is reduced to zero flux remains trapped in the centre of the sample but the edges are relatively flux free.

One of the first attempts to explain the irreversible behaviour of superconductors was made by Mendelssohn (1935). His sponge model is based on the flux trapping property of multiply-connected superconductors. It was shown in section 2.2 that a perfect conductor will trap flux within it. Similarly, if a ring of type 1 material becomes superconducting in a magnetic field flux is trapped within it by persistent currents in the inner surface of the ring. Mendelssohn suggested that hysteresis and flux trapping in superconductors were produced by thin multiply-connected filaments that remained superconducting at higher fields and temperatures than the bulk material. These filaments were supposed to form a 'sponge' within the superconductor identified with its defect structure. Bean (1962) based his early critical state model on this picture, and attempted to explain the behaviour of high-field, alloy superconductors on its predictions. He supposed that when flux penetrated the material at H_c currents up to a maximum value J_c were induced in successive filamentary circuits. As the critical current was reached in each circuit it was penetrated, but remained superconducting, while flux moved further into the sample.

As was shown in Chapter 2, the recognition of the existence of type II superconducting behaviour provided the correct explanation for many of the magnetic properties of alloy superconductors. However, as Mendelssohn (1964) has pointed out, it is incorrect to regard the sponge and flux line models as competing theories. The division into type I and II superconductors defines two different modes of reversible magnetic behaviour. The sponge model is a complication arising from an imperfect crystalline structure

which may produce irreversible behaviour in either type.

The realization that flux penetrated a type II superconductor in the form of flux lines led a number of authors (see section 3.2.) to suggest that these small flux units might interact more readily with specimen inhomogeneities than the large, normal regions of the intermediate state. Magnetic irreversibility and hysteresis could then be explained by the 'trapping' of individual flux lines at crystalline defects. A consequence of this picture is that type II superconductors should be more sensitive to structural changes, and show greater irreversibility, than type I materials. Livingston (1964) confirmed that Pb-Cd alloys showed such an increased hysteresis when they changed from type I to type II materials at higher cadmium concentrations. The trapping of individual flux lines is now usually known as flux pinning to distinguish it from the trapping produced by multiply-connected circuits.

The concept of flux pinning has been introduced by discussion of the magnetic behaviour of superconductors. The high current carrying capacity of the hard, type II superconductors in the mixed state is an equally important consequence of the same phenomenon. Rose-Innes and Rhoderick (1969) show that when a transport current flows through an array of straight flux lines each line experiences a Lorentz force, F_L per unit length, perpendicular to the current, which is given by

$$F_L = J \phi_o \sin \theta$$

where J is the current density, ϕ_o the flux quantum and θ is the angle between the vortex lines and the current. Evetts and Campbell (1966) proved that for a general array in three dimensions the force may be written

$$\underline{F_L} = - \phi_o \wedge \text{curl } \underline{H}\ (\underline{B})$$

where $\underline{B}$ is the local flux density and $\underline{H}\ (\underline{B})$ the external field in equilibrium with $\underline{B}$ in a reversible material. Since the flux lines are stationary the Lorentz force must be balanced by a pinning force, F_p. Cape and Silvera (1968), amongst others, have found that when flux lines are freed from the pinning

forces their motion produces a voltage across the sample. Bardeen and Stephen (1965) have shown that the flux-flow resistance producing this voltage arises from viscous drag. Hence, a superconductor in the mixed state can carry significant lossless currents only if pinning prevents the motion of flux lines.

Two other irreversible phenomena arise from the pinning of flux, namely flux creep and flux jumping. Flux creep consists of a slow variation in time of the flux distribution in the mixed state in the absence of a transport current. It was first observed by Kim et al (1962), who noticed a logarithmic decay in persistent currents and a strong temperature dependence of the critical current. Anderson (1962) explained their results by supposing that flux lines could be freed from their pinning sites by thermal activation. However, Wade (1969) has presented results which indicate that thermal activation may not be the cause of flux creep. Flux jumping is the discontinuous motion of flux in a superconductor. In changing magnetic fields flux lines become depinned from their pinning sites and these micro flux jumps produce local heating. Under certain circumstances this heating may produce a sufficient change in local superconducting properties to nucleate a large flux jump. This in turn may produce a normal region in the superconductor which, if an alternative current path is not available, may destroy the conductor. The experimental work on flux jumping has been reviewed by Thomas (1969), and the conditions under which large flux jumps may occur are discussed by Wilson et al (1969).

Considerable efforts have been made over the last eight years to understand the irreversible properties of superconductors. Although this has occurred partly because of theoretical interest in the interactions between flux lines and crystalline defects, the major effort has resulted from the need to produce commercial materials with predictable superconducting properties. It has been important to improve the flux pinning and hence the critical current while, at the same time, reducing the possibility of flux jumps destroying superconducting devices. The work on irreversible behaviour

has been reviewed by Thomas (1969). The effects of crystalline structure on the electro-magnetic properties of superconductors has been discussed by Livingston and Schadler (1964) and van Gurp and van Ooijen (1966).

The a.c. losses exhibited by superconductors at low frequencies are a result of their irreversible magnetic behaviour. Consequently, a knowledge of flux pinning and its effects on the magnetic properties is required to understand the loss mechanisms. The interactions between flux lines and specimen inhomogeneities are briefly reviewed in sections 3.2. and 3.3. Section 3.4. contains a description of some of the models for the irreversible behaviour and hysteresis which have been developed by various authors. The way in which these models may be used to calculate a.c. losses is described both in section 3.4. and section 4.4.

3.2. Flux Pinning

The study of flux pinning mechanisms has proved difficult. Experimentally, the isolation of different defects presents problems, theoretically, exact calculations are complex. The first estimate of the magnitude of the pinning energy was made by Anderson (1962). He showed that the maximum free energy barrier, $\Delta G_{max} = (\mu_o H_c^2/2)d^3$ where d^3 is the volume of pinned flux. And suggested that the pinning exerted by a single dislocation of radius r might be proportional to r^2/d^2. Friedel et al (1963) and Silcox and Rollins (1963) considered the pinning force exerted on a flux line by a void in the superconductor, suggesting that such voids might appear in incompletely sintered Nb_3Sn. They showed that the interaction force is $(H_{c1}\phi_o 1nd/\lambda)/M$ where d is the distance between flux lines and M is the number of flux lines pinned at one void. For most effective pinning d should be of the same order as the radius of the void and M equal to 1, when the pinning force for niobium is of order 10^{-10} N.

It seems unlikely that voids are responsible for pinning in the majority of materials, but Livingston (1964) has pointed out that normal, second-phase precipitates are rather similar to voids. He measured the magnetization curves of a ternary Pb-In-Sn alloy and showed that, for a constant volume fraction of

precipitate, the hysteresis decreased as the particle size increased. He interpreted his results in terms of the void model of Friedel et al. Campbell et al (1968) investigated the effects of normal Bi precipitates in Pb-Bi alloys, and also observed that irreversibility decreased as the particle size increased. However, they found that the pinning force was directly proportional to the area of phase boundary, and used a 'surface barrier' model (Bean and Livingston 1964) to develop an expression for the pinning force namely

$$F_p = \frac{\phi_o}{\lambda} M(\text{Rev.}) \approx 10^{-4}\ \text{Nm}^{-1}$$

where M(rev.) is the Abrikosov magnetization of the reversible matrix at a given induction, B. They showed that this expression accounted for the dependence of the magnetization and critical current on field in their specimens, and gave qualitative agreement (within an order of magnitude) with their results.

Irreversibility and hysteresis are also observed (Livingston 1964, Narlikar and Dew-Hughes 1964) in single phase alloys and elements. Pinning in these materials may be attributed to the effects of point defects (vacancies and interstitial impurities), dislocations and grain boundaries. A number of calculations of the pinning force have been made for the comparatively simple case of the interaction between a single dislocation and a flux line. Webb (1963) calculated the force between a flux line and the stress field produced by a perpendicular screw dislocation. He showed that the force was repulsive, and was maximum for a forest of dislocations at a density of $10^{14}\ m^{-2}$. In this case the force per unit length is of order $10^{-6}\ N\ m^{-1}$. Kramer and Bauer (1967) performed a similar calculation for an edge dislocation parallel to the flux line and showed that, in this case, the force was attractive. These calculations did not take into account the effect of neighbouring flux lines on the interaction energy between a defect and a flux line. Labusch (1968) and Miyahara et al (1968) showed that when this effect is included the interaction force is considerably reduced. Measurements have been made by Nembach (1966) of the pinning forces in a torsion-deformed, niobium single crystal containing a homogeneous array of screw dislocations perpendicular to the flux lines. He found that for a dislocation density of about $10^{14}\ m^{-2}$ the

force on a unit length of flux line was 10^{-7} Nm^{-1}. Freyhardt (1969) repeated these measurements using an improved technique, and showed that the correct pinning force was of order 10^{-12} N, i.e. for a dislocation density of 10^{14} m^{-2} about 10^{-5} N m^{-1}. This value is ten times larger than the force calculated by Webb (1963).

While there is some evidence that isolated point defects and dislocations can pin flux, many experiments indicate that extended defects play a more significant role. DeSorbo (1963) found that the magnetization curves of niobium containing oxygen and carbon were fairly reversible up to the solubility limit of these impurities. He concluded that the subsequent irreversibility was produced by second phase precipitates. Kernohan and Sekula (1967) found that neutron irradiation only produced large irreversibility at dosages sufficient to create dislocation loops within the sample. Narlikar and Dew-Hughes (1964 and 1966) measured the zero-field, trapped flux in their deformed niobium and niobium alloy samples and found that it increased most markedly at deformations large enough to produce dislocation tangles and cells. They suggested (Narlikar and Dew-Hughes 1964) that the pinning was due to local variations in κ at the cell walls. However, they have also suggested (Narlikar and Dew-Hughes 1966) that the pinning is produced in the cell walls by the same surface barrier proposed by Campbell et al (1968) for precipitate pinning. Whichever explanation is correct, it seems clear that a non-uniform distribution of dislocations is a strong source of pinning.

The surface-barrier model of Bean and Livingston (1964) used by Campbell et al (1968) to calculate the pinning force exerted by a phase-boundary was originally formulated as a surface pinning mechanism. The role of surfaces in pinning, which has been the subject of some controversy, will be discussed in the next section.

3.3. Surface Pinning

Bean and Livingston developed their surface barrier model to explain the hysteresis observed near H_{c1} in otherwise reversible samples. When a

flux line approaches a surface the shielding currents are distorted so that the current normal to the surface remains at zero. The effects of this distortion may be allowed for by adding an equal image flux line of opposite sign outside the surface. The force between the flux line and the surface then consists of an attraction between the flux line and its image, and a repulsion between the field of the flux line and the external field within the penetration depth. A similar situation exists for a flux line entering the superconductor from outside. Bean and Livingston showed that the net effect of these two terms is a repulsive force near the surface at fields above H_{c1}. For a material with a κ of 10 this barrier to penetration exists up to a field H_s equal to twice H_{c1}. There is a barrier to the exit of flux at all fields.

Campbell et al (1968) extended the calculation to an array of flux lines near a surface. They showed that this surface pinning could account for all the hysteresis they observed in a reversible, single phase Pb-Bi alloy. Lowell (1969) also performed this type of calculation. He measured the voltage across a semicylindrical sample in which a field was applied perpendicular to the axis, and either an electric or thermal current flowed parallel to the axis. He found that the critical current (i.e. that at which a voltage first appeared) had a strong maximum where the field was parallel to the plane surface of the semicylinder, and explained his results in terms of the Bean-Livingston barrier.

The discovery (Sandiford and Schweitzer 1964) that currents in the DeGennes surface sheath could produce hysteretic magnetization loops above H_{c2}, led Fink (1965) and Park (1965) to propose that mixed state hysteresis could be produced by similar currents flowing below H_{c2}. Both authors showed that suitable solutions to the Ginzburg-Landau equations existed below H_{c2}, and they, and earlier Abrikosov (1964), calculated the maximum current the sheath could carry. Barnes and Fink (1966) reported that mixed-state hysteresis was reduced by plating the surface with a normal metal and suggested that this was best explained in terms of DeGennes currents.

Hart and Swartz (1967) found that the maximum lossless (i.e. critical) current that thin films could support in the mixed state increased if the sample surfaces were roughened. They rejected both the Bean-Livingston barrier and the DeGennes surface current as explanations of their results because these both predict a decreased critical current (or hysteresis) for a rough surface. They proposed instead a 'flux-spot' pinning model. In this, they call the surface exit point of a flux line a flux spot, and assume that, because of the currents circulating around it, there will be a dipole moment $\underline{\mu}$ associated with it directed normally to the local surface. A term $-\underline{\mu}.\underline{H}$ then appears in the free energy of the flux line. For a surface everywhere parallel to an applied field $\underline{\mu}.\underline{H}$ is zero. For a rough surface $\underline{\mu}.\underline{H}$ will vary along the sample according to the relative orientation of the local field and surface. Flux lines will be pinned where their free energy is minimum, i.e. where $|\underline{\mu}.\underline{H}|$ is maximum. Hence rough surfaces will provide greater pinning. Hart and Swartz assume that the critical current for their films is reached when flux lines begin to move through the sample. This will not occur until the pinning force has been exceeded. The critical current below H_{c2} will, therefore, be higher in rough films. Increased critical currents have also been observed in roughened cylindrical samples by Jones and Rose-Innes (1966). Both Hart and Swartz (1966) and Lowell (1969) have pointed out that, although the Fink and Park calculations give the maximum current which can flow before the sheath reverts to the normal state, the mixed state, surface critical current is probably reached (i.e. a voltage appears) when flux lines begin to cross the surface.

We can therefore distinguish four sources of currents which may flow in addition to the Abrikosov magnetization current and will support hysteresis. These are :

(i) The Bean-Livingston surface barrier

(ii) The DeGennes surface sheath

(iii) Flux spot pinning

(iv) Defect pinning

It is interesting to note that Campbell et al (1968) suggested that the first two of these may be different ways of describing the same phenomenon. Although defect pinning (iv) is not a specifically surface phenomenon, it has been included because the high defect densities which can be produced near the surface of otherwise reversible materials can give rise to large pseudo surface currents (Kwasnitza and Winkler 1969).

In summary, experimental evidence exists that flux pinning may be produced by a variety of crystalline inhomogeneities. While it is generally difficult to isolate the roles played by different types of defects, it is clear that inhomogeneities such as second-phase precipitates, extended defects and surfaces are most effective in pinning. Because of the complexity of this type of defect, expressions for the pinning force have been derived only in isolated cases. Fortunately, satisfactory models of the effects of pinning on the magnetic properties of superconductors have been developed without detailed knowledge of the pinning mechanisms. Some of these models will be described in the next section.

3.4. Models

The work of DeSorbo and Healey (section 3.1.) and others has shown that the flux distribution in an irreversible superconductor is inhomogeneous i.e. that flux gradients exist within the superconductor. To satisfy the Maxwell equation

$$\text{curl } \underline{H} = \underline{J}$$

current must flow wherever there is a gradient. In terms of the slab of superconductor shown in Figure 3.2.1., the variation in the field H_z as it penetrates the superconductor in the x direction requires that a current flows in the y direction whose density J_y is given by

$$dH_z/dx = J_y$$

If flux penetrates in the form of flux lines the flux gradient must correspond to a variation in the flux line density, N. There will be a Lorentz force

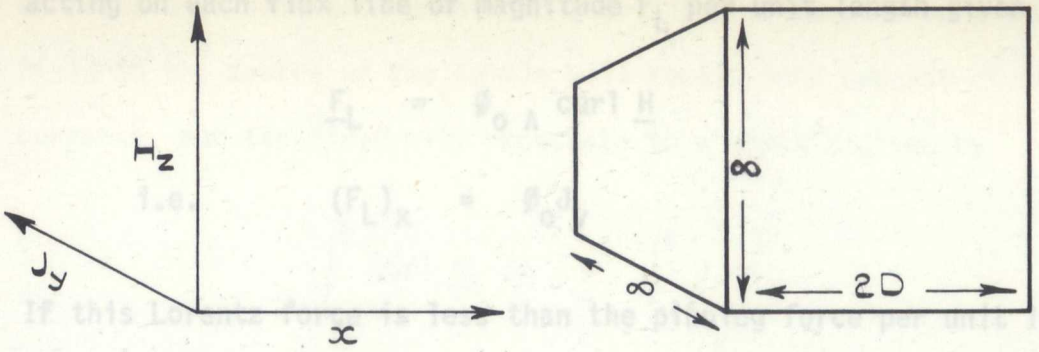

Figure 3.2.1. SLAB DIMENSIONS AND CO-ORDINATES.

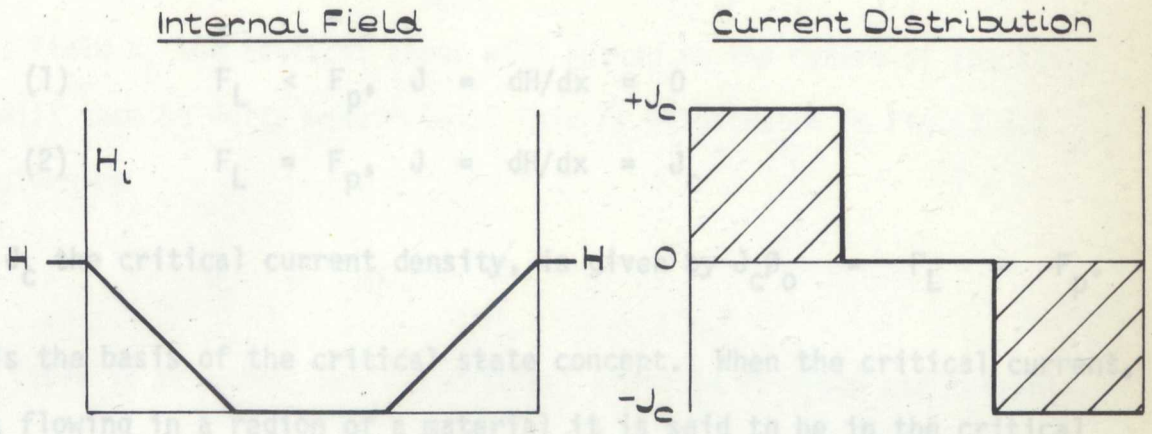

Figure 3.2.2. AT FIELD H.

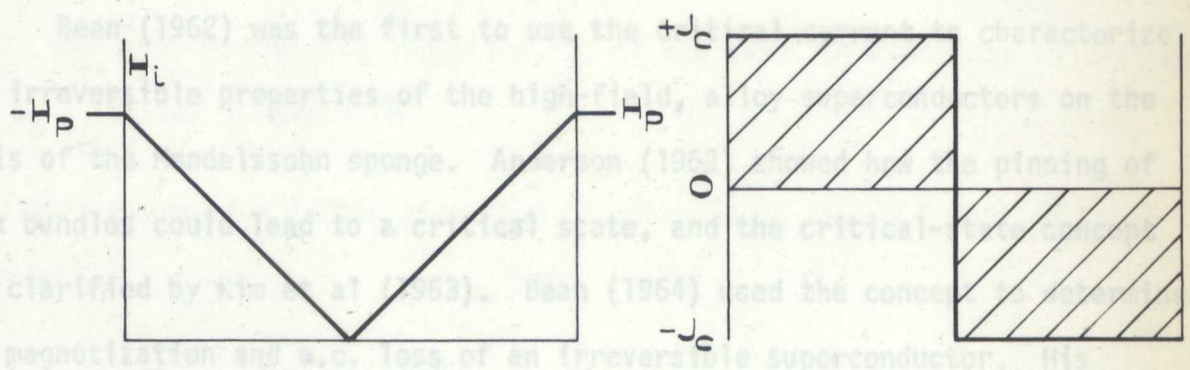

Figure 3.2.3. AT H_p.

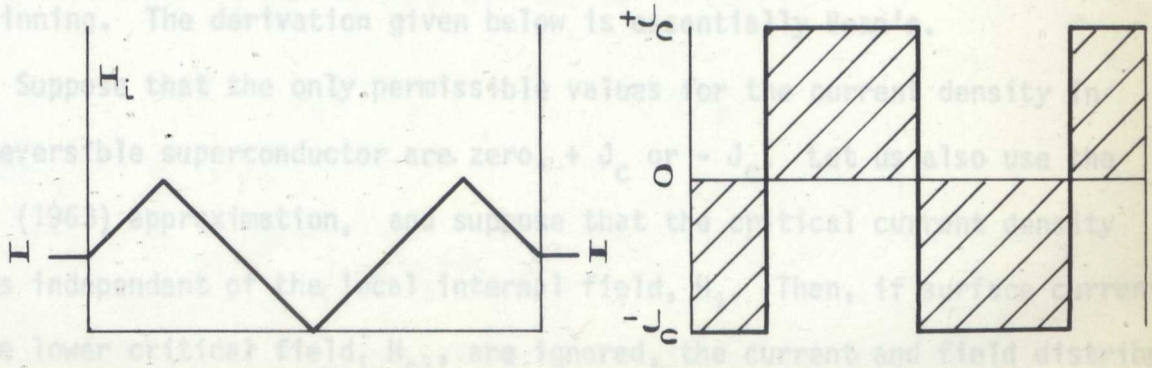

Figure 3.2.4. DECREASING FIELD H.

Figure 3.2.

acting on each flux line of magnitude F_L per unit length given by

$$\underline{F_L} = \phi_o \wedge \text{curl } \underline{H}$$

$$\text{i.e.} \qquad (F_L)_x = \phi_o J_y$$

If this Lorentz force is less than the pinning force per unit length, F_p, no flux can penetrate. If F_L is greater than F_p flux lines will move until an equilibrium flux distribution where $F_L = F_p$ is reached. Therefore the only possible static conditions are :

(1) $\quad F_L < F_p, \quad J = dH/dx = 0$

(2) $\quad F_L = F_p, \quad J = dH/dx = J_c$

Where J_c the critical current density, is given by $J_c \phi_o = F_L = F_p$.

This is the basis of the critical state concept. When the critical current, J_c, is flowing in a region of a material it is said to be in the critical state.

Bean (1962) was the first to use the critical current to characterize the irreversible properties of the high-field, alloy superconductors on the basis of the Mendelssohn sponge. Anderson (1962) showed how the pinning of flux bundles could lead to a critical state, and the critical-state concept was clarified by Kim et al (1963). Bean (1964) used the concept to determine the magnetization and a.c. loss of an irreversible superconductor. His calculation was based on the sponge model, but is equally applicable to flux-line pinning. The derivation given below is essentially Bean's.

Suppose that the only permissible values for the current density in an irreversible superconductor are zero, + J_c or - J_c. Let us also use the London (1963) approximation, and suppose that the critical current density $|J_c|$ is independent of the local internal field, H_i. Then, if surface currents and the lower critical field, H_{c1}, are ignored, the current and field distributions in a slab of the material when a magnetic field, H, is applied will be those shown in Figure 3.2.2. The flux penetration will generate shielding

currents and field gradients, and a critical state will be produced. The field in the centre of the sample will remain zero because of the shielding currents, and the field will penetrate to a depth x given by

$$\int_0^H \text{curl } \underline{H_i}\, \underline{dx} = \int_0^x \underline{J}.\underline{dx}$$

i.e. since we have assumed that constant = $J_c = dH/dx$

3.4.1. $$H = Jx$$

At some field H_p the critical state will extend to the centre of the slab, which will then be fully penetrated. This is illustrated in Fig. 3.2.3. H_p is given by

3.4.2. $$H_p = JD$$

If the field is reversed then the critical state is reversed and currents flow in the opposite direction, the resulting current and field distributions are shown in Figure 3.2.4.

The average magnetic induction, $\overline{B}$, of the superconductor may be defined as $\mu_o \int_o^V H_i\, dv \Big/ \int_o^V dv = \overline{B}$

Using this expression in the situation illustrated in Figure 3.2.2., $\overline{B}$ is given by

$$\overline{B} = \mu_o \frac{H}{2} \frac{x}{D}$$

Using Equations 3.4.1. and 3.4.2., this may be written as

3.4.3a. $$\overline{B} = \mu_o H^2/2H_p \qquad H < H_p$$

while for $H > H_p$

3.4.3b. $$\overline{B} = \mu_o(H - H_p/2)$$

Once the critical state has been set up in a region of the superconductor no changes in field can remove it. Equation 3.4.3. therefore defines the 'virgin' magnetization. The induction at any subsequent field may be calculated on the

same principles. Bean (1964) shows that the hysteresis loop followed by a superconductor between peak applied fields of $\pm H_m$ is given by

$$\overline{B} = \mu_o \left| HH_m/2H_p \pm (H^2 - H_m^2)/4H_p \right| \qquad H_m \leq H_p$$

where the plus sign refers to fields going from $-H_m$ to H_m and the negative sign to fields going from H_m to $-H_m$. The loss per cycle in tracing this magnetization loop can be calculated from

$$W_V = \mu_o \oint_{\text{cycle}} H \, d\overline{B}$$

and Bean shows that for both slabs and cylinders the loss per cycle per unit surface area is given by

3.4.4. $$L = 2 \mu_o H_m^3/3J_c \qquad H_m << H_p$$

The assumption that J_c is independent of H_i corresponds to assuming that the pinning force, F_p, is independent of field, and that the number of pinning centres acting on a single line remains constant. At a given field the number of flux lines per unit area, N, is given by

$$\overline{B} = N\emptyset_o$$

If the external field is 2 Tesla then, since $\emptyset_o = 2 \times 10^{-15}$ Weber, N is equal to 10^{15} lines m^{-2}. If each line only occupies one pinning centre a very high defect density is required to provide sufficient sites. This assumption also leads to Equation 3.4.3b

$$\overline{B} = \mu_o(H - H_p/2)$$

which shows that the superconductor will have a finite magnetization $-H_p/2$ at all fields. Clearly the London approximation is not valid at all fields, and Kim et al (1963) proposed that the experimental critical current data was better fitted by the expression

$$J_c = \alpha/(B + B_o)$$

which is known as the Kim approximation.

Silcox and Rollins (1963) derived the induction B(x) at any point within an irreversible superconductor by using an expression for the pinning force which allowed for the change of flux line density with field. They assumed that for a material containing n voids per unit volume the pinning force exerted by each void remained constant, but that the number of pinning sites associated with a unit length of one flux line, f, was given by :

$$f = n/N = n/|\phi_0 B(x)|$$

The total pinning exerted on one flux line is thus a function of the local induction. They equated their pinning force to the Friedel et al (1964) expression for the Lorentz driving force, and obtained the equation

3.4.5. $$B^2(x) = B^2(o) - \beta x$$

where B(o) is the induction at the surface of the superconductor in equilibrium with the external field and β is a pinning constant related to n. If Equation 3.4.5. is differentiated with respect to x, we obtain the expression

$$2B\frac{dB}{dx} = \text{constant}$$

i.e. $$BJ_c = \text{constant}$$

which is similar to the Kim approximation.

An equivalent expression to Equation 3.4.5. for the Bean-London model may be derived from Equation 3.4.1. i.e.

3.4.6. $$B(x) = B(o) - J_c x$$

Yasukochi et al (1964) assumed a different relationship between the flux line and defect densities for the case of a cold-drawn wire in a perpendicular field, namely :

$$f^2 = (2/\sqrt{3})n_1^2/N$$

where n_1 is the number of pinning filaments per unit cross section of wire produced by the cold working. They showed that the corresponding expression for B(x) is

3.4.7. $$B^{3/2}(x) = B^{3/2}(o) - \alpha x$$

where α is another pinning constant. Clearly equations 3.4.5., 3.4.6. and 3.4.7. are different 'one parameter' expressions for B(x), in which the experimentally determined constants J_c, β and α determine the pinning strength and the different powers of B correspond to different relations between the pinning centres and flux lines.

These critical state models suffer from two difficulties. The first is that the effects of surface currents and H_{c1} are not specifically included, although they can be allowed for by suitable selection of B(o). The second difficulty is that dynamic effects which are important when considering a.c. losses in low pinning materials are not included. The latter problem has been overcome by Irie and Yamafuji (1967) who proposed two equations for the motion of flux in superconductors

$$\underline{F}_L + \underline{F}_p + \underline{F}_V = 0$$

and $$\nabla_\Lambda(\underline{V}_L \Lambda \underline{N}) = \partial \underline{N}/\partial t$$

where $\underline{F}_L$ is the Lorentz force, $\underline{F}_p$ the pinning force, $\underline{F}_V$ the viscous drag (Bardeen and Stephen 1965), $\underline{V}_L$ the flux line velocity and $\underline{N}$ the number density of flux lines defined by $\underline{B} = \underline{N}\,\emptyset_0$. The first of these equations defines a dynamic critical state, and the second is the continuity equation of the flux lines. In the static case, $V_L = 0$ and choosing axes as before the equations become

3.4.8. $$\lambda(x)B^{2-\gamma}(x) = \lambda(o)B^{2-\gamma}(o) - (2-\gamma)\alpha x/2$$

$$dN/dt = 0$$

where $\lambda = \pm 1$ depending on the changes of the applied field, and α and γ are constants determined experimentally from a static magnetization loop.

Equation 3.4.8. is a 'two-parameter' pinning generalization of equations 3.4.5., 3.4.6. and 3.4.7. Irie and Yamafuji point out that values for γ of 1, $\frac{1}{2}$ and 0 correspond to the Bean-London, Yasukochi et al and Rollins and Silcox expressions respectively. Dunn and Hlawiczka (1968) have derived a generalized critical state model which includes the effects of surface currents and H_{c1}. This will be discussed further in section 4.4.

These critical state models and others (e.g. Campbell et al 1968) have been shown to give good agreement with the magnetization curves and critical current versus field relationships of a wide range of irreversible type II superconductors. It would be more satisfactory to be able to calculate the pinning constants directly than to obtain them from magnetization curves. Nevertheless the basic concepts of flux pinning and the critical state have proved extremely useful in investigating irreversibility and a.c. losses in superconductors.

4. A.C. LOSSES

4.1. Introduction

The importance of the a.c. behaviour of superconductors for their technical applications has led to a considerable effort over the past few years in measuring and understanding their a.c. properties. This work has been reviewed by Goodman (1969) and Wipf (1968) who lists over a hundred references pertinent to the subject, 44 of which deal explicitly with a.c. losses.

In discussing the response of superconductors to transient fields it is useful to distinguish between four regions of the peak applied alternating field, H_m. Wipf (1968) defines these as :

Region I : $H_m < H_{C1}$ (or H_c for Type I materials)

Region II : $H_{C1} < H_m < H_p$

Region III : $H_p < H_m < H_{C2}$

Region IV : $H_{C2} < H_m$ (or $H_c < H_m$ for Type II materials)

where H_p is the field at which the sample is completely penetrated.

This chapter contains a discussion of losses in each of these regions. To avoid duplication of Wipf's review we have concentrated on the measurement and theory of losses for $H_m < H_{C1}$. Region II is dealt with less thoroughly, one section is devoted to tracing the growth in theoretical understanding of the losses in that regime. Since our results were obtained mainly in Regions I and II, Regions III and IV are only covered briefly. The chapter is concluded with a description of the specific objects of our research.

The early measurements of losses showed that, at least where $H_m < H_p$, the losses were hysteretic in nature depending only on the peak applied field, and arose mainly at the surface. It is useful therefore to measure losses in terms of the energy loss per cycle which is independent of frequency, and to express them as loss per unit surface area, which is independent of the size

and geometry of the sample. The unit of loss used throughout this thesis is watts per hertz per square metre ($WHz^{-1}\ m^{-2}$) equivalent to joules per cycle per square metre. The term 'dissipation' is used to refer to the energy loss per second, in watts per square metre (Wm^{-2}).

4.2. Measurements in the Meissner State

In the region below H_{C1} in a Type II superconductor or H_C in a Type I material no flux penetrates an ideal sample beyond the penetration depth. Losses due to magnetic hysteresis are therefore zero. Some losses may arise from the motion of normal electrons produced by the fields required to accelerate superconducting electrons within the penetration depth. At low frequencies the dissipation from this source will be negligible. However, a number of workers have reported losses in this regime in both Type I and II materials. Among the first of them were Buchhold and Molenda (1962) who observed losses in both lead and niobium using an adiabatic calorimeter. The dissipation at a fixed field varied linearly with frequency between 0 and 500 Hz. They concluded that the losses were of hysteretic origin. They found that the loss per cycle, L, depended strongly on the peak applied field, H_m, and could be expressed as

4.2.1. $$L = CH_m^n$$

where C and n were constants for a given material, n varying between 2.5 and 7.0. In a low-loss lead sample the loss depended on the field in which the sample was cooled, the presence of the earth's field being sufficient to increase it by a factor of three. Buchhold and Molenda also noted that the loss appeared to depend on the surface properties of the sample.

Buchhold (1963) reported new measurements using an electrical technique (see Chapter 5) which enabled him to observe the flux penetration waveform and to measure hysteresis loops of the flux, ϕ vs H_m. These showed that flux penetrated even in the Meissner state. The waveform was asymmetric for samples cooled in a magnetic field, and the loss depended on the magnetic history of the specimens. In this paper Buchhold also presented a model for

the a.c. loss mechanism which will be discussed in section 4.3.

Bogner and Heinzel (1963) measured the voltage across the ends of bifilar wound coils of niobium and niobium-zirconium (Nb-33% Zr) with alternating currents flowing in them. They confirmed Buchhold and Molenda's findings that the dissipation varied linearly with frequency and that the loss depended strongly on the applied magnetic field. They reported that L was proportional to $H_m^{4.4}$, and that losses were lower in niobium than niobium-zirconium wire.

Further measurements were made on bifilar coils by Rhodes et al (1964). In their experiments the loss was determined by noting the helium boiled off by the coil in a fixed time while a current was flowing. Once again losses were observed in fields below H_{c1} in niobium and below H_c in lead, which depended strongly on the applied field. Values of n in Equation 4.2.1. were found to be between 6.5 and 12.5. Of particular importance was their finding that the loss in an annealed niobium wire at a given self-field was much higher than in as-drawn wires. The value of n also appeared to depend on the degree of cold-work.

Rocher and Septfonds (1967) measured the dissipation in niobium cylinders at peak fields between 0 and 40 kAm^{-1} (500 Oe) for frequencies between 500 and 10,000 hertz using an adiabatic calorimeter. They observed non-linear variations of dissipation with frequency, particularly above 5kHz. These non-linear effects appear to have been more pronounced in outgassed, electropolished samples. The losses obeyed equation 4.2.1. with values of n between 2.5 and 3.5. Loss at a given field was higher before a sample was electropolished i.e. smoothed, and increased when it was outgassed in ultra-high vacuum or cooled in a non-zero, transverse field. The high resistance ratio, outgassed samples which trapped little flux in d.c. measurements were insensitive to the cooling field. The authors suggested that the higher losses in outgassed samples were related to the decrease in critical current produced by this treatment, and arose because a field could penetrate further into their surface protrusions.

Easson and Hlawiczka (1967a, 1967b and 1968) reported that the

loss below H_{C1} in niobium samples was below the sensitivity of their measuring apparatus provided the surface was sufficiently smooth. Linford and Rhodes (1968) showed that the nature of the loss above H_{C1} depended on the bulk metallurgical properties. Loss increased rapidly at H_{C1} in a single crystal, but slowly in a polycrystalline sample. The loss below H_{C1} was lower in the polycrystalline sample. However, Brankin and Rhodes (1969) reported losses in a niobium single crystal with an extremely good surface finish as low as those measured by Easson and Hlawiczka (1968) in mechanically polished samples. A mechanically polished single crystal with a bright surface but some surface irregularities produced by the polishing exhibited fairly high losses below H_{C1}, although the losses above H_{C1} (100 kAm^{-1}, 1300 Oe) remained low up to 145 kAm^{-1} (1800 Oe).

Both Rocher and Septfonds (1967) and Linford and Rhodes (1968) concluded that losses in niobium below H_{C1}, i.e. in the Meissner state were higher in samples with low defect densities. Brankin and Rhodes (1969) suggested that, provided the samples had similar surface finishes, the defect density might not be very important. Further doubt has been thrown on the conclusions of the earlier workers by the work of Beall and Meyerhoff (1969). They measured losses in niobium below H_{C1} both electrically, thermally, and from d.c. magnetization curves. The results agreed well and showed the losses to be hysteretic. The loss in an ultra-high vacuum-annealed sample was lower than in a heavily cold-worked sample. Beall and Meyerhoff suggested that this was due to the increased reversibility of the annealed sample. All their results fitted equation 4.2.1., the value of n being between 2 and 4.

Buchhold and Rhodenizer (1969) have reported that the loss in a cold-worked niobium sample depended on the rate of cooling from room temperature. The loss below H_{C1} was an order of 100 greater in a sample cooled overnight to liquid nitrogen temperatures. This effect was associated with visible surface deformation produced on slow-cooled, highly-polished samples.

Few detailed investigations have been undertaken on the losses in type I materials. The majority of the work has been done by Seebold and Rhodes (1969) who measured losses below H_c in lead and lead-indium solid solutions. They found that for surfaces roughened by spark-machining the loss depended on the degree of roughness, and was below the sensitivity of their equipment for smooth, chemically polished surfaces. The loss per cycle was independent of frequency between 50 and 600 Hz both for pure lead and the solid solutions. For a given surface the loss was independent of the normal state resistivity of the sample which was two orders of magnitude higher in a lead 0.4wt % indium alloy than in pure lead.

Before proceeding to discuss the theories which have been developed for the losses in the Meissner state it is useful to summarize the experimental results we have described above. There are five conclusions that can be drawn, namely :

(i) The loss per cycle is independent of frequency below 500 Hz. It depends only on the peak value of the applied field and is supposed to be hysteretic.

(ii) Losses depend strongly on the peak applied field and may be expressed as

$$L = CH_m^n$$

where n has values between 2 and 12 and C is constant for a given sample.

(iii) The loss can be reduced by smoothing the surface of a sample, and is extremely low in samples with very smooth surfaces.

(iv) The losses depend on the metallurgy of both the bulk material and surface layer of the sample. There is some evidence that high defect densities in cold-worked samples produce low losses but the position is not yet clear.

(v) The loss in a given sample increases when it is cooled in a transverse field. Cooling in the earth's field can increase the losses by tenfold.

This effect is greater in samples which trap more flux, and is most pronounced for very low-loss samples.

4.3. Theories of Loss in the Meissner State

A detailed analysis of the Meissner state losses is extremely difficult. Not only do they vary non-linearly with magnetic field, but they also depend on a number of ill-defined material properties. The first attempt to explain the experimental data was made by Buchhold (1963). Buchhold and Molenda (1962) drew an analogy between ferromagnetic materials and superconductors and suggested two sources of loss; eddy currents which would produce dissipation increasing with the square of the frequency, and magnetic hysteresis which would give a dissipation proportional to frequency. Buchhold states that eddy currents will flow in resistive normal regions produced when flux penetrates a superconductor. He shows that the loss arising from these currents in a sample of conductivity σ penetrated to a depth d by a field of peak value B_m and frequency f would be

4.3.1. $$L = 2\sigma f(\pi B_m)^2 d^3$$

Taking $B_m = 0.1$ Tesla, $\sigma = 10^9$ mhos m^{-1} and $d = 10^{-6}$ m this gives

$$L = 10^{-10} \text{ WHz}^{-1} \text{ m}^{-2} \text{ at a frequency of 50 Hz.}$$

This loss is considerably below the sensitivity of any of the measurements discussed in section 4.2. At a frequency of 5 kHz the loss is 10^{-8} WHz^{-1} m^{-2} which is of the order of those reported by Rocher and Septfonds (1967). If eddy currents were the source of these losses the higher, non-linear dissipation they measured in samples with higher resistance ratios (and therefore higher helium temperature conductivities) would be explained. This point will be discussed again later in this section. The majority of loss measurements have been made at lower frequencies and higher loss levels. Buchhold dismisses the possibility of eddy currents contributing to the losses in these cases.

A second source of loss is magnetic hysteresis. Buchhold considers this in two parts. First, he develops a microscopic model by assuming that regions at the surface such as voids, normal inclusions and asperities can form multiply connected circuits which trap flux. Each circuit is penetrated once a field large enough to induce a critical current in it is reached. The circuit then becomes resistive, and losses occur in this resistance which adjusts its value in fields of different magnitude and frequency so that the circuit current remains at the critical value. When the field reverses the circuit becomes superconducting again trapping flux within it until the critical current is induced in the opposite direction. Buchhold shows how this variable resistance circuit will produce a hysteresis loop and loss per cycle independent of frequency. The model may be criticised on the grounds that loss occurs only in fields greater than that at which the critical current is exceeded. In practice, the loss would probably occur only at the point where flux penetrated when the critical current was first exceeded.

In the second part of his consideration of hysteretic losses Buchhold derives an expression for the losses. This calculation is independent of the microscopic model, and only assumes that flux penetrates the superconductor and is trapped giving rise to a hysteretic magnetization loop. The derivation given below leads to the same result, and gives more insight into the mechanisms involved.

A superconductor which is penetrated at a field H_c and traps flux completely will have a magnetization curve as shown in Fig. 4.1. The energy dissipated per unit volume in going once around the loop from H_c to $-H_c$ will be equal to the area enclosed by the loop. It can be seen from Fig. 4.1. that this area is eight times the area under the reversible magnetization curve, and is equal to $4\mu_o H_c^2$. A constant K may be defined such that the energy dissipated by a sample of volume V which does not trap flux completely when taken through the same field cycle is given by $4\mu_o H_c^2 KV$. A typical curve is shown in Fig. 4.2. Suppose a cylindrical

MODEL HYSTERSIS LOOPS

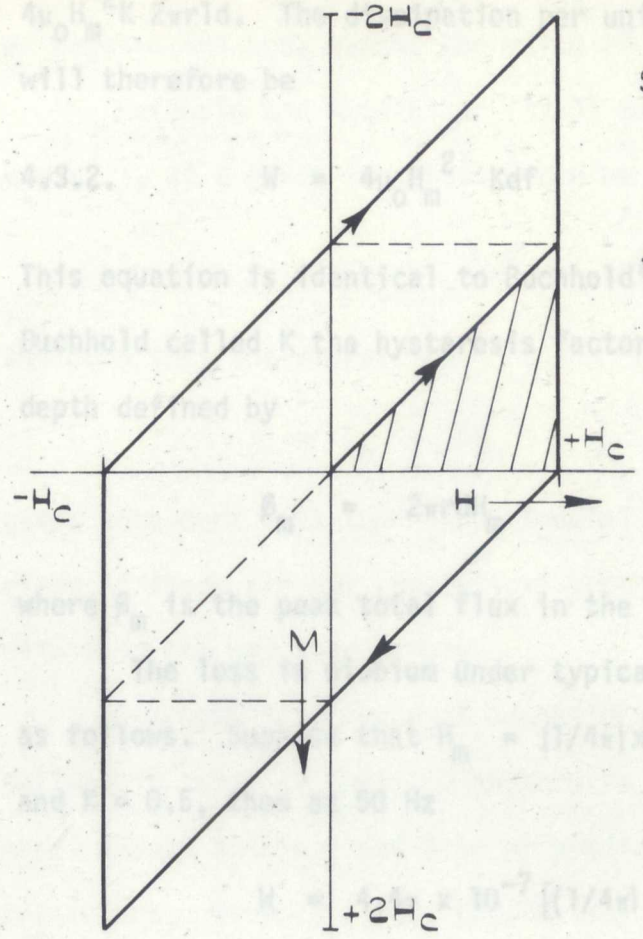

Shaded Area(Virgin Loop)

$= \mu_o H_c^2/2$

Total Area $= 8\mu_o H_c^2/2$

Figure 4.1

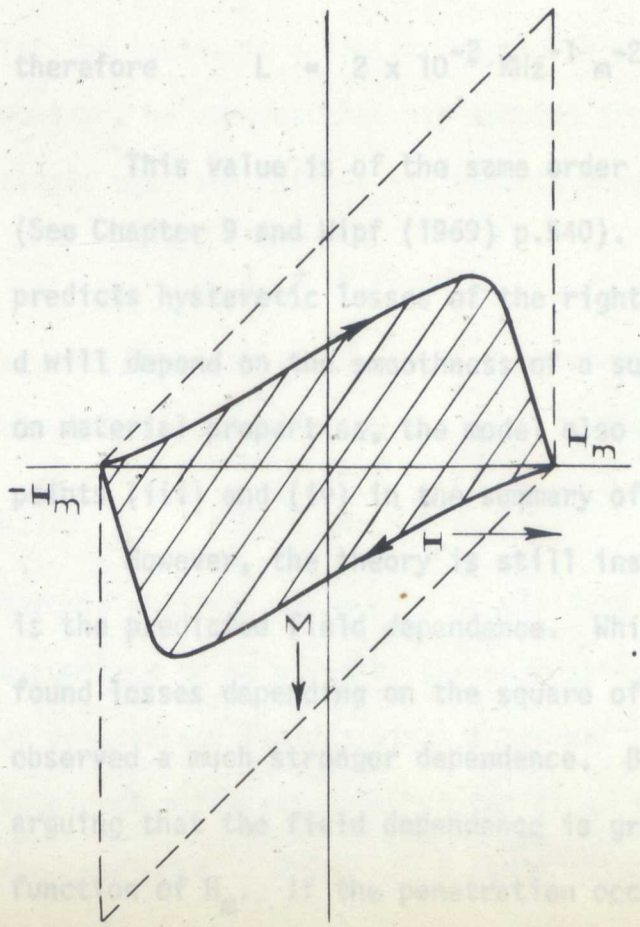

Shaded Area $= 4\mu_o H_m^2 K$

$\therefore$ Dissipation/Unit Volume

$= 4\mu_o H_m^2 Kf$

$\therefore$ Dissipation/Unit Surface Area

$= 4\mu_o H_m^2 Kdf \ Wm^{-2}$

Figure 4.2.

sample of radius r and length l is penetrated to a depth d by an alternating field of peak value H_m, the energy dissipated in one cycle will be $4\mu_o H_m^2 K\, 2\pi rld$. The dissipation per unit surface area at a frequency f will therefore be

4.3.2. $$W = 4\mu_o H_m^2 \, Kdf \qquad (W\, m^{-2})$$

This equation is identical to Buchhold's when converted to c.g.s. units. Buchhold called K the hysteresis factor, and d the effective penetration depth defined by

$$\phi_m = 2\pi rdH_m$$

where ϕ_m is the peak total flux in the sample.

The loss in niobium under typical condition near H_{c1} may be calculated as follows. Suppose that $H_m = (1/4\pi) \times 10^6\ Am^{-1}$ (1000 Oe), $d = 10^{-6}$m, and K = 0.5, then at 50 Hz

$$W = 4.4\pi \times 10^{-7} [(1/4\pi) \times 10^6]^2 \cdot 50 \cdot 10^{-6} \cdot 0.5$$

$$\approx 1\ Wm^{-2}$$

therefore $$L \approx 2 \times 10^{-2}\ WHz^{-1}\, m^{-2}$$

This value is of the same order of magnitude as measured losses (See Chapter 9 and Wipf (1969) p.540). Buchhold's expression, therefore, predicts hysteretic losses of the right order. Since it seems likely that d will depend on the smoothness of a surface, and that d and K will depend on material properties, the model also accounts qualitatively for points (iii) and (iv) in the summary of experimental data in section 4.2.

However, the theory is still inadequate in some respects. The first is the predicted field dependence. While Beall and Meyerhoff (1969) found losses depending on the square of the field, the majority of workers observed a much stronger dependence. Buchhold (1963) explains this by arguing that the field dependence is greater than H_m^2 because d is a function of H_m. If the penetration occurs at surface asperities the

penetration is likely to increase with field. Furthermore, if there is a distribution of imperfections, each will have a characteristic field of penetration and, hence, the value of d will be a function of H_m.

Buchhold and Rhodinizer (1969) suppose that the Pippard penetration depth, λ, at a given temperature can be expressed as

$$\lambda = \lambda_o + aH^2 + bH^4 + \ldots\ldots$$

and show that the expression

$$\lambda = \lambda_o + bH_m^4$$

gives agreement with their experimental results for niobium. It is not clear if there are any theoretical grounds for assuming that λ varies with H in the way they assume.

A second inadequacy of Buchhold's theory is that d and K are defined in terms of measured hysteresis loops, whereas, a satisfactory model should enable d and K to be predicted from measurable material parameters. Seebold (1969, pp.123-130) has attempted with some success to relate the losses to material properties. He develops an expression for the losses in a similar way to that which was used to obtain 4.3.2. However, he assumes that his samples trap flux completely (i.e. that K equals one) and defines an 'effective penetration depth', δ, as

$$\delta = \phi_m/2\pi r H_c$$

arguing that the field within a penetrated region will be H_c. The resulting expression for the loss is then

4.3.3. $$L = 4\mu_o H_c^2 \delta$$

Seebold obtains values of δ by dividing measured losses by $4\mu_o H_c^2$, and, assuming δ to be given by the expression $C(H_m/H_c)^n$ due to a distribution of penetration fields, plots δ against (H_m/H_c). The results for one sample at different temperatures (i.e. varying H_c) plotted thus lie on the same curve. Values of δ for samples of lead, indium and tin with similar surface treatments are also in remarkable agreement when plotted

against H_m/H_c. Hence, for a given surface, δ appears to be a universal function of H_m/H_c and, at least in type I materials, the loss is related to only two material parameters δ and H_c.

The major differences between this model and Buchhold's is that in the former H_c is taken to be the penetration field while in Buchhold's model H_m is used. However, the effective penetration depth will be a universal function of H_m/H_c in both models. Seebold's results show that

$$\delta = \frac{L}{4\mu_o H_c^2} = C\left(\frac{H_m}{H_c}\right)^n$$

Where, for a given surface, the values of C and n are the same for all materials. This expression may be rewritten as

$$L = 4\mu_o H_c^2 C(H_m/H_c)^n = 4\mu_o H_c^2 C(H_m/H_c)^{n-2}(H_m/H_c)^2$$

therefore

4.3.4. $$L = 4\mu_o H_m^2 C(H_m/H_c)^{n-2}$$

If we define an 'effective penetration depth' from Buchhold's equation (4.3.2.) namely

$$dK = \frac{L}{4\mu_o H_m^2}$$

then 4.3.4. shows that if δ is a universal function of (H_m/H_c) then dK will be one also. Either model will, therefore, explain the experimental results, although the field dependence of the 'effective penetration depth' will be different in the two cases. In practice it is probably impossible to distinguish between the models.

Unfortunately, although this approach shows the importance of H_c and an 'effective penetration depth' in determining the losses two problems remain unsolved. The first is to relate δ or dK to measurable properties of a given surface, the second is to determine the values of C and n in the expression

$$dK = C \left(\frac{H_m}{H_c} \right)^n$$

In fact experiments show that n is not constant and it is better to write F (H_m/H_c). Furthermore, it is not immediately clear if H_c is the correct normalization field to use in the case of type II superconductors, nor if K can also be assumed to be constant for such materials.

An analysis of the losses in terms of flux trapped at surface imperfections is reasonable for samples with rough surfaces, i.e. with asperities greater than 0.1 μm or in samples known to have chemically inhomogeneous surfaces or voids below the surface. It is clearly not applicable where losses are observed in samples with smooth, homogeneous surfaces which depend on the field in which they are cooled - point (v) in the summary of section 4.2.

A general qualitative description of the losses in such cases has been given by Rocher and Septfonds (1967). They distinguish two types of loss. One is hysteretic due to pinning of flux lines, and the other is associated with motion of the flux lines. The latter produces dissipation which is non-linear with frequency. They reject eddy currents as a source of non-linear dissipation because comparison of equations 4.3.1. and 2 show that they are smaller than hysteretic losses except for very rough samples where the penetration depth is greater than 0.1 mm, or at frequencies higher than 10^{10} Hz. Instead they propose that resonant modes of the flux line system (DeGennes and Matricon, 1964) or viscous damping of the flux line motion (Baixeras and Fournet 1966, Bardeen and Stephen 1965) are responsible. Both of these mechanisms produce loss proportional to the square of the frequency. Their observation of larger dissipation, non-linear with frequency, in outgassed samples bears out the conclusion that moving flux lines are responsible for these losses.

Rocher and Septfonds point out that both hysteretic and viscous losses may arise either from flux which penetrates the sample at surface imperfections, or from flux trapped within the sample - for instance, on cooling in the earth's field. One would expect a somewhat different field

dependence of the losses to arise from these two sources. For penetrating flux the losses should increase more rapidly with the external field as the penetration increases. Rocher and Septfonds observed no such differences in the variation of loss with applied field. Since one cannot assume a constant penetration depth and still explain the observed field dependence, this is somewhat difficult to understand. One possible solution is to assume a variety of strengths of pinning centre so that already trapped flux-lines contribute to the losses at different fields. Alternatively Buchhold (1963) suggested that points where flux is already trapped might provide easy sites for further flux penetration.

Rocher and Septfonds do not suggest how loss might arise from trapped flux. Wipf (1968) pointed out, however, that each trapped flux-line will have an entry and exit point at the surface. These 'flux-spots' will be subject to an alternating Lorentz force in an alternating applied field. Wipf suggests that the spots and the flux-lines immediately below the surface will oscillate under the influence of this force. Dissipation will be produced both on pinning and depinning of the flux-spots, and whilst they are moving.

In summary we can say that qualitative explanations are available for all five points in our summary of the experimental data, and most of the experimental results are understood. Losses arise from motion at the sample surface of flux which is either trapped in the sample or penetrates at surface imperfections. At low frequencies the dissipation is hysteretic arising from flux pinning in type II superconductors or from normal state transitions in type I materials. At higher frequencies 'viscous' losses due to movement of the flux lines also produce significant dissipation. The amount of flux which penetrates or is trapped, and hence the loss, depends on the detailed metallurgy of the sample and the applied magnetic field.

A quantitative model of dissipation due to flux penetrating the surface at imperfections has been given. This is in reasonable agreement

with some of the experimentally observed features. The relation of the losses to material parameters in this model and the field dependence it predicts are still uncertain.

4.4. Losses Above H_{c1} - Region II

The a.c. losses in superconductors above H_{c1} have probably been studied more closely than in any other field region and a satisfactory theoretical description of the loss has been developed. There are a number of reasons for this. Except at very low fields the commercially important superconductors operate in this regime and it is here that reduction in the a.c. losses must be achieved. Theoretically the losses are easier to understand because they arise in the bulk of the superconductor, and are dependent on more easily defined material properties. Wipf (1968) has given a comprehensive review of the experimental work in Region II, and it is intended to concentrate in this section on the theoretical ideas mentioning only selected, confirmatory experiments.

Wipf points out that four equivalent methods are available for calculating the loss, namely :

(i) Calculation of the area under the magnetization curve,

(ii) Calculation of the energy put into the sample and the energy taken out using the Poynting Vector,

(iii) Calculation of the joule heating,

(iv) Calculation of the product of the pinning forces and the distance they move.

The first paper containing a calculation of the a.c. losses in superconductors was published by London (1963). He used the first method to obtain the loss. He calculated B using the Bean (1962) critical state model assuming a constant critical current density, J_c, in the same way we have done in section 3.4. The result he obtained was therefore similar to that derived by Bean (1964) namely :

3.4.4. $$L = \frac{2}{3} \frac{\mu_0}{J_c} H_m^3 \quad W\,Hz^{-1}\,m^{-2}$$

London showed that this expression was in agreement with experiments by Kamper (1962) in that the frequency dependence was linear and the results were of the same order of magnitude.

The macroscopic critical current density, J_c, was assumed to be constant in the Bean-London calculations. Losses may also be calculated using the Kim et al (1963) approximation to the critical current-field relation namely :

$$J_c = \frac{\alpha}{(B_o + B)}$$

and the Bean critical state model. Hancox (1966) used both the Kim and London approximations to calculate the loss for superconductors of a number of different geometries. Taylor (1968) analysed his data taken on Nb-25%Zr wires in terms of a Bean-Kim model and concluded that the agreement was generally good over a wide range of fields. The Bean model therefore gives a reasonable description of the high field losses in the hard type II superconductors. The microscopic origin of the loss is not clear, although Bean (1964) suggested that they were produced by the local electric fields which exist during a change of magnetization. The product of these fields and the local current density gives rise to local joule heating.

Irie and Yamafuji (1967) calculated the a.c. loss using their general equation for the motion of flux described in section 3.4. They calculated the static hysteresis loss from these equations by neglecting the viscous force, and integrating the product of the pinning force density, F_p, and the flux line velocity V_L over time and distance. For a slab of thickness 2d they find that the loss per unit volume L_p is given by :

4.4.1. $$L_p = 2/3\mu_o (2 - \gamma) H_m^{4-\gamma}/H_a^{2-\gamma}$$

where $H_a^{2-\gamma} \equiv (2 - \gamma)\alpha d/2$ and H_a and γ may be found from the static magnetization loop. Irie and Yamafuji show that equation 4.4.1. gives

better agreement than the Bean-Kim model to the results of Yasukochi et al (1964) on Nb-25%Zr. It also agrees with the measurements of Pech et al (1965) on the same material. The microscopic picture of the losses in this case is that dissipation occurs when a flux line is pinned or depinned at a pinning site.

While equations 3.4.4. and 4.4.1. agree with the experimental data at high fields the models for the behaviour of superconductors from which they are derived ignore the effects of H_{c1} and surface currents on the flux penetration. These are of great importance in niobium and at low fields in hard type II materials. Since it is found experimentally that the losses depend only on the peak applied field, Ullmaier (1966) suggested that the effects could be allowed for by using an effective applied field. If ΔH is the field change from which the bulk sample is shielded by surface currents when the applied field is reversed, a sample in a field alternating between H_m and $-H_m$ will be subject to an effective peak applied field $(H_m - \Delta H/2)$. The Bean-London equation (3.4.4.) therefore becomes

4.4.2. $$L = \frac{2}{3} \frac{\mu_o}{J_c} (H_m - \Delta H/2)^3 \quad WHz^{-1} \quad m^{-2}$$

ΔH will, in general, be a function of the applied field. It is equal to twice the maximum current the surface can carry at a particular field.

A similar equation has been derived by Dunn and Hlawiczka (1968), from their generalized, critical-state model. This incorporates four material-dependent parameters, H_{c1}, ΔH^*, k and n, k and n are defined by

$$F_p = \pm k|H|^n = F_L = \emptyset_o J_c \quad \text{(in the critical state)}$$

ΔH^* is not identical to the ΔH defined by Ullmaier. In this case it is equal to half the field change which occurs with no change in internal flux, and is equivalent to the critical surface current, j_c. These four parameters define a magnetization loop from which Dunn and Hlawiczka calculate the loss on the assumption that n = 0, and therefore

$$J_c = k/\emptyset_o = C \quad \text{(the London approximation)}$$

The loss is then given by

$$4.4.3. \quad L = \frac{2}{3}\frac{\mu_o}{J_c}(H_m - \Delta H^* - H_{c1})^2 \; (H_m + 2\Delta H^* + \tfrac{1}{2}H_{c1}) \; \text{WHz}^{-1} \; \text{m}^{-2}$$

To compare equations 4.4.2. and 3 with measured losses it is necessary to know the values of J_c, H_{c1} and ΔH or ΔH^*. Wipf (1968) used a value of 4×10^9 Am^{-2} for J_c, and Ullmaier and Gauster's (1966) values of ΔH for Nb-25%Zr in equation 4.4.2., and showed that the majority of the published data on niobium alloys agrees with this equation. Linford (1968) found that equation 4.4.2. described the behaviour of annealed polycrystalline niobium above H_{c1}. He put $\Delta H/2$ equal to H_{c1} equal to 103.5 kAm^{-1} (1300 Oe). For Nb-Zr, NbTi and rolled niobium strip he found that equation 4.4.3. gave better agreement. Easson and Hlawiczka (1968) reported good agreement between their results and equation 4.4.3., although in that case ΔH^* was taken to be zero.

Little experimental work has been undertaken on very reversible type II superconductors, for example, well annealed niobium or suitable Nb-Ta and NbMo alloys. For these materials the viscous forces, F_V, neglected in all the calculations mentioned so far, will become significant and higher losses, increasing with non-linear frequency dependence, may be expected. Irie (1970) has presented calculations of the losses in weak-pinning superconductors and has shown that at low frequencies the loss is increased by a term linear in frequency. At high frequencies the hysteretic loss can be neglected, and the losses are inversely proportional to the square root of the frequency.

4.5. Losses above H_{c1} - Regions III and IV

In this region the whole volume of the superconductor has been penetrated. Wipf (1968) points out that because of this the loss per unit volume rather than the loss per unit surface area is the correct unit for comparisons between samples. Few measurements have been reported in this regime because the losses are so high that the

temperature of the superconductors may rise significantly producing thermal runaway. The temperature rise will be proportional to the total heat dissipated divided by the rate of removal of heat. Since the former will be proportional to the volume of material, and the latter to the surface area, the temperature rise will be proportional to the volume to surface-area ratio. Hence thermal runaway will be less likely to occur for thin sheets or wires.

Region III is of interest because of the potential uses of coils wound from type II superconductors able to operate in these high a.c. fields. London (1963) showed that for conductors of normal size the losses at 50 Hz are so high that operation would be impractical. He pointed out that the losses could be reduced by using smaller conductors of order 1 μm or even 10^{-2} μm in thickness. Recently coils able to operate in high, low frequency (0 - 1Hz) magnetic fields have been the subject of a considerable amount of theoretical and practical work because of their intended application in high-energy particle accelerators. Composite conductors have been developed which consist of large numbers (61-1045) of thin (10-1 μm) superconducting filaments of niobium-titanium embedded in a matrix of copper or cupro-nickel or a combination of these.

The theory and behaviour of such composites has been discussed by Smith et al (1970). The initial goal in developing them was to obtain intrinsically stable conductors in which the microscopic flux jumps, which occur in changing fields, would not avalanche and quench the superconducting state. However, the small sized superconducting filaments used to obtain stability also have low losses. If the composites are twisted the losses induced in the normal matrix by the a.c. currents are also considerably reduced. Consequently these materials may be used to produce magnetic fields of the order of 5 Tesla at frequencies of up to 1Hz.

In Region IV the superconductor is normal except for a surface sheath during part of the cycle and the losses are so high that it is of no practical interest. Very little experimental or theoretical work has

been published except that Seebold (1969) has reported some measurements on lead and its alloys with $H_m > H_c$. In these measurements either eddy current or hysteretic losses were of greater importance depending on the resistivity of the sample. We have made no measurements in this regime and will not discuss it further.

4.6. Aims of Research

Our experiments were aimed at extending the available data on losses, and verifying some aspects of the theories described earlier in this chapter. Niobium was chosen as the material for our investigations because it was readily available, and because considerable expertise in its treatment was at our disposal. Moreover, its high value for H_{c1} makes it a commercially interesting material as was shown earlier.

It is clear from the experimental evidence summarized in section 4.2. that the metallurgical state of the sample, and in particular, the geometry and physical condition (i.e. chemical composition, defect density) of its surface have a major effect on the dissipation when a superconductor is subjected to an alternating field below H_{c1}. Many of the reported investigations were carried out without sufficient attention being paid to control of these parameters. For instance, many of the accounts (Easson and Hlawiczka 1967a, Linford 1968) of lower losses in samples whose surface roughness had been reduced ignored the fact that the methods of reducing the roughness (chemical or mechanical polishing) had probably altered either the chemical or physical nature of the surface. Chemical polishing, for example, may increase the dissolved hydrogen content of a surface, mechanical polishing may introduce high defect densities. In other experiments where the effect of heat-treatments on the losses was investigated e.g. Beall and Meyerhoff (1969), no attempts were reported to measure the surface geometry before and after treatment to ensure that thermal etching or surface diffusion had not altered the profile. Rocher and Septfonds (1967) annealed their electropolished samples in ultra-high vacuum and then re-electropolished them! They did not discuss

the possibility that the second electropolish had altered the chemical composition of the surface, nor the possibility that the electropolish had produced quite different surface profiles in the cold-worked and annealed materials.

In our experiments we aimed to measure the effects on the losses in the Meissner state of the surface geometry, the dissolved gas content, and the degree of cold-working independently of each other. The model for a.c. losses in the Meissner state developed by Buchhold (1963) and modified by Seebold (1969) seemed to provide a satisfactory method of analysing the losses. We hoped, therefore, to check these theories by measuring the variation of losses with frequency, with surface roughness and with the primary superconducting properties H_c and κ.

In the discussion of the loss measurements below H_{c1} (section 4.2.) it was pointed out that the fields in which the samples were cooled affected the loss. However, these effects were only noted on very low loss samples, and, where the cooling field was less than or equal to the earth's field, the losses in such samples were always lower than 10^{-4} watts hertz^{-1} metre^{-2}. Since, in most cases, this was the lower limit of sensitivity of the technique used for our measurement, no attempt was made initially to study the effects of a cooling field on the loss or to cool the samples in other than the earth's field.

Catterall (1968) has pointed out that any method of increasing the field at which losses in niobium become high is of interest because it might enhance the economic viability of a superconducting power cable. Equations 4.4.2. and 4.4.3. developed by Ullmaier (1966) and Dunn and Hlawiczka (1968) indicate a way of achieving such an improvement. They predict that there will be no loss where the applied field H_m is less than $H_{c1} + \Delta H^*$. Hence if ΔH^* can be increased significantly the field at which bulk flux penetration occurs and losses become large will be raised above H_{c1}. Linford (1968) showed that mechanical polishing delayed the onset of the high-loss regime in a niobium single crystal to a field of about 160 kAm^{-1} (2000 Oe). We were interested in pursuing this work, and in attempting to increase ΔH^*

by such methods as cold-working, neutron-irradiation and ion-implantation. We wished to investigate the effects of these treatments on the losses above H_{c1}, and, where possible, to relate any changes to the magnetization curves and critical currents of the treated samples.

The theories for losses in fields greater than H_{c1} (see section 4.4.) appear to work well for hard type II superconductors. We wished to see how well these theories described the behaviour of our niobium samples particularly after they had been annealed. To do this it was necessary to obtain values for ΔH^*, J_c and H_{c1}, and measurement of these parameters were undertaken. The method adopted to measure ΔH^* and J_c (described in Chapter 5) also enabled us to check the validity of using a critical state model to describe the behaviour of our samples.

In summary, it was planned to make the following loss measurements :

Below H_{c1}

As a function of :

(i) frequency

(ii) of surface roughness on materials of similar properties

(iii) dissolved gas content on material with similar surfaces

(iv) cold work on materials with similar surfaces

Above H_{c1}

On samples which had been :

(i) cold worked

(ii) neutron irradiated

(iii) ion-implanted

and as a function of :

(i) annealing treatment

(ii) surface roughness

In all cases we wished to correlate the losses with other appropriate measurements of surface profiles, magnetization curves, critical currents (bulk and surface), dissolved gas content and crystalline structures.

5. LOSS MEASUREMENT

5.1. Introduction

The experimental programme described in section 4.6. required the measurement of three superconducting properties: a.c. loss, magnetization and critical current. Techniques and apparatus for making all three types of measurement were already available at Warwick. These have been described by Linford (1968), Goodfellow (1969) and Seebold (1969). In deciding which of the available techniques for making each type of measurement was most suitable for our purposes, a major consideration was the geometrical form and size of the samples.

Short, cylindrical samples were chosen because they could be prepared from as-received rods and as-grown, single crystals with a minimum of machining. The field distribution about cylindrical samples in axial fields is symmetric and, apart from the ends, calculable. For this reason, short samples were used as opposed to wires because the latter must usually be wound into a bifilar coil in which the field and current distribution are uncertain. Short samples also have the advantage that they are easier to prepare than wires. No wire drawing facilities were available and producing wires with a homogeneous, uniform surface or bulk treatment is difficult. A further disadvantage of wires is that cold work is often introduced into high-purity, annealed samples when they are mounted in experimental apparatus. Because of the difficulty of fixing current leads on niobium, the choice of short samples necessitated the use of measuring techniques in which currents were induced in the samples by external magnetic fields.

The apparatus chosen for measuring a.c. loss was originally constructed by Linford. Attempts were made to improve its accuracy and sensitivity and these are described in section 5.4. The vibrating sample magnetometer used by Linford and Seebold was also modified, and an integrating magnetometer was built (Brankin, Eastham and Rhodes 1970). These, together with a new apparatus for measuring critical current, will be described in Chapter 6.

5.2. Selection of Technique

Seebold (1969 p.23-39) has critically reviewed the techniques used for loss measurement by different authors. He distinguishes between two distinct classes of techniques, these are the thermal (calorimetric) and electrical methods. The thermal calorimeters are either adiabatic or isothermal. In the adiabatic type the sample is thermally isolated as well as possible, and an a.c. field applied. The time taken to produce a given temperature rise at this field is then noted. The dissipation may then be calculated if the specific heat of the sample is known. However, the calorimeter is usually calibrated using a known dissipation in a standard resistor. Because of the need for thermal isolation the technique is not suitable for transport currents, and the current is induced by an external field. The isothermal calorimeter, on the other hand, is kept at a constant temperature and is suitable for either induced or transport current measurements. In this method, the helium boiled off in a given time when the field or current is applied is measured or, alternatively, the rate of boil-off is determined. Both calorimetric techniques have the disadvantage that when induced currents are used the dissipation in the whole sample is measured. Since the losses at the ends may be completely different to those in the central region, measurements are not directly comparable with those taken by other techniques or using different calorimeters. The problem has been overcome (Buchhold and Molenda, 1962) by using a profiled magnet producing a field only over the middle of the specimen.

Electrical techniques may be either direct or inductive. In the former, the loss is determined directly by measuring the a.c. voltage across the specimen. Wire specimens are used to obtain a sufficiently high potential difference at a reasonable current. The voltage is either measured with a phase-sensitive detector to extract the non-inductive component, which is in any case reduced either by a bifilar winding or compensation, or multiplied by the applied current in a wattmeter. In the inductive technique, a current, I_s, is induced in a sample by an applied alternating field, H_m. A pick-up

coil is wound on the sample and the voltage induced in it by the changing flux within the sample, $d\phi/dt$, is multiplied by a signal proportional to the field. Since the field is proportional to the current induced in the sample, and the rate of change of flux is proportional to the voltage around the sample surface, V_s, the product $H_m \frac{d\phi}{dt}$ is proportional to $V_s I_s$ the surface dissipation in the sample.

In his review, Seebold (1969) concludes that the thermal techniques give greater sensitivity. The adiabatic technique is limited only by the thermal isolation of the sample and gives the greatest sensitivity of all. This was the technique used by Rocher and Septfonds (1967). The lower sensitivity of the electrical methods is compensated for by their ease of use, rapid presentation of results and convenience for variable temperature measurements. The problem concerning the sample ends which arises with induced current, calorimetric measurements does not arise in the inductive, electrical technique in which only the loss in the region of the sample below the pick-up coil is measured.

An electronic wattmeter was available at Warwick. It had a sensitivity of about 10^{-5} Watts Hz^{-1} m^{-2} at 50 Hz, and, at 80 kA m^{-1} (1000 Oe) it gave reasonably accurate (±10%) results for losses greater than 10^{-3} WHz^{-1} m^{-2}. It had the advantage of giving quick results, samples could be changed easily and the cryostat consumed only about 1 litre of helium in a six hour run. Typically 40 experimental points were obtained in a run, twice this number were taken in some cases. This compares with a maximum of about 7 points in 3 hours using 4 litres of helium for our isothermal calorimeter. The acceptable level of a.c. loss for a cable conductor has been set at 0.1 Wm^{-2} (i.e. 2×10^{-3} WHz^{-1} m^{-2}) (Taylor 1969, Goodman 1969). It was decided, therefore, that provided the apparatus could be improved to give good results at 10^{-4} WHz^{-1} m^{-2} or lower in fields of 80 kA m^{-1} (1000 Oe), this apparatus would be adequate for our measurements.

5.3. Apparatus

The apparatus consists of a tailed helium dewar with a copper solenoid

fitted co-axially with the tail. The solenoid and dewar both fit inside a nitrogen dewar. The sample, in a nylon holder, is inserted into the prefilled helium dewar at the end of a thin-walled, stainless-steel tube which projects from the dewar. The helium dewar is closed at the top with a vacuum-tight sliding seal between the steel tube and a brass top plate. This plate is O-ring sealed onto a flanged collar in which the dewar is fixed with black wax. The sample holder is fitted with spacers to keep the sample co-axial with the tail of the dewar, and has large cooling slits along the sample length. To facilitate cooling, the sample itself is held only at the ends by two thin, nylon rings making a good fit both on the sample and the holder. A pick-up coil of approximately 100 turns of 46 S.W.G., enamelled, copper wire is wound directly on the centre of the sample and held in place with a thin coat of epibond. The leads to the coil are twisted up to the point they leave the solenoid where they are soldered to a terminal block. A second 'compensation' coil is wound on the sample holder 30 mm from the sample end and the leads taken to the same terminal block. Separate screened leads from the coils carry signals out of the cryostat via the stainless-steel support tube and a vacuum seal.

A block diagram of the electronic measuring apparatus is shown in Fig. 5.1. Current for the solenoid is supplied either directly from the 50 Hz mains via two Variac's, an isolating transformer and tuning capacitors, or from a 100 Watt Derritron power amplifier via a matching transformer and tuning capacitors. The tuning capacitors form a series-tuned circuit with the solenoid so that their effective impedance is only the coil resistance. The capacitance may be varied to tune at different frequencies. A total of twelve, 300 V A.C. power-factor capacitors are used at low-frequencies, and various 1, 0.1 and 0.01 μF, 1000 V D.C., paper capacitors for higher frequencies. The coil is not tuned exactly in the 50 Hz mode to reduce instability in the field, particularly at high currents. An 0.1 Ω ± 0.02%, AC/DC standard resistor is fitted in the field supply circuit for current measurement, the voltage across it being measured with a Solartron LM 1219

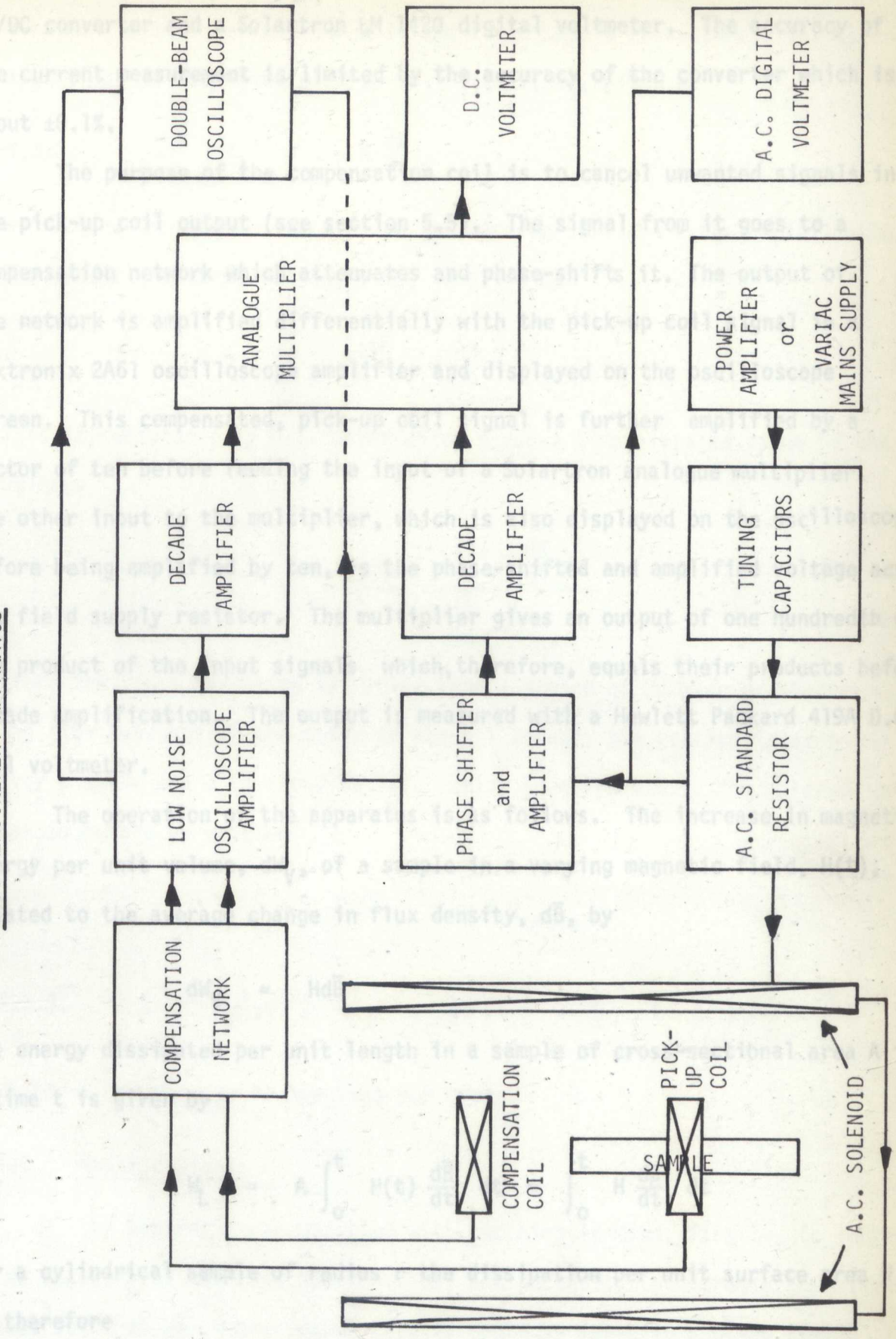
LOSS MEASUREMENT APPARATUS
DOUBLE-BEAM OSCILLOSCOPE
D.C. VOLTMETER
A.C. DIGITAL VOLTMETER
ANALOGUE MULTIPLIER
POWER AMPLIFIER or VARIAC MAINS SUPPLY
DECADE AMPLIFIER
DECADE AMPLIFIER
TUNING CAPACITORS
LOW NOISE OSCILLOSCOPE AMPLIFIER
PHASE SHIFTER and AMPLIFIER
A.C. STANDARD RESISTOR
COMPENSATION NETWORK
COMPENSATION COIL
PICK-UP COIL
SAMPLE
A.C. SOLENOID

FIGURE 5.1.

AC/DC converter and a Solartron LM 1420 digital voltmeter. The accuracy of the current measurement is limited by the accuracy of the converter which is about ±0.1%.

The purpose of the compensation coil is to cancel unwanted signals in the pick-up coil output (see section 5.5). The signal from it goes to a compensation network which attenuates and phase-shifts it. The output of the network is amplified differentially with the pick-up coil signal in a Tektronix 2A61 oscilloscope amplifier and displayed on the oscilloscope screen. This compensated, pick-up coil signal is further amplified by a factor of ten before feeding the input of a Solartron analogue multiplier. The other input to the multiplier, which is also displayed on the oscilloscope before being amplified by ten, is the phase-shifted and amplified voltage across the field supply resistor. The multiplier gives an output of one hundredth of the product of the input signals which, therefore, equals their products before decade amplification. The output is measured with a Hewlett Packard 419A D.C. null voltmeter.

The operation of the apparatus is as follows. The increase in magnetic energy per unit volume, dW_V, of a sample in a varying magnetic field, H(t), is related to the average change in flux density, $d\bar{B}$, by

$$dW_V = H d\bar{B}$$

The energy dissipated per unit length in a sample of cross-sectional area A in a time t is given by

$$W_L = A \int_0^t H(t) \frac{d\bar{B}}{dt} dt = \int_0^t H \frac{d\phi}{dt} dt$$

For a cylindrical sample of radius r the dissipation per unit surface area W is therefore

5.3.1. $$W = \frac{1}{2\pi r} \int_0^t H \frac{d\phi}{dt} dt$$

In the wattmeter, two signals are fed to the multiplier. One, proportional to the magnetic field, is given by $V_H = \beta RH/K$.

where β is the amplification factor of the electronics, K is the solenoid constant in Am^{-1} per Amp and R is the field supply resistance. The second signal is the amplified pick-up coil signal, V_s, given by

5.3.2. $$V_s = \alpha N \frac{d\phi}{dt}$$

where N is the number of turns on the pick-up coil and α the amplification. The product of these voltages, V_L, is given by

$$V_L = \frac{\alpha\beta NR}{K} H \frac{d\phi}{dt}$$

This is measured on a D.C. meter which gives a time averaged value of the voltage

$$\overline{V}_L = \frac{\alpha\beta NR}{K} \frac{\int_0^t H \frac{d\phi}{dt}\, dt}{\int_0^t dt}$$

Since the field variation is cyclic with a period of 20 msec or shorter and the time constant of the meter is about 1 second, the voltage is averaged over a cycle and t is equal to 1/f. Using Equation 5.3.1. the meter output can therefore be written

$$\overline{V}_L = \frac{\alpha\beta NR}{K} 2\pi r f W_{cycle} \qquad \text{or}$$

5.3.3. $$L = \frac{1}{2\pi r} \cdot \frac{1}{\alpha\beta} \cdot \frac{1}{N} \cdot \frac{1}{f} \cdot \frac{K}{R} \overline{V}_L \quad WHz^{-1} m^{-2}$$

where $L = W_{cycle}$ is the loss per cycle.

5.4. Modifications

The apparatus was modified with two aims in mind, firstly, to increase the accuracy of the loss measurements, and secondly, to decrease the minimum loss level at which meaningful results could be taken in a given field. It will be shown in the next section that this minimum loss level, which will be called the sensitivity of the loss measurement, is limited by the accuracy with which the compensation can be carried out. Compensation is achieved

by observation of the pick-up coil waveform on the oscilloscope. It depends, therefore, on the sensitivity of the pick-up coil signal measurement. Sensitivity in this section will be arbitrarily defined as the input signal level at which the signal to noise ratio is one. The noise level at the output of the Tektronix amplifier is about 5 μV peak to peak with the filters set at 0.6 Hz (low-pass) and 6 KHz (high-pass). The sensitivity is therefore about 5 μV peak to peak, which was usually found to correspond to a loss of about 5×10^{-4} WHz^{-1} m^{-2}. The sensitivity of the wattmeter was much greater than this. Experimentally the noise at the D.C. meter for a field of 80 kA m^{-1} (1000 Oe) was about 10 mV. If this figure is substituted in Equation 5.3.3. using typical values of 3×10^5 for α, 100 for N, 50 for f, 1.5×10^{-3} m for r and 4.5×10^4 for $K/R\beta$ the minimum detectable loss is

$$L = 3 \times 10^{-3} \bar{V}_L = 3 \times 10^{-5} \text{ WHz}^{-1} \text{ m}^{-2}$$

Equation 5.3.2. shows that the sensitivity of the pick-up coil measurement may be improved by increasing N, or $d\phi/dt$, i.e. the frequency of the field, or by increasing α. Increase in any of these must be achieved without altering the noise level at the output of the Tektronix. Since this is determined by internal noise, increasing N or f will not affect it. Increases in α may do so, and in practice before α is increased the signal to noise ratio must be improved. This latter method was attempted first. T. Pech (1968) described a loss measuring system based on a P.A.R. Lock-In amplifier. This is a phase-sensitive detector preceded by a tuned amplifier. The theory of the technique is as follows :

The induction in a sample subjected to a field $H = H_m \sin \omega t$ may be written

$$\bar{B} = H_m \sum_{n=1}^{n=\infty} (\mu_n' \sin n\omega t + \mu_n'' \cos n\omega t)$$

where μ_n' and μ_n'' are Fourier coefficients.

Since ϕ is equal to $A\bar{B}$ where A is the area of the sample this expression for $\bar{B}$ may be differentiated and substituted into the expression for W derived in section 5.3. i.e.

5.3.1. $$W = \frac{1}{2\pi r} \int_0^t H(t) \frac{d\phi}{dt} \, dt$$

which gives

$$W = \frac{A}{2\pi r} H_m^2 \int_0^t \left| \sum_{n=1}^{n=\infty} n\omega \, (\mu_n' \cos n\omega t - \mu_n'' \sin n\omega t) \right| \sin\omega t \, dt$$

The only term in the integral which gives a non-zero result when it is integrated over a cycle is

$$\int_0^{1/f} \omega \, \mu_1'' \sin \omega t \sin \omega t \, dt = \tfrac{1}{2} \int_0^{1/f} \omega \, \mu_1'' \, (1 - \cos 2\theta) \, dt = \omega\mu_1''/2f$$

The loss is therefore given by

5.4.1. $$L = W_{cycle} = \frac{A}{2\pi r} H_m^2 \cdot \omega \frac{\mu_1''}{2f}$$

The voltage across the ends of a pick-up coil is given by

$$V_s = -N\frac{d\phi}{dt} = -NAH_m \sum_{n=0}^{n=\infty} n\omega \, (\mu_n' \cos n\omega t - \mu_n'' \sin n \, \omega t)$$

When detected by a correctly adjusted phase-sensitive detector this signal will give an output, V_o, given by

$$V_o = C \, NA \, \omega H_m \, \mu_1''$$

where C is a constant.

μ_1'' can, therefore, be measured and substituted in Equation 5.4.1. to give the loss. The importance of this analysis is that it demonstrates that only the component of the pick-up coil signal at the fundamental frequency and in

quadrature with the inductive signal contributes to the loss voltage, hence the other harmonics may be filtered out. This result applied equally to the wattmeter technique in which wide-band amplifiers had been used previously. However, improving the signal to noise ratio by the use of filters introduces two problems. The first is that the $d\emptyset/dt$ waveform then appears as a sinusoid, which means that it cannot be used for compensation or interpretation. The second problem is that conventional filters introduce large phase-shifts at frequencies near the pass-band. Since the phase-sensitive detector depends on phase coherence between the reference and input signals, the frequency of the a.c. field must therefore be held constant for overall phase-stability. Also, as mentioned in section 5.3., the field supply was tuned which meant that the field frequency and phase was not very stable. A combined filter and phase-sensitive detector system was tried to see if the sensitivity of the wattmeter could be improved. Although this system was much simpler, the overall sensitivity was no better. When no filters were used problems were encountered with the higher harmonics which are measured by the phase-sensitive detector. For this reason, and because the multiplier automatically takes the product of the coil signal and the field, the phase-sensitive detector was abandoned.

Experiments were then made using larger pick-up coils. A 1000 turn coil wound on a nylon former was used in early experiments. This coil not only produced a larger signal due to flux penetration but also increased (by a factor of nearly 1000) the signal due to flux linkage with parts of the coil not filled by the sample. Consequently the compensation had to be effected more precisely. It was calculated that for a sensitivity of 10^{-5} Watts Hz^{-1} m^{-2} compensation to 1 part in 10^6 was required. A new compensator was constructed using fixed resistors and helipots for the amplitude voltage divider and fixed capacitors and helipots for the phase-shifter. Compensation to the required order of magnitude can be obtained for short periods with this system, but mechanical and thermal instabilities in the variable resistors and fixed capacitors make it difficult to sustain for the duration

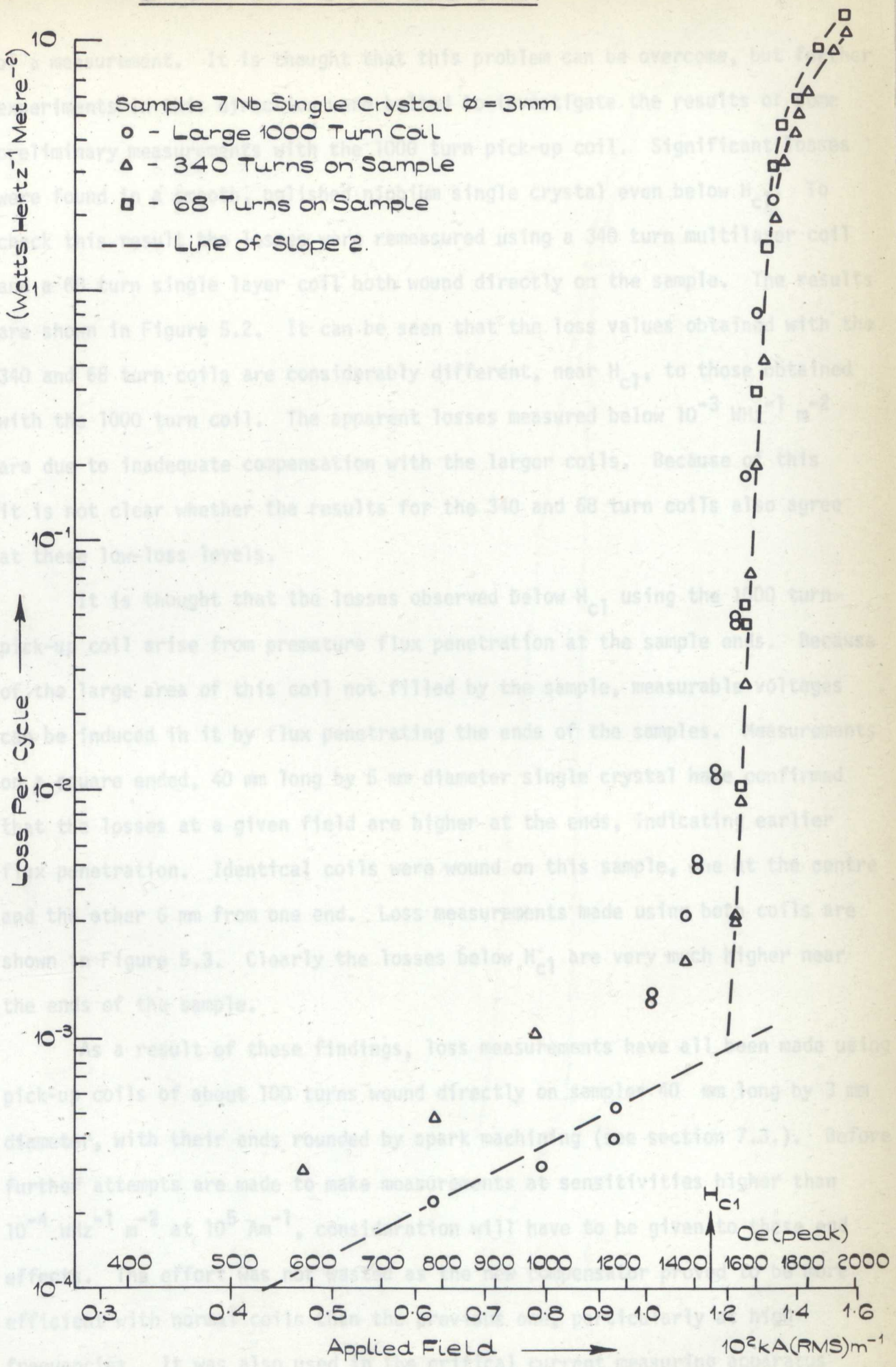
Sample 7 Nb Single Crystal ø = 3mm
o - Large 1000 Turn Coil
Δ - 340 Turns on Sample
□ - 68 Turns on Sample
— — — Line of Slope 2.
Loss Per Cycle (Watts Hertz⁻¹ Metre⁻²)
10
1
10⁻¹
10⁻²
10⁻³
10⁻⁴
Hc1
Oe(peak)
400 500 600 700 800 900 1000 1200 1400 1600 1800 2000
0·3 0·4 0·5 0·6 0·7 0·8 0·9 1·0 1·2 1·4 1·6
Applied Field
10²kA(RMS)m⁻¹

Figure 5.2.

of a measurement. It is thought that this problem can be overcome, but further experiments in this direction were halted to investigate the results of some preliminary measurements with the 1000 turn pick-up coil. Significant losses were found in a smooth, polished niobium single crystal even below H_{c1}. To check this result the losses were remeasured using a 340 turn multilayer coil and a 68 turn single layer coil both wound directly on the sample. The results are shown in Figure 5.2. It can be seen that the loss values obtained with the 340 and 68 turn coils are considerably different, near H_{c1}, to those obtained with the 1000 turn coil. The apparent losses measured below 10^{-3} WHz^{-1} m^{-2} are due to inadequate compensation with the larger coils. Because of this it is not clear whether the results for the 340 and 68 turn coils also agree at these low-loss levels.

It is thought that the losses observed below H_{c1} using the 1000 turn pick-up coil arise from premature flux penetration at the sample ends. Because of the large area of this coil not filled by the sample, measurable voltages can be induced in it by flux penetrating the ends of the samples. Measurements on a square ended, 40 mm long by 5 mm diameter single crystal have confirmed that the losses at a given field are higher at the ends, indicating earlier flux penetration. Identical coils were wound on this sample, one at the centre and the other 6 mm from one end. Loss measurements made using both coils are shown in Figure 5.3. Clearly the losses below H_{c1} are very much higher near the ends of the sample.

As a result of these findings, loss measurements have all been made using pick-up coils of about 100 turns wound directly on samples 40 mm long by 3 mm diameter, with their ends rounded by spark machining (see section 7.3.). Before further attempts are made to make measurements at sensitivities higher than 10^{-4} WHz^{-1} m^{-2} at 10^{5} Am^{-1}, consideration will have to be given to these end effects. The effort was not wasted as the new compensator proved to be more efficient with normal coils than the previous one, particularly at high frequencies. It was also used in the critical current measuring apparatus described in the next chapter.

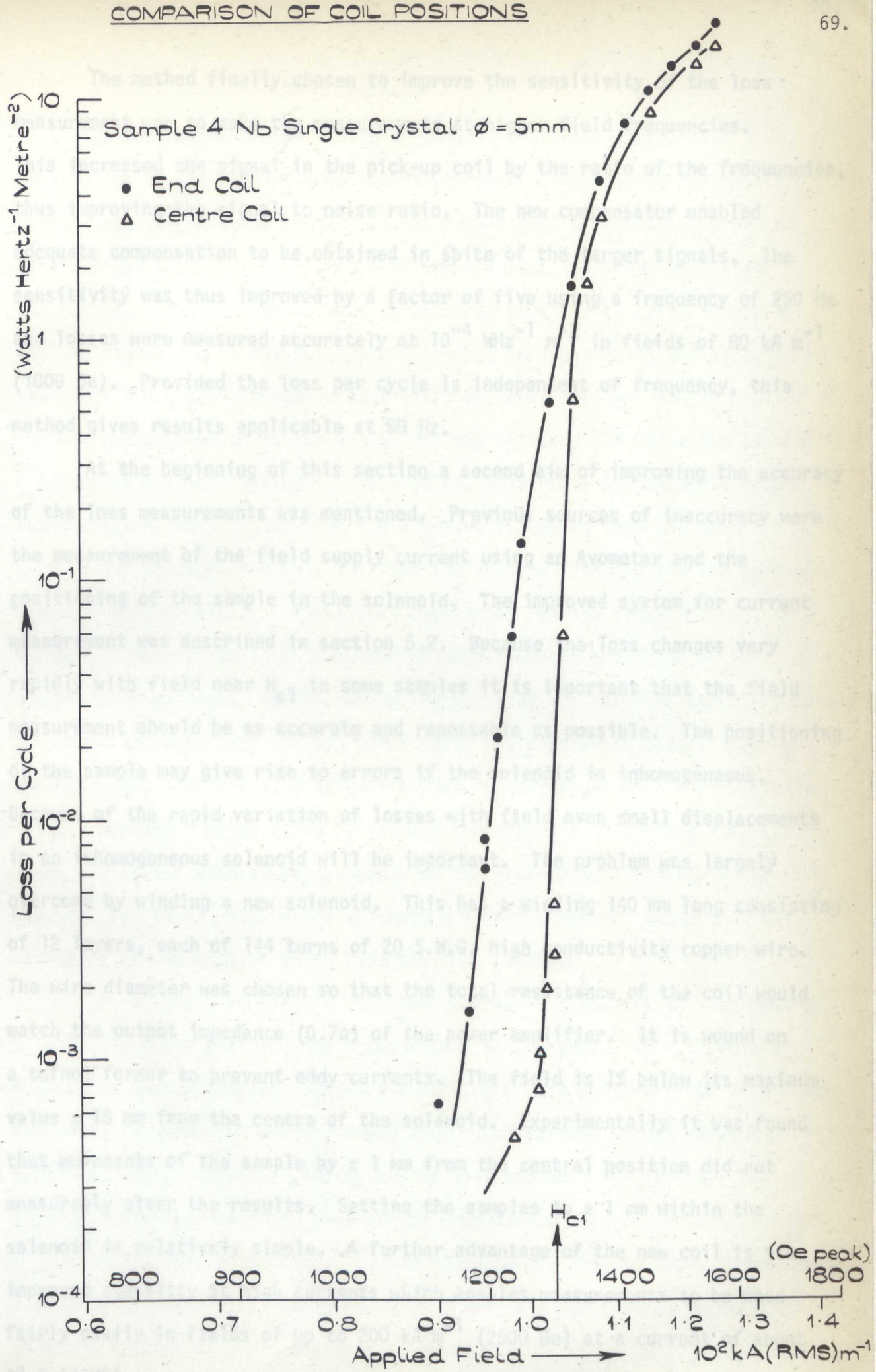
Sample 4 Nb Single Crystal ø = 5mm
• End Coil
△ Centre Coil
(Watts Hertz⁻¹ Metre⁻²)
Loss per Cycle
10
1
10⁻¹
10⁻²
10⁻³
10⁻⁴
Hc1
800
900
1000
1200
1400
1600
1800
(Oe peak)
0·6
0·7
0·8
0·9
1·0
1·1
1·2
1·3
1·4
Applied Field
10²kA(RMS)m⁻¹

Figure 5.3.

The method finally chosen to improve the sensitivity of the loss measurement was to make the measurements at higher field frequencies. This increased the signal in the pick-up coil by the ratio of the frequencies, thus improving the signal to noise ratio. The new compensator enabled adequate compensation to be obtained in spite of the larger signals. The sensitivity was thus improved by a factor of five using a frequency of 250 Hz and losses were measured accurately at 10^{-4} WHz^{-1} m^{-2} in fields of 80 kA m^{-1} (1000 Oe). Provided the loss per cycle is independent of frequency, this method gives results applicable at 50 Hz.

At the beginning of this section a second aim of improving the accuracy of the loss measurements was mentioned. Previous sources of inaccuracy were the measurement of the field supply current using an Avometer and the positioning of the sample in the solenoid. The improved system for current measurement was described in section 5.2. Because the loss changes very rapidly with field near H_{cl} in some samples it is important that the field measurement should be as accurate and repeatable as possible. The positioning of the sample may give rise to errors if the solenoid is inhomogeneous. Because of the rapid variation of losses with field even small displacements in an inhomogeneous solenoid will be important. The problem was largely overcome by winding a new solenoid. This has a winding 140 mm long consisting of 12 layers, each of 144 turns of 20 S.W.G. high conductivity copper wire. The wire diameter was chosen so that the total resistance of the coil would match the output impedance (0.7Ω) of the power amplifier. It is wound on a tufnol former to prevent eddy currents. The field is 1% below its maximum value ± 18 mm from the centre of the solenoid. Experimentally it was found that movements of the sample by ± 1 mm from the central position did not measurably alter the results. Setting the samples to ± 1 mm within the solenoid is relatively simple. A further advantage of the new coil is its improved stability at high currents which enables measurements to be made fairly easily in fields of up to 200 kA m^{-1} (2500 Oe) at a current of about 12.5 A(RMS).

5.5. Compensation and Phase Setting

No discussion of the wattmeter technique is complete without a description of the compensation techniques used. The need to compensate arises from the presence in the pick-up coil signal of a voltage produced by 'leakage' flux in those regions of the coil and its leads not filled by the sample. This voltage is kept as small as possible by using fine wire (0.1 mm diameter - 46 S.W.G.), wound directly on the sample, and by twisting the leads. A small leakage voltage still appears, however, and determines the maximum gain at which the amplifiers may be used, and hence the sensitivity for a given detector system. This problem is overcome by placing a second (compensation) coil in the same field but well removed from the sample. A part of the voltage from this coil and the voltage from the pick-up coil are measured differentially. The signal due to the leakage flux can then, in theory, be made as small as required by adjusting the amplitude of the compensation voltage. Unfortunately, in practice, it has been found impossible to obtain voltages from the two coils which are exactly in phase. Hence, when they are subtracted, a voltage almost in quadrature with the inductive voltage remains. As equation 5.4.1. and the analysis of section 5.4. has shown, it is the quadrature component of the pick-up coil voltage which measures the loss. This other quadrature signal therefore appears at the output of the multiplier as an apparent loss voltage.

In our experiments this unwanted quadrature signal is in turn removed by slightly phase shifting the compensation coil signal. This immediately introduces a complication because the setting of the phase-shifter determines the point at which the losses become zero. Unless this is set carefully incorrect, even 'negative', losses may be observed and, in any case, the smallest quadrature voltage that can be compensated sets the effective limit to the lowest loss measurable. In our measurements this is taken to be about 1 μV peak to peak which, using equation 5.3.3. and the typical constants given in section 5.4, gives a loss of about 5×10^{-4} WHz^{-1} m^{-2}. At higher frequencies this is, of course, reduced by the ratio of the frequencies.

Two criteria have been suggested for setting the compensators. Both of these involve observation of the pick-up coil signal on an oscilloscope. Seebold (1969) adjusted the amplitude compensator so that there appeared to be no signal on the oscilloscope at a field just below that at which a loss waveform was observed. The phase-shifter was then adjusted, at the same field, so that the multiplier output was zero. This technique suffers from two drawbacks. The first is that the point at which losses first appear is not clearly defined, particularly for samples with losses at low field. The second is that because any uncompensated voltage produces loss increasing with the square of the applied field, compensation at low field is not sufficiently accurate. A second, alternative, criterion (Easson and Hlawiczka 1967b) is to adjust the compensators so that $d\phi/dt$ and $d/dt(d\phi/dt)$ are zero at the turning points of the applied field (i.e. $\pm H_m$) where dH/dt is zero. If sheath currents are present then $d\phi/dt$ remains zero over a field interval and this technique is very satisfactory. However, for some of our annealed samples this was not the case, and the compensation was difficult, particularly at low loss levels below H_{cl}.

The technique finally adopted will be described with reference to Fig. 5.4. which shows typical $d\phi/dt$ waveforms. The field was set to about 400 Oe peak and the amplitude and phase-shift of the compensation signal adjusted so that a straight line was present on the oscilloscope screen. If an obvious loss signal was present the field was reduced and the procedure repeated. Then the field was increased until an observable penetration signal appeared. This is characterized by the 'double-lump' appearance of Fig. 5.4.1. The field was further increased until the loss signal was about 40-50 μV peak to peak at the maximum sensitivity of the oscilloscope (1 μV/mm). The loss signal was then, typically, of the form shown in Fig. 5.4.3. The upper trace in this photograph shows an incorrectly compensated loss signal, and the lower trace shows the corresponding field signal. Because the two traces are synchronized an examination of the two signals with respect to each other reveals which compensator requires adjusting. The inductive pick-up coil signal is 90^0 out of phase with the field signal, $H = H_m \sin \omega t$, producing it. An

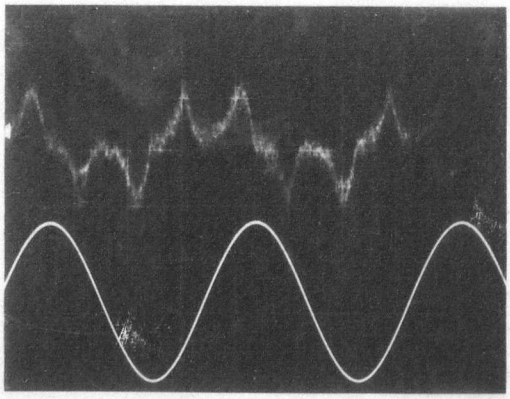

FIG. 5.4.1. Sample 17
78·5 kA (RMS)m^{-1} - 1395 Oe (Peak)

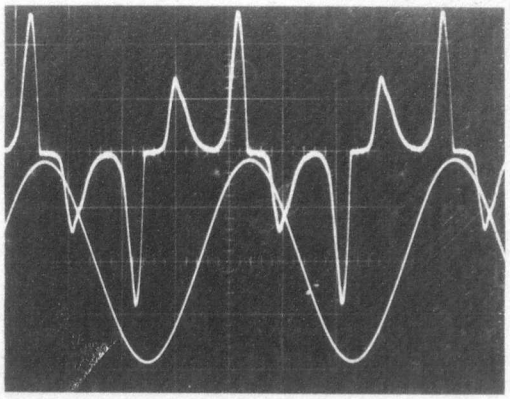

FIG. 5.4.2. Sample 17
89·5 kA(RMS)m^{-1} - 1590 Oe (Peak)

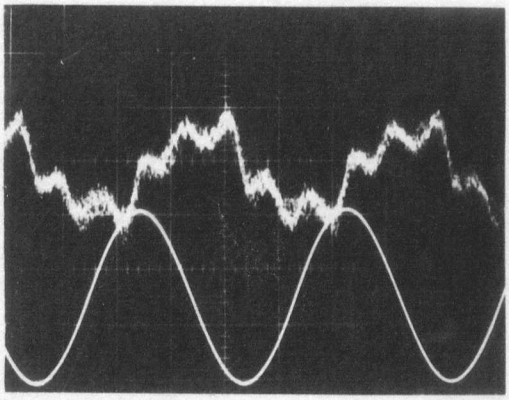

FIG. 5.4.3. Sample 9
82·6 kA(RMS)m^{-1} - 1468 Oe(Peak)

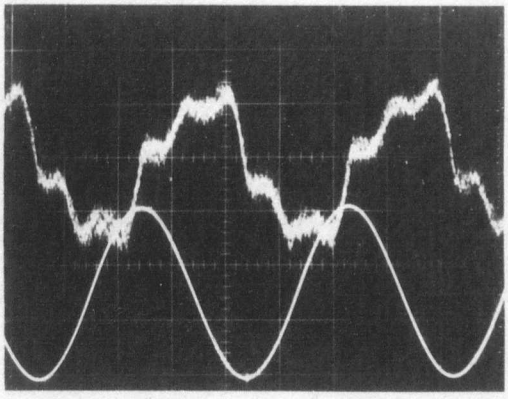

FIG. 5.4.4. Sample 9
82·6 kA(RMS)m^{-1} - 1468 Oe(Peak)

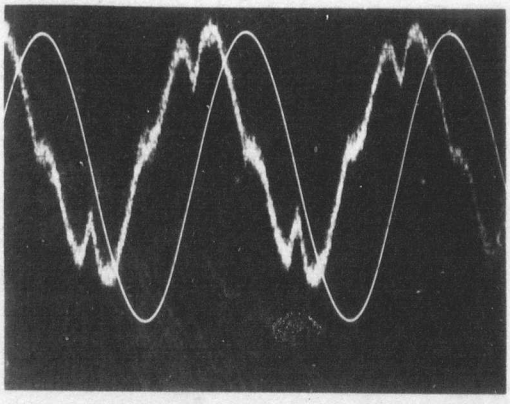

FIG. 5.4.5. Sample 16
30·1 kA(RMS)m^{-1} - 535 Oe (Peak)

Upper Trace : 0·01 mV/ Div.
except FIG.5.4.2. = 0·1 mV/ Div.

Lower Trace : 2 V/Div.
except FIG.5.4.5. = 0·2 V/ Div.

Horizontal : 5 mSec/ Div.

Figure 5.4. $d\phi/dt$ AND H WAVEFORMS.

uncompensated inductive component will, therefore, appear as a sinusoid with maxima where H is zero. On the other hand an uncompensated quadrature signal will appear as a sinusoid with maxima where H is $\pm H_m$. Hence, the difference in height of the kinks at $\pm H_m$ in the $d\emptyset/dt$ waveform shown in Fig. 5.4.4. indicates the presence of an uncompensated quadrature signal. The presence of an uncompensated inductive signal (requiring adjustment of the amplitude compensator) is revealed by the slope of the $d\emptyset/dt$ waveform beyond $\pm H_m$ seen in Fig. 5.4.3. A correctly compensated waveform is shown in Fig. 5.4.1. After this type of signal was obtained, the compensation was always checked at higher fields and a typical waveform is shown in Fig. 5.4.2.

After this initial compensator setting the field was again reduced below the point at which a loss signal was visible, the flatness of the $d\emptyset/dt$ waveform was checked and the compensators adjusted as necessary. The whole procedure was repeated until a satisfactory result was obtained. Compensation was relatively straightforward with signals of the type shown in Fig. 5.4.1. - 4, but for a waveform like that of Fig. 5.4.5. it was much more difficult. Two things were always avoided, firstly, 'negative' losses at low fields, and secondly, crossing of the axis by the $d\emptyset/dt$ waveform between $\pm H_m$. The latter can occur if the amplitude compensator is set incorrectly.

The above technique has been critized by Campbell (1969) on the grounds that 'in-phase' or inductive voltage components are present even when surface currents are shielding the sample from flux penetration. Because the product of two similar sinusoids in quadrature is zero when integrated over a cycle, this in-phase signal will not produce a loss voltage. However, its presence may account for the discrepancies which have been observed by the present author, Linford (1968) and Dunn (private communication) in the 'correct' compensator settings at high and low fields.

Besides setting the compensation, the phase relation between the field signal and the compensated pick-up coil signal must be correctly adjusted. The product of the field signal and a pure inductive signal from the coils must be zero over a cycle (i.e. as seen on the D.C. meter) because they

should be in quadrature (i.e. at 90^{o}). This relationship was obtained exactly by slightly phase shifting the field supply signal to allow for the effects of phase shifts in the amplifiers. The phase shifter was adjusted at about 42 kA(RMS) m^{-1} (400 Oe peak), so that the product of the field signal and the compensation coil signal was equal to the product of the field signal and the grounded-input signal. The compensation coil signal in these conditions is purely inductive, and (apart from loss signals) exactly in phase with the pick-up coil signal. The field and pick-up coil signal are therefore in quadrature, probably to better than 0.1^{o}.

6. MAGNETIZATION AND CRITICAL CURRENT MEASUREMENTS

6.1. Vibrating Sample Magnetometer

The magnetization curves of our samples were measured to obtain values for the critical fields H_{c1} and H_{c2}, and to determine their reversibility, zero-field trapped flux and surface sheath currents. A vibrating sample magnetometer of the type described by Zijlstra (1967) was constructed by Linford (1968), and a modified version of this magnetometer was used for most of the measurements presented in this thesis. It is similar to the magnetometer described by Foner (1959), with the important difference that the direction of vibration in our instrument is parallel to both the field and the sample, whereas in the Foner design the motion is perpendicular to the field.

A block diagram of the apparatus is shown in Fig. 6.1. A magnetic field is applied to the sample by a superconducting solenoid. This was constructed by Oxford Instruments Ltd., has a bore of 30 mm and produces a maximum field of 3 Tesla. Current is supplied by an Oxford Instruments 30A power supply controlled by a variable rate (30 sec. to 30 min. full sweep time) sweep unit. The sample is vibrated along the axis of the solenoid at the end of a thin-walled, stainless-steel tube by a Pye-Ling vibrator and power amplifier. The oscillating dipole field of the sample induces voltages in two identical, pick-up coils located at either end of the sample and co-axial with both the sample and the solenoid. These coils are connected in the same sense to a differential amplifier so that the voltages induced by the sample are added, but voltages induced by other alternating fields are cancelled. A phase-sensitive detector measures the output of the amplifier. This type of detector is fed with a reference signal, and produces a d.c. output V_0 given by

$$V_0 = V_I \cos \theta$$

where V_I is the r.m.s. value of the component of the input signal at the

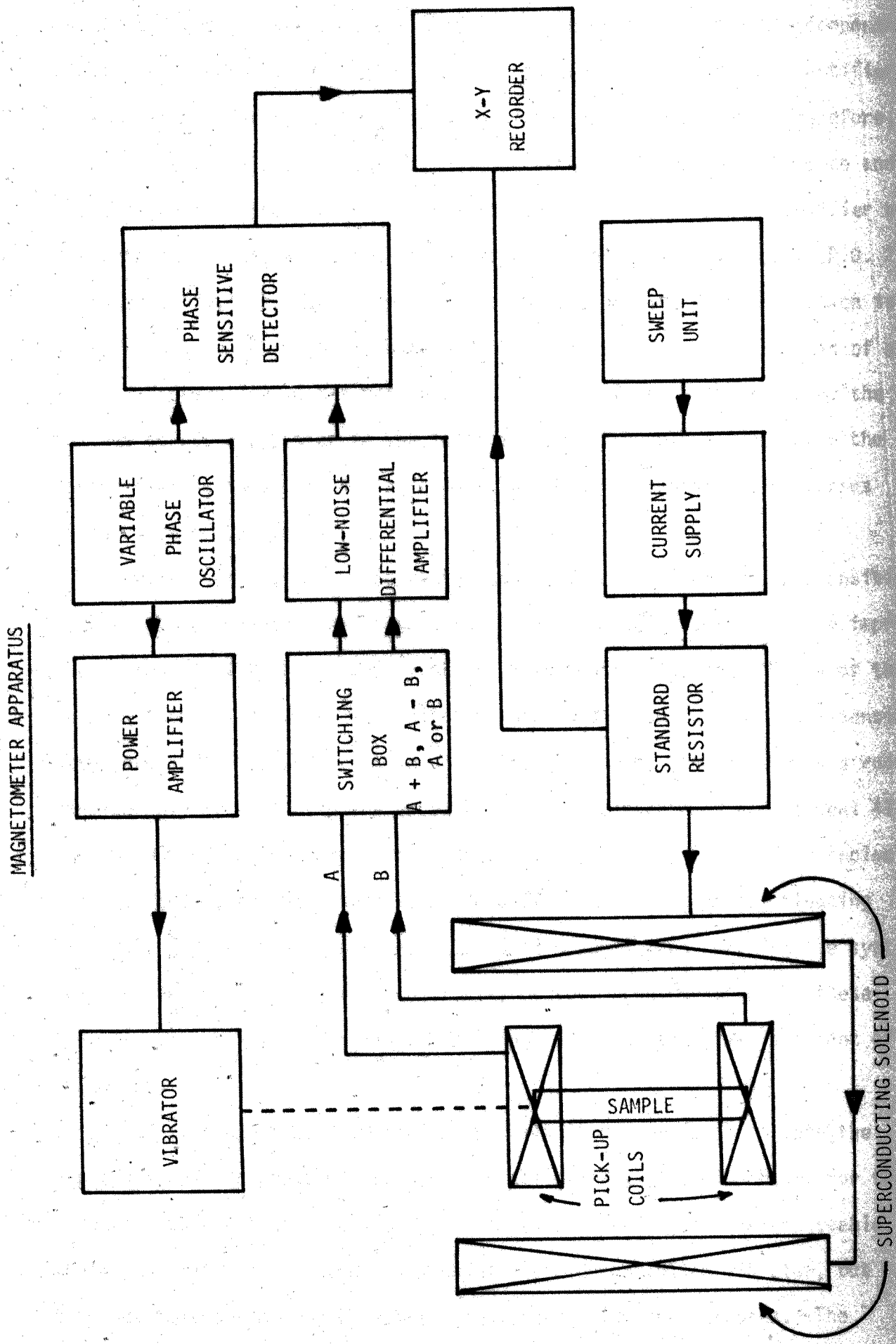
MAGNETOMETER APPARATUS
X-Y RECORDER
PHASE SENSITIVE DETECTOR
SWEEP UNIT
VARIABLE PHASE OSCILLATOR
LOW-NOISE DIFFERENTIAL AMPLIFIER
CURRENT SUPPLY
POWER AMPLIFIER
SWITCHING BOX A + B, A - B, A or B
STANDARD RESISTOR
A
B
VIBRATOR
SAMPLE
PICK-UP COILS
SUPERCONDUCTING SOLENOID

FIGURE 6.1.

frequency of the reference, and θ is the phase angle between this component and the reference signal. This detector is superior to a simple rectifier because it can detect a change in sign of the input signal and, therefore, of the magnetization. To ensure phase coherence between the reference and input signals to the detector, the input to the vibrator power amplifier and the reference voltage are both supplied from the same oscillator (V.P.O. 230 - Feedback Ltd.). The d.c. output of the phase-sensitive detector, which is proportional to the magnetization of the sample, is fed to the Y-axis of a Hewlett-Packard 7000 A X-Y recorder, the X-axis of which is driven by the voltage across a resistor in the solenoid current supply. Thus, when the magnet current is swept, the recorder plots out the magnetization versus field curve of the sample.

Modifications were made to the magnetometer to increase the sensitivity with which the surface sheath magnetization could be measured, and to improve the reproducibility and accuracy of the instrument. The sensitivity of the magnetization measurement is limited by the noise input to the phase-sensitive detector, and noise and drift in the detector output. The latter were reduced considerably by replacing the Brookdeal PM.322a detector by a Brookdeal 411. The common-mode noise rejection of the whole system was improved by replacing a single-ended, earthed amplifier by a differential, low-noise, floating amplifier (CR4 - Princeton Applied Research Corpn.), and earthing the system only at the oscillator. The sensitivity of the magnetometer after these changes was about 10 Am^{-1} (12μTesla) using an integrating time constant of 100 msec.

Since the output of the pick-up coils is proportional to both the amplitude and frequency of the sample oscillations, it is important for the accuracy and reproducibility of the magnetometer that these remain stable. Their stability can be ensured by using a servo-controlled vibrator, but this was felt to be an unnecessary complication for our purposes. The stability of the system was, however, improved by substituting the V.P.O. 230 oscillator, which is amplitude and frequency stable to 0.1%, for the original

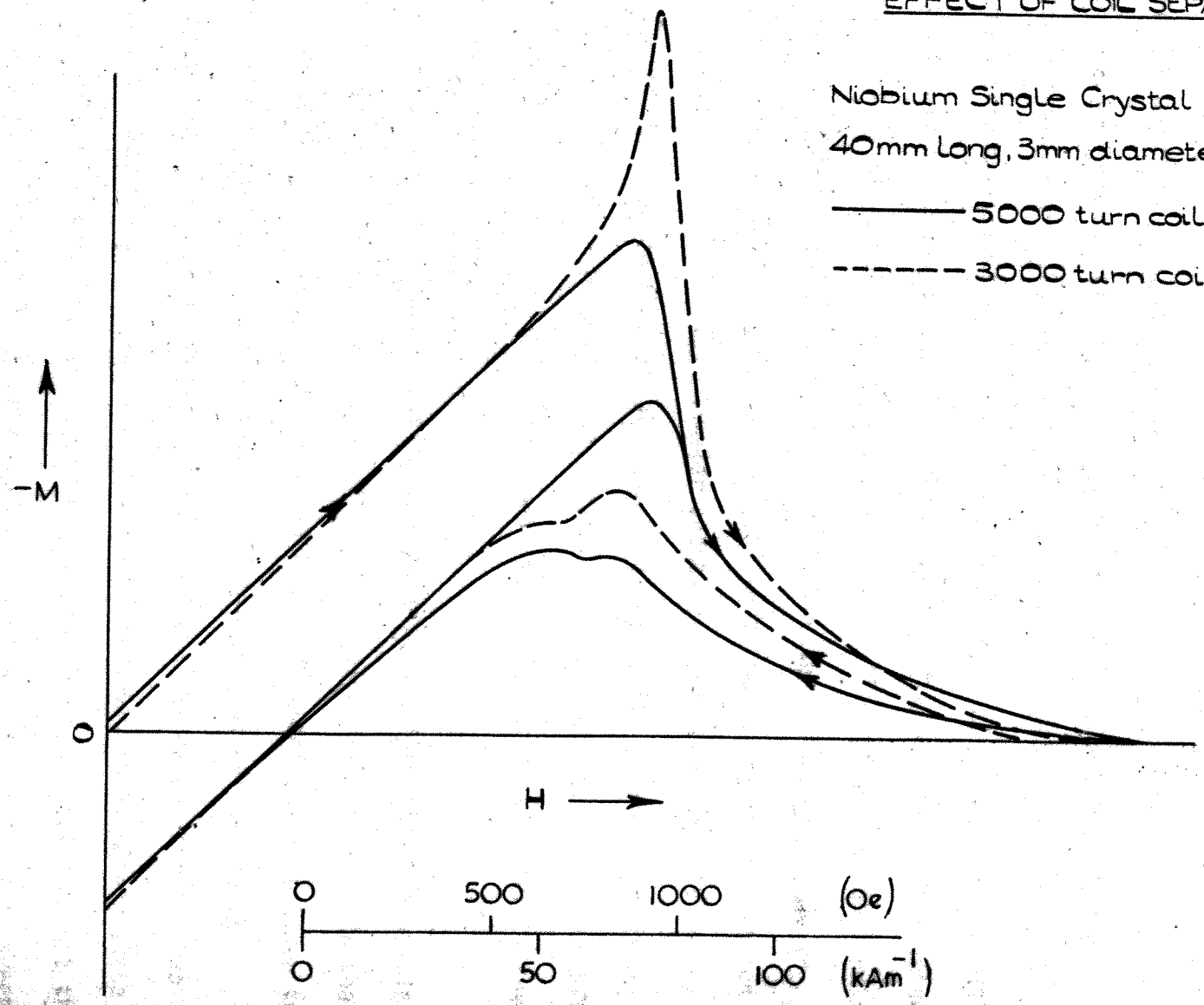
EFFECT OF COIL SEPARATION.
Niobium Single Crystal - Sample 7
40mm long, 3mm diameter, Annealed, Polished.
5000 turn coils, 26mm sepn.
3000 turn coils, 38mm sepn.
-M
0
H
0
500
1000
(Oe)
0
50
100
(kAm⁻¹)

Figure 62

one. The mechanical oscillation was also improved by substituting a P.T.F.E. sample holder for a tufnol one, and taking care to prevent ice forming on the sliding surfaces while changing samples.

Another fault of the original instrument is illustrated in Fig. 6.2. This shows the magnetization curve of an annealed, niobium single crystal 40 mm long. The broken curve was drawn using the original, 5000-turn, pick-up coils 26 mm apart, and the solid curve using the 3000-turn coils 38 mm apart with which they were replaced. The apparent increase in diamagnetism near H_{c1} on the broken curve probably arises from flux penetration near the sample ends. Because the ends of a 40 mm sample will project beyond coils separated by 26 mm, the polarity of the voltage induced in a coil by the sample ends will be opposite to that induced by the centre. Hence flux penetration at the ends will produce an apparent increase in diamagnetism if, as is likely near H_{c1}, it takes place before penetration of the centre of the sample. Similar anomalies have been observed in the surface sheath region (between H_{c2} and H_{c3}) when coils separated by 26 mm were used. The drop in sensitivity which resulted from the use of the 3000-turn in place of the 5000-turn coils was adequately compensated for by the absence of these effects.

Fig. 6.3, shows the magnetization curve of a polycrystalline sample (8) taken on two different occasions at an interval of two months. On the first occasion the frequency of oscillation was 85 Hz and the time taken to sweep between zero and maximum field was 10 minutes; on the second, the frequency was 63 Hz and the sweep time 5 minutes. The curves for the two cases are practically identical. The small differences in the mixed state may be sweep rate effects. The results shown in Fig. 6.3. indicate that the magnetometer results are virtually independent of small variations in sweep-rate, frequency and sample alignment.

In operation, a sample was placed in the holder and inserted in the cryostat with no current flowing in the solenoid. Care was taken to prevent ice formation, and the top of the cryostat was sealed by an O-ring and

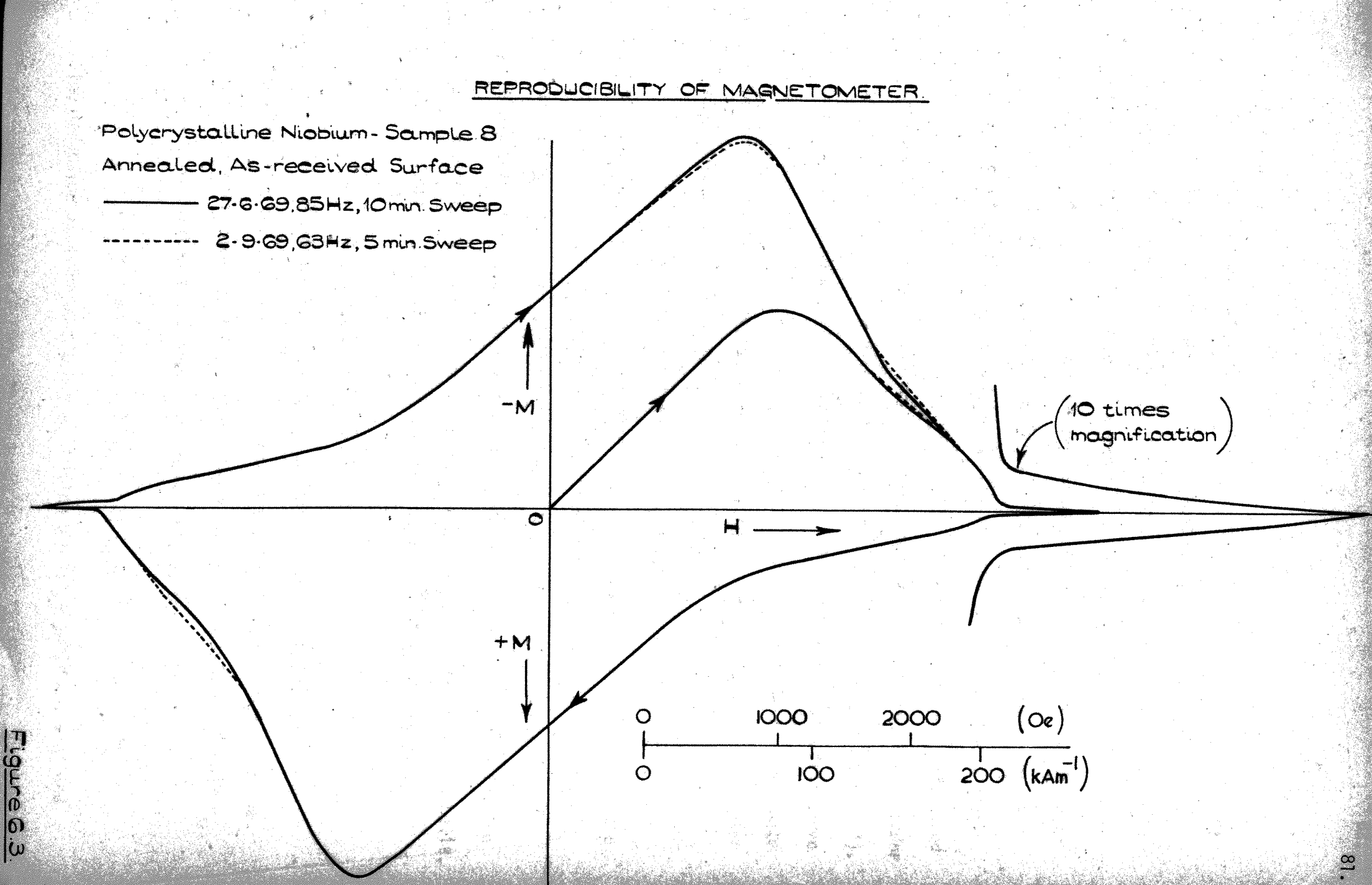
REPRODUCIBILITY OF MAGNETOMETER.
Polycrystalline Niobium - Sample 8
Annealed, As-received Surface
27-6-69, 85Hz, 10min. Sweep
2-9-69, 63Hz, 5 min. Sweep
-M
+M
H
0
(10 times magnification)
0
1000
2000
(Oe)
0
100
200
(kAm⁻¹)

Figure 6.3

flexible bellows between the top-plate and vibrator rod. After insertion, the magnetic field was increased to a low value and the vibrator was switched on. The position of the sample relative to the two pick-up coils was then adjusted over a range of about 5 mm so that the signals from the two coils after subtraction gave zero output. The position of the vibrator was also adjusted to give the maximum, undistorted output signal, and the phase of the oscillator supply to the vibrator was set so that the phase-sensitive dctector gave the maximum output. The magnetometer was calibrated by slowly sweeping the field up, and adjusting the Y-gain of the X-Y recorder so that the slope of the diamagnetic curve was 45^{o} (i.e. the gradient was 1). The accuracy of this setting was about ± 1%. The virgin magnetization curve was usually repeated after the setting-up procedure. To do this, the sample was driven normal by passing a current through a small, copper, heating coil wound on the sample-holder.

In spite of its sensitivity, reproducibility and simplicity, the vibrating sample magnetometer suffers from a number of disadvantages related to penetration at the sample ends which make the interpretation of bulk sample properties, especially the value of H_{c1}, difficult. To overcome this problem and to enable consecutive measurement of loss and magnetization to be made in the same cryostat, an integrating sample magnetometer was built. This is described in Brankin, Eastham and Rhodes (1970) (see Appendix).

6.2. A.C. Permeability of Superconductors

When an alternating field, $h = h_m \sin \omega t$, is applied to a superconductor in the presence of a steady magnetic field, H, a voltage will be induced in a pick-up coil wound about the sample. For a coil of N turns and area A_1 surrounding a sample of area A this voltage will be

$$V = -NAdb/dt - N(A_1 - A)\,\mu_0\, dh/dt$$

The induction b in the sample may be written $b = (\mu' + i\mu'')h$ where μ' and

μ'' are the real and imaginary components respectively of the magnetic permeability of the superconductor at the field H. Hence, V will be given by

6.2.1. $$V = -NAd|(\mu' + i\mu'')h|/dt - N(A_1 - A)\,\mu_o\, dh/dt$$

Measurement of the amplitude and phase of V will give μ' and μ''. The induction in the sample may also be expressed as a Fourier series (as in section 5.4. p.64) in which case the coil voltage may be expressed as :

6.2.2. $$V = -NAn\omega h_m \sum_{n=1}^{\infty} | \mu_n' \cos n\omega t - \mu_n'' \sin n\omega t |$$

where μ_n' and μ_n'' are the Fourier components of the real and imaginary permeabilities and the term $N(A_1 - A)\,\mu_o\, dh/dt$ produced by the leakage flux has been omitted. Measurement of the amplitude and phase of the various frequency components of V will give μ_n' and μ_n''.

Measurement of V and derivation of the different components of μ from equations 6.2.1. and 6.2.2. have been used by Bean (1964), Ullmaier (1966), Rollins and Silcox (1967), Brankin (1968), Campbell (1969) and others to obtain information about the flux distribution and critical currents in superconductors. In general, such measurements are difficult to interpret. The permeabilities depend not only on the magnitude and frequency of the a.c. field and the magnitude of the d.c. field, but also on the metallurgy of the bulk material and the surface of the sample. The loss measurement techniques described in sections 5.3. and 5.4. are examples of permeability measurements, and although only the fundamental component of the permeability, μ_1'', is measured and no steady field is present the results are very complex (see chapter 4).

In principle, the surface critical current, $j_c(H)$, may be obtained very easily by permeability measurement. If the applied a.c. field, h, is less than j_c it will not alter the flux within the superconductor, but only induce an alternating surface current equal to h. Hence the voltage in the pick up coil will be zero until h exceeds j_c, which can be defined

as the induced surface current at which a voltage is first detected. A permeability apparatus was originally built to measure j_c in this way. Unfortunately, as in the case of the loss measurement, the voltage from the pick-up coil is never zero because of the leakage flux, which induces a voltage equal to $N(A_1 - A)\ \mu_o\ dh/dt$ (Equation 6.2.1.) in the coil. This voltage can be reduced by compensation, but it is still difficult to detect the point at which the permeability becomes zero (see chapter 10). The problem can be overcome by developing a model (e.g. Fink 1967) for the magnetic behaviour of the superconductor in terms of j_c, and using this to predict values of μ_n' and μ_n'' at particular values of j_c. This technique has been used by the author (Brankin 1968) and others (e.g. Rollins and Silcox 1967), to obtain values of the critical currents in the Saint-James, DeGennes sheath above H_{c2}.

In the mixed state, the magnetic behaviour of the superconductor also depends on its bulk properties, and the permeability can be calculated from the models developed in section 3.4. Since some of these models contain both the bulk and surface critical currents as parameters, values of J_c and j_c can be derived from measurements of μ. This is a valuable method of measuring J_c under a.c. conditions, and it was adopted for our experiments. Two methods of analysis were employed. The first used the Ullmaier (1966) expression for the losses in superconductors. The second method was developed by Campbell (1969). His technique enables the flux distribution within the superconductor to be measured directly. The bulk and surface critical currents can then be obtained from the flux profile.

Ullmaier's (1966) modified version of Bean's (1964) expression for the loss is given in equation 4.4.2. namely

$$L = \frac{2}{3}\ \frac{\mu_o}{J_c}\ (h_m - \frac{\Delta H}{2})^3$$

Equation 5.4.1. shows that the loss is also given by

$$L = \frac{A}{2\pi r}\ \pi\mu_1''\ h_m^2$$

where for a cylinder $A = \pi r^2$.

Combining these equations we obtain

6.2.3. $$\mu_1'' = \frac{4}{3r\pi} \frac{\mu_o}{J_c} (h_m - 3j_c)$$

where $\Delta H/2$ has been taken as being equal to j_c.

Hence, values of J_c and j_c may be obtained from measurements of μ_1'' as a function of h_m.

In Campbell's method, the conventional permeability apparatus described in section 6.3. is used, but a wide-band amplifier preceeds the phase-sensitive detector in place of the narrow band amplifier employed when measuring the component permeabilities μ_1' and μ_1''. Campbell (1969) shows that if the detector is of the full-wave type (e.g. the Brookdeal 411), it can be regarded as a switch which inverts the sign of the input signal, V, when the reference signal changes sign. If this occurs at $\omega t = \theta$. the output is

6.2.4. $$\frac{\omega}{2\pi} \left| \int_o^{\theta} V dt - \int_{\theta}^{\theta + \pi} V dt + \int_{\theta + \pi}^{2\pi} V dt \right| = \frac{\omega}{2\pi} N\alpha \left| \phi(\theta) - \phi(\theta + \pi) \right|$$

where ϕ is the flux which has crossed the specimen boundary, N is the number of turns on the pick-up coil and α is the amplification factor of the electronics. Hence, if the 'in-phase' inductive signal is measured, i.e. the reference is set in quadrature with the field, the output, V_0, is proportional to the flux in the sample at the peaks of the a.c. field.

When a small a.c. field, $h = h_m \sin \omega t$, is applied to an irreversible superconductor in the mixed state, variations to a depth d will take place in the critical state in the sample where, on the Bean-London model, $dJ_c = h_m$. Provided the oscillation is small enough for J_c to independent of H over the amplitude of the a.c. field, the extra flux introduced into the sample at the peaks of the field when its amplitude h_m is increased by δh_m is given by

$$\delta\phi = \mu_o(\pi r^2 - \pi x^2)\delta h_m$$

where r is the sample radius and x (equals r - d) is the radius to which the critical state is altered. Hence

$$\frac{d\phi}{dh_m} = \mu_o(\pi r^2 - \pi x^2)$$

and since, from equation 6.2.4., the 'in-phase' voltage $V_o = 2\omega N\alpha\phi/2\pi$ then

$$\frac{dV_o}{dh_m} = \frac{\alpha\omega N}{\pi}\frac{d\phi}{dh_m} = \mu_o\alpha\omega N(r^2 - x^2)$$

i.e.

$$\frac{dV_o}{dh_m} = C\left|1 - \left(\frac{x}{r}\right)^2\right|$$

where $C = \mu_o\alpha\omega N r^2$

Therefore the penetration depth d (equals r - x) is given by

6.2.5. $$r\left|1 - \left(1 - \frac{1}{C}\frac{dV_o}{dh_m}\right)^{\frac{1}{2}}\right| \approx \frac{r}{2C}\frac{dV_o}{dh_m} \qquad d \ll r$$

Hence, if V_o is measured as a function of h_m, the gradient, dV_o/dh_m, at a given value of h_m gives the depth d to which that field penetrates. A graph of h_m against d shows the flux profile within the sample.

The apparatus built to make these a.c. permeability measurements is described in the next section.

6.3. Apparatus

A block diagram of the electronics used for the permeability measurements is shown in Figure 6.4. A similar apparatus has been described in detail by the author elsewhere (Brankin 1968 pp.37 - 52). Rollins and Silcox (1967) and Campbell (1969) have described similar equipments.

A d.c. field is applied to the sample by an Oxford Instruments, 3 Tesla, 30 mm bore, superconducting solenoid, driven from a B.O.C. 60A current supply which is stable to 0.1% and has a very low ripple content.

ELECTRONICS FOR A.C. PERMEABILITY MEASUREMENTS

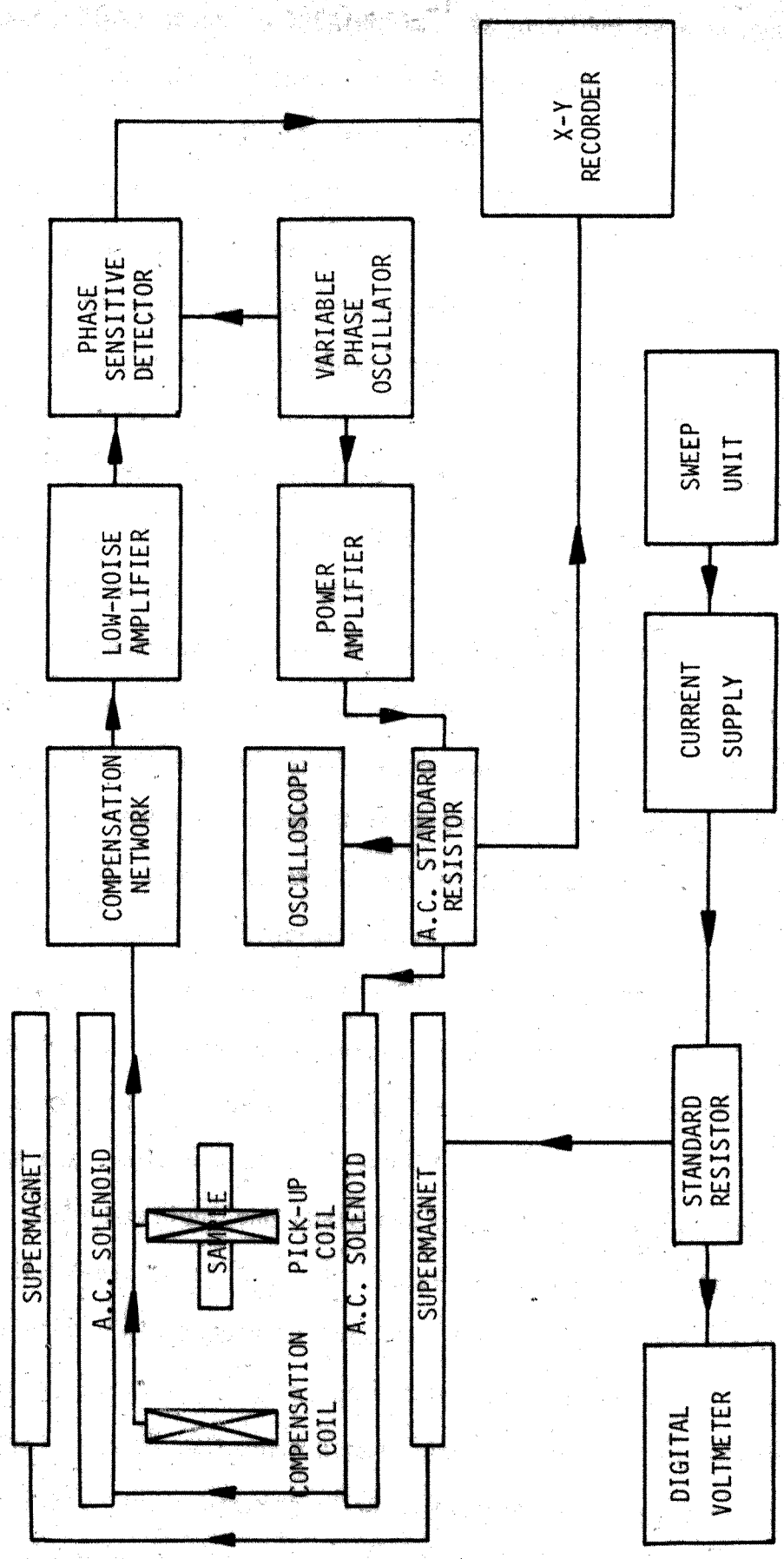

FIGURE 6.4.

10⁵ of the signal from either coil alone.

An a.c. field of up to 15kA(RMS)m^{-1} is provided by a second solenoid. This consists of 1400 turns, in a double layer, of 40 S.W.G. enamelled copper wire, wound on a tufnol coil former to avoid the eddy currents which arise if a metal is used. The former is a good fit on the super-magnet bore, and the axes of the two solenoids are parallel to $\pm 0.1^{0}$. Current for the a.c. field is provided by a Derritron 100W power amplifier driven from the variable phase output of a V.P.O. 230 (Feedback Ltd.), variable-phase oscillator.

The pick-up and compensation coils each consist of 1000 turns of 46 S.W.G., copper wire wound on a nylon sample holder. The compensation coil is 40 mm above the pick-up coil. Signals from both coils are fed to the compensator used for the a.c. loss measurements (section 5.4.), in which the amplitude voltage divider is modified to provide the extra compensation signal required by the large, poorly-filled, pick-up coil. The output from the compensator is taken to a Princeton Applied Research Corpn., CR-4, low-noise amplifier which has an adjustable bandwidth. The amplifier output is phase-sensitive detected by a Brookdeal 411, references for which are supplied from the 0^{0} and 90^{0} outputs (which are in quadrature) of the variable-phase oscillator. The output of the detector drives the Y-axis of an X-Y recorder, whose X axis is fed from a standard resistor in the a.c. solenoid current supply.

In operation, the phase and compensator settings were first checked at a low field below H_{c1}. The phase was set by adjusting the phase of the oscillator field supply so that the detector gave zero output when the compensation-coil signal alone was measured using the 0^{0} reference signal. The field and 0^{0} reference signal phases were then in quadrature within about 0.2^{0}. The compensators were adjusted at large a.c. field amplitude so that the compensated pick-up coil voltage gave zero output from the detector using either reference signal, the amplitude compensator being adjusted using the 90^{0} reference and the phase-shift using the 0^{0} reference. The compensated pick-up coil voltage could thus be reduced to one part in 10^{5} of the signal from either coil alone.

After these adjustments, the phase setting was rechecked and the compensated voltage was measured as a function of the a.c. field to provide a zero line for the measurements at higher fields in the mixed state. Then the d.c. field was increased to the desired measuring field and a plot was made of the required component of the compensated pick-up coil voltage as a function of the a.c. solenoid current. The 90^{o} reference was used to measure the in-phase signal, and the 0^{o} reference to obtain the quadrature signal. The low-noise amplifier bandwidth was adjusted to measure either the fundamental component of the permeability only, or the wide-band value. Measurements were taken in progressively increasing d.c. fields because it was found that the results depended on the way the field was produced (e.g. either by sweeping up or down) and on whether the sample had been previously exposed to a higher field. The phase and compensator settings were checked at low field between the measurements at each of the high field settings.

6.4. Measuring Techniques for the Radioactive Sample

Loss and magnetization measurements were made on a single crystal of niobium which had been exposed to a fast neutron flux of 4.6×10^{17} neutrons m^{-2} s^{-1} for 28 days. The total fast neutron dose was 9.7×10^{23} m^{-2}. After irradiation its activity was measured at AERE-Harwell as about 120 millicuries. It produced about 1 Rad/hr of ionizing radiation at 50 mm of lead, 500 mRads/hr at 0.3 m in air and less than 1 mRad/hr at 3 m in air.

For safety all the measurements on this sample were made at a range of greater than 4 m. During the magnetization measurements the vibrator power amplifier was left near the cryostat and was fed via a 3 m co-axial lead from the variable-phase oscillator. Similarly, the low-noise amplifier was left close to magnetometer, and its high level (±5V Peak) output was taken along a second, 3 m, co-axial cable to the detector. This procedure was not possible in the case of the loss measurements because of

the need to switch ranges on the oscilloscope coil-signal amplifier. The coil signals were, therefore, transmitted directly along twin, 3 m, co-axial links, with the result that these voltages had both a considerably higher noise level than usual and extra phase shifts. Current was supplied to the a.c. solenoid for the loss measurement and to the superconducting solenoid for the magnetometer through four 30 A braids of copper insulated by P.V.C. piping.

Extreme care was taken in loading the sample into the cryostats. It was handled using 1 m long tongs, and the probes were lowered into the cryostats from a similar distance. All leads were connected and filling was completed before the sample was removed from its lead transport flask. Because of its activity, a coil could not be wound on the sample for loss measurement. Instead, it was mounted in a thin (0.1 mm) walled, close fitting, tufnol coil former carrying a 140 turn coil of 46 S.W.G. copper wire. This coil gave rise to a 100 times larger than normal leakage-flux voltage because of the poor filling factor. As a result of this and the extra noise in the coil signals mentioned earlier, correct compensation was more difficult to achieve. Consequently, the lowest level at which satisfactory loss measurements were obtained was 10^{-3} WHz^{-1} m^{-2}.

7. SAMPLE PROPERTIES

7.1. Introduction

The following three chapters contain an account of the results obtained from our experiments. For clarity, all the descriptions of sample preparation and the measurements of sample properties, such as the magnetization curves and surface profiles, have been grouped together in Chapter 7. Chapters 8 and 9 contain discussions of the loss measurements. For convenience, the descriptions and properties of all the samples are summarized in Tables 7.1. and 7.2. respectively.

The superconducting properties of niobium may be severely modified by the presence of interstitial impurities (Desorbo 1963) and cold work (Narlikar and Dew-Hughes 1964). The published results summarized in Chapter 4 show that the a.c. losses are particularly affected by the metallurgical conditions of the specimen. It is necessary therefore, when making comparisons between measurements on different samples, to ensure that the initial properties of the samples are similar.

To this end, our early measurements were made on niobium single crystals prepared by electron-beam, zone melting. However, it was found that the properties of single crystals are also strongly affected by their purity, orientation and detailed preparation. Because of difficulties in preparing our own single crystals, their use was abandoned.

A second approach to the problem is to use starting material from a single source and treat all samples in the same way. Therefore, although some results were obtained using single crystals, the majority of our measurements were made on samples taken from the same batch of commercial polycrystalline niobium. This latter material was obtained from Murex Ltd. in rods of 3 mm diameter. The niobium was electron-beam melted, and then swaged and centre-less ground to size. The as-received rods were heavily cold worked, and had fairly smooth (C.L.A. about 1 μm - see section 7.3.), matt surfaces. Some later measurements were made on a second batch of niobium

SAMPLE DESCRIPTIONS

Sample No.	Source	Diameter [1]	Surface	TREATMENT: Heat	TREATMENT: Other
4 X [2]	Birmingham	5 mm	Chemical Polish	-	Neutron Irradiation
6 X	Birmingham	5 mm	Mechanical Polish	-	-
7 X	Oxford	3 mm	Electropolish	2500°C, 10^{-10} torr	-
8 [3]	Murex 1	3 mm	As Received	24 hrs, 1100°C, $<10^{-4}$ torr	-
9	Murex 1	3 mm	As Received	-	-
10	Murex 1	3 mm	As Received	24 hrs, 900°C, 10^{-5} torr	-
30	Murex 2	3 mm	As Received	1 hr, 900°C, $<10^{-5}$ torr	-
11	Murex 1	3 mm	Spark Energy 3	48 hrs, 1100°C	Furnace Failure
12	Murex 1	2.9 mm	Spark Energy 5	48 hrs, 1100°C, $<10^{-4}$ torr	-
13	Murex 1	2.9 mm	Spark Energy 7	48 hrs, 1100°C,	Furnace Failure
14	Murex 1	3.0 mm	Chemical Polish	48 hrs, 1100°C, $<10^{-4}$ torr	-
15	Murex 1	2.93 mm	Spark Energy 7 only	-	-
16	Murex 1	2.90 mm	Spark Energy 3,5,7	-	-
17	Murex 1	2.96 mm	Chemical Polish	-	-
29	Murex 2	2.7 mm	Spark Energy 1	10 hrs, 1100°C, $<10^{-5}$ torr	-
23	Murex 1	2.8 mm	Spark Energy 3	10 hrs, 1100°C, $<10^{-5}$ torr	-
24	Murex 1	2.7 mm	Spark Energy 5	10 hrs, 1100°C, $<10^{-5}$ torr	-
25	Murex 1	2.7 mm	Spark Energy 7	10 hrs, 1100°C, $<10^{-5}$ torr	-
26	Murex 1	2.9 mm	Electropolish	10 hrs, 1100°C, $<10^{-5}$ torr	-
27 [4]	Murex 1	2.8 mm	Electropolish		Ion-implantation
31	Murex 2	2.8 mm.	Mechanical Polish	4 hr, 1100°C, $<10^{-5}$ torr	-

(1) All samples were 40 mm long and, except for the single crystals, had ellipsoidal ends produced by spark machining.

(2) X indicates a single crystal.

(3) 1 and 2 indicate the first and second batches respectively.

(4) Vertical brackets indicate one group of samples.

TABLE 7.1.

SAMPLE PROPERTIES AT 4.2K

Sample No.	H_{c1} kAm^{-1}	H_{c1} KOe	H_{c2} kAm^{-1}	H_{c2} KOe	$B_T(o)$ Tesla[1]	C.L.A. μm
4	105	1.32	290	3.65	0.311	-
6	-		253	3.20	0.113	-
7	111	1.41	221	2.78	0.044	-
8	104	1.31	273	3.45	0.163	1
9	-		307	3.85	0.313	1
10	110	1.37	242	3.05	0.117	1
30	-		233	2.95	0.166	0.9
11	72	0.90	352	4.40	0.205	3.1
12	-		250	3.15	0.177	-
13	-		292	3.67	0.205	-
14	-		262	3.30	0.161	-
15	-		295	3.70	0.290	0.35
16	-		295	3.70	0.304	1.1
17	-		295	3.70	0.304	-
29	-		235	2.95	0.194	5.0
23	-		232	2.90	0.182	3.3
24	-		232	2.90	0.182	1.45
25	-		232	2.90	0.152	0.33
26	108	1.36	228	2.86	0.004	0.3
27	107	1.34	232	2.90	0.008	0.3
31	-		239	3.00	0.060	0.22

1 $B_T(o)$ is the zero-field trapped flux density.

The Figures given are those measured <u>after</u> sample treatment.

TABLE 7.2.

manufactured by Murex. Little difference between the two batches was detected in our measurements. Table 7.1. gives a complete list of the samples used, their sources, sizes and treatments.

As a further means of ensuring the comparability of our measurements on different samples, only one parameter, e.g. the surface roughness, was varied at a time in so far as possible. A group of samples (usually four) was cut from the same rod of niobium, and each was then given the same treatment, apart from that required to change the parameter under investigation. A different parameter was varied for each group of samples. The following sections contain descriptions of each of these groups, and of some specimens, including the single crystals given individual treatments.

7.2. Heat-Treated Samples

Three samples, Nos. 8 to 10, cut from the same rod of niobium together with a fourth, No.30, from the second batch were used to observe the effect of annealing the cold-worked material for different times and at various temperatures. Sample 9 was untreated and the others were given the heat treatments shown in Table 7.1. The magnetization curves of the samples are shown in Fig. 7.1. and their grain structure in Fig. 7.2. Table 7.3. gives a mass spectrographic analysis of a section cut from the end of and treated with samples 8 and 10, and a section from the as-received sample 15 which is similar to 9.

The heat treatments were carried out in recrystallized-alumina crucibles in a Metals Research, 2" diameter, 'Vacseal' furnace. This has a 'Mullite' furnace tube which is silicone rubber-sealed to stainless-steel end caps, enabling the tube to be easily evacuated. The furnace is pumped by a 2", Edwards, oil-diffusion pump with a baffle valve and liquid-nitrogen trap, capable of reducing the pressure, measured by a Birvac Penning gauge at the end of the tube, below 10^{-5} torr. The furnace tube is capable of operating at up to 1400°C but the 'Kanthal' heater winding is only usable up to 1200°C. The hot-zone of the furnace is uniform to about ± 0.2% over the central 150 mm of the tube.

Two problems were encountered in the initial operation of this furnace.

ANALYSIS REPORT FROM UNIVERSITY OF BIRMINGHAM CENTRE FOR MATERIALS SCIENCE

Mass Spectrographic analysis of Niobium samples 29.10.69.

ELEMENT	IMPURITY CONCENTRATION (p.p.m. atomic)		
	Sample 8, 24 hrs, 1100°C, $<10^{-4}$ torr	Sample 10, 24 hrs, 900°C, 10^{-5} torr	Sample 15 (as sample 9) As-Received
W	1.5	1.5	1.5
Ta	30	30*	30
Mo	0.8	0.8	0.8
Br	0.6*	3	0.6*
Ni	0.75	3	0.45*
Fe	0.3*	0.2*	3*
Cr	1.2	0.1*	0.2*
Ca	1	0.2	0.5*
K	10*	5	3*
Cl	1.3*	0.3	0.4*
S	2.1*	0.5	0.3*
Si	11	5	3*
Na	20*	30	30*
F	30*	3	2*
O	300	50	200
N	10	5	5
C	500	75	50
B	0.4	4	1.2

Only elements with concentrations greater than 1 p.p.m. included

* Denotes impurity distributed inhomogeneously.

F is possibly contamination from the etch. Au, P, Be and Li could not be detected because of interference from other ions.

TABLE 7.3.

The first was contamination of specimen surfaces by material from the walls and the nickel radiation shields; the second was a high concentration of oxygen and carbon in the annealed samples (e.g. No.8, Table 7.3.). The contamination was reduced by baking out the furnace in air at 1100°C for 24 hours to oxidize any deposits on the walls, and by then repeating the bake with radiation shields and crucible in place under a vacuum of 10^{-5} torr. The vapour pressure of nickel is about 10^{-5} torr at 1200°C (Smithell 1967), so care was taken to ensure that the radiation shields were outside the hot zone. At a later stage, the nickel shields were replaced with tantalum.

The oxygen and carbon content of the samples was found to depend on the vacuum maintained in the furnace during annealing. When the vacuum was kept low, the interstitial impurity content was low. Lower annealing vacuums were achieved by the bake-out already described, which was repeated before each anneal. However, it was found that the most important requirement was to keep the liquid-nitrogen trap full throughout the anneal. This was not done in the case of sample 8 and the annealing pressure rose about 10^{-5} torr. As a result, the oxygen and carbon contents (Table 7.3.) are 300 and 500 p.p.m. respectively, and the H_{c2} value is 273 kAm^{-1} (3450 Oe) as opposed to that of about 233 kAm^{-1} (2950 Oe) for sample 30 annealed at $<10^{-5}$ torr.

Annealing produces two distinct metallurgical changes which have rather different effects on the superconducting behaviour of a sample. As already mentioned, one of these is to alter the concentrations of interstitial impurities such as oxygen and nitrogen. De Sorbo (1963) and Tedmon et al (1964) have measured the effects of these impurities on the superconducting properties of niobium and, in general, it was shown that an increase in the dissolved impurity concentrations reduces the electron mean free path. This produces an increase in the resistivity, ρ, and the Ginzburg-Landau parameter, κ. The thermodynamic critical field, H_c, is not, however, greatly affected and the effect of the changes on the magnetization curve is to reduce H_{c1} and increase H_{c2}. If the impurity concentration increases but the impurities remain in the form of second-phase precipitates, then the value of κ may not

HEAT-TREATED SAMPLES

Polycrystalline Niobium, As Received Surfaces.

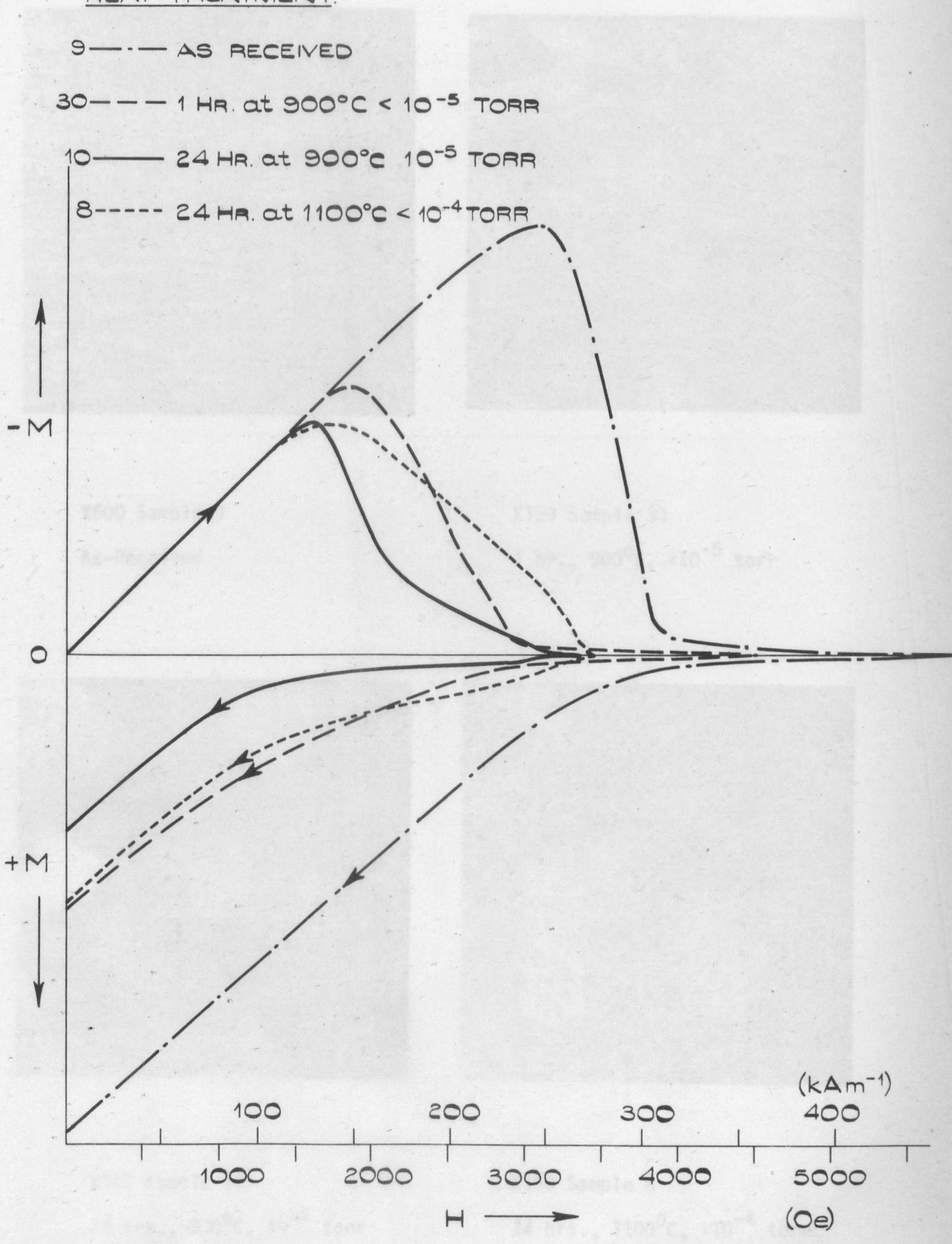

Figure 7.1.

GRAIN STRUCTURE OF ANNEALED SAMPLES

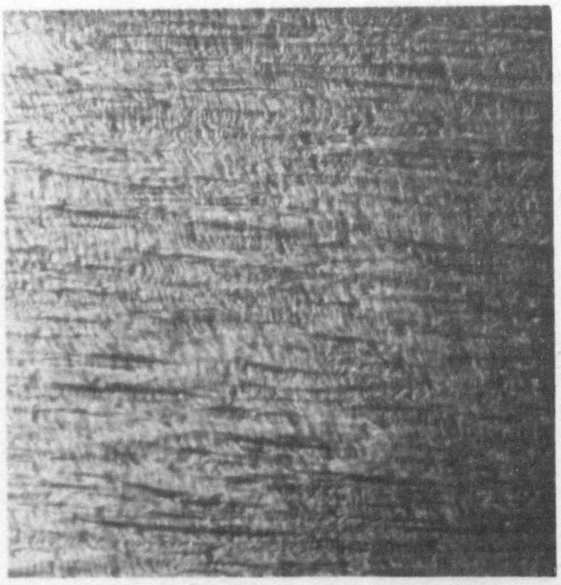

X600 Sample 9

As-Received

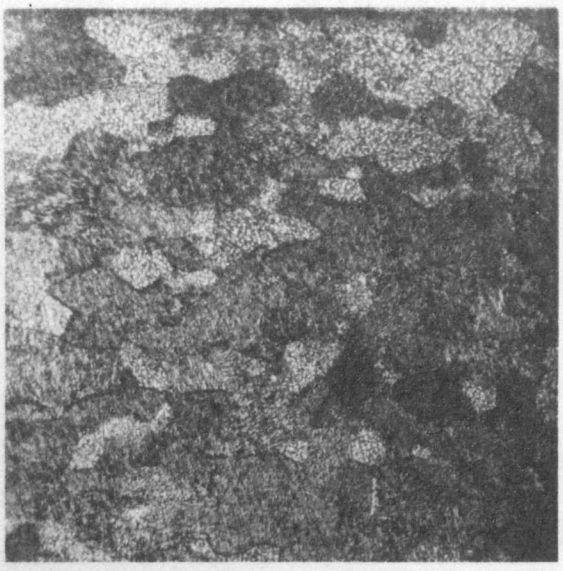

X150 Sample 30

1 hr., 900°C, $<10^{-5}$ torr

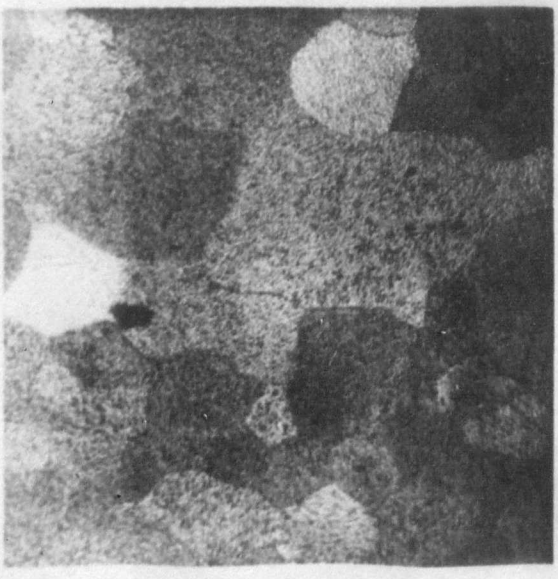

X150 Sample 10

24 hrs., 900°C, 10^{-5} torr

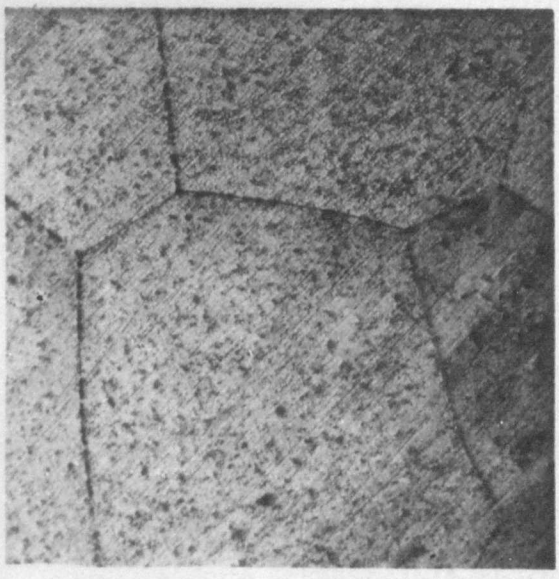

X150 Sample 8

24 hrs., 1100°C, $<10^{-4}$ torr

FIGURE 7.2.

be much affected; but the magnetic irreversibility will be increased by the presence of the precipitates.

The second of the changes resulting from annealing a cold-worked specimen is a reduction in the density of dislocations, dislocation tangles and grain boundaries. This reduction is produced by dislocation interaction, vacancy diffusion, recrystallization and grain growth. The improved homogeneity in turn produces two effects, the most important of these is a reduction in the magnetic irreversibility of the sample, and the other is an increase in the electron mean free path. The latter will produce similar changes in ρ, κ, H_{c1} and H_{c2} to those arising from dissolved impurities.

Applying this discussion to the effects of annealing in our samples, it is clear from the magnetization curves (Fig. 7.1.) that the major change is a reduction in irreversibility. This is characterized both by the reduction in the zero-field trapped flux and by the earlier penetration of flux in the mixed state. The increase in grain size after annealing revealed in the micrographs of Fig. 7.2., indicates that the reduced irreversibility results from a decrease in the defect density in the samples.

A second change in the annealed samples is a lowering of the upper critical field, H_{c2}, indicating a decrease in κ. This probably results from the combined effects of the lower defect density and a reduction in the dissolved gas content. The mass analysis (Table 7.3.) shows that sample 9 has a lower oxygen and carbon content than 8, the higher H_{c2} value of sample 9 must, therefore, be produced by its high defect density. Sample 10 has a much lower dissolved impurity content than 8 and 9, and its H_{c2} value is still lower than that of specimen 8. The complexity of the effects produced by annealing is illustrated by the fact that H_{c2} appears to be slightly lower for sample 30 than for 10, even though the former is more irreversible and was annealed for a shorter time. Presumably, because it was annealed at a lower pressure, the dissolved impurity content of 30 is lower than that of sample 10.

7.3. Surface-Treated Samples

The effects of different surface profiles on samples with similar bulk

properties were examined in three groups of samples. The techniques used to prepare the surfaces were spark machining, chemical polishing and electro-polishing. The spark machining was carried out in the lathe of a Metals Research 'Servomet'. To produce a uniform finish, the whole length of the specimen was machined at once. The unmachined piece held in the chuck jaws was subsequently removed by lowering a V-shaped tool onto the sample. (This same tool was used to produce ellipsoidal shaped ends on all the poly-crystalline samples). Initial machinings almost always took place at spark energy 3 to produce a true cylinder quickly. When a smoother final finish was required, subsequent machining at lower spark energies was continued until sufficient material had been removed to ensure that the surface profile produced by the previous machining was obliterated. In general, about 50 μm of material was removed on energy 5 after machining at 3, and about 25 μm on 7 after machining at 5. These numbers refer to the settings of the machine control which alters the energy of the spark. The low numbers correspond to high spark energies which remove more material and, consequently, produce a rougher surface.

The chemical and electropolishing procedures were standard treatments described by Tegart (1959). A mixture of 75% fuming nitric acid with 25% concentrated (60%) hydrofluoric acid was used for chemical polishing. Electro-polishing was carried out in a platinum beaker used as the cathode. The electrolyte (90% concentrated sulphuric acid with 10% hydrofluoric acid) was stirred magnetically, and current densities of about 1000 Am^{-2} were passed. It was found that while excellent results could be obtained by chemically polishing single crystals, electro-polishing was preferable for polycrystalline samples particularly if they were cold worked. This was because the grain boundaries in annealed samples were preferentially attacked by the chemical polish, and because in cold-worked samples a surface structure of longitudinal ridges appeared. This structure may have been a result of directional hardening produced by the swaging. In any case, the finishes produced by chemically polishing annealed and cold-worked polycrystalline specimens were

very different. A similar effect, but much reduced, was produced by an electropolish; we believe this may explain the different loss measurements obtained by Rocher and Septfonds (1967) before and after annealing.

Three of the first group of surface treated samples (Nos. 11 to 14) were each machined at a different spark energy and the fourth was chemically polished. To enable the effect of the different surface profiles to be studied in isolation, the samples were then annealed for 24 hrs at 1100°C to remove the damage produced by the spark machining and the original cold working. Because no sufficiently large crucible was available, samples 12 and 14 were annealed separately from 11 and 13. The latter pair of samples became heavily contaminated when air leaked into the furnace during their heat treatment. All four samples were then annealed together for a further 24 hrs in an unsuccessful attempt to produce uniform properties. The magnetization curves of the samples after treatment are shown in Fig. 7.3. The samples all have different values of H_{c2} which, presumably, result from differences in impurity concentration. It is interesting to note that the differences in zero-field trapped flux are rather less than those in H_{c2}, indicating that the latter do not arise from differences in defect density. The second anneal was probably unsuccessful in removing the impurities because insufficient care was taken to maintain a low vacuum. The results for these samples have been included because an interesting comparison is possible between this and a second group of surface treated specimens.

This group, samples 29 and 23 to 26, were prepared in a second attempt to produce specimens having the same properties but with different surface profiles. Samples 23 to 26 were cut from the same rod, 29 came from the second batch of material. Their treatments are shown in Table 7.1.; samples 23 to 26 were annealed together and 29 was given a similar, but separate, heat treatment. The annealing temperature was chosen so as to be above the recrystallization temperature of niobium, which Miller (1959) gives as 1050°C. This is confirmed by the micrograph of sample 8 (Fig. 7.2.) which shows that the grain size is of order 1 mm after annealing at 1100°C. The

EFFECT OF SURFACE PROFILE - 1.

Polycrystalline Niobium, Annealed (See Text)

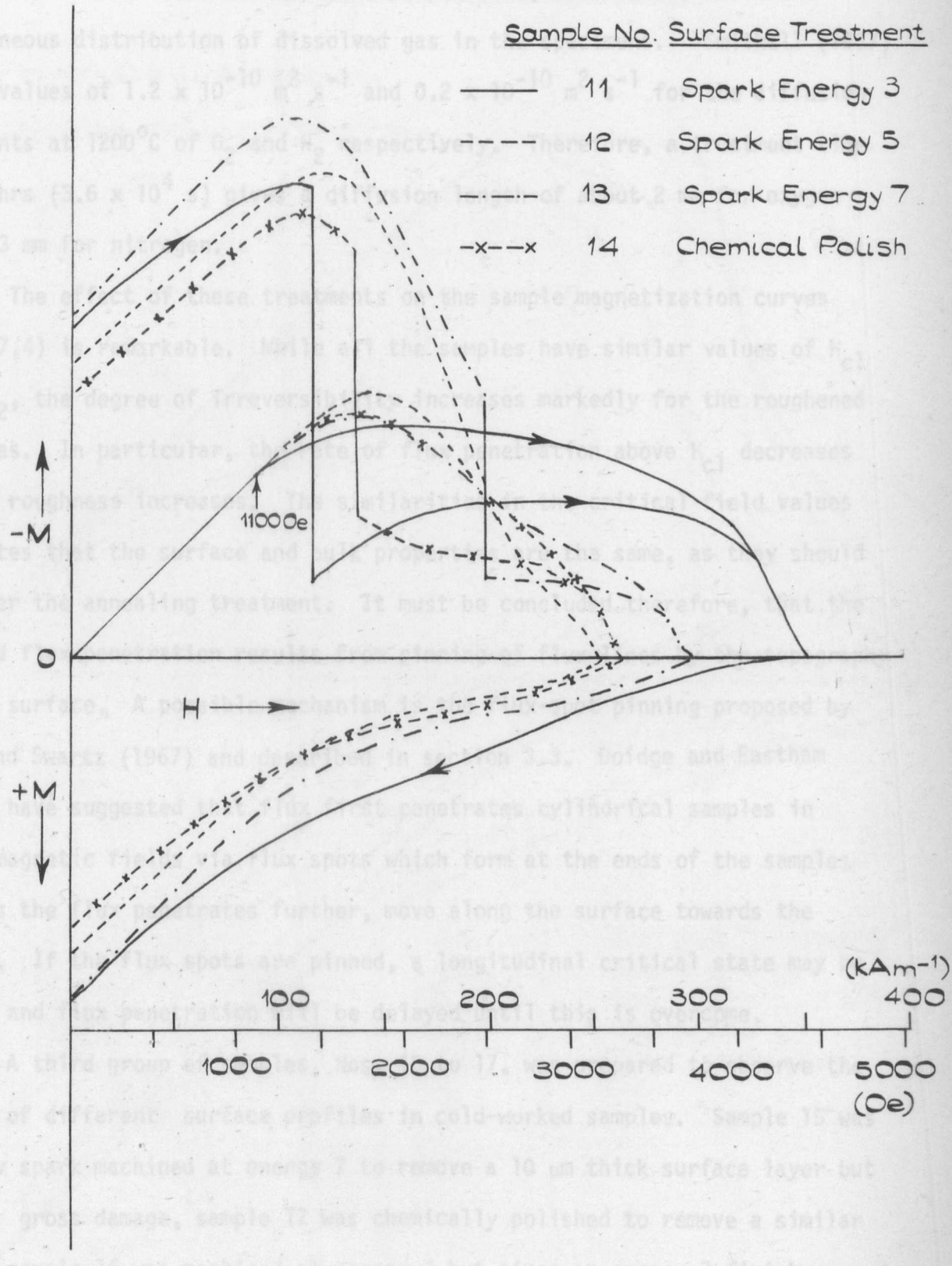

Figure 7.3.

annealing time (10 hrs) was chosen not only to ensure complete recrystallization, which takes about 1 hr at this temperature, but also to achieve a homogeneous distribution of dissolved gas in the specimens. Smithell (1967) gives values of 1.2×10^{-10} m^2 s^{-1} and 0.2×10^{-10} m^2 s^{-1} for the diffusion constants at 1200°C of O_2 and N_2 respectively. Therefore, a treatment time of 10 hrs (3.6×10^4 s) gives a diffusion length of about 2 mm for oxygen and 0.3 mm for nitrogen.

The effect of these treatments on the sample magnetization curves (Fig. 7.4) is remarkable. While all the samples have similar values of H_{c1} and H_{c2}, the degree of irreversibility increases markedly for the roughened surfaces. In particular, the rate of flux penetration above H_{c1} decreases as the roughness increases. The similarities in the critical field values indicates that the surface and bulk properties are the same, as they should be after the annealing treatment. It must be concluded therefore, that the delayed flux penetration results from pinning of flux lines by the topography of the surface. A possible mechanism is the flux-spot pinning proposed by Hart and Swartz (1967) and described in section 3.3. Doidge and Eastham (1970) have suggested that flux first penetrates cylindrical samples in axial magnetic fields via flux spots which form at the ends of the samples and, as the flux penetrates further, move along the surface towards the middle. If the flux spots are pinned, a longitudinal critical state may be set up and flux penetration will be delayed until this is overcome.

A third group of samples, Nos. 15 to 17, was prepared to observe the effect of different surface profiles in cold-worked samples. Sample 15 was lightly spark machined at energy 7 to remove a 10 μm thick surface layer but avoid gross damage, sample 17 was chemically polished to remove a similar layer, sample 16 was machined at energy 3 but given an energy 7 finish. Fig. 7.5. shows the magnetization curves of these samples, together with that of specimen 9 for comparison. Although the surface treatments have produced little effect on the bulk properties of the samples apart from small reductions in H_{c2} and the zero-field trapped flux, the surface currents have been noticeably

EFFECT OF SURFACE PROFILE - 2.

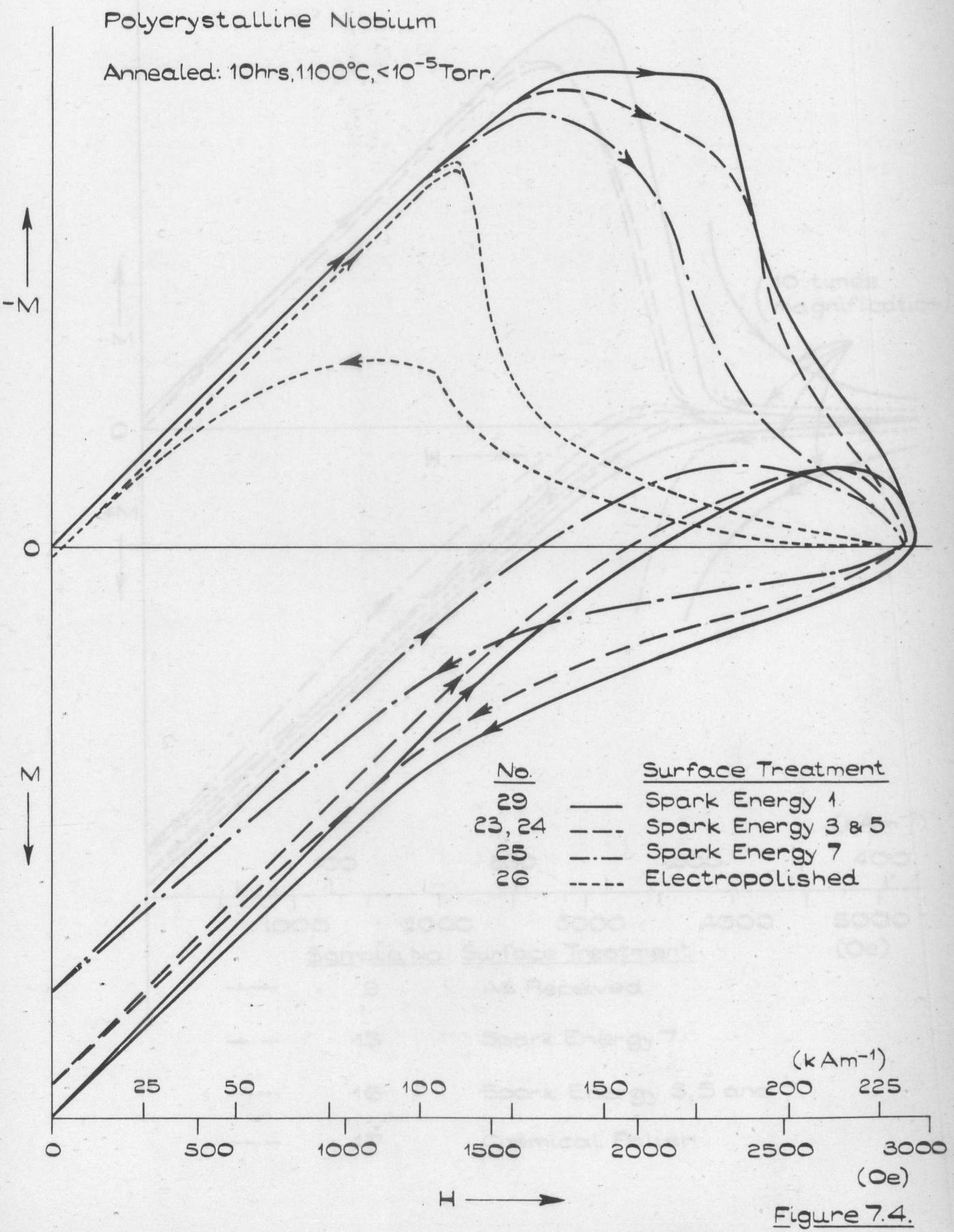

Figure 7.4.

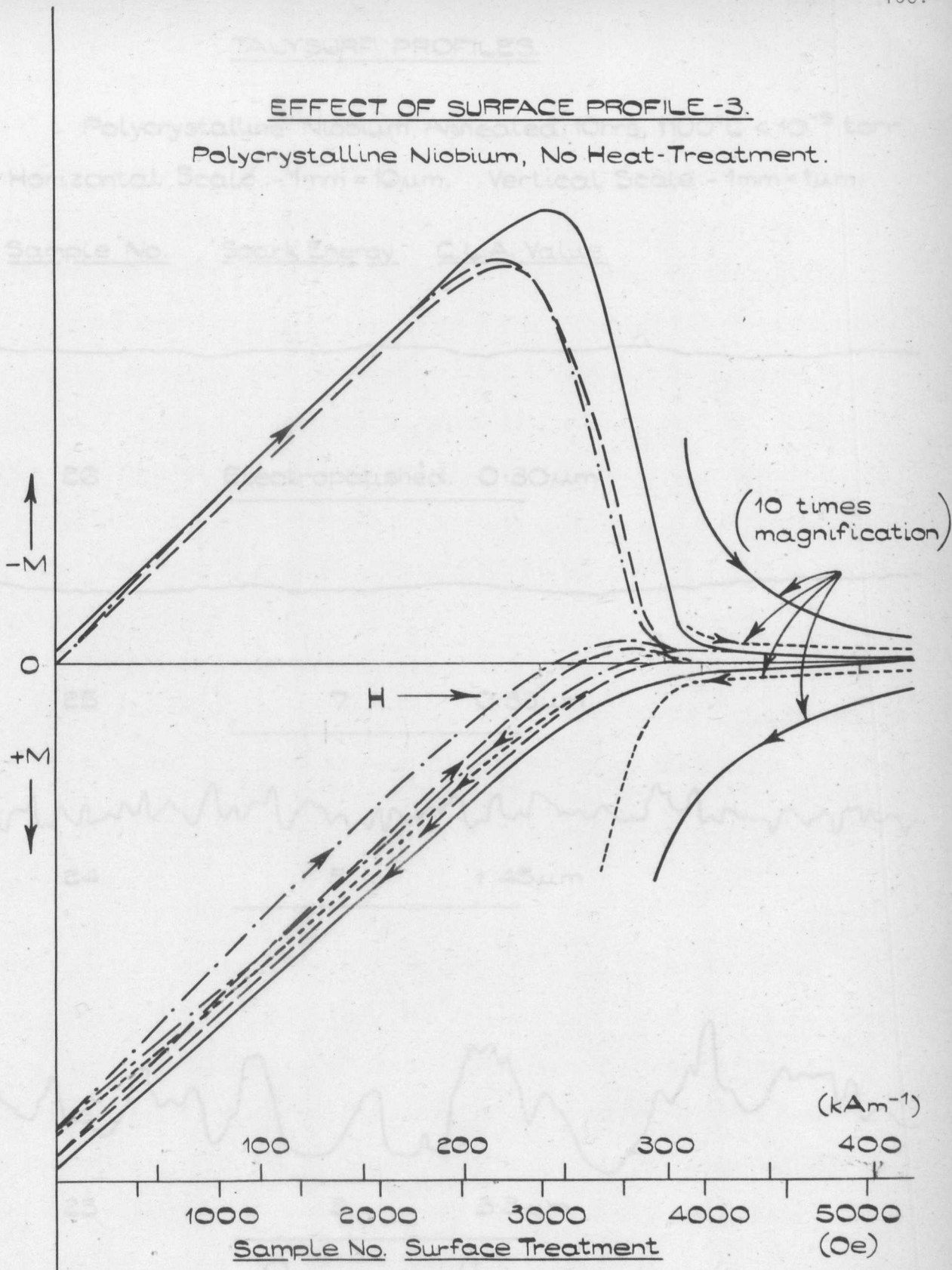
EFFECT OF SURFACE PROFILE -3.
Polycrystalline Niobium, No Heat-Treatment.
-M
0
+M
H
(10 times magnification)
(kAm⁻¹)
100
200
300
400
1000
2000
3000
4000
5000
(Oe)
Sample No.
Surface Treatment
9
As Received
15
Spark Energy 7
16
Spark Energy 3, 5 and 7.
17
Chemical Polish

Figure 75.

TALYSURF PROFILES.

Polycrystalline Niobium, Annealed: 10hrs, 1100°C < 10^{-5} torr.

Horizontal Scale :- 1mm = 10μm. Vertical Scale:- 1mm = 1μm.

Sample No.	Spark Energy.	C.L.A. Value.
26	Electropolished.	0·30μm
25	7	0·33μm
24	5	1·45μm
23	3	3·3μm
29	1	5·0μm

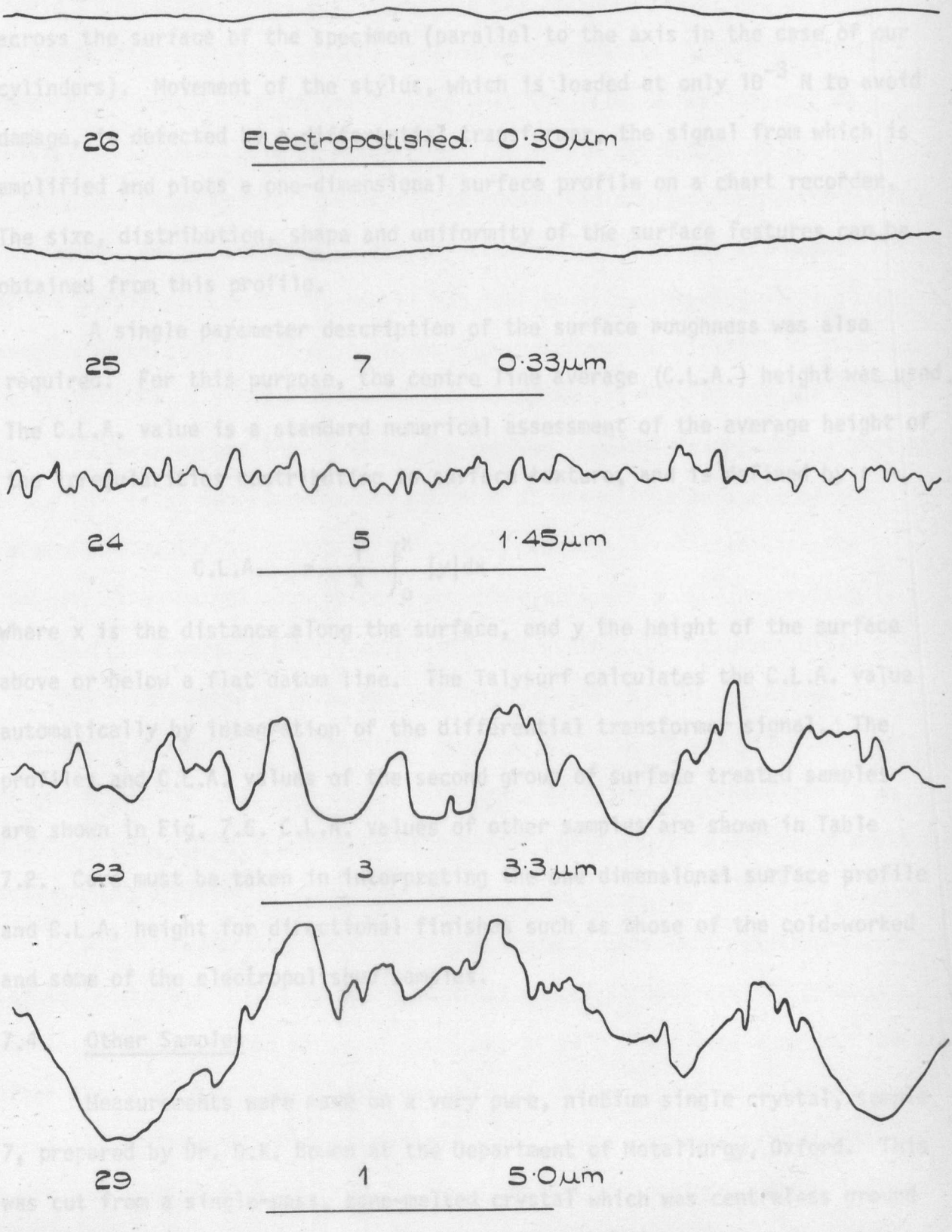

Figure 7.6.

reduced. They are a factor of four smaller in sample 16 than 9, and were still smaller in samples 15 and 17.

To enable the effects of the different surface profiles of our samples on their superconducting properties to be usefully compared, a 'Talysurf' was used to obtain a quantitative description of the profiles. The Talysurf consists of a stylus with a 2.5 μm diameter tip which is drawn across the surface of the specimen (parallel to the axis in the case of our cylinders). Movement of the stylus, which is loaded at only 10^{-3} N to avoid damage, is detected by a differential transformer, the signal from which is amplified and plots a one-dimensional surface profile on a chart recorder. The size, distribution, shape and uniformity of the surface features can be obtained from this profile.

A single parameter description of the surface roughness was also required. For this purpose, the centre line average (C.L.A.) height was used. The C.L.A. value is a standard numerical assessment of the average height of the irregularities contributing to surface texture, and is defined by :

$$\text{C.L.A.} = \frac{1}{x}\int_0^x |y|\,dx$$

where x is the distance along the surface, and y the height of the surface above or below a flat datum line. The Talysurf calculates the C.L.A. value automatically by integration of the differential transformer signal. The profiles and C.L.A. values of the second group of surface treated samples are shown in Fig. 7.6. C.L.A. values of other samples are shown in Table 7.2. Care must be taken in interpreting the one dimensional surface profile and C.L.A. height for directional finishes such as those of the cold-worked and some of the electropolished samples.

7.4. Other Samples

Measurements were made on a very pure, niobium single crystal, sample 7, prepared by Dr. D.K. Bowen at the Department of Metallurgy, Oxford. This was cut from a single-pass, zone-melted crystal which was centreless ground to 3 mm diameter, the damaged surface being removed by chemical polishing.

After annealing at 2500°C in a vacuum of about 2 x 10^{-10} torr, the sample had a very smooth bright surface and a resistance ratio of about 1000. Its magnetization curve is shown in Fig. 6.2.

Four other samples were given individual treatments intended to increase their flux pinning properties, particularly near the surface. Sample 4 was taken from a niobium single crystal prepared by Dr. D. Jones of the Materials Science Centre, Birmingham University. This single-pass, zone-melted crystal had an orientation near the |110| direction, and an initial resistance ratio of about 200. The sample was shaped on the spark machine and after chemical polishing to remove the damaged layer, its surface was smooth, bright and fairly free of etch-pits. The losses and magnetization of the sample were measured, and it was sent to AERE, Harwell, where it was neutron irradiated for 28 days in the Dido reactor. To minimize temperature rises produced by γ-ray absorption, the specimen was immersed in the deuterium cooling stream during irradiation, its surface temperature thus being kept at 50°C. The total neutron flux was measured at Harwell by analysis of the induced radioactivity in cobalt and nickel monitors irradiated with the niobium. The thermal neutron dose was given as 1.077 x 10^{24} neutrons m^{-2}, and the fast (Energy > 1MeV) neutron dose as 9.656 x 10^{23} neutron m^{-2}.

A second sample, No.6, was cut from the same single crystal as 4. After being turned to a cylindrical shape on a lathe, it was given a succession of mechanical polishes commencing with emery cloth and finishing with 1 μm diamond paste. This treatment left a bright surface with a number of scratches from the emery cloths.

Sample 31 was also mechanically polished. This is a polycrystalline sample, which was initially spark machined and electropolished to produce a smooth surface and then annealed for 4 hrs at 1100°C and less than 10^{-5} torr. After heat treatment, the sample was rotated at high speed in a lathe and carefully polished by holding 'Metron' suede cloths impregnated with diamond paste and lubricated with 'Dialap' fluid against its surface. 1 and 1/4 μm grades of diamond paste were used successively, polishing with each being

continued for about 30 minutes.

Another polycrystalline sample, No.27, was annealed and given a smooth bright surface by electropolishing. It was then irradiated with 40 kV niobium ions at the University of Surrey. To obtain a uniform implantation, the specimen was rotated at about 60 r.p.m. in a niobium chuck, driven through a rotary vacuum seal by a motor external to the target chamber. The total sample current during implantation was about 50 nA, but it was estimated that 90% of this current might be secondary electron emission. The depth of implantation was calculated to be about 10 nm so that, assuming the ion current was 5 nA, the dosage in the penetrated layer was at least 3×10^{25} ions m^{-3}.

The magnetization curve of sample 4 is compared with an untreated specimen in Fig. 7.7., the curves of samples 6 and 31 are shown in Fig. 7.8 and that of sample 27 in Fig. 7.10. The zero-field trapped flux of the neutron-irradiated sample has been greatly increased and there is also a rise in its H_{c2} value. Flux penetration is detectable below 150 kAm^{-1} (1885 Oe) and the surface currents are not particularly high, being a factor of ten smaller than those in the as-received, cold-worked, polycrystalline sample (No.9) shown in Fig. 7.1. Kernohan and Sekula (1967) and Kuhn (1962) have previously reported measurements on irradiated niobium. The magnetization curve shown in Fig. 7.7. is similar in shape to that reported by Kernohan and Sekula for a similar sample after irradiation with 1.7×10^{23} neutrons m^{-2}. However, the upper critical field of their sample, 222 kAm^{-1} (2800 Oe), was little affected by the irradiation.

These magnetization curves indicate that, although neutron irradiation produces considerable bulk damage, the surface flux pinning is not particularly affected. This is to be expected. Neutron damage arises mainly from the fast neutrons, which displace atoms from their lattice sites on collision and produce vacancies, interstitials and clusters of these point defects. Because of their long range, the defects produced by fast neutrons are uniformly distributed in the sample (Harwood et al 1958). This has been

NEUTRON-IRRADIATED SAMPLE-4.

Niobium Single Crystal, Chemically Polished, 40mm long
5mm diameter, Resistance Ratio ≙ 200

—— After Neutron Irradiation (see text) 9.7×10^{23} Neutrons m^{-2}

------ Untreated Sample.

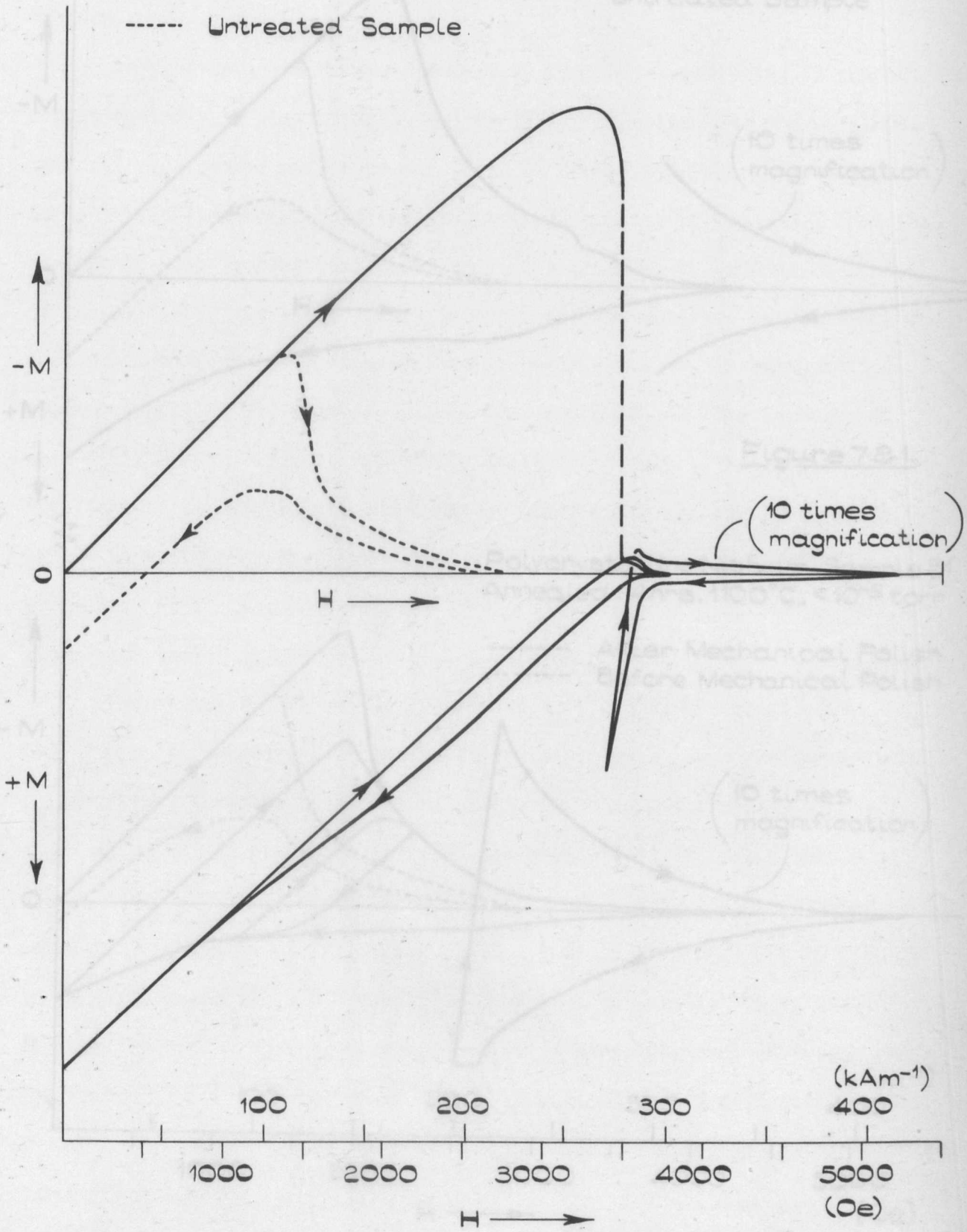

Figure 7.7.

MECHANICALLY POLISHED SAMPLES.

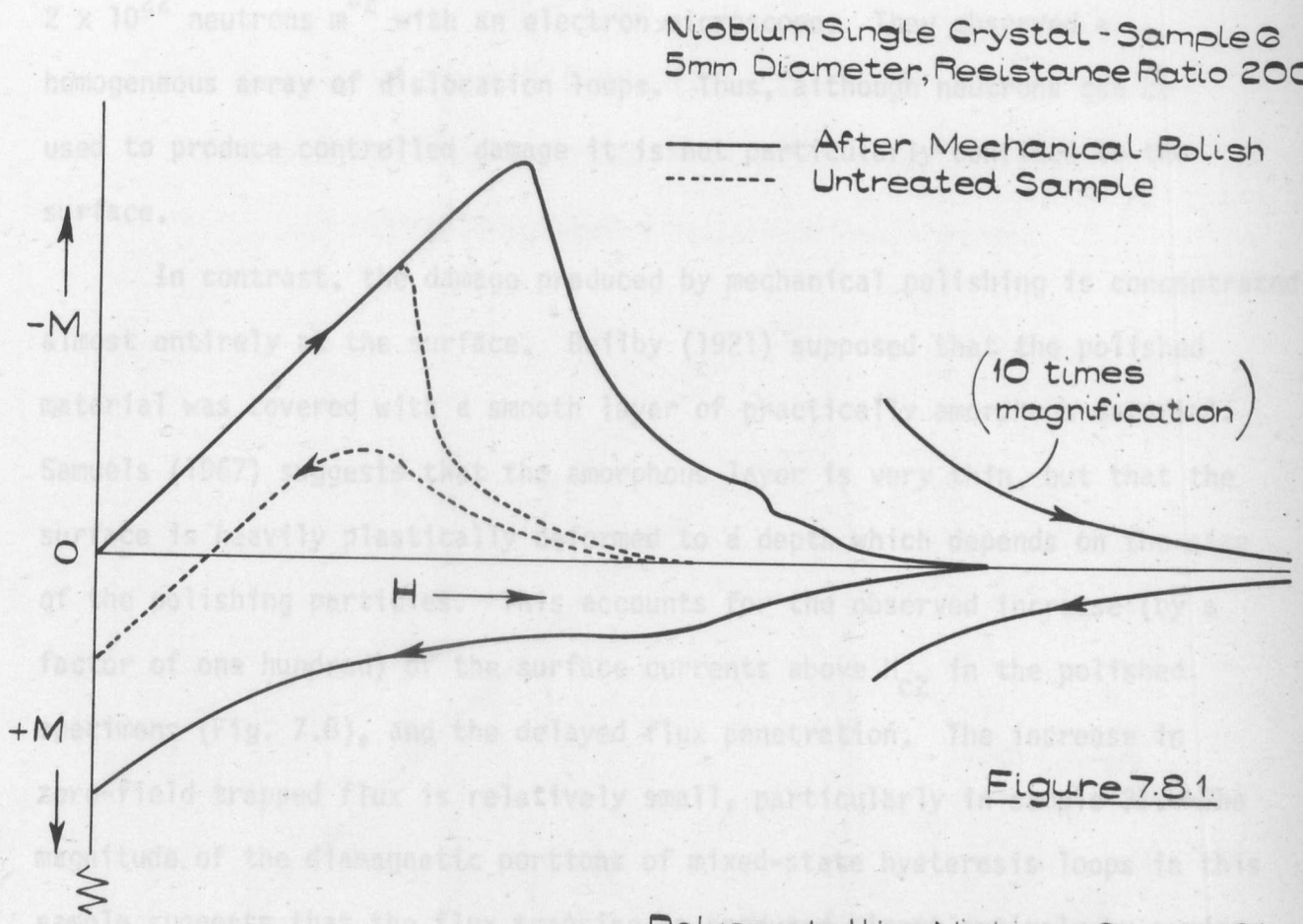

Figure 7.8.1.

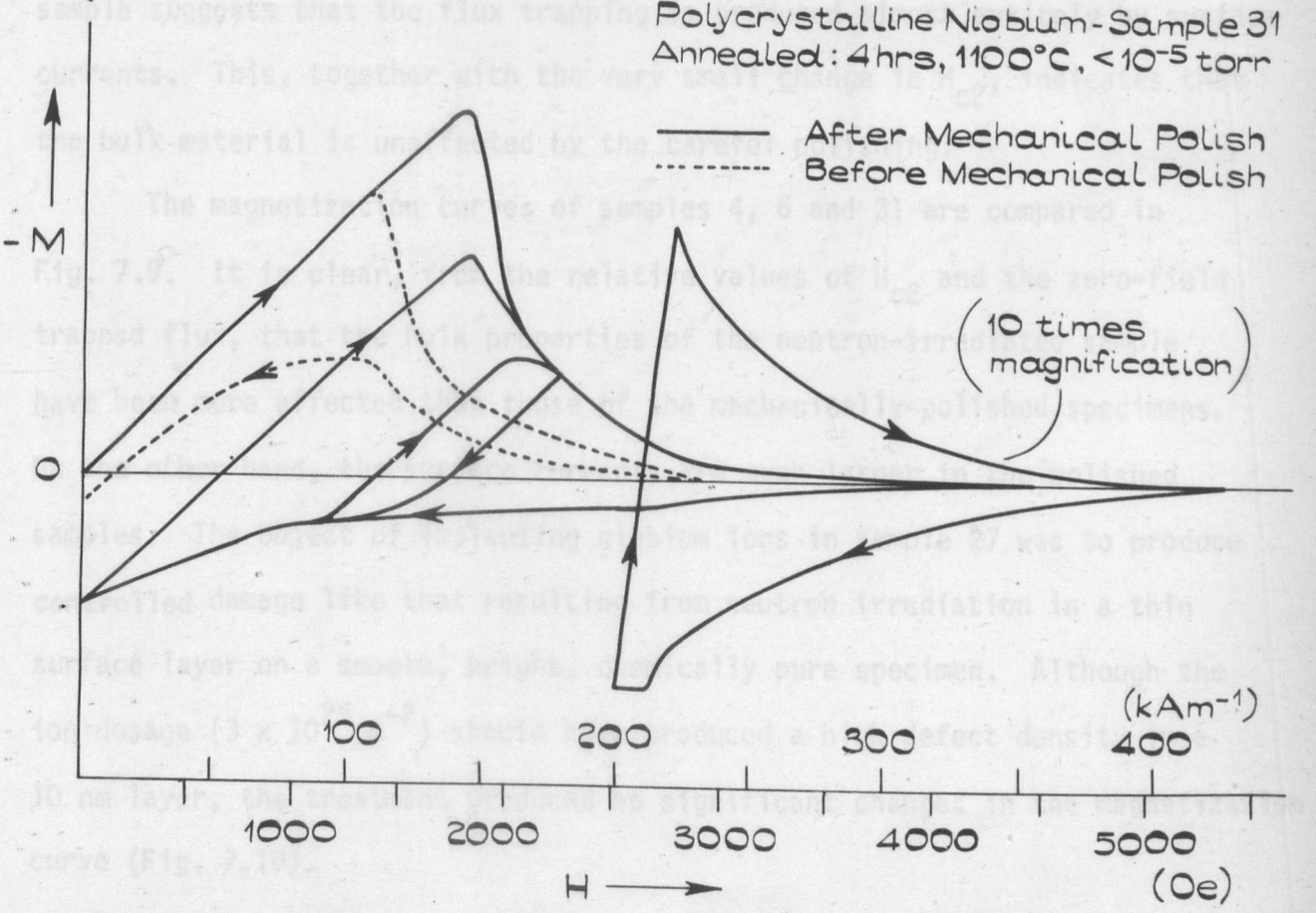

Figure 7.8.2.

confirmed by Tucker and Ohr (1967) who examined niobium irradiated with 2×10^{22} neutrons m^{-2} with an electron microscope. They observed a homogeneous array of dislocation loops. Thus, although neutrons can be used to produce controlled damage it is not particularly confined to the surface.

In contrast, the damage produced by mechanical polishing is concentrated almost entirely at the surface. Beilby (1921) supposed that the polished material was covered with a smooth layer of practically amorphous material. Samuels (1967) suggests that the amorphous layer is very thin, but that the surface is heavily plastically deformed to a depth which depends on the size of the polishing particles. This accounts for the observed increase (by a factor of one hundred) of the surface currents above H_{c2} in the polished specimens (Fig. 7.8), and the delayed flux penetration. The increase in zero-field trapped flux is relatively small, particularly in sample 31. The magnitude of the diamagnetic portions of mixed-state hysteresis loops in this sample suggests that the flux trapping is produced almost entirely by surface currents. This, together with the very small change in H_{c2}, indicates that the bulk material is unaffected by the careful polishing.

The magnetization curves of samples 4, 6 and 31 are compared in Fig. 7.9. It is clear, from the relative values of H_{c2} and the zero-field trapped flux, that the bulk properties of the neutron-irradiated sample have been more affected than those of the mechanically-polished specimens. On the other hand, the surface currents are much larger in the polished samples. The object of implanting niobium ions in sample 27 was to produce controlled damage like that resulting from neutron irradiation in a thin surface layer on a smooth, bright, chemically pure specimen. Although the ion dosage (3×10^{25} m^{-2}) should have produced a high defect density in a 10 nm layer, the treatment produced no significant changes in the magnetization curve (Fig. 7.10).

COMPARISON OF DAMAGED SAMPLES.

Samples

——— 4, Neutron Irradiated Single Crystal.

– – – 6, Mechanically Polished Single Crystal.

—.—. 31, Mechanically Polished Polycrystal.

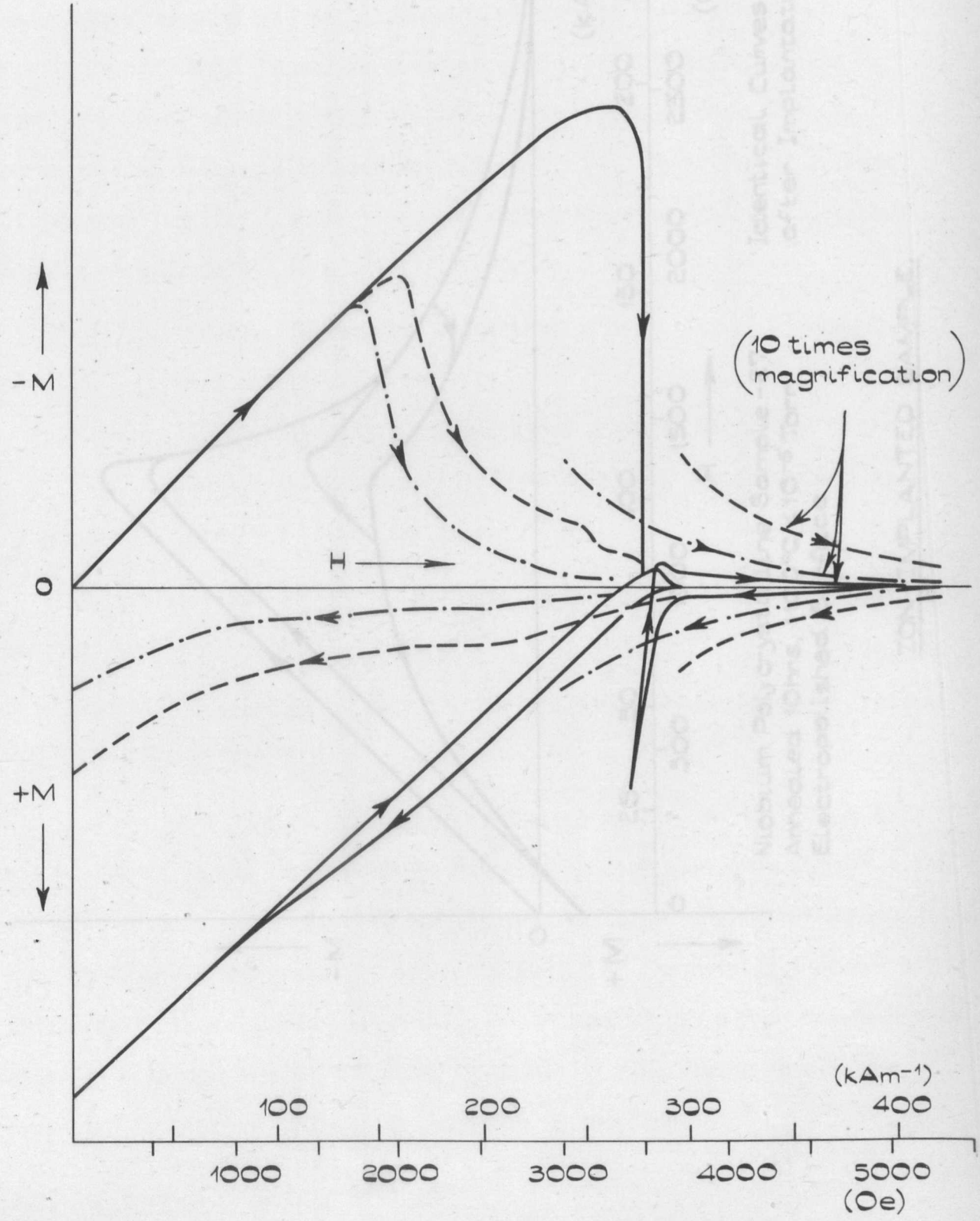

Figure 7.9

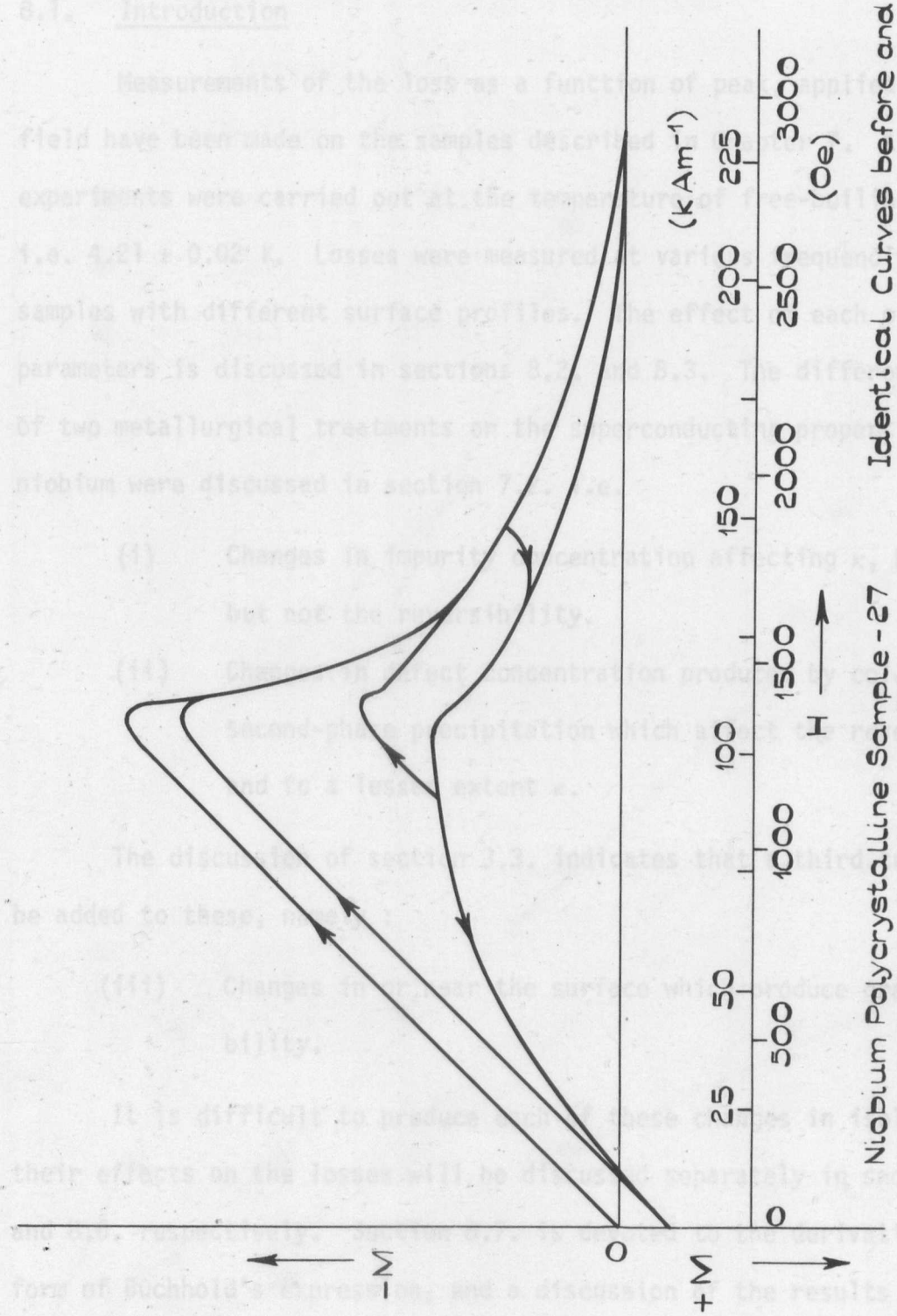
-M
0
+M
0
25
50
500
1000
100
1500
150
2000
200
2500
225
3000
(kAm⁻¹)
(Oe)
H
Niobium Polycrystalline Sample-27
Annealed 10hrs, 1100°C, <10⁻⁵ Torr
Electropolished Surface
Identical Curves before and after Implantation.
ION-IMPLANTED SAMPLE.

Figure 7.10

8. LOSSES BELOW H_{c1}

8.1. Introduction

Measurements of the loss as a function of peak, applied, magnetic field have been made on the samples described in Chapter 7. All these experiments were carried out at the temperature of free-boiling helium i.e. 4.21 ± 0.02 K. Losses were measured at various frequencies and in samples with different surface profiles. The effect of each of these parameters is discussed in sections 8.2. and 8.3. The different effects of two metallurgical treatments on the superconducting properties of niobium were discussed in section 7.2. i.e.

(i) Changes in impurity concentration affecting κ, H_{c1} and H_{c2} but not the reversibility.

(ii) Changes in defect concentration produced by cold-work and second-phase precipitation which affect the reversibility and to a lesser extent κ.

The discussion of section 3.3. indicates that a third treatment should be added to these, namely :

(iii) Changes in or near the surface which produce greater irreversibility.

It is difficult to produce each of these changes in isolation, but their effects on the losses will be discussed separately in sections 8.4., 8.5., and 8.6. respectively. Section 8.7. is devoted to the derivation of a modified form of Buchhold's expression, and a discussion of the results in terms of this model. It was found that the losses in some of our samples changed when they had been completely penetrated by an a.c. field. These results are presented in section 8.8. and discussed in section 8.9.

8.2. Effect of Frequency

The frequency dependence of the loss was measured firstly, to determine

EFFECT OF FREQUENCY.

Polycrystalline Niobium - Sample 15

Cold Worked, Spark Energy 7 Surface.

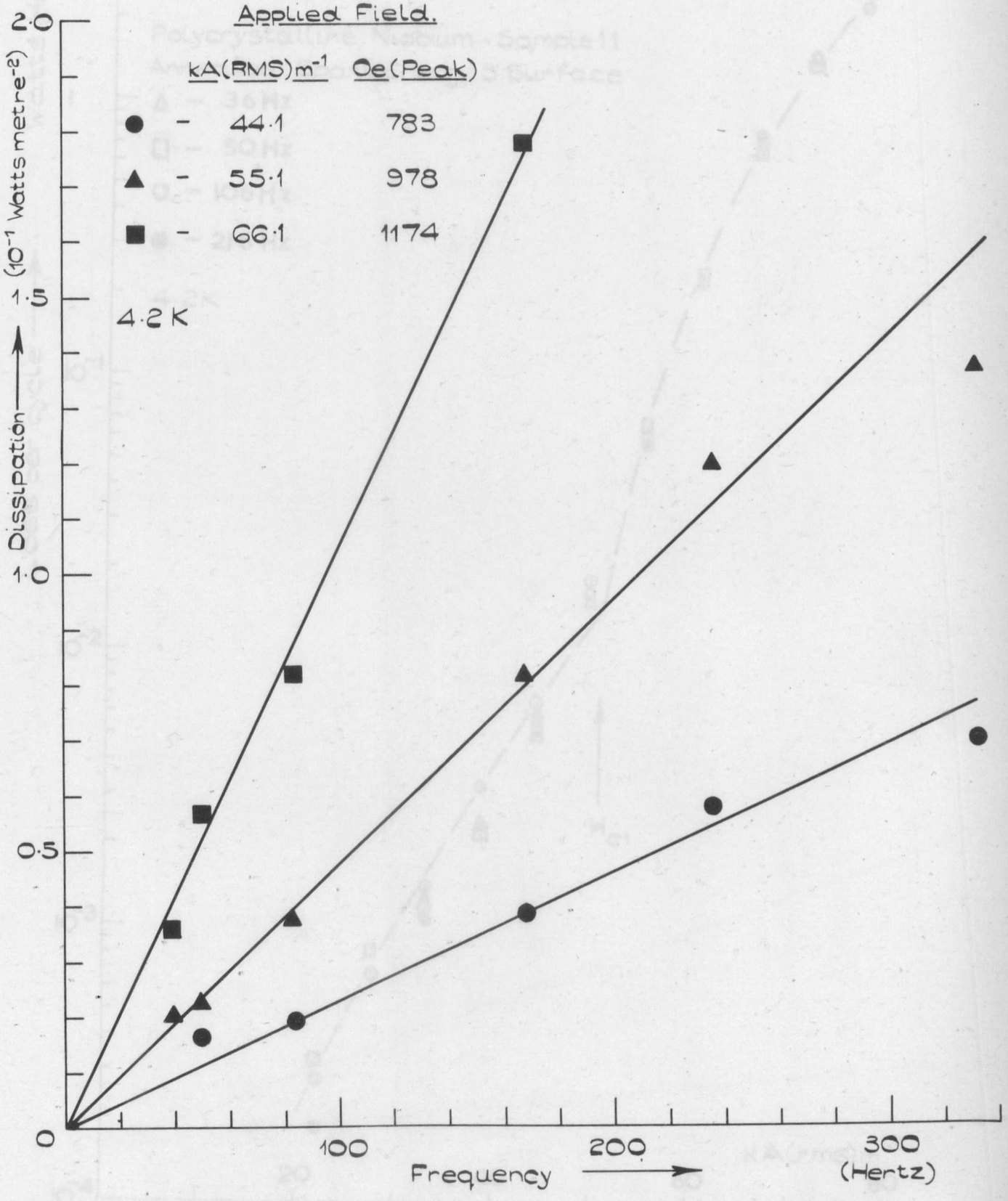

Figure 8.1.

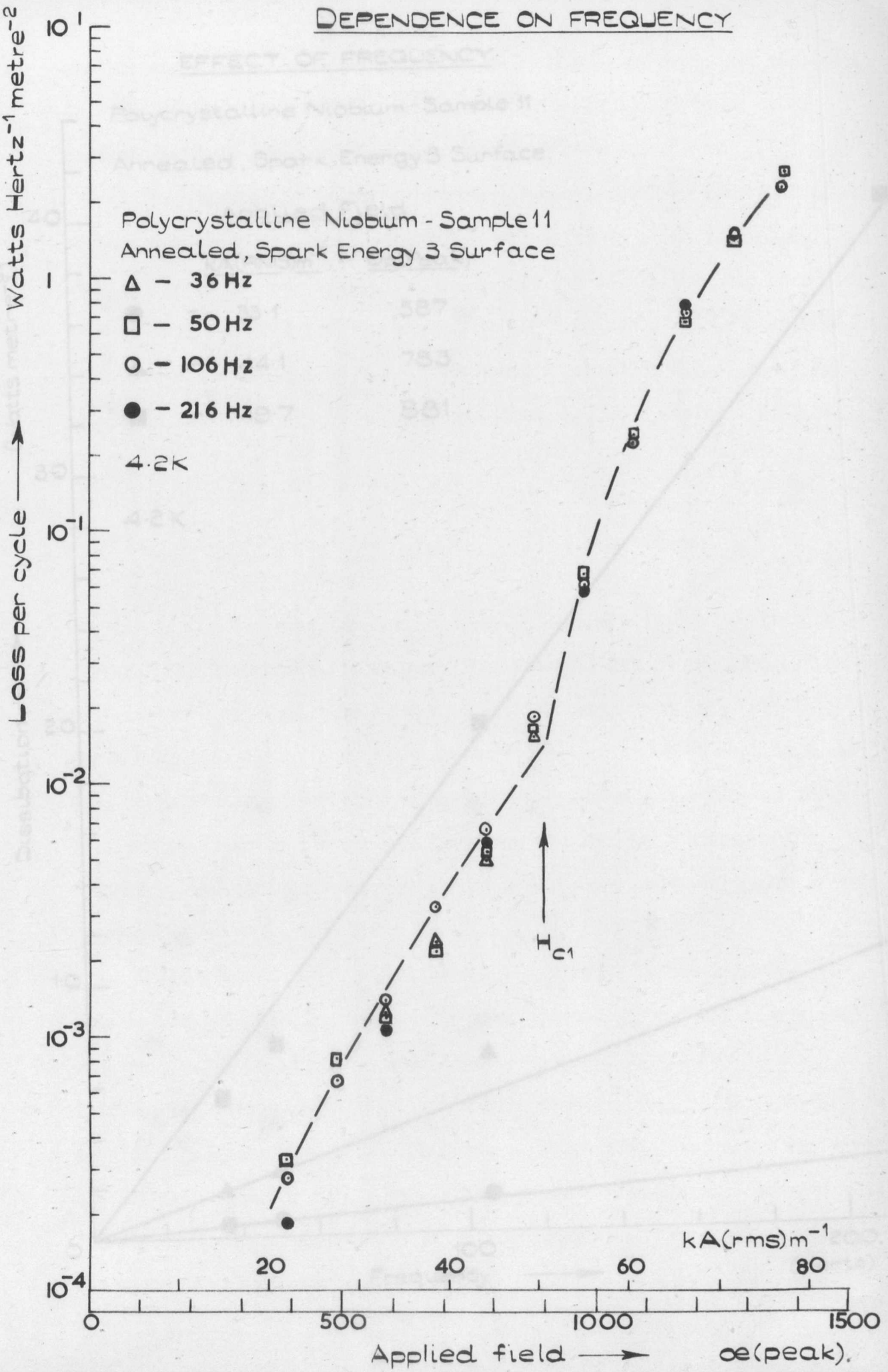
DEPENDENCE ON FREQUENCY
Polycrystalline Niobium - Sample 11
Annealed, Spark Energy 3 Surface
Δ – 36 Hz
□ – 50 Hz
○ – 106 Hz
● – 216 Hz
4·2K
Loss per cycle → Watts Hertz⁻¹ metre⁻²
10⁻¹
1
10⁻¹
10⁻²
10⁻³
10⁻⁴
H_{c1}
kA(rms)m⁻¹
20
40
60
80
0
500
1000
1500
Applied field → oe(peak).

Figure 8.2.

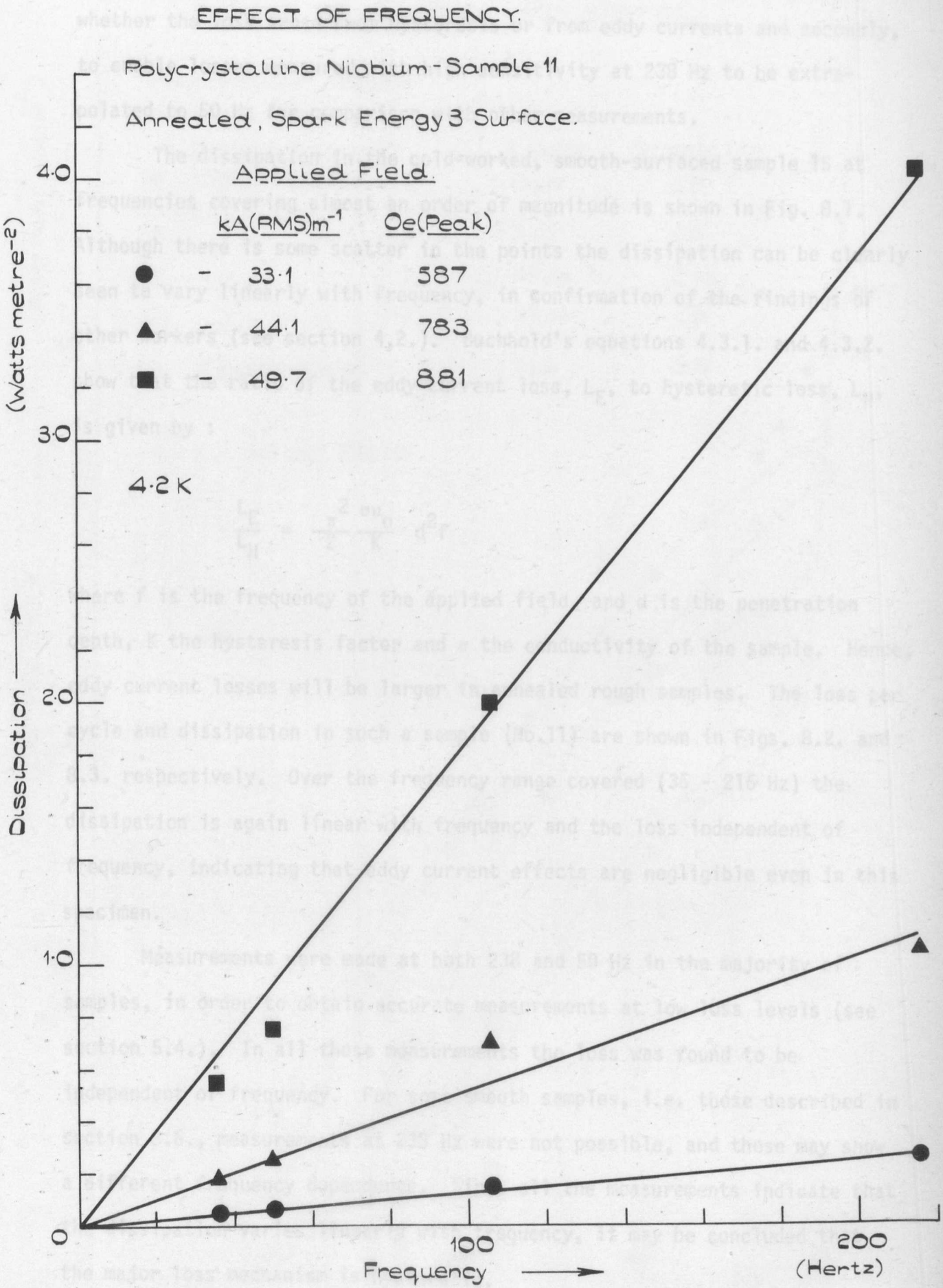
EFFECT OF FREQUENCY.
Polycrystalline Niobium - Sample 11
Annealed, Spark Energy 3 Surface.
Applied Field.
kA(RMS)m⁻¹ Oe(Peak)
● - 33·1 587
▲ - 44·1 783
■ - 49·7 881
4·2 K
Dissipation (Watts metre⁻²)
4·0
3·0
2·0
1·0
0
100
200
Frequency (Hertz)

Figure 8.3.

whether the loss arose from hysteresis or from eddy currents and secondly, to enable losses measured with high sensitivity at 238 Hz to be extrapolated to 50 Hz for comparison with other measurements.

The dissipation in the cold-worked, smooth-surfaced sample 15 at frequencies covering almost an order of magnitude is shown in Fig. 8.1. Although there is some scatter in the points the dissipation can be clearly seen to vary linearly with frequency, in confirmation of the findings of other workers (see section 4.2.). Buchhold's equations 4.3.1. and 4.3.2. show that the ratio of the eddy current loss, L_E, to hysteretic loss, L_H, is given by :

$$\frac{L_E}{L_H} = \frac{\pi^2}{2} \frac{\sigma \mu_o}{K} d^2 f$$

where f is the frequency of the applied field, and d is the penetration depth, K the hysteresis factor and σ the conductivity of the sample. Hence, eddy current losses will be larger in annealed rough samples. The loss per cycle and dissipation in such a sample (No.11) are shown in Figs. 8.2. and 8.3. respectively. Over the frequency range covered (36 - 216 Hz) the dissipation is again linear with frequency and the loss independent of frequency, indicating that eddy current effects are negligible even in this specimen.

Measurements were made at both 238 and 50 Hz in the majority of samples, in order to obtain accurate measurements at low loss levels (see section 5.4.). In all these measurements the loss was found to be independent of frequency. For some smooth samples, i.e. those described in section 8.6., measurements at 238 Hz were not possible, and these may show a different frequency dependence. Since all the measurements indicate that the dissipation varies linearly with frequency, it may be concluded that the major loss mechanism is hysteretic.

8.3. Surface Roughness

The losses in samples 23 to 26 and 29 which were prepared with

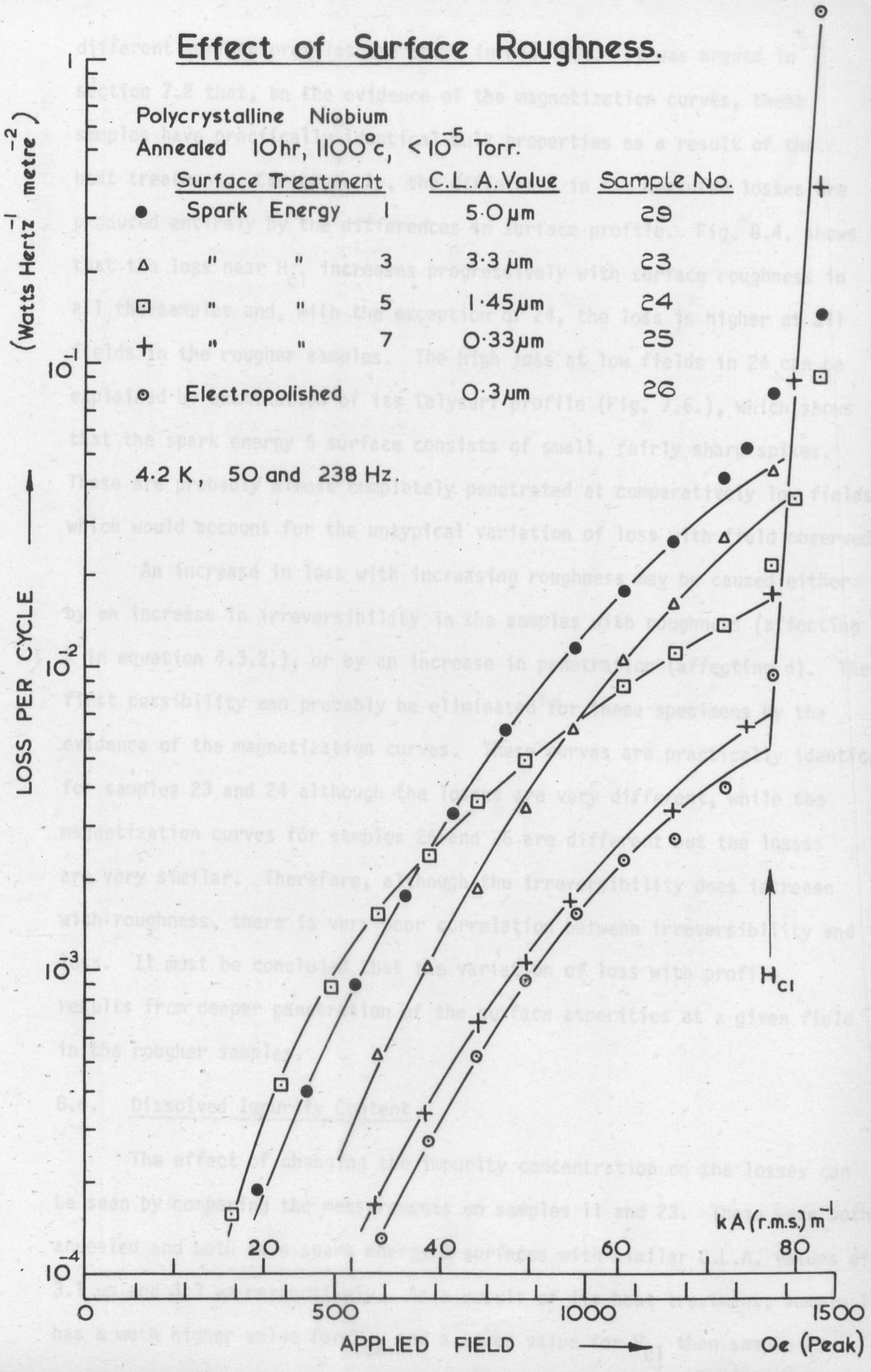
Effect of Surface Roughness.
Polycrystalline Niobium
Annealed 10hr, 1100°c, < 10⁻⁵ Torr.
Surface Treatment
C.L.A. Value
Sample No.
Spark Energy 1
5·0 μm
29
" " 3
3·3 μm
23
" " 5
1·45 μm
24
" " 7
0·33 μm
25
Electropolished
0·3 μm
26
4.2 K, 50 and 238 Hz.
LOSS PER CYCLE (Watts Hertz⁻¹ metre⁻²)
1
10⁻¹
10⁻²
10⁻³
10⁻⁴
H_c1
kA (r.m.s.) m⁻¹
20
40
60
80
0
500
1000
1500
APPLIED FIELD
Oe (Peak)

Figure 8.4.

different surface profiles are shown in Fig. 8.4. It was argued in section 7.2 that, on the evidence of the magnetization curves, these samples have practically identical bulk properties as a result of their heat treatment. Consequently, the difference in the measured losses are produced entirely by the differences in surface profile. Fig. 8.4. shows that the loss near H_{c1} increases progressively with surface roughness in all the samples and, with the exception of 24, the loss is higher at all fields in the rougher samples. The high loss at low fields in 24 can be explained by examination of its Talysurf profile (Fig. 7.6.), which shows that the spark energy 5 surface consists of small, fairly sharp spikes. These are probably almost completely penetrated at comparatively low fields which would account for the untypical variation of loss with field observed.

An increase in loss with increasing roughness may be caused either by an increase in irreversibility in the samples with roughness (affecting K in equation 4.3.2.), or by an increase in penetration (affecting d). The first possibility can probably be eliminated for these specimens by the evidence of the magnetization curves. These curves are practically identical for samples 23 and 24 although the losses are very different, while the magnetization curves for samples 25 and 26 are different but the losses are very similar. Therefore, although the irreversibility does increase with roughness, there is very poor correlation between irreversibility and loss. It must be concluded that the variation of loss with profile results from deeper penetration of the surface asperities at a given field in the rougher samples.

8.4. Dissolved Impurity Content

The effect of changing the impurity concentration on the losses can be seen by comparing the measurements on samples 11 and 23. These were both annealed and both have spark energy 3 surfaces with similar C.L.A. values of 3.1 μm and 3.3 μm respectively. As a result of its heat treatment, sample 11 has a much higher value for H_{c2} and a lower value for H_{c1} than sample 23

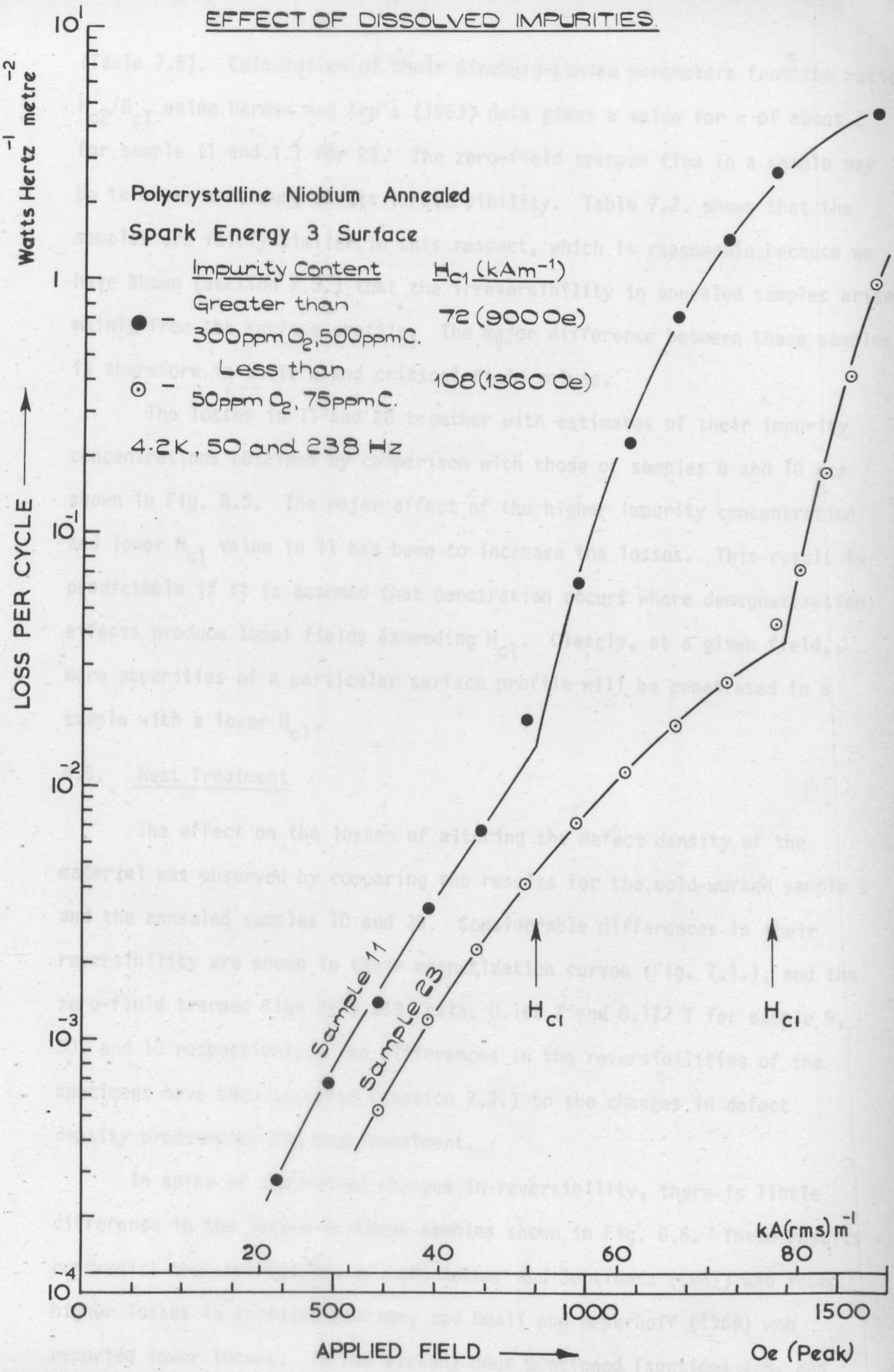
EFFECT OF DISSOLVED IMPURITIES.
Polycrystalline Niobium Annealed
Spark Energy 3 Surface
Impurity Content
H_c1 (kAm^-1)
● – Greater than 300ppm O2, 500ppm C. 72 (900 Oe)
⊙ – Less than 50ppm O2, 75ppm C. 108 (1360 Oe)
4.2K, 50 and 238 Hz
Sample 11
Sample 23
H_c1
H_c1
LOSS PER CYCLE → Watts Hertz^-1 metre^-2
10^1
1
10^-1
10^-2
10^-3
10^-4
0
500
1000
1500
APPLIED FIELD → Oe (Peak)
kA(rms) m^-1
20
40
60
80

Figure 8.5.

(Table 7.2). Calculation of their Ginzburg-Landau parameters from the ratio H_{c2}/H_{c1} using Harden and Arp's (1963) data gives a value for κ of about 2 for sample 11 and 1.1 for 23. The zero-field trapped flux in a sample may be taken as a measure of its irreversibility. Table 7.2. shows that the samples are fairly similar in this respect, which is reasonable because we have shown (section 7.3.) that the irreversibility in annealed samples arises mainly from the surface profile. The major difference between these samples is therefore in their κ and critical field values.

The losses in 11 and 23 together with estimates of their impurity concentrations obtained by comparison with those of samples 8 and 10 are shown in Fig. 8.5. The major effect of the higher impurity concentration and lower H_{c1} value in 11 has been to increase the losses. This result is predictable if it is assumed that penetration occurs where demagnetization effects produce local fields exceeding H_{c1}. Clearly, at a given field, more asperities of a particular surface profile will be penetrated in a sample with a lower H_{c1}.

8.5. Heat Treatment

The effect on the losses of altering the defect density of the material was observed by comparing the results for the cold-worked sample 9 and the annealed samples 10 and 30. Considerable differences in their reversibility are shown in their magnetization curves (Fig. 7.1.), and the zero-field trapped flux is 0.313 Tesla, 0.166 T and 0.117 T for sample 9, 30, and 10 respectively. The differences in the reversibilities of the specimens have been ascribed (section 7.2.) to the changes in defect density produced by the heat-treatment.

In spite of the marked changes in reversibility, there is little difference in the losses in these samples shown in Fig. 8.6. These results contradict the observations of both Rocher and Septfonds (1967) who found higher losses in annealed niobium, and Beall and Meyerhoff (1969) who reported lower losses. It has already been mentioned (sections 4.6. and

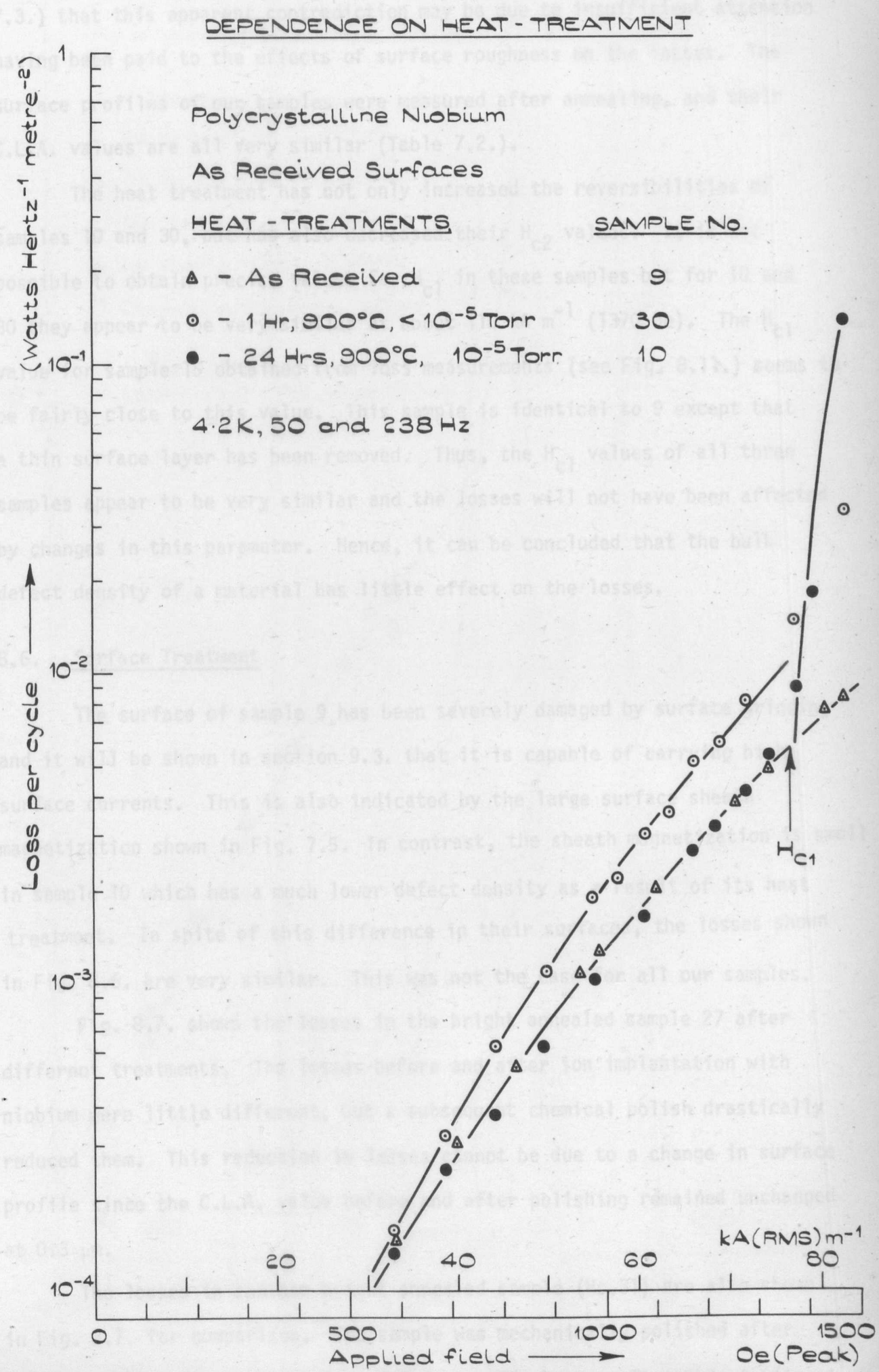
DEPENDENCE ON HEAT - TREATMENT
Polycrystalline Niobium
As Received Surfaces
HEAT - TREATMENTS
SAMPLE No.
△ - As Received 9
⊙ - 1 Hr, 900°C, < 10⁻⁵ Torr 30
● - 24 Hrs, 900°C, 10⁻⁵ Torr 10
4·2K, 50 and 238 Hz
Loss per cycle (Watts Hertz⁻¹ metre⁻²)
1
10⁻¹
10⁻²
10⁻³
10⁻⁴
H_c1
kA(RMS)m⁻¹
20
40
60
80
0
500
1000
1500
Applied field
Oe(Peak)

Figure 8.6.

7.3.) that this apparent contradiction may be due to insufficient attention having been paid to the effects of surface roughness on the losses. The surface profiles of our samples were measured after annealing, and their C.L.A. values are all very similar (Table 7.2.).

The heat treatment has not only increased the reversibilities of samples 10 and 30, but has also decreased their H_{c2} values. It is not possible to obtain precise values for H_{c1} in these samples but for 10 and 30 they appear to be very similar at about 110 kA m^{-1} (1370 Oe). The H_{c1} value for sample 15 obtained from loss measurements (see Fig. 8.11.) seems to be fairly close to this value. This sample is identical to 9 except that a thin surface layer has been removed. Thus, the H_{c1} values of all three samples appear to be very similar and the losses will not have been affected by changes in this parameter. Hence, it can be concluded that the bulk defect density of a material has little effect on the losses.

8.6. Surface Treatment

The surface of sample 9 has been severely damaged by surface grinding and it will be shown in section 9.3. that it is capable of carrying high surface currents. This is also indicated by the large surface sheath magnetization shown in Fig. 7.5. In contrast, the sheath magnetization is small in sample 10 which has a much lower defect density as a result of its heat treatment. In spite of this difference in their surfaces, the losses shown in Fig. 8.6. are very similar. This was not the case for all our samples.

Fig. 8.7. shows the losses in the bright annealed sample 27 after different treatments. The losses before and after ion implantation with niobium were little different, but a subsequent chemical polish drastically reduced them. This reduction in losses cannot be due to a change in surface profile since the C.L.A. value before and after polishing remained unchanged at 0.3 μm.

The losses in another bright annealed sample (No.31) are also shown in Fig. 8.7. for comparison. The sample was mechanically polished after annealing and has a C.L.A. value of 0.2 μm. The losses after this treatment

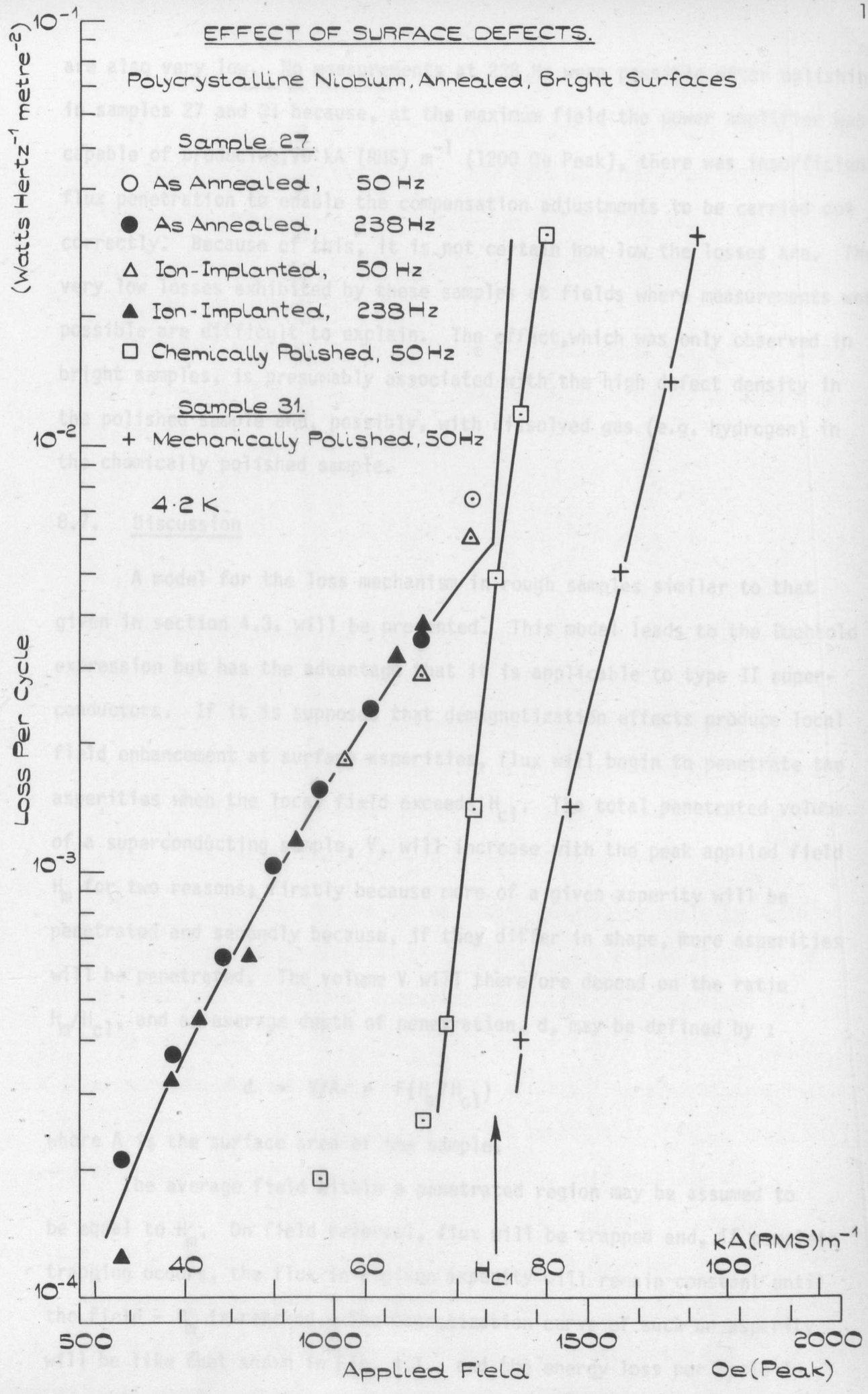
EFFECT OF SURFACE DEFECTS.
Polycrystalline Niobium, Annealed, Bright Surfaces
Sample 27.
As Annealed, 50 Hz
As Annealed, 238 Hz
Ion-Implanted, 50 Hz
Ion-Implanted, 238 Hz
Chemically Polished, 50 Hz
Sample 31.
Mechanically Polished, 50 Hz
4·2 K
(Watts Hertz⁻¹ metre⁻²)
Loss Per Cycle
10⁻¹
10⁻²
10⁻³
10⁻⁴
kA(RMS)m⁻¹
40
60
80
100
Hc1
500
1000
1500
2000
Applied Field
Oe(Peak)

Figure 8.7.

are also very low. No measurements at 238 Hz were possible after polishing in samples 27 and 31 because, at the maximum field the power amplifier was capable of producing,70 kA (RMS) m^{-1} (1200 Oe Peak), there was insufficient flux penetration to enable the compensation adjustments to be carried out correctly. Because of this, it is not certain how low the losses are. The very low losses exhibited by these samples at fields where measurements were possible are difficult to explain. The effect,which was only observed in bright samples, is presumably associated with the high defect density in the polished sample and, possibly, with dissolved gas (e.g. hydrogen) in the chemically polished sample.

8.7. Discussion

A model for the loss mechanism in rough samples similar to that given in section 4.3. will be presented. This model leads to the Buchhold expression but has the advantage that it is applicable to type II superconductors. If it is supposed that demagnetization effects produce local field enhancement at surface asperities, flux will begin to penetrate the asperities when the local field exceeds H_{c1}. The total penetrated volume of a superconducting sample, V, will increase with the peak applied field H_m for two reasons; firstly because more of a given asperity will be penetrated and secondly because, if they differ in shape, more asperities will be penetrated. The volume V will therefore depend on the ratio H_m/H_{c1}, and an average depth of penetration, d, may be defined by :

$$d = V/A = F(H_m/H_{c1})$$

where A is the surface area of the sample.

The average field within a penetrated region may be assumed to be equal to H_m. On field reversal, flux will be trapped and, if complete trapping occurs, the flux in a given asperity will remain constant until the field - H_m is reached. The magnetization curve of such an asperity will be like that shown in Fig. 4.1., and the energy loss per cycle in traversing the magnetization loop will be $4\ \mu_o H_m^2\ V_a$, where V_a is the

penetrated volume of the asperity.

In practice, some flux will leave the asperity on field reversal and the flux trapping will be incomplete. The real magnetization curve will be like that shown in Fig. 4.2., and the energy dissipation may be written as $4\ \mu_o H_m^2 V_a K_a$ where K_a is a constant equal to the ratio of the areas of the real and ideal magnetization curves.

The total loss per cycle in the sample will equal $4\ \mu_o H_m^2\ VK$, where K is an average of the K_a's, and the loss per cycle per unit surface area will be given by

8.7.1. $$L = 4\ \mu_o H_m^2 \frac{V}{A} K = 4\ \mu_o H_m^2 F\ (H_m/H_{c1})\ K$$

Three of the predictions of this expression are confirmed by our measurements, namely :

(i) The loss per cycle is independent of frequency (section 8.2.)

(ii) The dissipation is larger in samples with a larger volume of surface asperities i.e. rougher surfaces (section 8.3.)

(iii) The losses are higher in a sample with a lower H_{c1} (section 8.4.)

These predictions may be put on a more quantative basis by defining an effective depth of penetration dK (= $KF(H_m/H_{c1})$. Values of dK may be obtained from the experimental measurements of L by using Equation 8.7.1. which shows that $dK = L/4\ \mu_o H_m^2$. The expression also predicts that, for a given surface, dK will have the same value for all samples at a particular value of H_m/H_{c1}, i.e. that dK is a universal function of H_m/H_{c1}. This will also be true for type I superconductors if H_c is used in place of H_{c1}. Fig. 8.8. shows $L/4\ \mu_o H_m^2$ plotted against H_m/H_{c1} for the two niobium samples (Nos. 11 and 23) with differing H_{c1} values described in section 8.4. As predicted, the dK values are in good agreement. Seebold (1969) has observed a similar result in type I materials by plotting $L/4\ \mu_o H_c^2$ against H_m/H_c. As shown in section 4.3., these two relationships are equivalent.

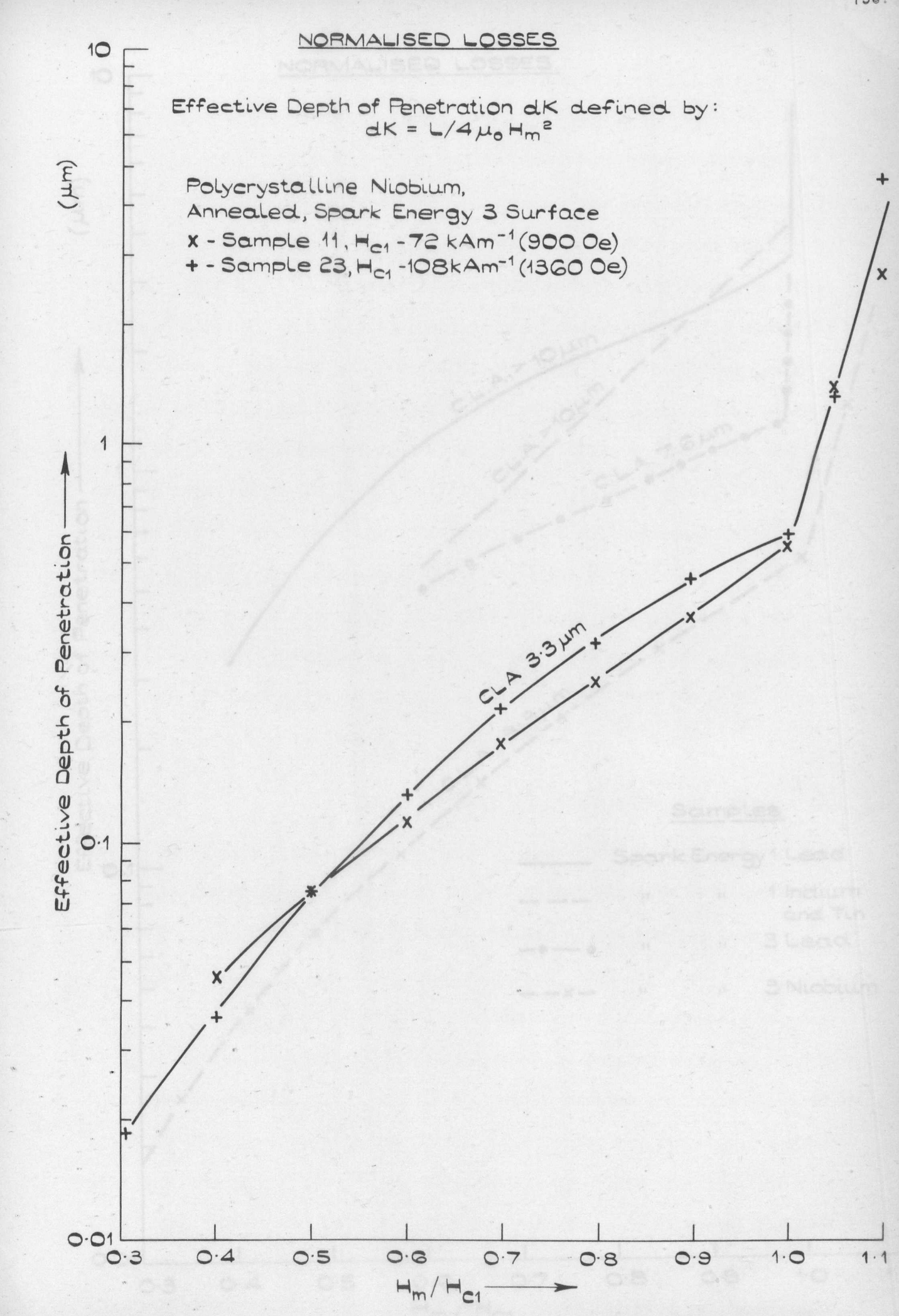
NORMALISED LOSSES
Effective Depth of Penetration dK defined by:
dK = L/4 μ0 Hm²
Polycrystalline Niobium,
Annealed, Spark Energy 3 Surface
x - Sample 11, Hc1 - 72 kAm⁻¹ (900 Oe)
+ - Sample 23, Hc1 - 108 kAm⁻¹ (1360 Oe)
CLA 3·3 μm
Effective Depth of Penetration (μm)
10
1
0·1
0·01
0·3
0·4
0·5
0·6
0·7
0·8
0·9
1·0
1·1
Hm / Hc1

Figure 8.8.

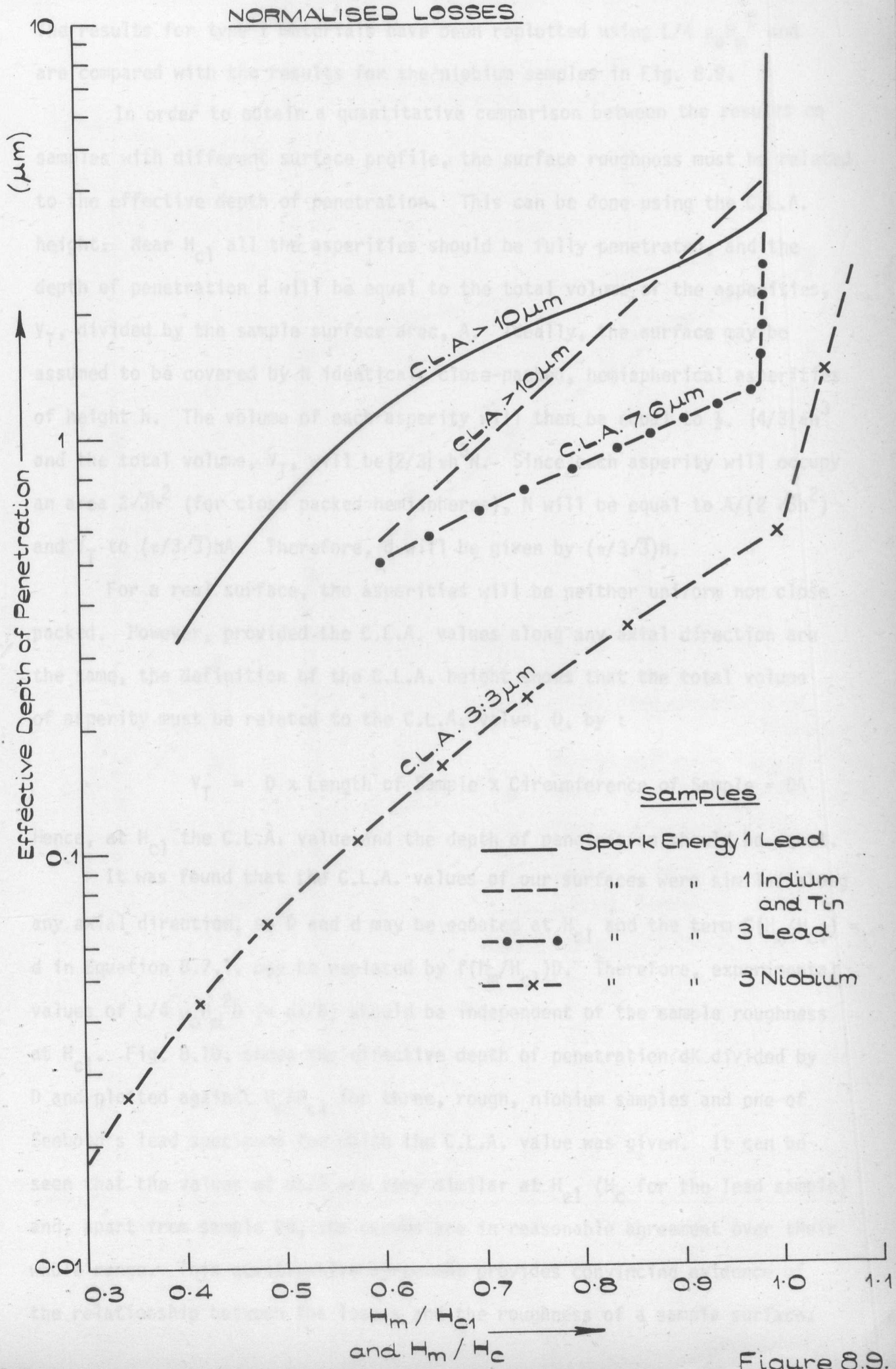
NORMALISED LOSSES
Effective Depth of Penetration (μm)
10
1
0·1
0·01
C.L.A. > 10 μm
C.L.A. > 10 μm
C.L.A. 7·6 μm
C.L.A. 3·3 μm
Samples
Spark Energy 1 Lead
" " 1 Indium and Tin
" " 3 Lead
" " 3 Niobium
0·3
0·4
0·5
0·6
0·7
0·8
0·9
1·0
1·1
Hm / Hc1
and Hm / Hc

Figure 8.9.

The results for type I materials have been replotted using $L/4\ \mu_o H_m^2$ and are compared with the results for the niobium samples in Fig. 8.9.

In order to obtain a quantitative comparison between the results on samples with different surface profile, the surface roughness must be related to the effective depth of penetration. This can be done using the C.L.A. height. Near H_{c1} all the asperities should be fully penetrated, and the depth of penetration d will be equal to the total volume of the asperities, V_T, divided by the sample surface area, A. Ideally, the surface may be assumed to be covered by N identical, close-packed, hemispherical asperities of height h. The volume of each asperity will then be equal to $\frac{1}{2}.\ [4/3]\pi h^3$ and the total volume, V_T, will be $[2/3]\pi h^3 N$. Since each asperity will occupy an area $2\sqrt{3}h^2$ (for close packed hemispheres), N will be equal to $A/(2\sqrt{3}h^2)$ and V_T to $(\pi/3\sqrt{3})hA$. Therefore, d will be given by $(\pi/3\sqrt{3})h$.

For a real surface, the asperities will be neither uniform nor close packed. However, provided the C.L.A. values along any axial direction are the same, the definition of the C.L.A. height shows that the total volume of asperity must be related to the C.L.A. value, D, by :

$$V_T = D \times \text{Length of Sample} \times \text{Circumference of Sample} = DA$$

Hence, at H_{c1} the C.L.A. value and the depth of penetration should be equal.

It was found that the C.L.A. values of our surfaces were similar along any axial direction, so D and d may be equated at H_{c1} and the term $F(H_m/H_{c1}) = d$ in Equation 8.7.1. may be replaced by $f(H_m/H_{c1})D$. Therefore, experimental values of $L/4\ \mu_o H_m^2 D$ $(= dK/D)$ should be independent of the sample roughness at H_{c1}. Fig. 8.10. shows the effective depth of penetration dK divided by D and plotted against H_m/H_{c1} for three, rough, niobium samples and one of Seebold's lead specimens for which the C.L.A. value was given. It can be seen that the values of dK/D are very similar at H_{c1} (H_c for the lead sample) and, apart from sample 24, the curves are in reasonable agreement over their whole range. This quantitative agreement provides convincing evidence of the relationship between the losses and the roughness of a sample surface.

NORMALIZED LOSSES

$$\frac{dK}{D} = \frac{\text{Effective Depth of Penetration}}{\text{Centre-Line Average Value}}$$

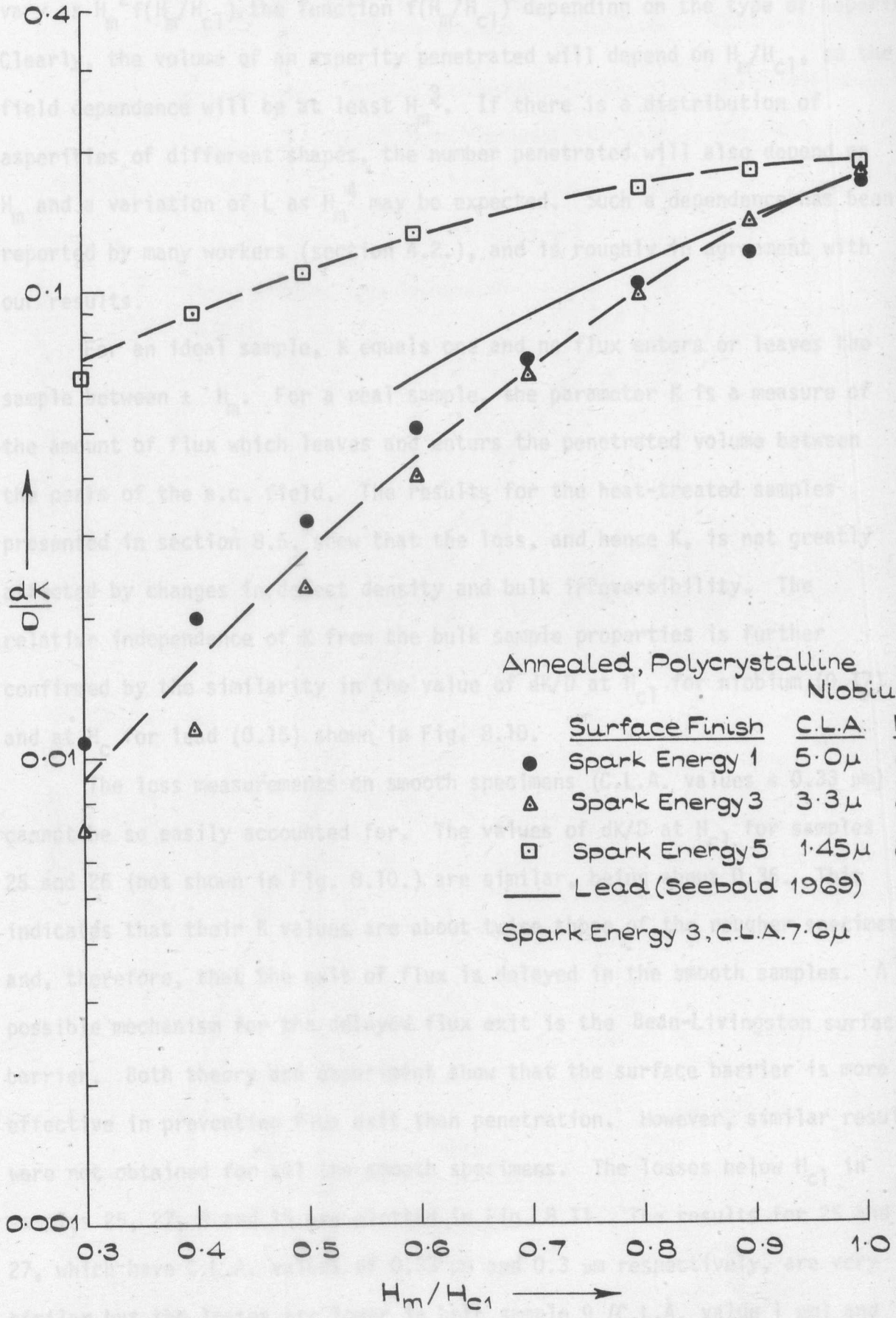

Figure 8.10.

Two further points for discussion are the field dependence of the losses and the parameter K. Equation 8.7.1. predicts that the losses will vary as $H_m^2 f(H_m/H_{c1})$, the function $f(H_m/H_{c1})$ depending on the type of asperity. Clearly, the volume of an asperity penetrated will depend on H_m/H_{c1}, so the field dependence will be at least H_m^3. If there is a distribution of asperities of different shapes, the number penetrated will also depend on H_m and a variation of L as H_m^4 may be expected. Such a dependence has been reported by many workers (section 4.2.), and is roughly in agreement with our results.

For an ideal sample, K equals one and no flux enters or leaves the sample between $\pm H_m$. For a real sample, the parameter K is a measure of the amount of flux which leaves and enters the penetrated volume between the peaks of the a.c. field. The results for the heat-treated samples presented in section 8.5. show that the loss, and hence K, is not greatly affected by changes in defect density and bulk irreversibility. The relative independence of K from the bulk sample properties is further confirmed by the similarity in the value of dK/D at H_{c1} for niobium (0.17) and at H_c for lead (0.15) shown in Fig. 8.10.

The loss measurements on smooth specimens (C.L.A. values $\leq$ 0.33 μm) cannot be so easily accounted for. The values of dK/D at H_{c1} for samples 25 and 26 (not shown in Fig. 8.10.) are similar, being about 0.36. This indicates that their K values are about twice those of the rougher specimens and, therefore, that the exit of flux is delayed in the smooth samples. A possible mechanism for the delayed flux exit is the Bean-Livingston surface barrier. Both theory and experiment show that the surface barrier is more effective in preventing flux exit than penetration. However, similar results were not obtained for all the smooth specimens. The losses below H_{c1} in samples 25, 27, 9 and 15 are plotted in Fig. 8.11. The results for 25 and 27, which have C.L.A. values of 0.33 μm and 0.3 μm respectively, are very similar but the losses are lower in both sample 9 (C.L.A. value 1 μm) and 15 which has a similar surface finish and C.L.A. value to sample 25. Why

LOSSES IN SMOOTH SAMPLES.

Sample	C.L.A. Value - Surface
——— 27, Annealed	0·30μm - Electropolished
—·—·— 25, Annealed	0·33μm - Spark Energy 7
x—x—x 15, Cold-Worked	0·35μm - Spark Energy 7
— — — 9+10, Cold-Worked	1·00μm - As Received

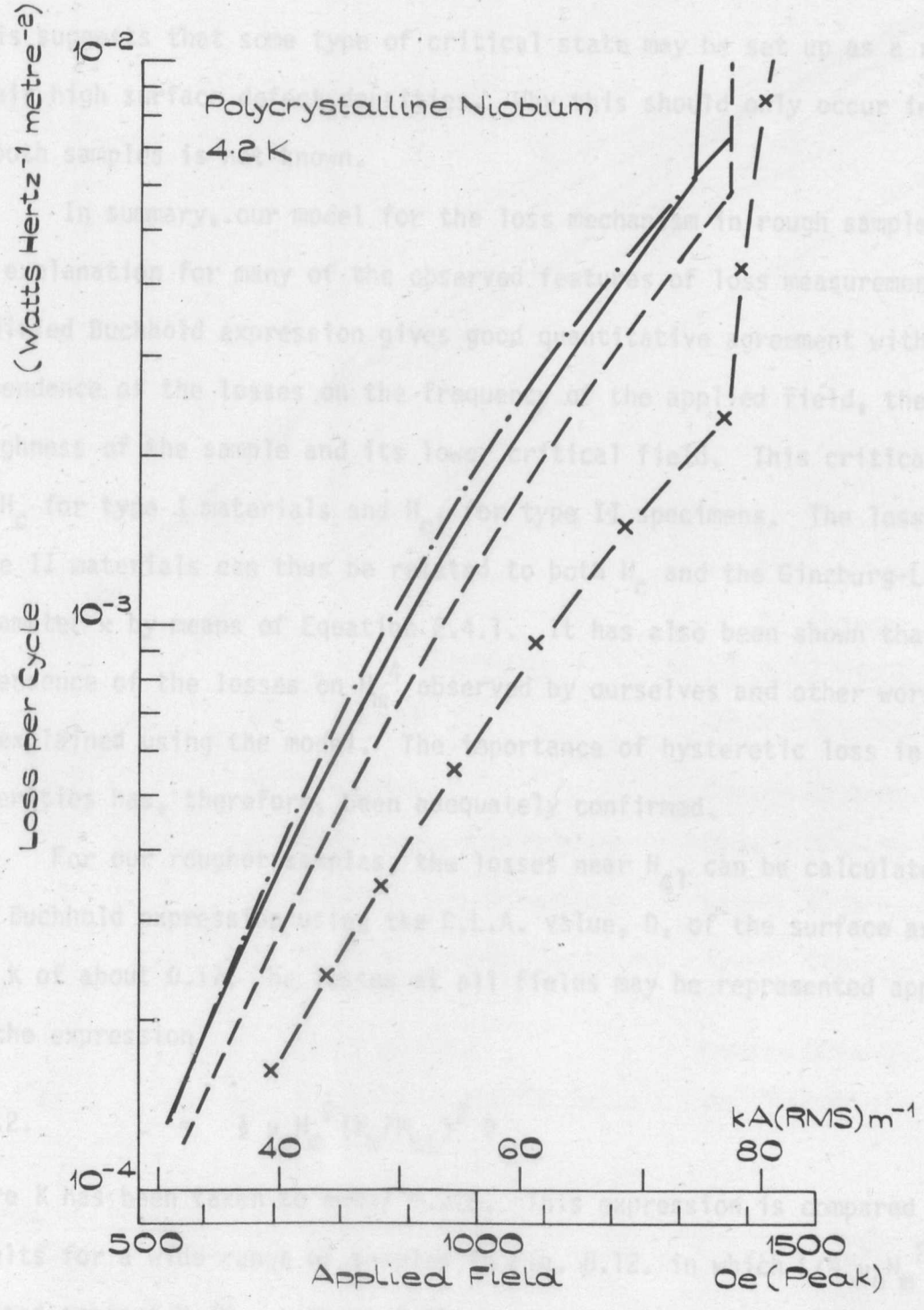

the Bean-Livingston barrier should be less effective for 15 than for 25 is not understood. An alternative explanation for the results is that a second loss mechanism is operative in samples 25 and 27. A further problem is presented by the results of section 8.6., which show that the loss in bright smooth samples has been greatly reduced by surface treatments. In this case, the results cannot be explained by changes in K because the $d\phi/dt$ waveforms showed that very little flux penetrated these samples, i.e. that d was small. This suggests that some type of critical state may be set up as a result of their high surface defect densities. Why this should only occur in bright smooth samples is not known.

In summary, our model for the loss mechanism in rough samples provides an explanation for many of the observed features of loss measurements. The modified Buchhold expression gives good quantitative agreement with the dependence of the losses on the frequency of the applied field, the surface roughness of the sample and its lower critical field. This critical field, H_{CL}, is H_c for type I materials and H_{c1} for type II specimens. The losses in type II materials can thus be related to both H_c and the Ginzburg-Landau parameter κ by means of Equation 2.4.1. It has also been shown that the dependence of the losses on H_m^4 observed by ourselves and other workers can be explained using the model. The importance of hysteretic loss in penetrated asperities has, therefore, been adequately confirmed.

For our rougher samples, the losses near H_{c1} can be calculated from the Buchhold expression using the C.L.A. value, D, of the surface and a value for K of about 0.17. The losses at all fields may be represented approximately by the expression

$$8.7.2. \qquad L = \tfrac{1}{2}\mu_o H_m^2 (H_m/H_{cL})^2 D$$

where K has been taken to equal 0.125. This expression is compared with the results for a wide range of samples in Fig. 8.12. in which $L/4\ \mu_o H_m^2 D$ is plotted against H_m/H_{cL}. None of the experimental results differ from this expression by more than a factor of two.

NORMALIZED LOSSES.

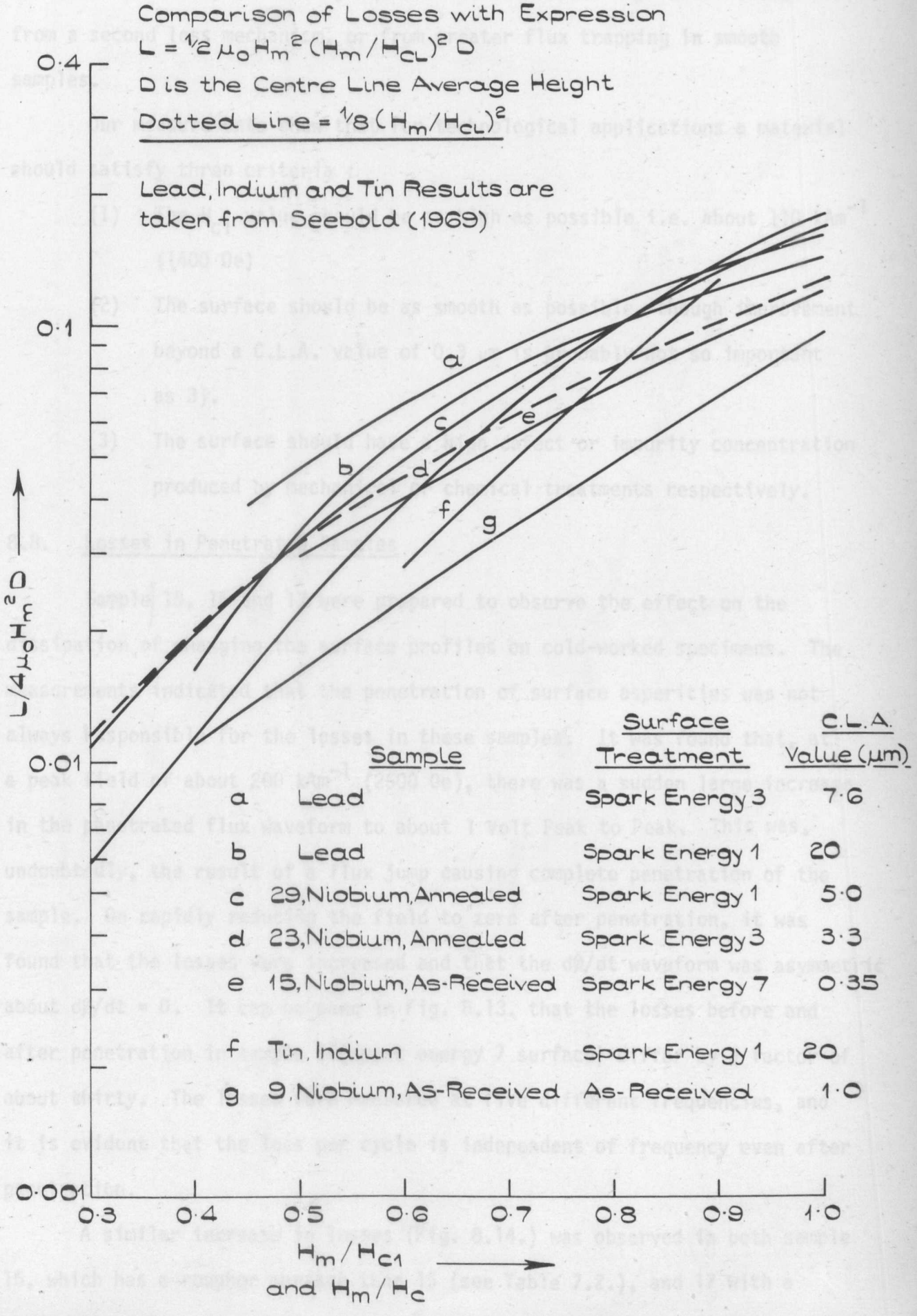

For smooth samples somewhat higher losses are observed in annealed specimens than is predicted by Equation 8.7.2. These may result either from a second loss mechanism, or from greater flux trapping in smooth samples.

Our measurements show that for technological applications a material should satisfy three criteria :

(1) The H_{c1} value should be as high as possible i.e. about 110 kAm^{-1} (1400 Oe)

(2) The surface should be as smooth as possible, though improvement beyond a C.L.A. value of 0.3 μm is probably not so important as 3).

(3) The surface should have a high defect or impurity concentration produced by mechanical or chemical treatments respectively.

8.8. Losses in Penetrated Samples

Samples 15, 16 and 17 were prepared to observe the effect on the dissipation of changing the surface profiles on cold-worked specimens. The measurements indicated that the penetration of surface asperities was not always responsible for the losses in these samples. It was found that, at a peak field of about 200 kAm^{-1} (2500 Oe), there was a sudden large increase in the penetrated flux waveform to about 1 Volt Peak to Peak. This was, undoubtedly, the result of a flux jump causing complete penetration of the sample. On rapidly reducing the field to zero after penetration, it was found that the losses were increased and that the $d\phi/dt$ waveform was asymmetric about $d\phi/dt = 0$. It can be seen in Fig. 8.13. that the losses before and after penetration in sample 15(spark energy 7 surface) differ by a factor of about thirty. The losses were measured at five different frequencies, and it is evident that the loss per cycle is independent of frequency even after penetration.

A similar increase in losses (Fig. 8.14.) was observed in both sample 16, which has a rougher surface than 15 (see Table 7.2.), and 17 with a chemically polished surface. Although the losses below H_{c1} in samples 15

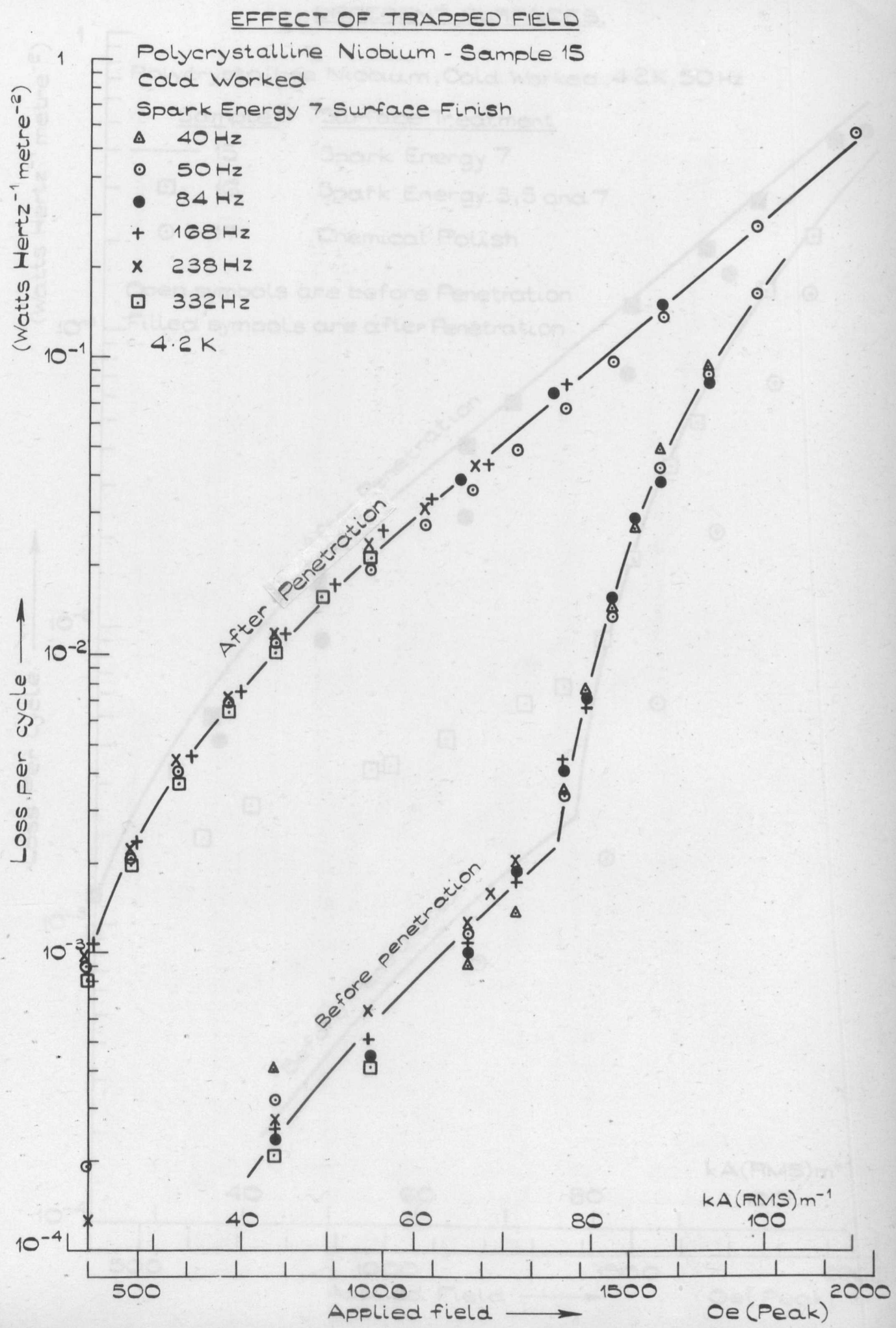
EFFECT OF TRAPPED FIELD
Polycrystalline Niobium - Sample 15
Cold Worked
Spark Energy 7 Surface Finish
40 Hz
50 Hz
84 Hz
168 Hz
238 Hz
332 Hz
4.2 K
After Penetration
Before penetration
Loss per cycle (Watts Hertz⁻¹ metre⁻²)
1
10⁻¹
10⁻²
10⁻³
10⁻⁴
kA (RMS) m⁻¹
40
60
80
100
500
1000
1500
2000
Applied field
Oe (Peak)

Figure 8.13.

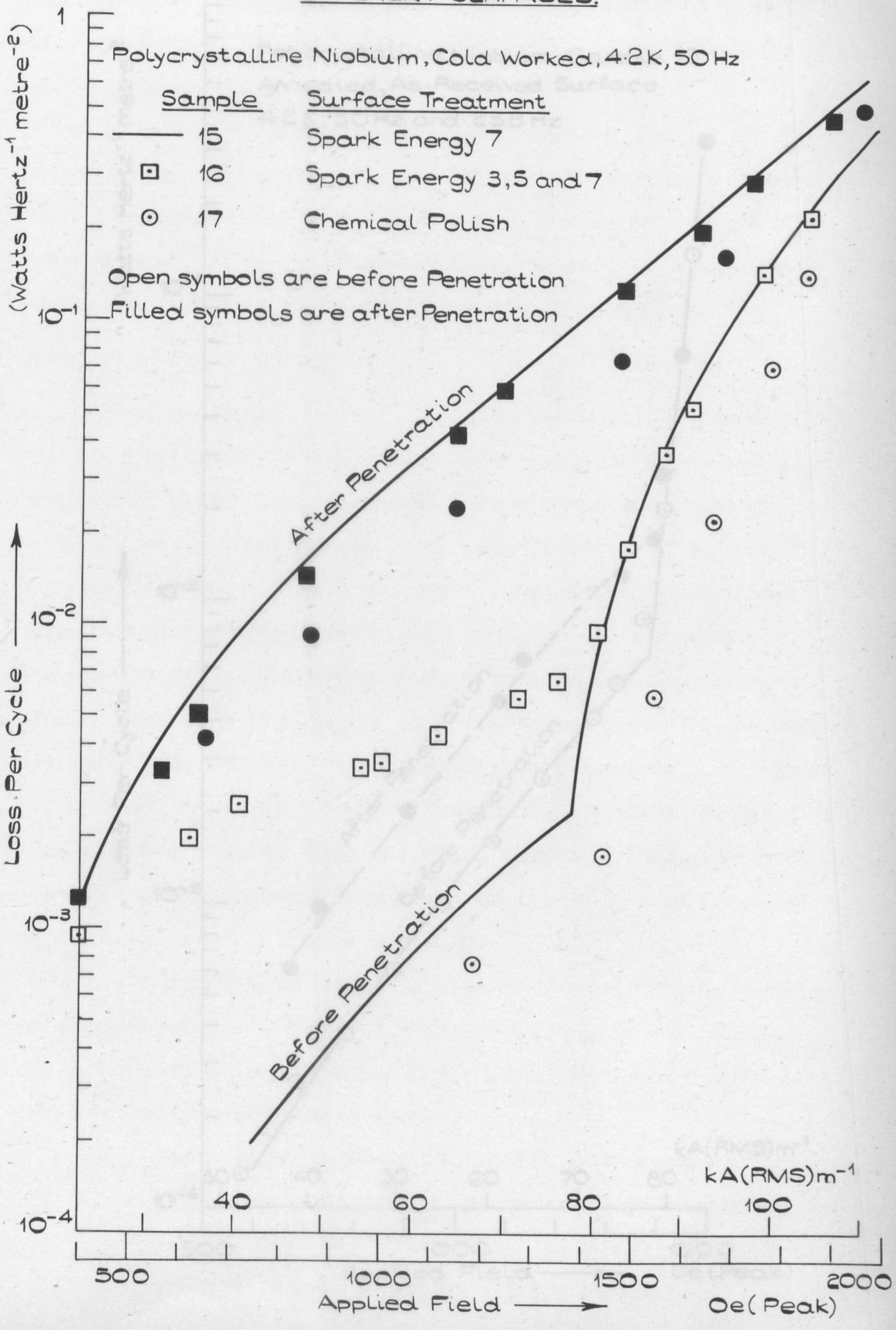
DIFFERENT SURFACES.
Polycrystalline Niobium, Cold Worked, 4·2K, 50 Hz
Sample
Surface Treatment
15
Spark Energy 7
16
Spark Energy 3, 5 and 7
17
Chemical Polish
Open symbols are before Penetration
Filled symbols are after Penetration
After Penetration
Before Penetration
(Watts Hertz⁻¹ metre⁻²)
Loss Per Cycle
1
10⁻¹
10⁻²
10⁻³
10⁻⁴
kA(RMS)m⁻¹
40
60
80
100
500
1000
1500
2000
Applied Field
Oe(Peak)

Figure 8.14.

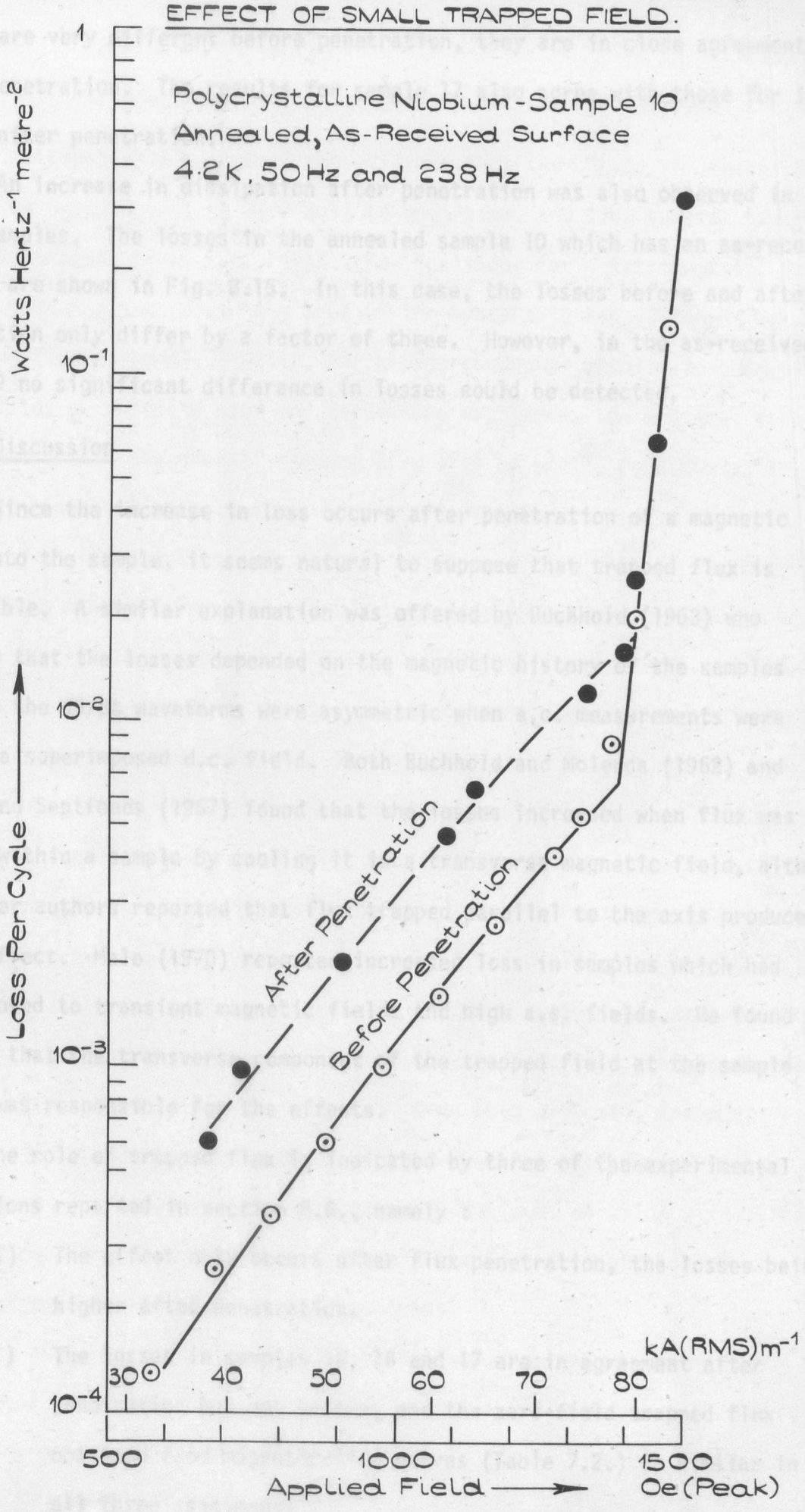
EFFECT OF SMALL TRAPPED FIELD.
Polycrystalline Niobium - Sample 10
Annealed, As-Received Surface
4.2K, 50Hz and 238Hz
Watts Hertz⁻¹ metre⁻²
Loss Per Cycle
1
10⁻¹
10⁻²
10⁻³
10⁻⁴
After Penetration
Before Penetration
kA(RMS)m⁻¹
30
40
50
60
70
80
500
1000
1500
Applied Field
Oe(Peak)

Figure 8.15.

and 16 are very different before penetration, they are in close agreement after penetration. The results for sample 17 also agree with those for 15 and 16 after penetration.

An increase in dissipation after penetration was also observed in other samples. The losses in the annealed sample 10 which has an as-received surface are shown in Fig. 8.15. In this case, the losses before and after penetration only differ by a factor of three. However, in the as-received sample 9 no significant difference in losses could be detected.

8.9. Discussion

Since the increase in loss occurs after penetration of a magnetic field into the sample, it seems natural to suppose that trapped flux is responsible. A similar explanation was offered by Buchhold (1963) who reported that the losses depended on the magnetic history of the samples and that the $d\phi/dt$ waveforms were asymmetric when a.c. measurements were made in a superimposed d.c. field. Both Buchhold and Molenda (1962) and Rocher and Septfonds (1967) found that the losses increased when flux was trapped within a sample by cooling it in a transverse magnetic field, although the latter authors reported that flux trapped parallel to the axis produced little effect. Male (1970) reported increased loss in samples which had been exposed to transient magnetic fields and high a.c. fields. He found evidence that the transverse component of the trapped field at the sample surface was responsible for the effects.

The role of trapped flux is indicated by three of the experimental observations reported in section 8.8., namely :

(i) The effect only occurs after flux penetration, the losses being higher after penetration.

(ii) The losses in samples 15, 16 and 17 are in agreement after penetration but not before, and the zero-field trapped flux obtained from magnetization curves (Table 7.2.) is similar in all three specimens.

(iii) The losses in sample 10 which has a much lower zero-field trapped flux are not so greatly increased after penetration.

Although this is convincing evidence that the change in losses results from flux trapping, it is difficult to understand how flux becomes trapped in a sample exposed to an a.c. field. For instance, for a ferromagnetic in a slowly reducing a.c. field the area of the hysteresis loops diminishes and the remanent flux is small. Equally, for a superconductor exposed to successive peak fields of opposite sign and decreasing magnitude, the critical state model shows that the overall trapped flux will be small, even though a critical state will remain everywhere in the sample.

In an attempt to obtain further evidence of the role of trapped flux, losses were measured in sample 15 after cooling in d.c. magnetic fields parallel to its axis and up to 160 kAm^{-1} (2000 Oe) in magnitude. To do this, the sample was heated above its transition temperature by passing current through a small coil wound on the sample holder. To check that the sample was normal, a small a.c. field was passed through the copper solenoid, and it was observed that this penetrated the sample. Then a large d.c. current was passed into the solenoid, and the heating current was removed. No significant difference in loss was detected after cooling the sample in this way. The reason for this is not clear. Possibly this sample trapped little flux on cooling or the amount of trapped flux must be very near the maximum for the effect to be observed. It would have been extremely informative to be able to measure the amount of flux trapped within the sample after penetration. An integrating magnetometer (Brankin et al 1970) was built for this purpose but, unfortunately, there was insufficient time to make the necessary modifications to the apparatus.

In spite of the negative result obtained from the measurements on a sample cooled in d.c. fields, the other evidence indicates that flux trapping is in some way responsible for the increase in losses. It was suggested (Brankin and Rhodes 1970) that a possible mechanism was motion of the surface exit-points of trapped flux lines (Wipf 1968). This model of flux-spot

motion is described in section 4.3. and would explain three of the experimental observations, i.e.

(i) The loss is similar in samples 15, 16 and 17 with similar values of zero-field trapped flux, i.e. similar numbers of flux spots.

(ii) The loss is lower in sample 10 which has a lower trapped flux i.e. less flux spots.

(iii) There is little change in losses in sample 9 which exhibits strong surface pinning.

It is more difficult to understand why the waveforms are asymmetric and why the increase in loss is so large when the flux spots might be expected to be concentrated at the sample ends. The distance that the trapped flux must move can be approximately estimated as follows :

The loss per cycle, L, is given by Equation 5.3.1.

$$L_{cycle} = 1/2\pi r \int_0^{1/f} H_m \frac{d\phi}{dt} \, dt$$

Assuming that under the influence of an a.c. field, the trapped flux B_T moves sinusoidally over a distance d then :

$$L_{cycle} = 1/2\pi r \, (2\pi rd) \int_0^{1/f} H_m \, B_T \sin^2\omega t \, dt$$

$$= \pi H_m B_T d$$

Values of d calculated from the losses after penetration in sample 15 assuming a value of 0.1 Tesla for B_T are shown in Fig. 8.16. These distances seem unreasonably large to result solely from flux-spot motion.

Therefore, although the Wipf mechanism may be responsible for the loss produced by small, transverse, trapped fields, a more likely explanation (Buchhold 1963) of the present effect is that the presence of the trapped flux provides 'weak spots' at which flux can penetrate more easily. The loss mechanism is then the same as for rough samples, and the effective depth of penetration (equal to $L/4\ \mu_o H_m^2$) is shown in Fig. 8.16. This explanation also enables the asymmetry of the $d\phi/dt$ waveforms to be under-

EFFECT OF TRAPPED FLUX.

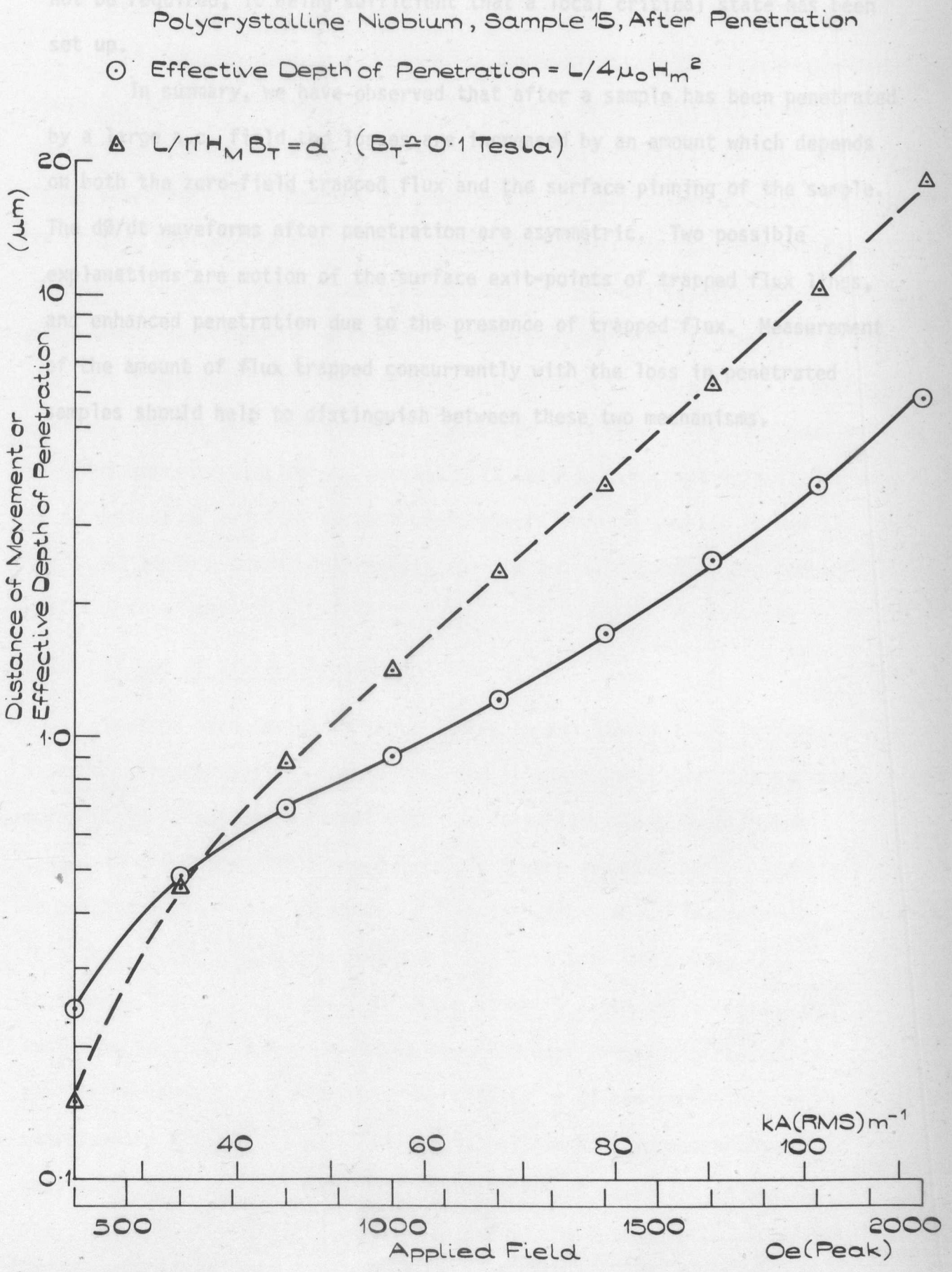

Figure 8.16.

stood, since penetration will be easier when the applied field is in the same direction as the local trapped field. A large trapped field might not be required, it being sufficient that a local critical state has been set up.

In summary, we have observed that after a sample has been penetrated by a large a.c. field the losses are increased by an amount which depends on both the zero-field trapped flux and the surface pinning of the sample. The $d\Phi/dt$ waveforms after penetration are asymmetric. Two possible explanations are motion of the surface exit-points of trapped flux lines, and enhanced penetration due to the presence of trapped flux. Measurement of the amount of flux trapped concurrently with the loss in penetrated samples should help to distinguish between these two mechanisms.

9. LOSSES ABOVE H_{c1}

9.1. Introduction

This chapter contains the results and analysis of the loss measurements above H_{c1} in some niobium samples. The primary object of these experiments was to investigate the effects of various surface treatments on the loss. These treatments were intended to enhance the surface currents which, according to theory, will reduce the losses. A secondary goal was the investigation of losses in annealed samples and a comparison of the results with the theoretical expressions described in section 4.4. using measured critical current values. The next three sections of the chapter are devoted to the surface-treated samples, section 9.4. containing a summary of this work. The loss measurements on annealed samples are presented in section 9.5., and this is followed by an account of critical current measurements made on samples 10 and 11. In the final section (9.7.) the results for the annealed samples are compared with the theories.

9.2. Effect of Neutron Irradiation

Neutron irradiation is known (Kernohan and Sekula 1967) to produce extreme irreversibility in niobium, and it was thought that the surface currents in irradiated material might be very high. Consequently, the losses in a niobium single crystal, sample 4, were measured before and after irradiation with a dose of about 10^{24} fast neutrons m^{-2}. The results (Fig. 9.1.) show that the losses above H_{c1} have been reduced by this treatment, but the rapid rise in losses at about 73 kA(RMS)m^{-1} (1300 Oe) indicates that the surface currents have not been greatly increased. A similar conclusion was reached in the discussion of the magnetization measurements (Fig. 7.7.) in section 7.4. Although no loss measurements were made below 3×10^{-3} WHz^{-1} m^{-2} for the reasons discussed in section 6.4., there is apparently a small increase in the losses below 73 kA(RMS)m^{-1} after irradiation which is due to an increase in κ and a reduction in H_{c1}.

EFFECT OF NEUTRON IRRADIATION.

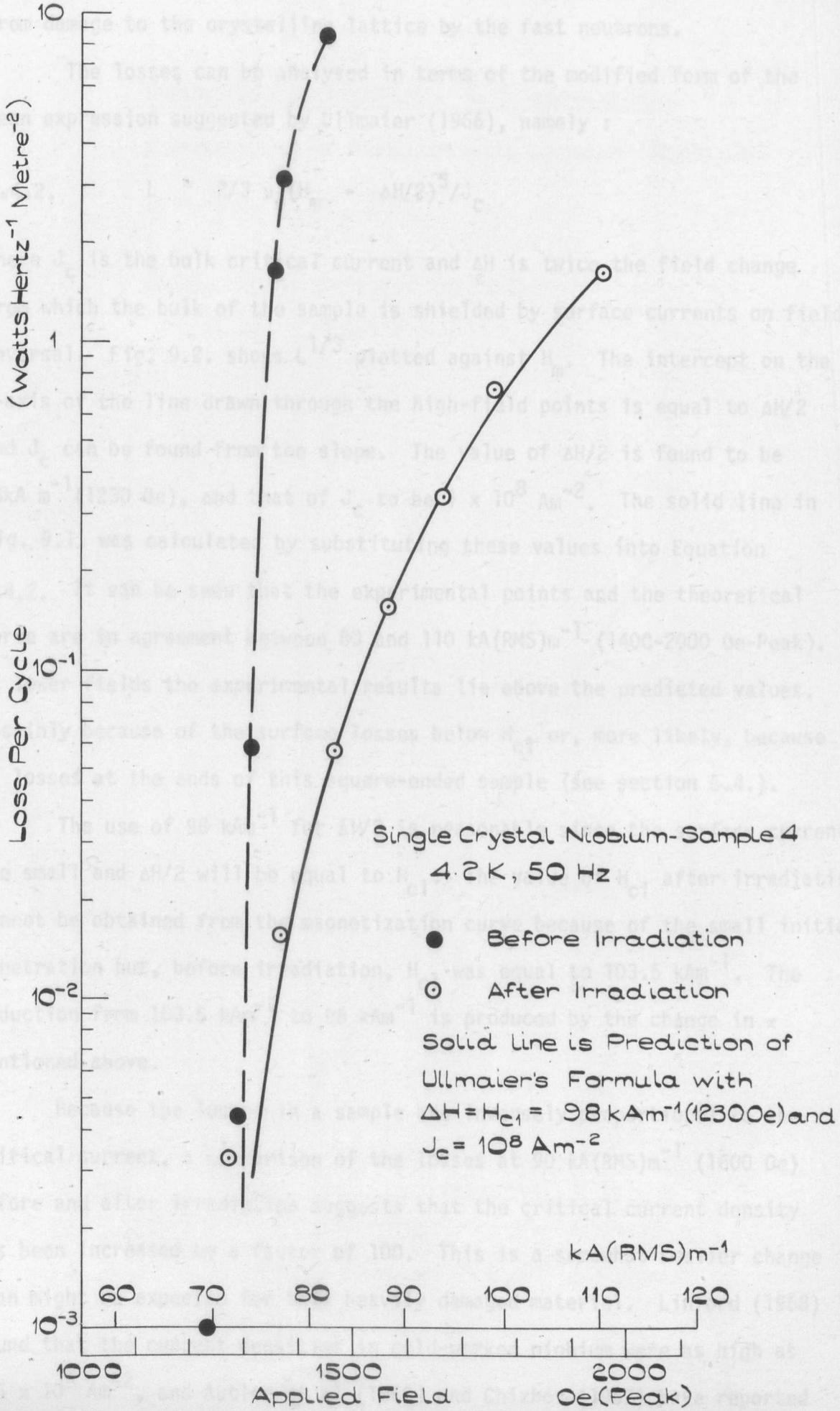

Figure 9.1.

This will arise from a decrease in the electron mean free path resulting from damage to the crystalline lattice by the fast neutrons.

The losses can be analysed in terms of the modified form of the Bean expression suggested by Ullmaier (1966), namely :

$$4.4.2. \qquad L = 2/3\ \mu_0(H_m - \Delta H/2)^3/J_c$$

where J_c is the bulk critical current and ΔH is twice the field change from which the bulk of the sample is shielded by surface currents on field reversal. Fig. 9.2. shows $L^{1/3}$ plotted against H_m. The intercept on the x-axis of the line drawn through the high-field points is equal to $\Delta H/2$ and J_c can be found from the slope. The value of $\Delta H/2$ is found to be 98kA m^{-1}(1230 Oe), and that of J_c to be 1 x 10^8 Am^{-2}. The solid line in Fig. 9.1. was calculated by substituting these values into Equation 4.4.2. It can be seen that the experimental points and the theoretical curve are in agreement between 80 and 110 kA(RMS)m^{-1} (1400-2000 Oe-Peak). At lower fields the experimental results lie above the predicted values, possibly because of the surface losses below H_{c1} or, more likely, because of losses at the ends of this square-ended sample (see section 5.4.).

The use of 98 kAm^{-1} for $\Delta H/2$ is reasonable since the surface currents are small and $\Delta H/2$ will be equal to H_{c1}. The value of H_{c1} after irradiation cannot be obtained from the magnetization curve because of the small initial penetration but, before irradiation, H_{c1} was equal to 103.5 kAm^{-1}. The reduction from 103.5 kAm^{-1} to 98 kAm^{-1} is produced by the change in κ mentioned above.

Because the losses in a sample are inversely proportional to the critical current, a comparison of the losses at 90 kA(RMS)m^{-1} (1600 Oe) before and after irradiation suggests that the critical current density has been increased by a factor of 100. This is a somewhat smaller change than might be expected for this heavily damaged material. Linford (1968) found that the current densities in cold-worked niobium were as high as 2.5 x 10^9 Am^{-2}, and Autler et al (1962) and Chizhov (1967) have reported

IRRADIATED NIOBIUM: $L^{1/3}$ versus H_m.

Comparison of Results with Ullmaier Formula:

$$L = \frac{2}{3\pi^2}\mu_0 \left(\frac{H_m - H_{c1}}{J_c}\right)^3$$

Gives $H_{c1} = 98\,kAm^{-1}$ (1230 Oe)

$J_c = 10^8\,Am^{-2}$

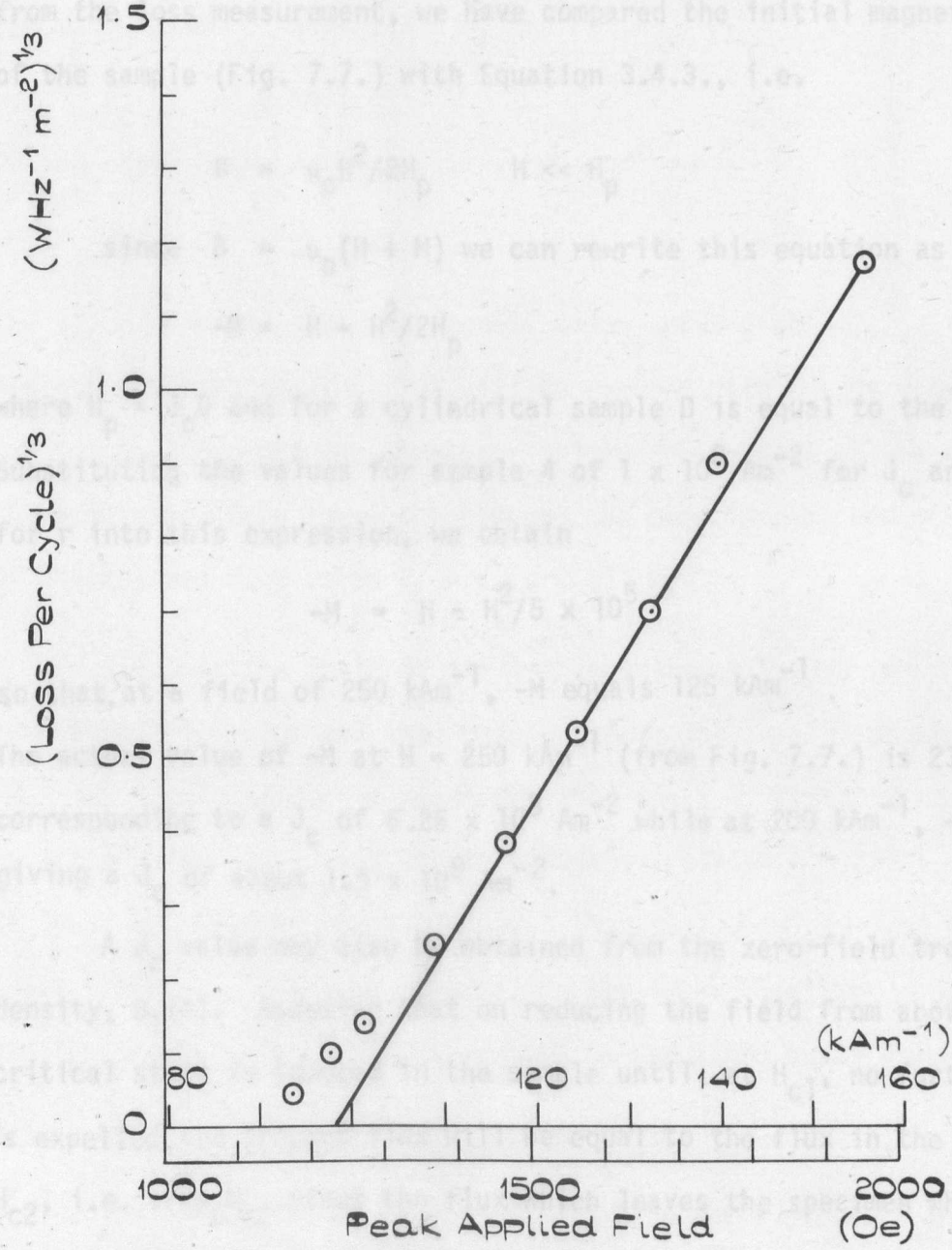

Figure 9.2.

currents of order 10^9 Am^{-2} in deformed polycrystalline samples at similar fields. Sekula (1970) has also studied the effects of neutron irradiation on the losses in niobium. He obtained values for J_c from loss measurements in d.c. fields in the mixed state. By analysing these in terms of the Bean expression (Equation 3.4.4.) he obtains values of 1×10^9 Am^{-2} for the critical current at 130 kAm^{-1} (1600 Oe) in a sample exposed to a dose of 6×10^{23} neutrons m^{-2}.

In order to check the critical current value of 1×10^8 Am^{-2} obtained from the loss measurement, we have compared the initial magnetization curve of the sample (Fig. 7.7.) with Equation 3.4.3., i.e.

$$B = \mu_o H^2/2H_p \qquad H \ll H_p$$

since $B = \mu_o(H + M)$ we can rewrite this equation as

$$-M = H - H^2/2H_p$$

where $H_p = J_c D$ and for a cylindrical sample D is equal to the radius, r. Substituting the values for sample 4 of 1×10^8 Am^{-2} for J_c and 2.5×10^{-3} m for r into this expression, we obtain

$$-M = H - H^2/5 \times 10^5$$

so that, at a field of 250 kAm^{-1}, -M equals 125 kAm^{-1}.
The actual value of -M at H = 250 kAm^{-1} (from Fig. 7.7.) is 230 kAm^{-1}, corresponding to a J_c of 6.25×10^8 Am^{-2} while at 200 kAm^{-1}, -M = 195 kAm^{-1} giving a J_c of about 1.5×10^9 Am^{-2}.

A J_c value may also be obtained from the zero-field trapped flux density, $B_T(o)$. Assuming that on reducing the field from above H_{c2} a critical state is induced in the sample until, at H_{c1}, no further flux is expelled, the trapped flux will be equal to the flux in the sample at H_{c2}, i.e. $\pi r^2 \mu_o H_{c2}$ minus the flux which leaves the specimen when the field decreases from H_{c2} to H_{c1}. The latter will be equal to the flux, ϕ, which penetrates a superconductor when exposed to a field H equal to $H_{c2} - H_{c1}$ and, according to Bean (1964), for a cylinder of radius r this is given by

$$\phi = \pi r^2 \mu_o (H^2/J_c r - H^3/3(J_c r)^2) \qquad H < J_c r$$

where the cubic term appears in the expression because of the cylindrical (as opposed to slab) geometry. Hence for this specimen

$$B_T(o) = \mu_o |H_{c2} - (H_{c2} - H_{c1})^2/J_c r + (H_{c2} - H_{c1}|^3/3(J_c r)^2|$$

provided $H_{c2} - H_{c1} < J_c r$

Substituting into this equation $H_{c2} = 282\ kAm^{-1}$, $H_{c1} = 98\ kAm^{-1}$, $r = 2.5 \times 10^{-3} m$ and $J_c = 10^8\ Am^{-2}$ we obtain

$$B_T(o) = 0.23\ Tesla$$

On the other hand, using $J_c = 6.25 \times 10^8\ Am^{-2}$

$$B_T(o) = 0.33\ Tesla$$

The value obtained from the magnetization curve (Table 7.2.) is 0.3 Tesla. Since the actual trapped flux will be reduced both by the drop in critical current near H_{c2} and the Abrikosov shielding currents in the mixed state, there is reasonable agreement between the experimental and theoretical values of the trapped flux using $J_c = 6.25 \times 10^8\ Am^{-2}$.

Since at the field of the loss measurements ($140\ kAm^{-1}$) J_c will be higher than both this value and that obtained from the initial magnetization curve at $-M = 195\ kAm^{-1}$, it can be concluded that the a.c. critical current obtained by fitting the loss measurements to the expression $L = 2/3\ \mu_o(H_m - H_{c1})^3/J_c$ is at least an order of magnitude lower than that obtained from the magnetization curve. The a.c. critical current is also lower than that obtained for a similar sample from loss measurements in the mixed state (Sekula 1970).

9.3. Effect of Mechanical Surface Treatment

The effect on the losses of polishing the surface of the annealed sample 31 with diamond paste is shown in Fig. 9.3. The decrease in the losses below H_{c1} has already been discussed in section 8.6. The reduction above H_{c1} is even more marked. At 90 kA(RMS)m^{-1} (1600 Oe) the losses in

EFFECT OF MECHANICAL POLISHING.

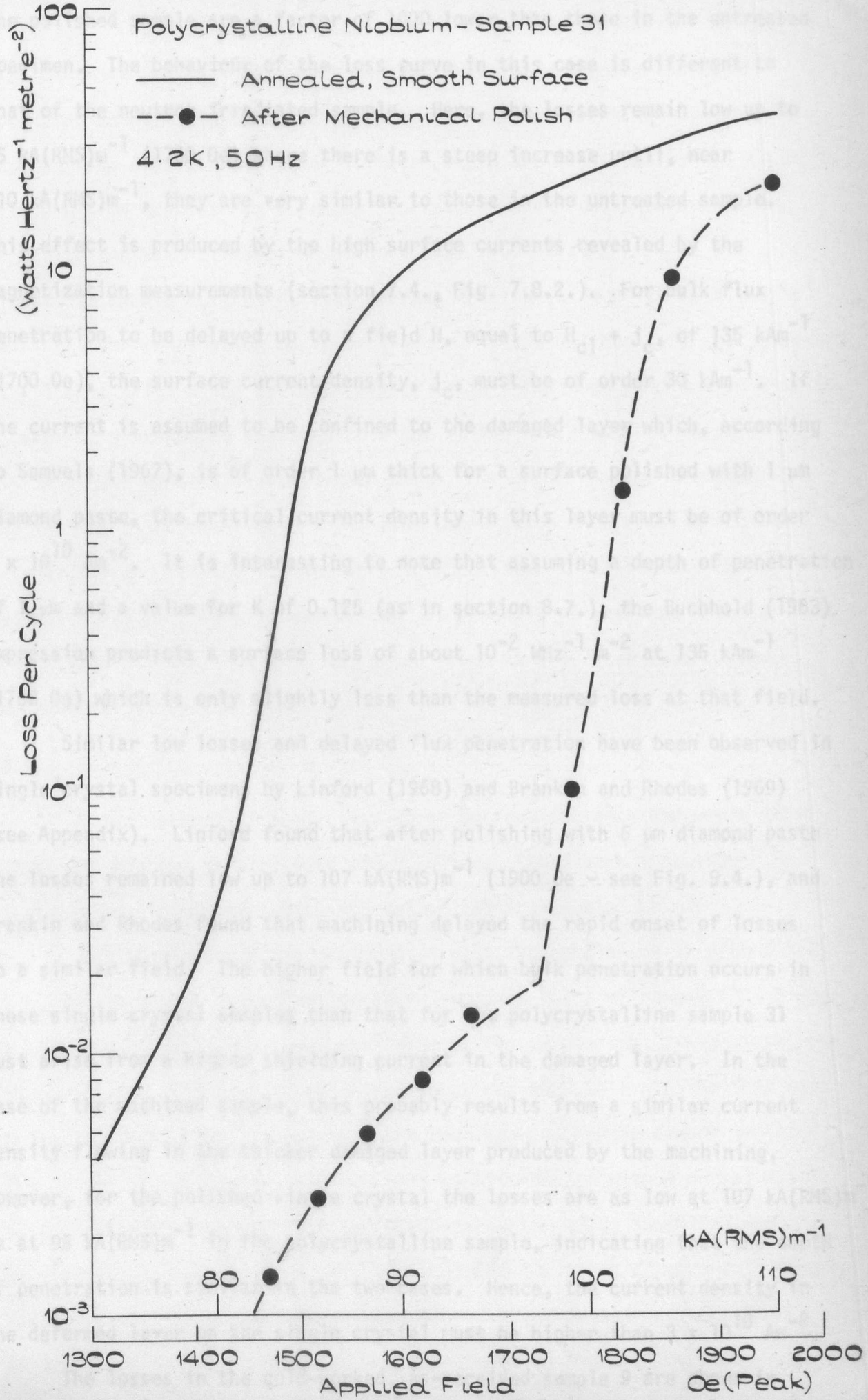

Figure 9.3

the polished sample are a factor of 1000 lower than those in the untreated specimen. The behaviour of the loss curve in this case is different to that of the neutron irradiated sample. Here, the losses remain low up to 95 kA(RMS)m^{-1} (1700 Oe) where there is a steep increase until, near 110 kA(RMS)m^{-1}, they are very similar to those in the untreated sample. This effect is produced by the high surface currents revealed by the magnetization measurements (section 7.4., Fig. 7.8.2.). For bulk flux penetration to be delayed up to a field H, equal to $H_{c1} + j_c$, of 135 kAm^{-1} (1700 Oe), the surface current density, j_c, must be of order 30 kAm^{-1}. If the current is assumed to be confined to the damaged layer which, according to Samuels (1967), is of order 1 μm thick for a surface polished with 1 μm diamond paste, the critical current density in this layer must be of order 3×10^{10} Am^{-2}. It is interesting to note that assuming a depth of penetration of 1 μm and a value for K of 0.125 (as in section 8.7.), the Buchhold (1963) expression predicts a surface loss of about 10^{-2} WHz^{-1} m^{-2} at 135 kAm^{-1} (1700 Oe) which is only slightly less than the measured loss at that field.

Similar low losses and delayed flux penetration have been observed in single crystal specimens by Linford (1968) and Brankin and Rhodes (1969) (see Appendix). Linford found that after polishing with 6 μm diamond paste the losses remained low up to 107 kA(RMS)m^{-1} (1900 Oe - see Fig. 9.4.), and Brankin and Rhodes found that machining delayed the rapid onset of losses to a similar field. The higher field for which bulk penetration occurs in these single crystal samples than that for the polycrystalline sample 31 must arise from a higher shielding current in the damaged layer. In the case of the machined sample, this probably results from a similar current density flowing in the thicker damaged layer produced by the machining. However, for the polished single crystal the losses are as low at 107 kA(RMS)m^{-1} as at 95 kA(RMS)m^{-1} in the polycrystalline sample, indicating that the depth of penetration is similar in the two cases. Hence, the current density in the deformed layer on the single crystal must be higher than 3×10^{10} Am^{-2}.

The losses in the cold-worked, as-received sample 9 are shown in

Fig. 9.5. The onset of high losses in this specimen is delayed to over 120 kA(RMS)m^{-1} (2100 Oe), which implies that the surface grinding has produced an even higher defect density and current carrying capacity in the surface layer. The losses in this sample are higher below 110 kA(RMS)m^{-1} (2000 Oe) because it has a rougher surface than the polished specimens. Applying the Bean-Ullmaier equation 4.4.2. (see Fig. 9.11), to the losses in sample 9, the critical current density is found to be 3.1×10^9 Am^{-2} and the penetration depth at 150 kAm^{-1} (2150 Oe) about 20 μm. However, the losses (Fig. 9.5.) are much higher at this field in sample 15. This is a similar as-received specimen to 9 but it has had a surface layer 10 μm in thickness removed by spark machining. The higher losses in sample 15 suggest that the observed delayed flux penetration in 9 results from a higher current density flowing in a thinner layer than predicted by equation 4.4.2. The critical current is probably of the same order as that for sample 31, i.e. 3×10^{10} Am^{-2}, and flows in a surface layer a few micrometres thick.

9.4. Discussion

Three methods of producing higher surface currents and hence lower losses in niobium samples were investigated. These were : neutron-irradiation, ion-implantation and mechanical treatment.

The ion-implantation produced no significant changes in either the a.c. losses or the magnetization curve (section 8.4.) of sample 27. Since a significant ion current was monitored at the sample, some damage must have been produced although no analytical check was made that niobium ions were being implanted. Whilst aligning the beam some copper ions were implanted. The effect of plating the surface of a superconductor with a normal metal is to reduce the irreversibility (Barnes and Fink 1966, Kwasnitza and Winkler 1969), but it seems unlikely that the implanted copper could have exactly cancelled any effects produced by damage. Little work on ion-implantation in superconductors has been reported by other workers, except that Chang and Rose-Innes (1970) found a significant change in the surface

critical currents of Nb-Mo samples whose surface composition had been altered by the implantation of Mo ions. Here, a significant concentration change was produced to a depth of order 25 nm in an alloy with a coherence length of order 15 nm. In our experiment, the depth of implantation was of order 10 nm and the coherence length approximately 40 nm. The absence of any measurable effect was therefore probably due to an insufficient depth of implantation.

Of the other two techniques, neutron-irradiation produced a significant increase in the bulk critical current but no similar change in the surface currents. Suitable mechanical treatment enhances both the bulk and surface critical currents and, when a surface is mechanically polished, the losses remain below 10^{-2} WHz^{-1} m^{-2} to fields of order 95 $kA(RMS)m^{-1}$ (1700 Oe). A comparison of the losses in a variety of treated single-crystal and polycrystalline samples is shown in Fig. 9.4. It is very clear that polycrystalline material with a mechanically-worked, smooth surface is capable of giving an excellent loss performance. We have shown that surface current densities of order 10^{10} Am^{-2} are obtainable by mechanical polishing, and there appears no reason why this might not be further increased by suitable treatments. The results for the mechanically-polished single-crystal and cold-worked polycrystalline sample suggest that niobium with losses below 2×10^{-3} WHz^{-1} m^{-2} (the economic level) up to 90 $kA(RMS)m^{-1}$ (1600 Oe - Peak) and below 2×10^{-1} WHz^{-1} m^{-2} at up to 130 $kA(RMS)m^{-1}$ could be produced commercially.

Our purpose in investigating the effects of neutron and ion bombardment on the losses was to induce high defect densities, similar to those produced by cold working, in a controlled manner without simultaneously altering the surface profile. Neutron irradiation has been shown to be a useful way of producing high uniform damage densities in bulk material. We believe that further experiments with ion-implantation are desirable using either more energetic niobium ions or lighter ions (e.g. protons) to produce deeper penetration, and that these will show that this technique is equally effective for producing controlled surface damage.

COMPARISON OF DIFFERENT TREATMENTS.

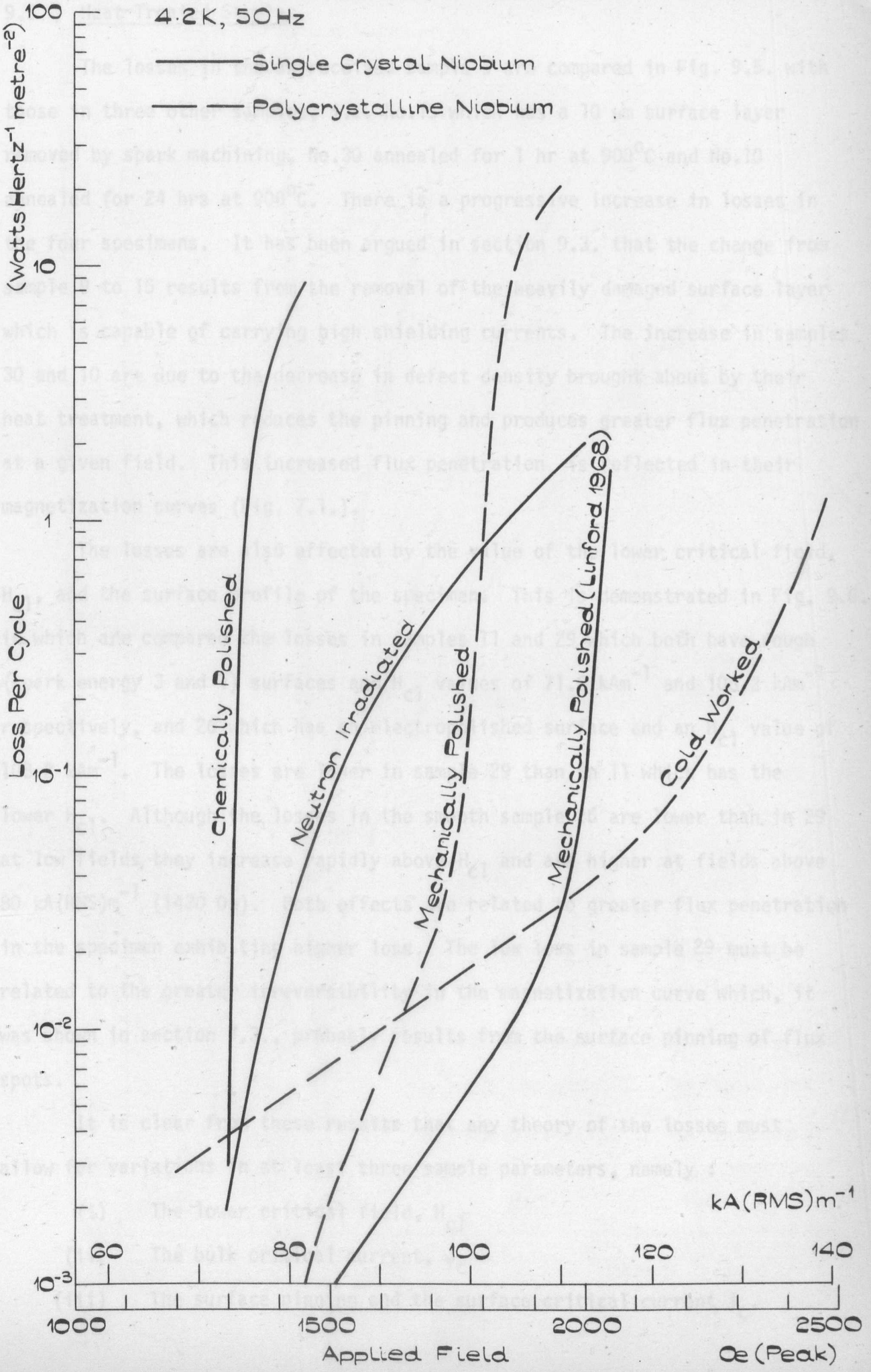

9.5. Heat-Treated Samples

The losses in the as-received sample 9 are compared in Fig. 9.5. with those in three other samples, i.e. No.15 which has a 10 μm surface layer removed by spark machining, No.30 annealed for 1 hr at 900°C and No.10 annealed for 24 hrs at 900°C. There is a progressive increase in losses in the four specimens. It has been argued in section 9.3. that the change from sample 9 to 15 results from the removal of the heavily damaged surface layer which is capable of carrying high shielding currents. The increase in samples 30 and 10 are due to the decrease in defect density brought about by their heat treatment, which reduces the pinning and produces greater flux penetration at a given field. This increased flux penetration is reflected in their magnetization curves (Fig. 7.1.).

The losses are also affected by the value of the lower critical field, H_{c1}, and the surface profile of the specimen. This is demonstrated in Fig. 9.6. in which are compared the losses in samples 11 and 29 which both have rough (spark energy 3 and 1) surfaces and H_{c1} values of 71.6 kAm^{-1} and 108.2 kAm^{-1} respectively, and 26 which has an electropolished surface and an H_{c1} value of 108.2 kAm^{-1}. The losses are lower in sample 29 than in 11 which has the lower H_{c1}. Although the losses in the smooth sample 26 are lower than in 29 at low fields, they increase rapidly above H_{c1} and are higher at fields above 80 $kA(RMS)m^{-1}$ (1430 Oe). Both effects are related to greater flux penetration in the specimen exhibiting higher loss. The low loss in sample 29 must be related to the greater irreversibility in the magnetization curve which, it was shown in section 7.3., probably results from the surface pinning of flux spots.

It is clear from these results that any theory of the losses must allow for variations in at least three sample parameters, namely :

(i) The lower critical field, H_{c1}

(ii) The bulk critical current, J_c

(iii) The surface pinning and the surface critical current, J_c.

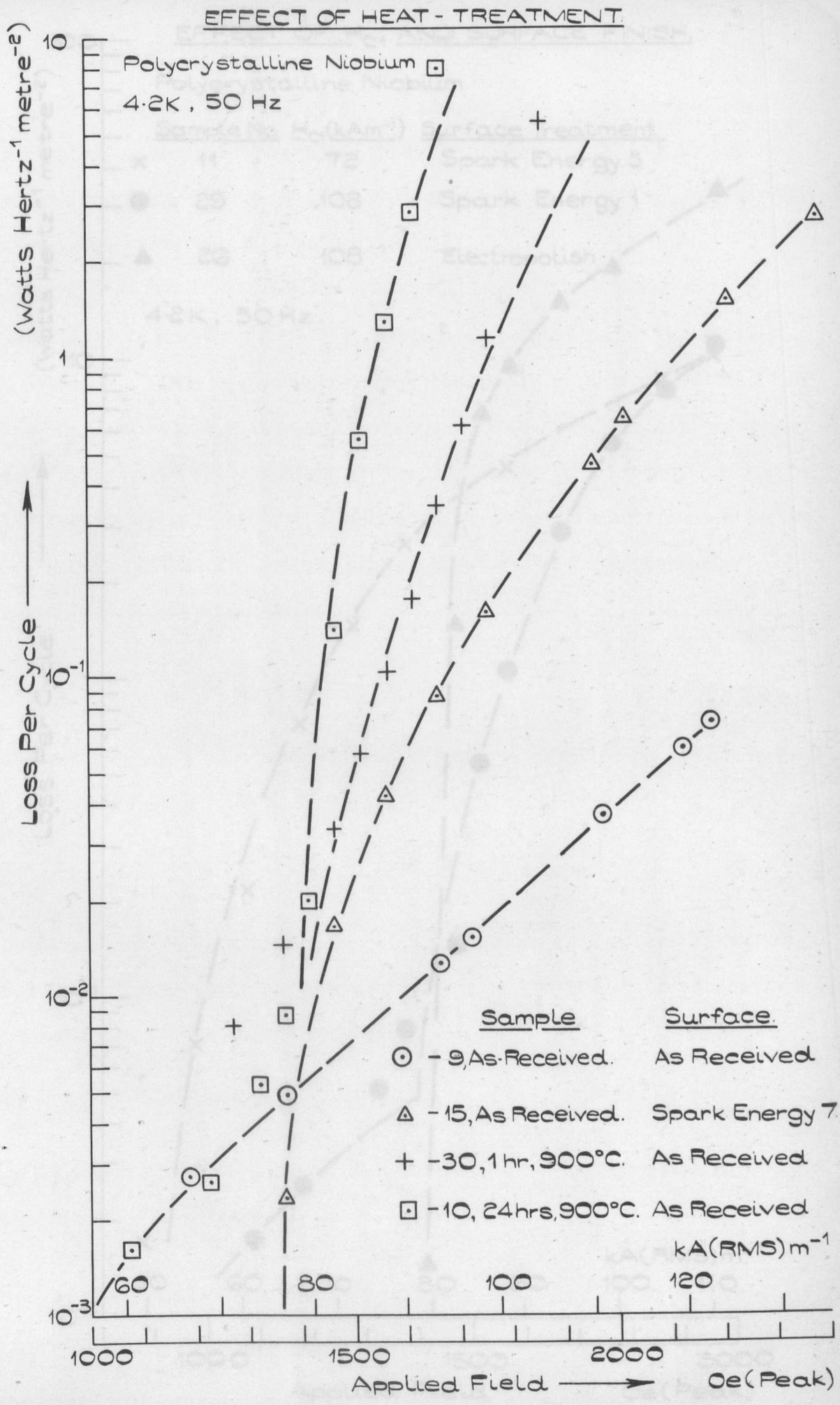
EFFECT OF HEAT - TREATMENT
Polycrystalline Niobium
4·2K , 50 Hz
(Watts Hertz⁻¹ metre⁻²)
Loss Per Cycle
10
1
10⁻¹
10⁻²
10⁻³
Sample
Surface.
⊙ - 9, As-Received. As Received
△ - 15, As Received. Spark Energy 7
+ - 30, 1 hr, 900°C. As Received
⊡ - 10, 24 hrs, 900°C. As Received
kA(RMS) m⁻¹
60
80
100
120
1000
1500
2000
Applied Field
Oe(Peak)

Figure 9.5.

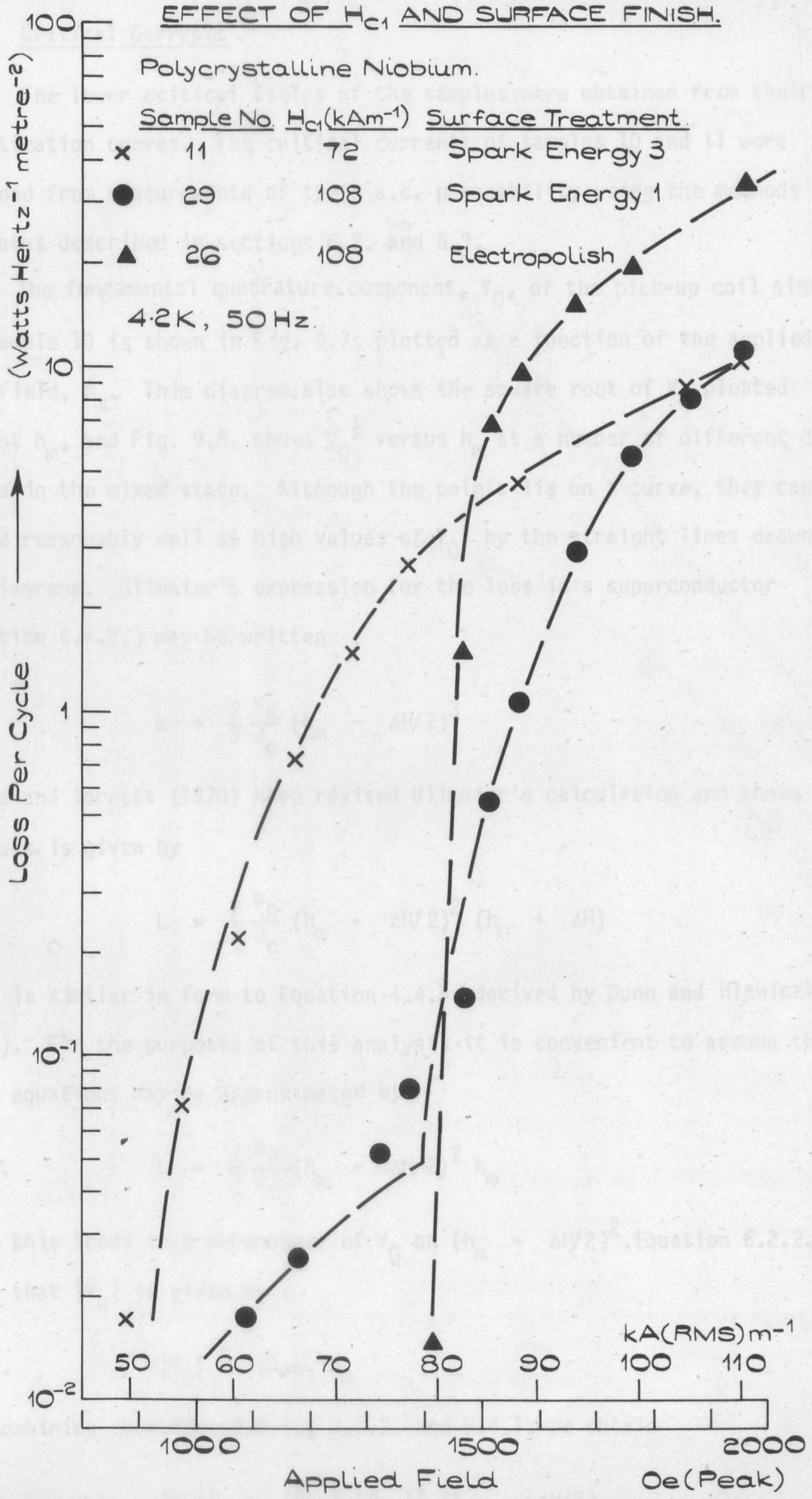
EFFECT OF H_{c1} AND SURFACE FINISH.
Polycrystalline Niobium.
Sample No. $H_{c1}(kAm^{-1})$ Surface Treatment
11 72 Spark Energy 3
29 108 Spark Energy 1
26 108 Electropolish
4·2K, 50Hz.
Loss Per Cycle (Watts Hertz^{-1} metre^{-2})
100
10
1
10^{-1}
10^{-2}
kA(RMS)m^{-1}
50 60 70 80 90 100 110
1000 1500 2000
Applied Field Oe(Peak)

Figure 9.6.

9.6. Critical Currents

The lower critical fields of the samples were obtained from their magnetization curves. The critical currents of samples 10 and 11 were obtained from measurements of their a.c. permeability using the methods and apparatus described in sections 6.2. and 6.3.

The fundamental quadrature component, V_Q, of the pick-up coil signal for sample 10 is shown in Fig. 9.7. plotted as a function of the applied a.c. field, h_m. This diagram also shows the square root of V_Q plotted against h_m, and Fig. 9.8. shows $V_Q^{\frac{1}{2}}$ versus h_m at a number of different d.c. fields in the mixed state. Although the points lie on a curve, they can be fitted reasonably well at high values of $V_Q^{\frac{1}{2}}$ by the straight lines drawn on the diagrams. Ullmaier's expression for the loss in a superconductor (Equation 4.4.2.) may be written

$$L = \frac{2}{3}\frac{\mu_o}{J_c}(h_m - \Delta H/2)^3$$

Sekula and Barrett (1970) have revised Ullmaier's calculation and shown that the loss is given by

$$L = \frac{2}{3}\frac{\mu_o}{J_c}(h_m - \Delta H/2)^2 (h_m + \Delta H)$$

which is similar in form to Equation 4.4.3. derived by Dunn and Hlawiczka (1968). For the purposes of this analysis it is convenient to assume that these equations may be approximated by

9.6.1. $$L = \frac{2}{3}\frac{\mu_o}{J_c}(h_m - \Delta H/2)^2 h_m$$

since this leads to a dependence of V_Q on $(h_m - \Delta H/2)^2$. Equation 6.2.2. shows that $|V_Q|$ is given by :

9.6.2. $$|V_Q| = NA\omega\mu_1'' h_m$$

and combining equations 9.6.1., 9.6.2. and 5.4.1. we obtain

9.6.3. $$|V_Q|^{\frac{1}{2}} = (\frac{2}{3}\frac{\mu_o}{J_c} 2Nr\omega)^{\frac{1}{2}} (h_m - \Delta H/2)$$

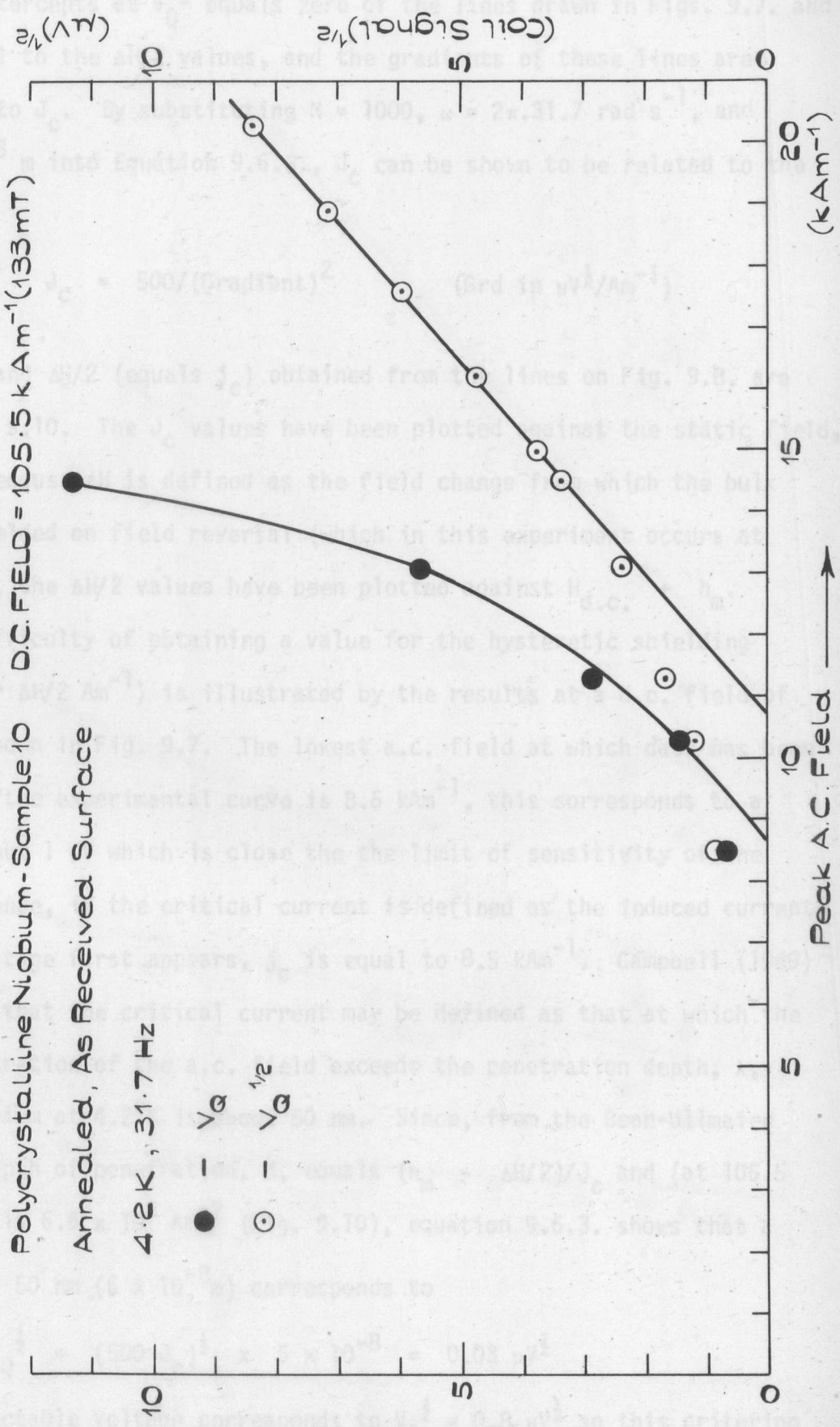
FUNDAMENTAL QUADRATURE COMPONENT OF PICK-UP COIL SIGNAL.
Polycrystalline Niobium-Sample 10
Annealed, As Received Surface
4.2 K, 31.7 Hz
D.C. FIELD = 105.5 kAm⁻¹ (133 mT)
● - V_Q
⊙ - $V_Q^{1/2}$
Coil Signal, V_Q (μV)
(Coil Signal)$^{1/2}$ (μV)$^{1/2}$
Peak A.C. Field (kAm⁻¹)
0
5
10
15
20

Figure 9.7.

Hence, the intercepts at $V_Q^{\frac{1}{2}}$ equals zero of the lines drawn in Figs. 9.7. and 9.8. are equal to the $\Delta H/2$ values, and the gradients of these lines are proportional to J_c. By substituting N = 1000, $\omega = 2\pi.31.7$ rad s^{-1}, and $r = 1.5 \times 10^{-3}$ m into Equation 9.6.3., J_c can be shown to be related to the gradients by

$$J_c = 500/(\text{Gradient})^2 \qquad (\text{Grd in } \mu V^{\frac{1}{2}}/Am^{-1})$$

Values of J_c and $\Delta H/2$ (equals j_c) obtained from the lines on Fig. 9.8. are shown in Fig. 9.10. The J_c values have been plotted against the static field, $H_{d.c.}$, but, because ΔH is defined as the field change from which the bulk sample is shielded on field reversal (which in this experiment occurs at $H_{d.c.} + h_m$), the $\Delta H/2$ values have been plotted against $H_{d.c.} + h_m$.

The difficulty of obtaining a value for the hysteretic shielding current j_c (or $\Delta H/2$ Am^{-1}) is illustrated by the results at a d.c. field of 105.5 kAm^{-1} shown in Fig. 9.7. The lowest a.c. field at which data has been obtained from the experimental curve is 8.5 kAm^{-1}, this corresponds to a voltage of about 1 μV which is close the the limit of sensitivity of the apparatus. Hence, if the critical current is defined as the induced current at which a voltage first appears, j_c is equal to 8.5 kAm^{-1}. Campbell (1969) has suggested that the critical current may be defined as that at which the depth of penetration of the a.c. field exceeds the penetration depth, λ, which for niobium at 4.2°K is about 50 nm. Since, from the Bean-Ullmaier theory, the depth of penetration, d, equals $(h_m - \Delta H/2)/J_c$ and (at 105.5 kAm^{-1}) J_c equals 6.6×10^8 Am^{-2} (Fig. 9.10), equation 9.6.3. shows that a penetration of 50 nm (5×10^{-8}m) corresponds to

$$V_Q^{\frac{1}{2}} = (500\ J_c)^{\frac{1}{2}} \times 5 \times 10^{-8} \simeq 0.03\ \mu V^{\frac{1}{2}}$$

The first detectable voltage corresponds to $V_Q^{\frac{1}{2}} = 0.8\ \mu V^{\frac{1}{2}}$ so this criterion also gives a j_c of 8.5 kAm^{-1}. These 'first penetration' criteria do not allow for voltages arising from penetrated surface asperities, and a third method of defining j_c as equal to the intercept of the straight line at $V_Q^{\frac{1}{2}}$ equals zero gives a higher value of 10.7 kAm^{-1}. In general these two methods

EFFECT OF DC. FIELD ON COIL SIGNAL
Numbers against lines are d.c. field values.
Polycrystalline Niobium, Sample 10
105.5 kAm⁻¹
143 kAm⁻¹
189 kAm⁻¹
222 kAm⁻¹
251 kAm⁻¹
Peak A.C. Field
(kAm⁻¹)
(Coil Signal)^½
(μV)^½
0
5
10
15
20

Figure 9.8.

of defining j_c give values which may differ by a factor of two. In plotting $\Delta H/2$ in Fig. 9.10., the values given by the intercepts of the straight line at $V_Q^{\frac{1}{2}} = 0$ have been used to give consistent results.

Campbell's method of analysis was used for the permeability measurements on sample 11. The in-phase, wideband, pick-up coil voltage, V_o, was measured at a number of fields and the gradient dV_o/dh_m of these curves is plotted against h_m in Fig. 9.9. In this case the curves show the flux profile within the sample. The advantage of Campbell's technique is illustrated by the calculation given above of the depth of penetration at a particular value of $V_Q^{\frac{1}{2}}$, in which the bulk value of the critical current, J_c, was substituted into Equation 9.6.3. The flux profiles show that J_c is higher near the surface and this calculation is incorrect. Using Campbell's expression (Equation 6.2.5.) which may be rewritten as

9.6.4. $$dV_o/dh_m = 2\mu_o\alpha\omega Nr\, d$$

the depth of penetration, d, may be found without assuming a value for J_c. A similar expression to Equation 9.6.4. may be obtained by differentiating Equation 9.6.3. By substituting d for $(h_m - \Delta H/2)/J_c$ into the resulting expression we obtain for V_Q' $(= \alpha V_Q)$ the signal measured at the phase-sensitive detector

9.6.5. $$dV_Q'/dh_m = 8/3\ \mu_o\alpha\omega Nr\, d$$

Equations 9.6.4. and 9.6.5. differ only by the constant 4/3. Hence, similar flux profiles may be obtained from measurements of either dV_o/dh_m or dV_Q'/dh_m. The analysis in terms of $V_Q^{\frac{1}{2}}$ has the advantage of simplicity and leads to the same values for J_c on the linear portions of the curve as those obtained from the flux profiles.

The flux profiles for sample 11 shown in Fig. 9.9. confirm that a critical state exists within this annealed sample and that, except near the surface, the London approximation $J_c = dB/dx$ = constant is obeyed for penetration of up to 100 μm. At larger penetrations where the internal

FLUX PROFILES.

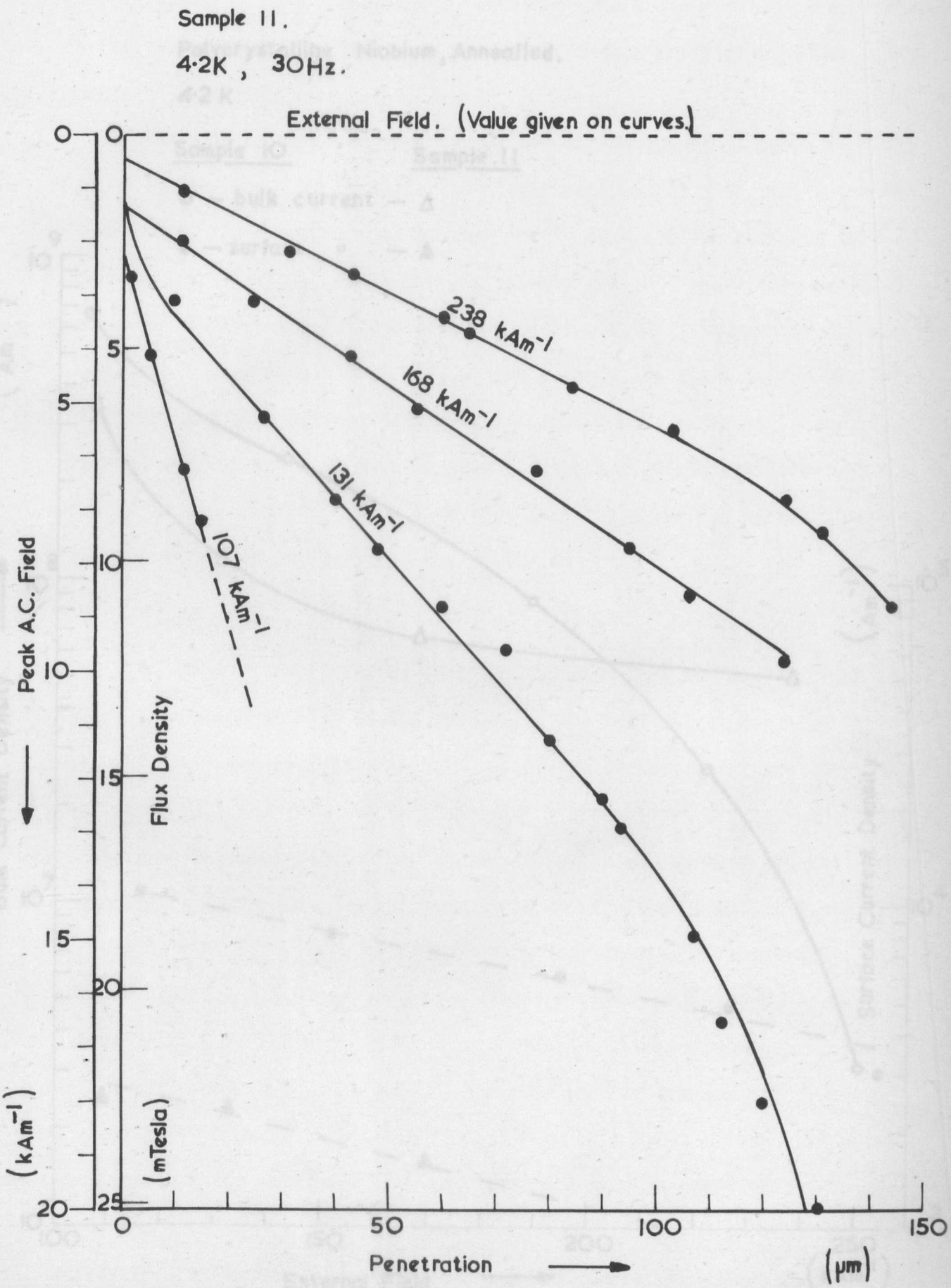

FIGURE 9.9.

CRITICAL CURRENTS.

Polycrystalline Niobium, Annealled.

4·2 K

Sample 10 Sample 11

o — bulk current — Δ

● — surface " — ▲

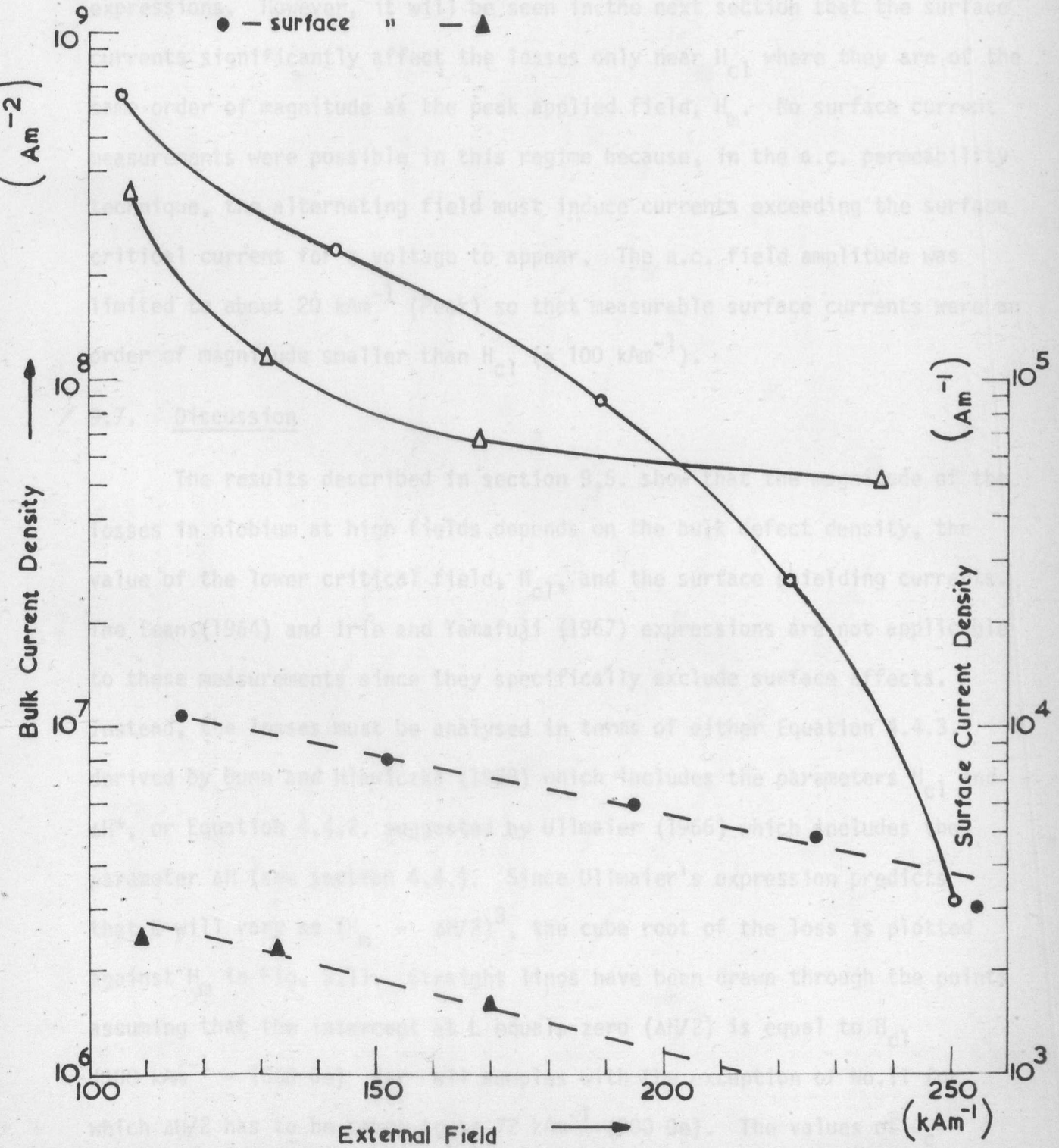

FIGURE 9.10.

field is significantly reduced, dB/dx rises because of the higher local-current density. The values for J_c obtained from these profiles are plotted in Fig. 9.10. together with j_c values obtained from profiles at lower penetration depths up to 10 μm.

The bulk critical current values of samples 10 and 11 shown in Fig. 9.10 are useful in comparing the loss measurements with the theoretical expressions. However, it will be seen in the next section that the surface currents significantly affect the losses only near H_{c1} where they are of the same order of magnitude as the peak applied field, H_m. No surface current measurements were possible in this regime because, in the a.c. permeability technique, the alternating field must induce currents exceeding the surface critical current for a voltage to appear. The a.c. field amplitude was limited to about 20 kAm^{-1} (Peak) so that measurable surface currents were an order of magnitude smaller than H_{c1} (≈ 100 kAm^{-1}).

9.7. Discussion

The results described in section 9.5. show that the magnitude of the losses in niobium at high fields depends on the bulk defect density, the value of the lower critical field, H_{c1}, and the surface shielding currents. The Bean (1964) and Irie and Yamafuji (1967) expressions are not applicable to these measurements since they specifically exclude surface effects. Instead, the losses must be analysed in terms of either Equation 4.4.3. derived by Dunn and Hlawiczka (1968) which includes the parameters H_{c1} and ΔH^*, or Equation 4.4.2. suggested by Ullmaier (1966) which includes the parameter ΔH (see section 4.4.). Since Ullmaier's expression predicts that L will vary as $(H_m - \Delta H/2)^3$, the cube root of the loss is plotted against H_m in Fig. 9.11. Straight lines have been drawn through the points assuming that the intercept at L equals zero ($\Delta H/2$) is equal to H_{c1} (108 kAm^{-1} - 1360 Oe) for all samples with the exception of No.11 for which $\Delta H/2$ has to be taken to be 72 kAm^{-1} (900 Oe). The values of J_c calculated from the gradients of these lines using the expression

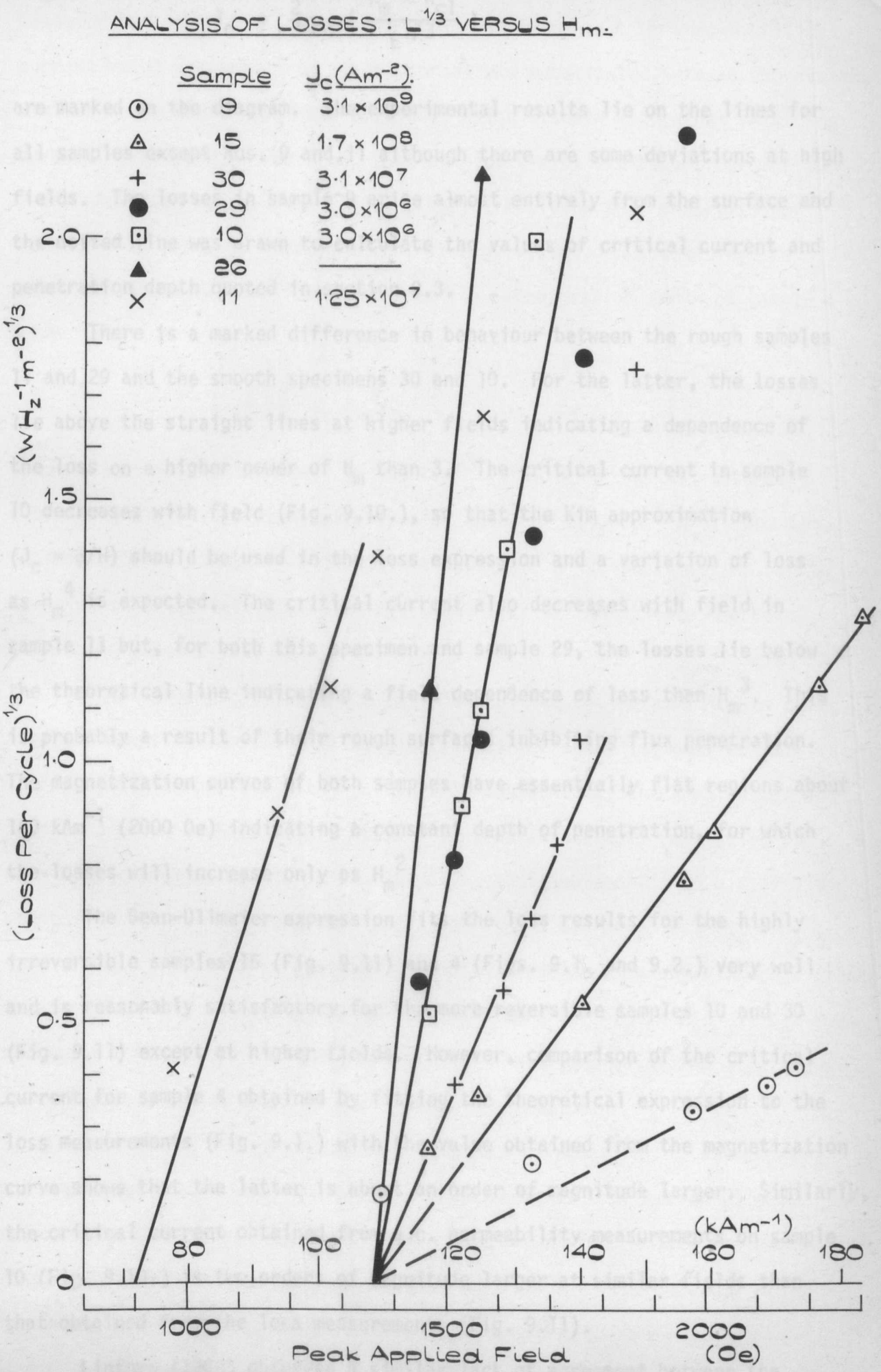
ANALYSIS OF LOSSES : L^1/3 VERSUS Hm.
Sample
Jc(Am-2).
9
3·1 x 10^9
15
1·7 x 10^8
30
3·1 x 10^7
29
3·0 x 10^6
10
3·0 x 10^6
26
11
1·25 x 10^7
(W Hz^-1 m^-2)^1/3
(Loss Per Cycle)^1/3
2·0
1·5
1·0
0·5
0
80
100
120
140
160
180
(kAm^-1)
1000
1500
2000
Peak Applied Field
(Oe)

$$J_c = \frac{2}{3}\mu_0 \left(\frac{H_m - H_{c1}}{L^{1/3}} \right)^3$$

are marked on the diagram. The experimental results lie on the lines for all samples except Nos. 9 and 11 although there are some deviations at high fields. The losses in sample 9 arise almost entirely from the surface and the dotted line was drawn to calculate the values of critical current and penetration depth quoted in section 9.3.

There is a marked difference in behaviour between the rough samples 11 and 29 and the smooth specimens 30 and 10. For the latter, the losses lie above the straight lines at higher fields indicating a dependence of the loss on a higher power of H_m than 3. The critical current in sample 10 decreases with field (Fig. 9.10.), so that the Kim approximation ($J_c = \alpha/H$) should be used in the loss expression and a variation of loss as H_m^4 is expected. The critical current also decreases with field in sample 11 but, for both this specimen and sample 29, the losses lie below the theoretical line indicating a field dependence of less than H_m^3. This is probably a result of their rough surfaces inhibiting flux penetration. The magnetization curves of both samples have essentially flat regions about 160 kAm^{-1} (2000 Oe) indicating a constant depth of penetration, for which the losses will increase only as H_m^2.

The Bean-Ullmaier expression fits the loss results for the highly irreversible samples 15 (Fig. 9.11) and 4 (Figs. 9.1. and 9.2.) very well and is reasonably satisfactory for the more reversible samples 10 and 30 (Fig. 9.11) except at higher fields. However, comparison of the critical current for sample 4 obtained by fitting the theoretical expression to the loss measurements (Fig. 9.1.) with the value obtained from the magnetization curve shows that the latter is about an order of magnitude larger. Similarly, the critical current obtained from a.c. permeability measurements on sample 10 (Fig. 9.10.) is two orders of magnitude larger at similar fields than that obtained from the loss measurements (Fig. 9.11).

Linford (1968) observed a similar lack of agreement between the

measured and theoretical losses in polycrystalline niobium when a critical current value obtained from other sources was substituted into an expression, similar to Dunn and Hlawiczka's (1968), which assumed a constant shielding current equal to H_{c1}. He found that at high fields the losses were of the order predicted by the Bean (1964) theory. Applying this theory to our results also leads to some agreement at high fields. Substituting the J_c value of 1.5×10^9 Am^{-2} obtained from the magnetization curve of sample 4 into

$$L = \frac{2}{3} \mu_o H_m^3 / J_c$$

gives a loss of 2.3 WHz^{-1} m^{-2} at 160 kAm^{-1} (2000 Oe) which is reasonably close to the (extrapolated) experimental value of 2.0 WHz^{-1} m^{-2}. The loss in sample 10 at 130 kAm^{-1} (1640 Oe) is 5.6 WHz^{-1} m^{-2}. Substitution of the J_c value at this field given in Fig. 9.10. (3×10^8 Am^{-2}) into the Bean expression gives a loss of 6.2 WHz^{-1} m^{-2}.

This agreement between the experimental and theoretical losses using the Bean equation implies that at high fields the shielding currents are negligible in comparison with H_m. This is confirmed by the $\Delta H/2$ values for sample 10 shown in Fig. 9.10. Linford arrived at the same conclusion by examining the $d\phi/dt$ waveforms of his polycrystalline samples in a.c. fields greater than H_{c1}. He found that $d\phi/dt$ was always non-zero for $-H_{c1} < H_{a.c.} < H_{c1}$. These results imply that the assumption made by Dunn and Hlawiczka (1968) that provided ΔH^* is negligible $d\phi/dt$ equals zero for $-H_{c1} < H_{a.c.} < H_{c1}$ does not apply to these niobium samples, so that a constant value for $\Delta H/2$ (equal to H_{c1}) should not be used in the Ullmaier expression.

Wipf (1968) has shown that for NbZr the Ullmaier theory agrees well with measured losses when the values for ΔH in Nb-Zr obtained by Ullmaier and Gauster (1966) are used. No similar comparison can be made for our results on sample 10 because, as was explained in the last section, no measurements of the shielding currents were obtained in the region near H_{c1} where they are significant. It seems possible however that the theory will

fit the results for niobium equally well, provided experimental values of J_c and ΔH are obtained from other measurements.

In summary, we have shown that the losses in niobium samples above H_{c1} depend on the bulk defect density, the lower critical field, H_{c1}, and the surface shielding currents. Only Ullmaier's (1966) expression correctly describes the form of these losses. A critical state has been shown to exist in annealed specimens, and the loss measurements for both irreversible and annealed samples fit the equation

$$L = \frac{2}{3} \mu_o (H_m - H_{c1})^3/J_c \qquad (J_c = \text{Constant})$$

However, the critical current values then obtained are at least an order of magnitude lower than those given by other measurement. At fields well above H_{c1}, the losses are in reasonable agreement with those predicted by the Bean (1964) equation using experimental values for J_c. It has been shown that this agreement with the Bean theory arises because the shielding currents are negligible at higher fields. It has been suggested that the correct Ullmaier expression

$$L = \frac{2}{3} \mu_o (H_m - \Delta H/2)^3/J_c$$

may be a good fit to the measured losses in niobium if experimental values for both J_c and ΔH are employed, but it has not been possible to verify this.

10. CONCLUSIONS

Magnetization and low-frequency a.c. loss measurements have been made at 4.2 K on a range of niobium single crystal and polycrystalline specimens. We have found that the losses above and below H_{c1} depend on different material parameters and our results from these two regimes show that :

Below H_{c1}

The losses in samples with rough surfaces (C.L.A. > 0.33 μm) cooled in the earth's field, arise from penetration of surface asperities by the applied a.c. field. A modified version of Buchhold's equation has been developed to analyse the results, namely :

$$L = 4 \mu_o H_m^2 f (H_m/H_{CL}) KD$$

where H_{CL}, the lower critical field, is equal to H_{c1} for type II and H_c for type I superconductors and D is the centre line average value of the surface profile. It has been shown that this expression agrees well with the experimental dependence of the losses on the frequency of the applied field, on the surface roughness and on the lower critical field of both type I and II superconductors. The expression

$$L = 1/2 \mu_o H_m^2 (H_m/H_{CL})^2 D$$

agrees within a factor of two with the measured losses in cold-worked and annealed niobium samples having C.L.A. values between 0.33 and 5.0 μm and the results obtained by Seebold (1969) for lead, indium and tin samples with C.L.A. values of 7.6 and 20 μm.

The losses in annealed, smooth specimens are somewhat higher than predicted by the above expression. It has been suggested that this is because either the exit of flux from the sample is delayed by the Bean-Livingston surface barrier or a second loss mechanism is operative.

In smooth samples having bright, polished surfaces the losses are strongly dependent on the surface treatment, a high defect density reducing

the losses by over an order of magnitude.

It has been found that the losses in specimens having a large, zero-field, trapped flux may be increased by up to thirty times after exposure to a.c. fields large enough to produce complete penetration. However, there was little change in the losses in a sample having a high surface defect density. It is thought that the increased losses result from flux trapped within the sample, although it is not clear whether these losses arise from the motion of the surface exit-points of trapped flux lines or from increased penetration of the applied field at 'weak-spots' produced by the presence of a local critical state.

Above H_{c1}

Measurements on samples in which high bulk or surface defect densities have been induced by neutron irradiation or mechanical treatment have shown that the critical currents are increased and the losses decreased by these treatments. High surface currents are particularly effective in reducing the losses in such damaged specimens. Neutron irradiation does not appear to be a satisfactory method for producing large surface currents, but mechanical treatment, e.g. grinding or polishing, is effective. Implantation of niobium ions into the surface of a niobium sample in an attempt to produce damage proved to have no measurable effect. However, it is thought that the depth of penetration (about 10 nm) of the ions was insufficient and that further experiments using more powerful or lighter ions should be attempted.

We have shown that the losses above H_{c1} depend on the bulk defect density, the lower critical field, H_{c1}, and the surface shielding currents. In annealed samples, the losses are significantly affected by the surface roughness. A rough surface reduces the losses, and this has been related to the delayed flux penetration and hysteresis revealed by the magnetization curves. This hysteresis can only be attributed to the rough surface profile, and it is thought that a longitudinal critical state may be produced by the pinning of flux spots on the surface profile.

The measured losses in both irreversible and annealed samples fit the expression

$$L = \frac{2}{3}\mu_o(H_m - H_{c1})^3/J_c \qquad (J_c = \text{constant})$$

but the critical current density, J_c, obtained is at least an order of magnitude lower than the value obtained from other measurements. It has been shown that this is because the shielding field, $\Delta H/2$, is not constant and for our samples is practically negligible except near H_{c1}.

Technological Aspects

Some of our conclusions are of more technical interest, namely :

(1) Since the losses below the lower critical field, H_{c1} or H_c, are intrinsically low, the niobium for an a.c. conductor should have as high a value for H_{c1} as possible, i.e. should be chemically pure.

(2) For low losses below H_{c1} an a.c. conductor should have :

(a) A smooth bright surface, although asperities with a C.L.A. value of less than about 0.3 μm may not be significant.

(b) A high surface defect density produced, for example, by mechanical polishing, rolling (of sheet) or drawing (of wires).

(3) For low losses above H_{c1} a conductor should have :

(a) A high surface defect density

(b) A high bulk defect density

A roughened surface reduces the losses in annealed samples but this effect was not found to be important in cold-worked materials.

(4) If flux becomes trapped within a superconductor the subsequent losses may be greatly increased. Since flux may be trapped in an a.c. conductor during overload conditions and can only be removed by warming above the transition temperature, devices should be designed to minimize the effect. This might be done, for example, by employing a suitable conductor geometry but a more satisfactory solution would be to use a conductor with a high surface defect density. The increase in losses in such materials appears to be practically negligible.

(5) Our results indicate that it is possible to produce a conductor with losses at 50 Hz below 0.1 W m^{-2} (2 x 10^{-3} WHz^{-1} m^{-2}) at currents of up to 80 kA(RMS)m^{-1}.

Further Work

It has been shown that the losses in niobium below H_{c1} can be made small enough for technical requirements. The greatest interest lies in producing materials with low losses at higher fields.

A considerable amount of work remains to be done on determining the relative effectiveness of surface treatments, particularly mechanical ones, in increasing the bulk and surface critical current densities. We believe that ion-implantation will prove to be a valuable means of producing controlled surface damage if the implantation depth is increased by using higher energy niobium ions or lighter ions such as protons. The latter alternative has the advantage that changes of the surface profile by sputtering should be minimized.

Work is also required on methods of producing niobium in suitable form for a conductor, e.g. by vapour deposition or electroplating onto hard type II superconductors or copper substrates.

Other topics of more academic interest arising directly out of this work are investigations of the mechanism producing losses in samples containing trapped flux and of the mechanism by which losses below H_{c1} are reduced in mechanically and chemically polished samples. An adequate investigation of these effects would require a more sensitive loss measuring apparatus than that used in our experiments. Because of the difficulties of compensation in the electrical method, an absolute calorimetric technique might be more satisfactory for this purpose.

Finally, the losses above H_{c1} in annealed niobium require further investigation. The surface shielding currents should be measured near H_{c1} and used together with measurements of the bulk critical current to test

Ullmaier's expression. The a.c. permeability technique is a useful method for measuring the flux profiles and bulk critical currents in superconductors under a.c. conditions. It could also be used for measuring the shielding currents near H_{c1} if the a.c. field amplitude is increased. The magnitude of the shielding currents can also be obtained from d.c. magnetization measurements, and comparison of the results from the two techniques would be of interest. Little work has been undertaken on the losses in low pinning materials. Such measurements should give considerable insight into the dynamics of flux motion in the mixed state.

REFERENCES

Abrikosov, A.A., 1957, Soviet Physics - JETP, 5, 1174-82.

Abrikosov, A.A., 1964, Soviet Physics - JETP (1965), 20, 480-8.

Anderson, P.W., 1962, Phys. Rev. Lett., 9, 309-11.

Autler, S.H. Rosenblum, E.S., and Gooen, K.H., 1962, Phys. Rev. Lett., 9, 489-93.

Baixeras, J., and Fournet, G., 1966, Phys. Lett., 20, 226-8.

Bardeen, J., Cooper, L.N., Schrieffer, J.R., 1957, Phys. Rev., 108, 1175-1204.

Bardeen, J., and Stephen, M.J., 1965, Phys. Rev., 140, A1197-1207.

Barnes, L.J., and Fink, H.J., 1966, Phys. Lett., 20, 583-4.

Beall, W.T., Jr., and Meyerhoff, R.W., 1969, J. Appl. Phys., 40, 2052-9.

Bean, C.P., 1962, Phys. Rev. Lett., 8, 250-3.

Bean, C.P., 1964, Rev. Mod. Phys., 36, 31-9.

Bean, C.P., and Livingston, J.D., 1964, Phys. Rev. Lett., 12, 14-6.

Becker, R., Heller, G., and Sauter, F., 1933, Z. Phys., 85, 772.

Beilby, G., 1921, Aggression and Flow of Solids, Macmillan : London.

Berlincourt, T.G., Hake, R.R., Leslie, D.H., 1961, Phys. Rev. Lett., 6, 671-4.

Bogner, G. and Heinzel, W., 1963, Solid-State Electronics, 7, 93-9.

Bon Mardion, G., Goodman, B.B. and Lacaze, A., 1964, Phys. Lett., 8, 15-17.

Brankin, P.R., 1968, M.Sc. Thesis, Manchester University.

Brankin, P.R. and Rhodes, R.G., 1969, Brit. J. Appl. Phys., Ser. 2, 2, 1775-8.

Brankin, P.R., Eastham, A.R. and Rhodes, R.G., 1970, J. Phys. E. Sci. Inst., 3, 312.

Brankin, P.R., and Rhodes, R.G., 1970, LT12-Kyoto., To be published.

Buchhold, T.A. and Molenda, P.J., 1962, Cryogenics, 2, 344-347.

Buchhold, T.A., 1963, Cryogenics, 3, 141-9.

Buchhold, T.A., and Rhodenizer, R.L., 1969, IEEE Trans., Mag - 5, 429-33.

Cairns, D.N.H., Minors, R.H., Norris, W.T. and Swift, P.A., 1969, L.T.E.P. Conference, London, Proceedings, 16-23.

Campbell, A.M., Evetts, J.E., and Dew-Hughes, D., 1968, Phil. Mag., 18, 313-43.

Campbell, A.M., 1969, J. Phys. C. : Solid St. Phys., Ser. 2, 2, 1492-1501.

Cape, J.A., and Silvera, I.F., 1968, Phys. Rev. Lett., 20, 326-9.

Catterall, A., 1968, Review Paper - Warwick Conference on A.C. Losses in Superconductors. Unpublished.

Chang, C.C., and Rose-Innes, A.C., 1970, LT12-Kyoto. To be published.

Chizhov, A. Kh., 1967, Soviet Physics - Technical Physics, 12, 555-60.

DeGennes, P.G., and Matricon, J., 1964, Rev. Mod. Phys., 36, 45-8.

DeGennes, P.G., 1966, Superconductivity of Metals and Alloys, W.A. Benjamin : New York.

DeSorbo, W., 1963, Phys. Rev., 132, 107-121.

DeSorbo, W., and Healey, W.A., 1964, Cryogenics, 4, 257-323.

Doidge, P.R., and Eastham, A.R., LT12-Kyoto., To be published.

Dunn, W.I., and Hlawiczka, P., 1968, Brit. J. Appl. Phys. : J. Phys. D., 1, 1469-76.

Easson, R.M. and Hlawiczka, P., 1967a, Phys. Stat. Sol., 23, K129.

Easson, R.M. and Hlawiczka, P., 1967b, Brit. J. Appl. Phys., 18, 1237-49.

Easson, R.M. and Hlawiczka, P., 1968, Brit. J. Appl. Phys. (J. Phys. D.), 1, 1477-85.

Essmann, U., and Träuble, H., 1967, Phys. Lett., 24A, 526-7.

Evetts, J.E., Campbell, A.M., 1966, LT10-Vol. IIB, Moscow : Venti, 1967.

Fink, H.J., 1965, Phys. Rev. Lett., 14, 309-12.

Fink, H.J., 1967, Phys. Rev., 161, 417-22.

Foner, S., 1959, Rev. Sci. Inst., 30, 548-57.

Foner, S., McNiff, E.J., Jr., Matthias, B.T., Corenzwit, E., 1968, LT11, St. Andrews, Proceedings, 1025-32.

Frazer, M.J., Hulm, J.K., Riamersa, H., Venturino, A.J., and Wein, R.E., 1961, Cryogenics, 2, 116-7.

French, R.A., Lowell, J., and Mendelssohn, K., 1967, Cryogenics, 7, 83-8.

Freyhardt, H., 1969, Z. Metallkde, 60, 409-12.

Friedel, J., DeGennes, P.G., and Matricon, J., 1963, Appl. Phys. Lett., 2119-21.

Garwin, R.L. and Matisoo, J., 1967, Proc. IEEE, 55, 538-48.

Ginzburg, V.L. and Landau, L.D., 1950, Z.E.T.F., 20, 1064-82.

Goodfellow, J.G., 1969, Ph.D. Thesis, Warwick University.

Goodman, B.B., 1961, Phys. Rev. Lett., 6, 597-9.

Goodman, B.B., 1966, Reports on Progress in Physics, Vol. 29, Part II, 445-87.

Goodman, B.B., 1969, A.C. Losses in Superconductors, British Oxygen Company Report.

Gor'kov, L.P., 1959, Soviet Physics - JETP, 9, 1364-7 also (Alloys), 1960, Soviet Physics - JETP, 10, 998-1004.

Gorter, C.J., and Casimir, H.B.G., 1934, Physica, 1, 306.

Hancox, R., 1966, Proc. IEE, 113, 1221-8.

Harden, J.L., and Arp., V., 1963, Cryogenics, 3, 105-8.

Hart, H.R., Jr., and Swartz, P.S., 1967, Phys. Rev., 156, 403-11.

Harwood, J.J., Hausner, H.H., Morse, J.G., and Rauch, W.G., 1958, Effect of Radiation on Materials, Rheinhold : New York.

Irie, F., and Yamafuji, K., 1967, J. Phys. Soc., Japan, 23, 255-68.

Irie, F., 1970, ICEC3-Berlin, Iliffe. To be published.

Jones, R.G., and Rose Innes, A.C., 1966, Phys. Lett., 22, 271-2.

Kamerlingh Onnes, H., 1913, Leiden Communications Supplement 34.

Kamper, R.A., 1962, Phys. Lett., 2, 290-2.

Kernohan, R.H., and Sekula, S.T., 1967, J. Appl. Phys., 38, 4904-10.

Kim, Y.B., Hempstead, C.F., and Strnad, A.R., 1962, Phys. Rev. Lett., 9, 306-9.

Kim, Y.B., Hempstead, C.F., and Strnad, A.R., 1963, Phys. Rev., 129, 528-35.

Kleiner, W.H., Roth, L.M., and Autler, S.H., 1964, Phys. Rev., 133, A1226-7.

Kramer, E.J., and Bauer, C.L., 1967, Phil. Mag., 15, 1189-99.

Kuhn, G., 1962, Compt. Rendus. Acad. Sci. (Paris), 255, 2923-5.

Kunzler, J.E., Buehler, E., Hsu, F.S.L., and Wernick, J.H., 1961, Phys. Rev. Lett., 6, 89-91.

Kunzler, J.E., 1962, Proc. 1st. Int. Conf. on High Magnetic Fields. Wiley : New York.

Kwasnitza, K., and Winkler, W., 1969, Z. Physik, 227, 391-8.

Labusch, R., 1968, Phys. Rev., 170, 470-4.

Landau, L.D., and Lifshitz, E.M., 1958, Quantum Mechanics, Vol. 3, of a Course of Theoretical Physics, Pergamon : London.

Landau, L.D., and Lifshitz, E.M., 1958, Statistical Physics, Pergamon : London.

Linford, R.M.F. and Rhodes, R.G., 1968, Phys. Stat. Sol., 28, K63-5.

Linford, R.M.F., 1968, Ph.D. Thesis, Warwick University.

Livingston, J.D., 1964, Rev. Mod. Phys., 36, 54-7.

Livingston, J.D., and Schadler, H.W., 1964, G.E. Report No. 64-RL-3765M.

London, F., and London, H., 1935, Proc. Roy. Soc. A149, 71-88.

London F., 1950, Superfluids Vol. I., 125-30, Dover : New York.

London, H., 1963, Phys. Lett., 6, 162-5.

Lowell, J., 1969, J. Phys. C. : Solid St. Phys., 2, 372-381.

Lynton, E.A., 1969, Superconductivity 3rd Ed. Methuen : London.

Male, J.C., 1970, Cryogenics, 10, 381-5.

Matricon, J., 1964, Phys. Lett., 9, 289-91.

Meissner, W., and Ochsenfeld, R., 1933, Naturweiss, 21, 787.

Mendelssohn, K., 1935, Proc. Roy. Soc., A152, 34-41.

Mendelssohn, K., 1964, Rev. Mod. Phys. 36, 50-1.

Miller, G.L., 1959, Tantalum and Niobium, Butterworths : London.

Miyahara, K., Irie, F., and Yamafuji, K., 1969, J. Phys. Soc. Japan, 27, 290-300.

Narlikar, A.V., and Dew-Hughes, D., 1964, Phys. Stat. Sol., 6, 383-90.

Narlikar, A.V., and Dew-Hughes, D., 1966, J. Mat. Sci., 1, 317-35.

Nembach, E., 1966, Phys. Stat. Sol., 13, 543-58.

Park, J.G., 1965, Phys. Rev. Lett., 15, 352-5.

Pech, T., 1968, Warwick Conference on A.C. Losses in Superconductors. Unpublished.

Pech, T., Duflot, J.P. and Fournet, G., 1965, Phys. Lett., 16, 201-2.

Pippard, A.B., 1950, Proc. Roy. Soc., A.203, 210-23.

Pippard, A.B., 1953, Proc. Roy. Soc., A216, 547-68.

Powell, J.R., and Danby, G.R., 1966, A.S.M.E. Publication No.66-WA/RR-5.

Rhodes, R.G., Rogers, E.C. and Seebold, R.J.A., 1964, Cryogenics, 4, 206-8.

Roberts, B.W., 1963, Superconducting Materials and Some of their Properties, G.E. Report No. 63-RL-3252M.

Rocher, Y.A. and Septfonds, J., 1967, Cryogenics, 7, 96-102.

Rogers, E.C., and Edwards, D.R., 1967, Electrical Review, 181, 348-51.

Rogers, E.C., 1969, LTEP Conference - London, Proceedings, 83-8.

Rollins, R.W., and Silcox, J., 1967, Phys. Rev., 155, 404-18.

Rose-Innes, A.C. and Rhoderick, E.H., 1969, Introduction to Superconductivity, Pergamon : London.

Saint-James, D. and DeGennes, P.G., 1963, Phys. Lett., 7, 306-8.

Samuels, L.E., 1967, Metallographic Polishing by Mechanical Means, Pitman : London.

Sandiford, D.J., and Schweitzer, D.G., 1964, Phys. Lett., 13, 98-100.

Seebold, R.J.A. and Rhodes, R.G., 1969, Brit. J. Appl. Phys., Ser. 2, 2, 1463-6.

Seebold, R.J.A., 1969, Ph.D. Thesis, Warwick University.

Sekula, S.T., and Barrett, J.H., 1970, Appl. Phys. Lett., 17, 204-5.

Sekula, S.T., 1970, Applied Superconductivity Conference - Boulder, J. Appl. Phys. To be published.

Shoenberg, D., 1940, Proc. Roy. Soc. A175, 49-70.

Silcox, J., and Rollins, R.W., 1963, Appl. Phys. Lett., 2, 231-3.

Smith, P.F., 1968, Proceedings of the 1968 Brookhaven Summer Study in Superconducting Devices and Accelerators, BNL-50155.

Smith, P.F., et al., 1970, S.R.C. Publication No. RPP/A73.

Smithell, C.J., 1967, Metals Reference Book, 4th Edition, Butterworths : London.

Taylor, H.F., 1968, Phys. Rev., 165, 517-21.

Taylor, M.T., 1969, LTEP Conference-London, Proceedings, 61-7.

Tedmon, C.S., Nr., Rose, R.M., and Wulff, J., 1964, J. Appl. Phys., 36, 164-7.

Tegart, W.J. McG., 1959, Electrolytic and Chemical Polishing of Metals, Pergamon : London.

Thomas, E.J., (also Saint-James, D., and Sarma, G.), 1969, Type II Superconductivity, Pergamon : London.

Tucker, R.P., and Ohr, S.M., 1967, Phil. Mag., 16, 643-6.

Ullmaier, H.A., 1966, Phys. Lett., 21, 507-8.

Ullmaier, H.A. and Gauster, W.F., 1966, J. Appl. Phys., 37, 4519-21.

Van Gurp, G.J., and van Ooijen, D.J., 1966, Journal de Physique, 27-C3, 51-67.

Wade, J.M.A., 1969, Phil. Mag., 20, 1107-14.

Webb, W.W., 1963, Phys. Rev. Lett., 11, 191-3.

Wilson, M.N., Walters, C.R., Lewin, J.D., and Smith, P.F., 1969, S.R.C. Publication No. RPP/A73.

Wipf, S.L., 1968, Proceedings of the 1968 Summer Study on Superconducting Devices and Accelerators, 571-43, Brookhaven National Labs. Publication No. BNL-50155(C-55).

Yasukochi, K.B. Ogasawara, T. and Usui, N., 1964, J. Phys. Soc. Japan, 19, 1649-61.

Zijlstra, H., 1967, Selected Topics in Solid State Physics, Vol. 9, Ed. E.P. Wohlfarth, (Amsterdam : North Holland).

1. LT-10, 11 and 12 refers to the 10th, 11th and 12th International Conferences on Low Temperature Physics.

2. LTEP refers to the International Institute of Refrigeration Conference on Low Temperatures and Electric Power, London, 1969.

3. ICEC3 refers to the Third International Cryogenic Engineering Conference, Berlin, 1970.

APPENDIX

Publications by the Author

(1) 'Critical Currents in the Superconducting Surface Sheaths of Some Indium-Lead Alloys'.

P.R. Brankin, M.Sc. Thesis, Manchester, 1968.

(2)* 'A.C. Losses in Niobium Single Crystals in the Meissner State'.

P.R. Brankin and R.G. Rhodes, Brit. J. Appl. Phys.: J.Phys.D. , 1969, 2, 1775-8.

(3)* 'A Simple Integrating Magnetometer'.

P.R. Brankin, A.R. Eastham and R.G. Rhodes, J. Phys. E.: Sci. Inst., 1970, 3, 312.

(4) 'Superconducting Materials for A.C. Power-Cables'.

P.R. Brankin, R.M.F. Linford, R.G. Rhodes and R.J.A. Seebold, ICEC3 Proceedings, Berlin, 1970. To be published.

(5) 'An Investigation of the A.C. Loss Mechanism below H_{c1} in a Type II Superconductor'.

P.R. Brankin and R.G. Rhodes, LT12 Proceedings, Kyoto, 1970. To be published.

The papers marked thus * are bound into the thesis after this page.

BRIT. J. APPL. PHYS. (J. PHYS. D), 1969, SER. 2, VOL. 2. PRINTED IN GREAT BRITAIN

RESEARCH NOTES

A.C. losses in niobium single crystals in the Meissner state

P. R. BRANKIN and R. G. RHODES

School of Engineering Science, University of Warwick, Coventry

MS. received 6th August 1969, in revised form 11th September 1969

Abstract. Losses at 50 Hz as a function of magnetic field and surface profile have been investigated in single crystal samples of niobium at 4·2 °K using an electronic wattmeter. The losses in samples with smooth surfaces were less than 5×10^{-4} W Hz^{-1} m^{-2} at 1×10^{5} A m^{-1} (1250 Oe). A sample with a cold-worked surface showed higher losses both before and after the surface was polished. It is concluded that the surface finish is of major importance in determining the magnitude of losses below the lower critical field.

1. Introduction

The subject of a.c. losses in superconductors is of considerable interest because of the potential application of these materials in a.c. devices. Buchhold and Molenda (1962) have shown that losses occur in superconductors subject to low-frequency magnetic fields or currents. Even when the superconductor exhibits perfect macroscopic diamagnetism in the Meissner state, where a d.c. current is carried without loss, some a.c. losses are detected.

Buchhold (1963) suggested that these losses were, in the main, due to local, hysteretic penetration of the a.c. field at surface imperfections. He proposed that the surface loss L(W m^{-2}) was related to the frequency f (Hz) and magnitude H_m (A m^{-1}) of the applied field, the average depth d (m) of penetration of the field and the hysteresis factor K, by the relation

$$L=4\mu_0 f H_m^2 dK.$$

K is a dimensionless constant related to the hysteresis associated with a given field penetration. This formula only applies in the Meissner state, and does not differentiate between type I and II superconductors. The terms d and K in this formula are both affected by sample properties. Buchhold (1963), Rocher and Septfonds (1967), Easson and Hlawiczka (1968) and Linford (1968) observed that the losses at a fixed field increased as the surface roughness increased. This they interpreted as an increase of the field penetration depth d with increasing surface roughness. On the other hand, one would expect d to decrease with an increase in flux-pinning. Above the lower critical field H_{C1} of niobium (a type II superconductor) the losses are found to decrease as the flux-pinning increases (e.g. Linford 1968). By analogy one would expect similar behaviour below H_{C1}.

Rocher and Septfonds (1967) have measured losses at frequencies between 1 and 50 kHz in polycrystalline niobium samples for fields up to 4×10^{4} A m^{-1} (500 Oe). They found that the losses depended on a number of factors, i.e. the frequency, the applied field, the field in which the sample was cooled, the surface finish and the resistance ratio of the materials. As a result of increasing the resistance ratio by outgassing the samples at 2100 °C in a vacuum of approximately 10^{-9} torr, the losses also increased, and this was explained by the lower flux-pinning in the outgassed samples. However, Seebold (to be published) has reported that, for pure lead samples in the Meissner state, no change in the losses occurred when their resistivity ratios differed by two orders of magnitude.

Linford and Rhodes (1968) have published results comparing the losses below H_{C1} in polycrystalline and single-crystal niobium samples. The losses in the polycrystal were found to be lower, presumably because of the greater amount of flux-pinning. Measurements on machined polycrystalline niobium by Easson and Hlawiczka (1968) showed that,

below H_{C1}, losses at a given field decrease sharply as the surface finish improves, and that losses in a very well polished sample are extremely low up to about 1500 Oe.

The purpose of the present experiments was to investigate the a.c. losses in niobium below its lower critical field H_{C1}, or, in the case of some samples, below the field of first flux penetration H_{FP}, i.e. in the Meissner state. To avoid any complicating effects of grain size and grain boundaries on the surface structure, single-crystal specimens were studied.

2. Measurements

Three samples of niobium single crystal, grown by electron-beam zone melting and having orientations near the [110] direction, have been measured. The samples were prepared in the form of solid cylinders 40 mm long and 3–5 mm in diameter. An alternating magnetic field was applied axially to the samples and losses were measured using an electronic wattmeter technique (Easson and Hlawiczka 1967, Linford 1968). Critical field values were obtained using a vibrating sample magnetometer.

Sample 1 was centreless ground to 3 mm diameter, chemically polished and finally outgassed near the melting point at a pressure of 10^{-10} torr. Its resistance ratio was 1040. The losses in this sample, as a function of the peak field, are shown in figure 1. The results from a low-loss polycrystalline sample, measured by Easson and Hlawiczka (1968), have also been plotted for comparison.

Figure 1 also shows the losses measured in sample 2 for two different surface treatments. The first measurements were made after spark-eroding the crystal to a cylindrical form. Final shaping to a diameter of 5 mm was carried out at spark energy 7. The losses were then remeasured after chemical polishing.

Sample 3 was cut from the same as-grown crystal as sample 2. It was machined to a cylinder of 5 mm diameter on an ordinary lathe. The losses measured after this treatment

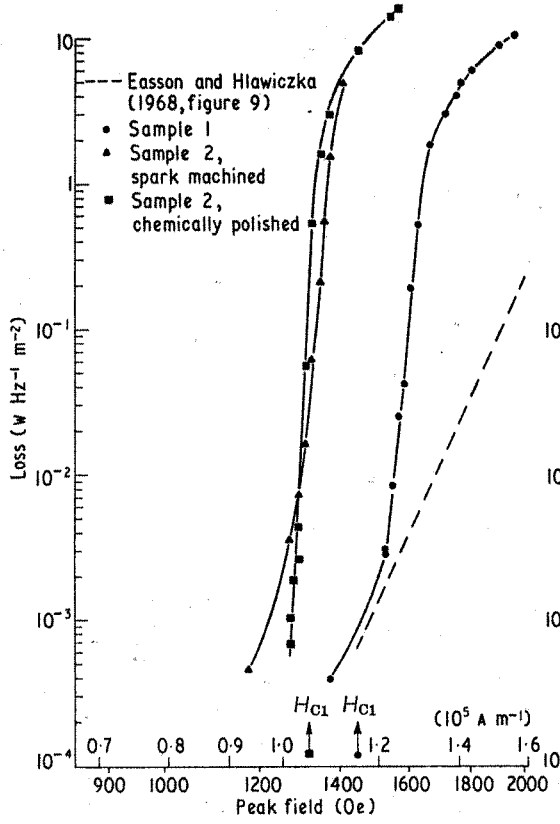

FIG. 1

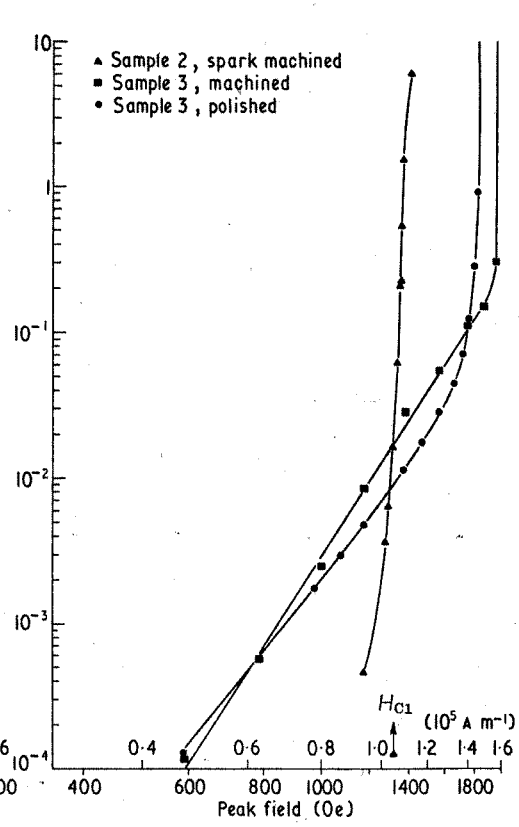

FIG. 2

are shown in figure 2. The sample was then mechanically polished with emery cloth and diamond paste to a 1 μm finish and the losses were remeasured. It can be seen in figure 2 that this mechanical polish has produced little effect. The results for sample 2 after spark-erosion are also shown for comparison.

Talysurf profiles of sample 3, taken after machining and after polishing, showed that the major surface features left by machining had been removed by polishing. However, some irregularities remained and the profile was very similar to that obtained from sample 2 after spark-erosion. Microscopic examination revealed these irregularities to be scratches from the emery cloths.

3. Discussion

From the measurements on samples 1 and 2 (figure 1) it is clear that, even for pure samples with low bulk flux-pinning, the losses below H_{C1} are very small if the surface finish is good. It is interesting to note that above H_{C1} the losses in the polycrystalline material are much lower than those in the single crystal, but below H_{C1} the losses are comparable. These measurements also show that the transition between high- and low-loss régimes occurs very close to H_{C1}. Chemical polishing of sample 2 has decreased the losses below H_{C1}, and the transition appears sharper.

The losses measured below H_{C1} on these two samples are lower than those reported by Linford and Rhodes (1968) for a niobium single crystal. This is possibly because of a better surface finish on the present samples, which had smooth bright etch-pit free surfaces after chemical polishing.

The results obtained on sample 3 (figure 2) are somewhat different. The losses do not undergo a transition to a high-loss régime until fields approaching $1{\cdot}5 \times 10^5$ A m^{-1} (1900 Oe). In general it has been found that single-crystal samples with worked surfaces behave in this manner. Magnetization measurements indicate that large-scale flux penetration is delayed to fields well above H_{C1}. It is thought that this effect is produced by defect stabilized surface currents shielding the interior of the sample. This hypothesis is confirmed by surface current measurements (to be published) in the mixed state which show a large increase as a result of surface treatment. The currents measured in sample 3 were of the correct order of magnitude to provide shielding up to $1{\cdot}6 \times 10^5$ A m^{-1} (2000 Oe).

A feature of the results for sample 3 which is more difficult to interpret is the small change in losses between the polished and unpolished surfaces. Moreover, although the surface profile of sample 3 after polishing was similar to that of sample 2 after spark machining, the losses were considerably higher (see figure 2). The heavily worked surface of sample 3 might be expected to provide strong flux-pinning and hence smaller losses. The reason that this was not observed is possibly that the surface layers were severely damaged by the machining and subsequent mechanical polishing.

4. Conclusions

These results confirm the conclusions of other workers that, to achieve minimum losses, it is of primary importance to use material with a smooth surface. Our measurements indicate that provided the surface is sufficiently smooth the bulk flux-pinning of the sample is not so important in losses below H_{C1}. The measurements also demonstrate that mechanical polishing may not always be a satisfactory way of achieving a smooth surface. Since losses increase sharply at H_{C1} or H_{FP} it is necessary to use a material treated so as to make this field as high as possible.

The results also indicate that the effect of the metallurgy of the surface layers on losses below H_{C1} requires further investigation. It is intended to measure losses in polycrystalline niobium samples as a function of their annealing treatment. Measurements will also be made on material with different surface finishes to obtain more quantitative data on the effect of surface finish.

Acknowledgments

This work was carried out under the terms of a research contract with the British Oxygen Company who have kindly agreed to the publication of these results. We wish to thank Dr. D. K. Bowen (Warwick University) and Dr. D. Jones (Birmingham University) for providing us with samples.

References

BUCHHOLD, T. A., 1963, *Cryogenics*, **3**, 141–9.
BUCHHOLD, T. A., and MOLENDA, P. J., 1962, *Cryogenics*, **2**, 344–7.
EASSON, R. M., and HLAWICZKA, P., 1967, *Brit. J. Appl. Phys.*, **18**, 1237–49.
—— 1968, *Brit. J. Appl. Phys.*, ser. 2, **1**, 1477–85.
LINFORD, R. M. F., 1968, *Ph.D. Thesis*, University of Warwick.
LINFORD, R. M. F., and RHODES, R. G., 1968, *Phys. Stat. Sol.*, **28**, K 63–5.
ROCHER, Y. A., and SEPTFONDS, J., 1967, *Cryogenics*, **7**, 96–102.

A simple integrating magnetometer

P R Brankin, A R Eastham and R G Rhodes
School of Engineering Science, University of Warwick, Coventry, Warwicks.
MS *received 2 December 1969*

Abstract Some problems with the vibrating sample technique for obtaining magnetization curves of superconducting samples are discussed. The construction and performance of a simple integrating magnetometer which overcomes some of these difficulties is described.

1 Introduction

This note describes a simple integrating magnetometer designed to obtain magnetization curves of superconducting samples. Hitherto, we have used a vibrating sample magnetometer of the type described by Zijlstra (1967) to carry out these measurements. However, it has been reported (Love *et al.* 1952, Finnemore *et al.* 1966, Campbell *et al.* 1968) that vibration or motion of a superconducting sample in a magnetic field may affect the penetration or expulsion of flux. Also, in conditions in which bulk flux changes are inhibited by surface flux-spot pinning (Hart and Swartz 1967), it has been shown that the magnetization near the sample ends differs from that of the central region (P R Doidge and A R Eastham to be published). With the vibrating sample magnetometer, the relative positions of the sample and pick-up coils are very critical and, in practice, anomalies in the shape of the magnetization curves obtained with this instrument are often observed. To overcome these difficulties, and because it was desired to make magnetization and ac measurements without disturbing a sample in the helium bath, it was decided to construct an integrating magnetometer.

2 Apparatus

A schematic diagram of the integrating magnetometer is shown in figure 1. The sample is placed in the centre of a coaxial pair of search coils which have an approximately equal number of area turns, and are connected in series opposition.

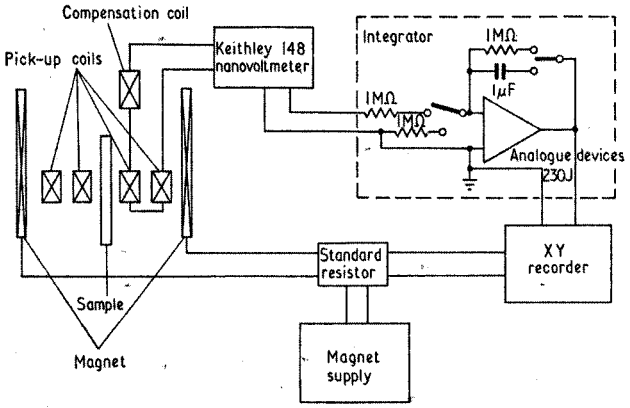

Figure 1 Schematic diagram of magnetometer

With the sample in the normal state, the coil system is made noninductive by adjusting the position of a small compensating coil. In a swept magnetic field H parallel to the axis of the sample, the voltage V across the coils is given by

$$V = -(n_1 - n_2)\, A \frac{dM}{dH}\frac{dH}{dt}.$$

Here A is the cross-sectional area of the sample, and dM/dH is the slope of the magnetization curve. In one experimental arrangement the search coils are 5 mm long. The inner coil has a mean diameter of 3·5 mm and $n_1 = 2100$ turns, while the outer coil has a mean diameter of 7·2 mm and $n_2 = 500$ turns.

After amplification by a Keithley nanovoltmeter, which has a very low drift (10 nV per day), the signal from the search coils is integrated to produce a voltage proportional to magnetization. The integrator is designed to have a stability of 0·1% over periods of up to 30 minutes. It consists of an input resistor and an operational amplifier with capacitive feedback. The output of the integrator may be set to zero by switching a 1 MΩ resistor in place of the feedback capacitor. A second switch enables the output to be held constant by connecting a 1 MΩ resistor between earth and the amplifier input. The input offset voltage of the amplifier may be reduced to zero by using the trimming facilities in the circuit and an external 10-turn 100 kΩ Helipot.

The chopper-stabilized amplifier is an Analogue Devices' type 230J. This has an input bias current drift of 1 pA degC^{-1} and an input offset voltage drift of 0·5 μV degC^{-1}. Two 0·5 μF (±½%) film capacitors (Salford Electrical Industries Ltd), having a temperature coefficient of -150 ± 80 p.p.m. and a leakage resistance of 5×10^{11} Ω are used for the feedback capacitors. The 1 MΩ (±¼%) input resistor (Paignton Ltd) is a metal oxide film type with a temperature coefficient of ±25 p.p.m. To minimize thermal voltages in the integrator all internal connections are made with untinned Cu wire and CdSn solder. Glass fibre insulation board is used wherever necessary to minimize leakage currents, and Radiospares Maka-Switch units, having a high leakage resistance ($> 10^{11}$ Ω) and low thermal emfs, are used for switching.

Before sweeping the magnetic field the gain of the nanovoltmeter is adjusted to keep the integrator input signal within the range 0–1 V to avoid saturation of the operational amplifier. The integrated voltage is fed to the Y axis of an XY recorder, while a signal proportional to the magnetic field is fed to the X axis.

3 Conclusions

The integrating magnetometer has provided a convenient and accurate method of obtaining the magnetization curves of cylindrical superconducting samples with diameters in the range 1–5 mm, at field sweep rates down to 10^3 A m^{-1} s^{-1} (about 10 Oe s^{-1}). The construction of the magnetometer presented no great difficulties, and it became operational in a very short time.

A comparison of the magnetization measurements on various samples using both the vibrating sample and integrating methods will be published shortly.

Acknowledgments

The authors wish to acknowledge financial support for this research from the British Oxygen Company (P R B) and the Ministry of Technology (A R E).

References

Campbell A M Evetts J E and Dew-Hughes D 1968 *Phil. Mag.* **18** 313–43

Finnemore D K Stromberg T F and Swenson C A 1966 *Phys. Rev.* **149** 231–43

Love W F Callen E and Nix F C 1952 *Phys. Rev.* **87** 844–7

Hart H R Jr and Swartz P S 1967 *Phys. Rev.* **156** 403–11

Zijlstra H 1967 *Selected Topics in Solid State Physics* Vol. 9 Ed. E P Wohlfarth (Amsterdam: North Holland)